Redox Activation of C–C and C–H Bonds Using Visible Light

by

Joel W. Beatty

A dissertation submitted in partial fulfillment
of the requirements for the degree of
Doctor of Philosophy
(Chemistry)
in the University of Michigan
2016

Doctoral Committee:

Professor Corey R. J. Stephenson, Chair
Assistant Professor Pavel Nagorny
Assistant Professor Corinna Schindler
Assistant Professor Matthew B. Soellner

DEDICATION

To Ellie, Dave, and Ian

ACKNOWLEDGEMENTS

There are a lot of people I need to thank for helping me through this process.

First, I must thank my advisor Corey Stephenson. I am very thankful for the opportunity he gave me in working in his lab, and for all of the advice and guidance I have received from him throughout the process. I am grateful for his high standards, and the expectations he placed upon me helped to motivate and drive me forwards. I was given opportunities to work on exciting chemistry, and I was given freedom to try ideas out for myself. I didn't have to teach the last three years of my studies, and I am very thankful for his willingness to fund me and support me in this endeavor. I'd also like to thank my committee: Professor Corinna Schindler, Professor Pavel Nagorny, and Professor Matt Soellner. Also thanks to faculty members at Boston University: Professor Ramesh Jasti, Professor John Snyder, and Professor John Porco.

I have been fortunate to have many smart, interesting, and hard-working co-workers. I'd especially like to thank Mitch Keylor, who started at the same time as me at Boston University. Graduate school is much better if you have a friend going through the same things at the same time as you. Thanks in particular to my friends Rebecca Watson, Bryan Matsuura, Verner Lofstrand, James Douglas, Alex Nett, and John Nguyen for making Michigan a better place for me. Also special thanks to those I have worked closely with on various projects: James Douglas, Joe Tucker, Alex Sun, Rory McAtee, Chris McAtee, and Tim Monos. All of my coworkers have been wonderful throughout the years. Post-docs: Daryl Staveness, Markus Kaerkaes, Irene Bosque-Martinez, Elizabeth Swift, Jim Devery, Milena Czyz, Jagan Narayanam, Calle Johan-

Wallentin, Dave Freeman. My fellow graduate students: Joe Tucker, Chunhui Dai, Laura Furst, John Nguyen, Bryan Matsuura, Mitch Keylor, Tim Monos, Martin Sevrin, Gabe Magallanes, Theresa Williams, Rory McAtee, Alex Sun, Christopher McAtee, Marlena Konieczynska, Long Nguyen, Zach Garletz, Leanne Sebren, and Sung Hun Park. Also my friends at BU: Evan Darzi, Gina Kim, Matt Goldberg.

Professor Michael Pollastri at Northeastern University has had a profound influence on me, and I am very thankful for his guidance and friendship. He made space for me in his lab when there wasn't any, and gave me excellent advice about graduate school and beyond. I am very grateful for all of this, as his advice has given me perspective on multiple occasions when I really needed it. Others at Northeastern University had a big influence on me, in particular my friend John Bottomy. Professor Mabrouk was very encouraging to me, and I always think about her words when I am feeling discouraged.

I was fortunate to have worked with Aaron Coffin and many others at GSK in Waltham. I am also very thankful for my time at W. R. Grace; Sal Crespo was a wonderful boss and I learned a lot from him.

So thank you to the many people who have supported me through my years of graduate school. I also need to thank my family and friends but I'll do most of that in person.

TABLE OF CONTENTS

LIST OF TABLES

LIST OF FIGURES

LIST OF ABBREVIATIONS

#	denotes position of additional functionalization
*	denotes position of regioisomeric functionalization
[O]	oxidant
°C	degree Celsius
Ac	acetyl
AIBN	azobisisobutyronitrile
aq	aqueous
Ar	aryl
ATRA	atom transfer radical addition
BF_4	tetrafluoroborate anion
Bn	benzyl
Boc	*tert*-butoxycarbonyl
bpy	2,2'-bipyridine
bpz	2,2'-bipyrazine
$BrCF_3$	bromotrichloromethane
Cbz	carboxybenzyl
CF_3	trifluoromethyl
CF_3I	trifluoromethyliodide
CFL	compact fluorescent lightbulb
cm	centimeter
Cr	chromium
Cu	copper
CV	cyclic voltammetry
d	doublet
DABCO	1,4-diazabicyclo[2.2.2]octane
Dap	2,9-bis(*para*-anisyl)-1,10-phenanthroline
DBU	1,8-diazabicyclo[5.4.0]undec-7-ene
DCM	dichloromethane
DDQ	2,3-dichloro-5,6-dicyano-1,4-benzoquinone
$dF(CF_3)ppy$	2-(2,4-difluorophenyl)-5-(trifluoromethyl)pyridine
DIPEA	*N*,*N*-diisopropylethylamine
DMF	dimethylformamide
DMSO	dimethylsulfoxide
dr	diastereomeric ratio
dtbbpy	4,4'-di-tert-butyl-2,2'-bipyridine
$E_{0,0}$	zero-zero excitation energy

ee	enantiomeric excess
equiv	equivalents
er	enantiomeric ratio
E_{red}	reduction potential
ESI	electrospray ionization
Et	ethyl
fac	facial
Fc	ferrocene
g	grams
h	hours
HCF_3	fluoroform
HRMS	high resolution mass spectroscopy
Hz	hertz
IR	infrared
Ir	iridium
J	coupling constant
K	Kelvin
L	liters
LED	light emitting diode
Li	lithium
M	molar concentration
m	multiplet
MCDFA	methyl chlorodifluoroacetate
Me	methyl
Mes	mesityl
MFC	mass-flow controller
mg	milligrams
MHz	megahertz
min	minutes
mL	milliliters
MLCT	metal to ligand charge transfer
mm	millimeters
mmol	millimoles
mol	moles
mol%	mole percent
MW	molecular weight
$NaSO_2CF_3$	sodium trifluoromethanesulfinate
NBS	*N*-bromosuccinimide
NHC	*N*-heterocyclic carbene
nm	nanometers
NMR	nuclear magnetic resonance
ns	nanosecond
ns	nanosecond
PC	photocatalyst
PF_6	hexafluorophosphate anion
Ph	phenyl

phen	1,10-phenanthroline
PNO	pyridine *N*-oxide
ppm	parts per million
PPNO	4-phenylpyridine *N*-oxide
ppy	2-phenylpyridine
ps	picoseconds
Py	pyridine
q	quartet
rt or RT	room temperature
Ru	ruthenium
s	singlet
SCE	saturated calomel electrode
SPhos	2-dicyclohexylphosphino-2',6'-dimethoxybiphenyl
t	triplet
Tf	triflyl
TFA	trifluoroacetic acid
TFAA	trifluoroacetic anhydride
TfCl	trifluoromethanesufonyl chloride
THF	tetrahydrofuran
THIQ	tetrahydroisoquinoline
TMEDA	tetramethylethylenediamine
$TMSCF_3$	trifluoromethyltrimethylsilane
t_R	residence time
UV	ultraviolet
V	volts
W	watt
δ	chemical shift in parts per million
λ_{max}	maximum wavelength
μL	microliters
τ	excited-state lifetime

ABSTRACT

Carbon-carbon and carbon-hydrogen bonds constitute essential components of organic frameworks and impart significant amounts of chemical inertness and stability to complex architectures. These bond types are common, and the ability to modify or selectively cleave these bonds in the presence of other sensitive functional groups is a worthy goal of synthetic chemistry. These operations not only are capable of functionalizing traditionally unreactive positions on molecules, but provide additional strategic options for the design and implementation of synthetic routes.

Due to the strength and ubiquity of these bonds, the development of methods to selectively cleave and functional groups is an important synthetic challenge. Here, efforts to use visible light as a chemical energy source to cleave C–C and C–H bonds selectively are outlined, with both single-electron oxidation and single-electron reduction as the key activation event.

The first two chapters of this thesis outline the factors which can be leveraged for the functionalization of atoms alpha to amine nitrogens. Upon single-electron oxidation of an amine to its corresponding radical cation, the bond strengths to all adjacent α-positions drop substantially, providing significant modulation of reactivity through a simple oxidation mechanism. This activation pathway can be used to selectively cleave C–C bonds in the presence of significant strain energy. In the absence of strain energy, C–H bonds react in preference. Both of these activation mechanisms are demonstrated in the semi-synthesis of three alkaloid natural products using photoredox catalysis.

Aside from single-electron oxidation, this work also details a reductive mechanism for the selective C–C bond cleavage of carboxylic acids. Through the use of pyridine *N*-oxide, a method has been developed to activate carboxylate esters to single-electron reduction, which is rapidly succeeded by a decarboxylative fragmentation event. This method has been used to trifluoromethylate a wide array of aromatic substrates, and has been demonstrated on significant scale. Mechanistic insights into this reactivity have revealed that under certain conditions intermolecular charge-transfer complexes can be formed, and these have been directly implicated in the trifluoromethylation reaction mechanism.

Chapter 1: Photoredox Catalysis in Amine Oxidation

*Portions of this chapter have been published in Beatty, J. W.; Stephenson, C. R. J. Amine functionalization via oxidative photoredox catalysis: Methodology development and complex molecule synthesis. *Acc. Chem. Res.* **2015**, *48*, 1474.

Introduction

The use of visible light in synthetic chemistry imparts selectivity that is unavailable through the use of ultraviolet (UV) light, as selective activation of reagents may be mediated through the use of a light-absorbing catalyst instead of through direct irradiation of the substrate.[1] UV irradiation is high in energy, and consequently its interaction with organic substrates often results in less selective bond-cleavages and molecular excitations. Furthermore, from a practical standpoint visible light is much easier to utilize, as there is less of a safety concern for light exposure and no special equipment is required other than a light source as simple as a desk lamp.

Photoredox catalysis uses visible-light absorbing catalysts to funnel light-based energy into chemical energy.[2] This is accomplished through the excitation of electrons in the photocatalysts to generate a reactive and versatile photo-excited state. The prototypical polypyridyl metal photocatalyst tris(bipyridyl)ruthenium dichloride ($Ru(bpy)_3Cl_2$) is shown in **Fig. 1.1**, and a schematic of its molecular orbitals serves to depict the electronic configuration of the photocatalyst upon absorption of a photon.[3] There are a number of features of this catalyst

which cause it to behave efficiently as a catalyst for organic transformations, one of which is that the excited state lifetime is relatively long-lived (approximately 1100 ns), allowing for intermolecular reactivity within the timeframe of excitation.[4] Furthermore, the quantum yield of the chemically reactive excited state $Ru(bpy)_3^{2+*}$ is near 100%,[5] which under standard conditions allows for a highly efficient conversion of light to chemical energy without promoting significant amounts of side-reactivity such as catalyst decomposition or ligand exchange.

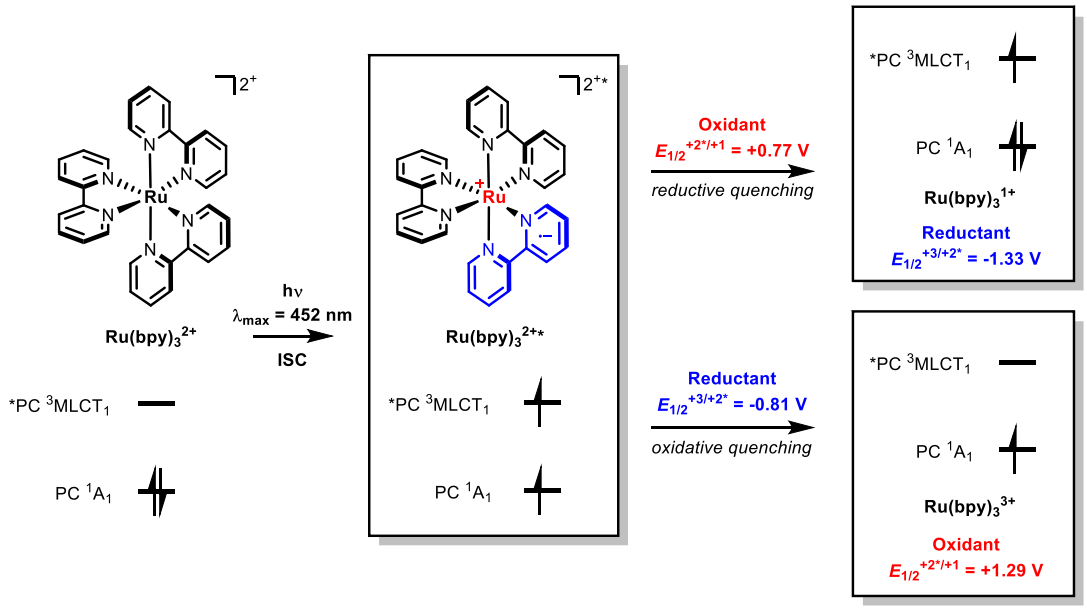

Figure 1.1 Molecular orbitals of the $Ru(bpy)_3Cl_2$ redox cycle

The photoexcited state of $Ru(bpy)_3^{2+*}$ is accessed *via* promotion of a single electron to an extremely short lived singlet excited state centered on the ligand ($^1MLCT_1$, not shown). There are numerous higher energy electronic bands available for excitation, as can be gleaned from the broad absorption of the catalyst in the UV spectrum;[3] these higher energy excited states ($^1MLCT_n$) rapidly decay to $^1MLCT_1$, which subsequently undergoes intersystem crossing (ISC) to form the long-lived and redox-active triplet excited state (**Fig. 1.1**). This excited state is capable of behaving as either an electron-acceptor (oxidant, reductive quenching of the excited state) or an electron-donor (reductant, oxidative quenching of the excited state), and may be

formally conceptualized as a Ru^{3+} metal center with radical anion character localized on one of the bipyridine ligands.[6] If the excited state is reduced, an electron is injected into the PC $^1A_1$ orbital, while oxidation of the catalyst unsurprisingly removes the highest-energy electron from the ligand. These events are depicted simply in the frontier molecular orbital diagram in **Fig. 1.1**, wherein reductive quenching results in the formation of the strong reductant $Ru(bpy)_3^{1+}$ and oxidative quenching correspondingly forms the strong oxidant $Ru(bpy)_3^{3+}$. Each of these ground-state species readily regenerate the initial $Ru(bpy)_2^{2+}$ oxidation state through an additional electron transfer event, thus closing the catalytic cycle.

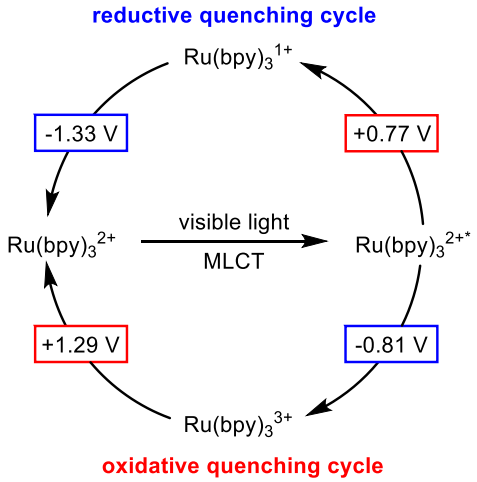

Figure 1.2 Reductive and oxidative quenching cycles of $Ru(bpy)_3Cl_2$

Each of these electron-transfer events is also characterized by a corresponding redox potential. Ground state redox couples (i.e. between Ru^{+1}, Ru^{2+}, and Ru^{3+}) can be measured directly through the use of cyclic voltammetry and have been shown to be empirically independent of solvent choice.[7] These values are cited in **Fig. 1.2** (left side), and are readily extracted from the corresponding voltammogram.[3] Redox potentials which describe the photoexcited state are challenging to directly measure due to the transient nature of the excited state; as a consequence these values are estimated from spectroscopic measurements of the

photocatalyst.[8] The peak phosphorescence emission wavelength of the photocatalyst (615 nm at 298 K for $Ru(bpy)_3Cl_2$) can be used directly to calculate the energy gap ($E_{0,0}$) between the ground state of the photocatalyst and the lowest triplet energy state $^3MLCT_1$ using the Planck-Einstein relation ($E_{0,0} = h \bullet c \bullet \lambda^{-1}$). As this value represents the difference in energy between the excited state and ground state of the photocatalyst, it is also representative of the sum of the energies of both the ground state redox potential and exited state redox potentials, which allows the excited state reduction potentials to be estimated from both $E_{0,0}$ and cyclic voltammetry measurements.

A wide array of transition-metal photocatalysts are used for photocatalysis, with well characterized redox potentials which can be tuned based upon the careful selection of both metal center and ligand. While not exhaustively listed in this document, a series of popular photocatalysts are listed along with their photophysical and electrochemical properties in MacMillan's review.[2] These catalyst redox values serve a valuable role in the rationalization of whether an electron-transfer process will be feasible; however, even ground-state redox potentials cannot be used as absolute guidelines for a number of reasons. First, the use of cyclic voltammetry for electrochemical measurement requires the use of superstoichiometric amounts of electrolyte in order to facilitate ion transport in solution; this as well as other physical considerations such as concentration, surface adsorption phenomena, and lack of other substrates and reagents results in an inability to accurately extrapolate measured redox potentials to a given reaction system. Furthermore, ground state and excited state potentials are often cited as half-wave potentials ($E_{1/2}$). This number does not take into consideration thermodynamically uphill electron transfer events which may also take place, which usually result in observed electric current during cyclic voltammetry measurements. Electron transfer can happen in an endergonic

fashion at milder potentials than that quoted as the value for $E_{1/2}$. Redox behavior of the photocatalyst excited state is subject to the same principals, and consequently the determination of fluorescence quenching is a much more reliable method of determining reactivity from the excited state.

The benefits of using photocatalysis are myriad. Light is a renewable resource, and the ability to promote reactivity in a catalytic fashion as opposed to the use of stoichiometric reagents is a hallmark of green chemical synthesis. Furthermore, the use of photoredox catalysis can obviate the need for more traditional reagents for radical organic chemical transformations, including triethylborane (pyrophoric), azobisisobutyronitrile (explosive), and tributyltin hydride (toxic). Trialkyltin reagents are especially problematic for environmental reasons.[9] The use of alkyltins as anti-fouling agents in boat paint led to the slow leaching of these chemicals into the marine environment, and as a consequence it has been found that these pollutants are highly persistent. Photoredox catalysis allows for the replacement of these reagents in synthesis, and with the development of further technologies such as flow processing, the ability to truly scale photoredox catalysis for industrial use is well within reach. The underlying focus of the presented research deals directly with developing the efficacy of photoredox catalysis in more complex and synthetically challenging environments, with the ultimate goal of demonstrating its relevance for solving real chemical problems in an environmentally benign fashion.

Amine Oxidation with Photoredox Catalysis

The use of amines in photoredox catalysis is widespread, as they are easily oxidized and readily quench the photoexcited state of a variety of photocatalysts.[2] Amine additives were essential to many of the initial reports concerning modern photoredox catalysis, including

Nicewicz's and MacMillan's seminal alpha-alkylation of aldehydes[10] and Yoon's [2 + 2] cycloadditions of enones.[11] Trialkylamines can be used as facile reductive quenchers of the photo-excited state of $Ru(bpy)_3Cl_2$ and similar photocatalysts, as often the catalyst ground-state reduction potential is more negative than that of the excited state. The oxidation potentials of trialkylamines are relatively low,[12] and in this way the use of amines as additives helps to enable more challenging reductions, such as light-promoted dehalogenation reactions.[13] The use of amines as substrates for photoredox catalysis has been well reviewed.[14,15]

Amines as Reductive Additives

Early attempts in the Stephenson laboratory to promote the radical functionalization of indoles using diethyl bromomalonate were inspired by a C–C bond disconnection in a retrosynthetic analysis of the natural product actinophyllic acid (**Fig. 1.3A**).[16] Specifically, the radical malonation of the 2-position of an indole intermediate was expected to provide the key quaternary carbon center of the natural product, as well as to allow the use of an indole derivative as a starting material. In preliminary attempts to promote the intermolecular malonation of indole, dehalogenated malonate was recovered as the major product from the reaction mixture when Hunig's base was used as the reductive quencher (**Fig. 1.3B**). This undesired side reaction is expected to proceed *via* reductive quenching of the $Ru(bpy)_3^{2+*}$ excited state, wherein the Ru^{1+} ground state is formed simultaneously with the diisopropylethylamine radical cation. This aminium ion is correspondingly expected to behave as a facile H-atom donor as well as a competent acid in the reaction conditions.

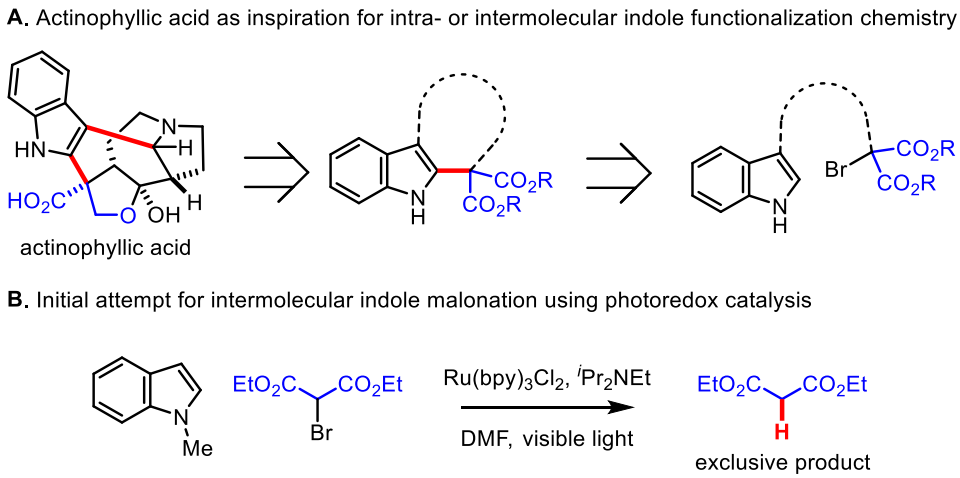

Figure 1.3: Early attempts and rationale for an intermolecular radical malonation

Precedent for this type of reactivity is extensive, as the dramatic acidification of α-amino C–H bonds upon single-electron oxidation of the neighboring nitrogen atom has been well studied; for example, this oxidation is estimated to result in a drop of roughly 25 pK_a units for the α-amino C–H bonds of trimethylamine (**Fig. 1.4A**).[17,18,19] Furthermore, the bond dissociation energy (BDE) of the α-C–H bond of the Et_3N radical cation is significantly weakened to roughly 42 kcal mol^{-1}.[20,21] These factors have significant implications for the synthetic utility of single-electron amine oxidation, and early studies by Lewis,[22,23] Mariano,[24] Saveant,[25] and others,[26,27] have shed significant light on this subject. Consequently, the amine radical cation is capable of the formation of α-amino radicals, iminium ions, and carbon centered radicals *via* β-scission—a significant array of mechanistic possibilities which, if controlled, hold significant promise for enabling synthetic strategy and design (**Fig 1.4B**).

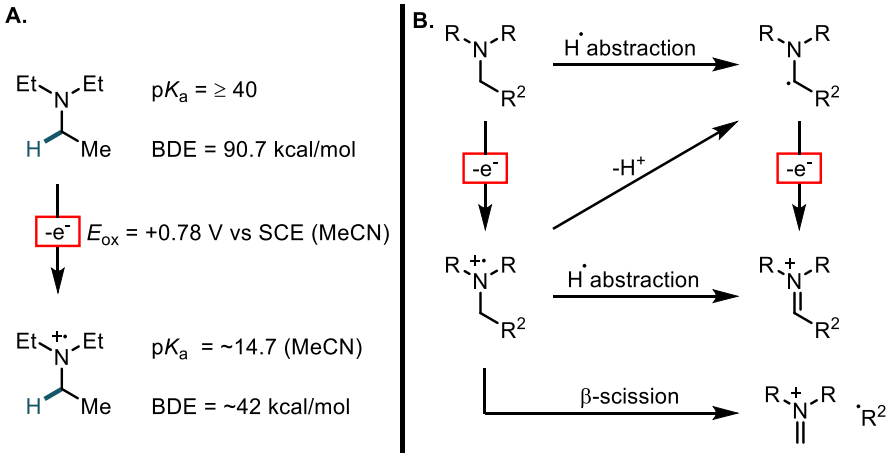

Figure 1.4 Amine reactivity upon single-electron oxidation

In the context of this complex mechanistic picture, we have empirically found that the use of triethylamine in the place of Hunig's base significantly decreases the amount of hydrodehalogenation reactivity when these amines are added as reductive quenchers, although this effect can only be efficiently exploited in intramolecular systems such as that shown in **Fig. 1.5A**.[28] Further evidence for the α-C–H bonds of the amine additive acting as either a proton or hydrogen-atom donor was obtained upon the isolation of the aldehyde product **1** (**Fig 1.5B**). This material is thought to arise from the formation of the enamine **2** through α-reactivity (deprotonation or H-atom abstraction) of the triethylamine radical cation (**Fig. 1.5C**), followed by addition of the electronically matched malonyl radical to the enamine, oxidation, and hydrolysis. Eventually, this reactivity was mitigated through the use of tertiary amine additives which do not possess the requisite C–H bonds alpha to the amine center. A triarylamine was found to effectively promote the intermolecular functionalization of indoles and pyrroles with diethyl bromomalonate, and the absence of C–H bonds for hydrogen atom donation entirely eliminated the formation of hydrodehalogenation byproducts.[29]

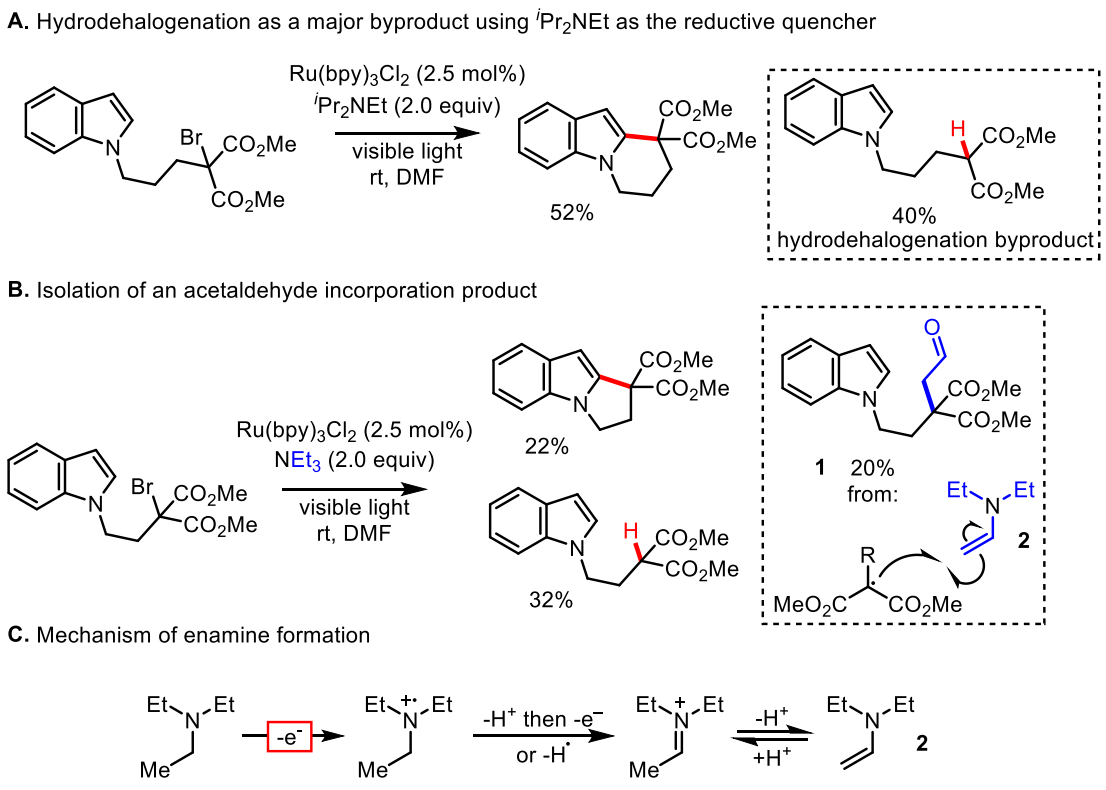

Figure 1.5 Hydrogen abstraction from trialkylamines

Amines as Substrates for Iminium Formation

This functional understanding of tertiary amine reactivity in reactions employing photoredox catalysis allowed for a reevaluation of their role from that of an additive to that of substrate. Specifically, the ability to activate the requisite C–H or C–C bonds adjacent to an amine center through simple single-electron oxidation holds significant potential from a synthetic standpoint, especially considering the large number of naturally occurring alkaloids which could be accessed using such a strategy. The first report of the synthetic utility of amines as substrates for photoredox catalysis was published in our lab, wherein the oxidation of tetrahydroisoquinolines (THIQ) was accomplished photochemically.[30] Using $Ru(bpy)_3Cl_2$ as the photocatalyst, oxidation of *N*-phenyl tetrahydroisoquinoline was accomplished in DMF using

diethyl bromomalonate **3** as the terminal oxidant. The product iminium ion was isolated as the methoxy aminal **4** after purification on silica gel with a mixture of CH_2Cl_2 and methanol as the eluent (**Fig 1.6B**). Further work revealed that the use of nitromethane as the solvent under aerobic conditions resulted in aza-Henry reactivity, and a wide variety of alkylated products could be produced with high efficiency. It should be noted with particular interest that *N*-phenyl pyrrolidine precursor to **5** underwent oxidation with very poor material recovery and yield. It was also found through control experiments that a slow background reaction is operative in the absence oxygen, suggesting that oxygen plays an accelerating role as a terminal oxidant but that nitromethane is also a competent oxidant for the system.

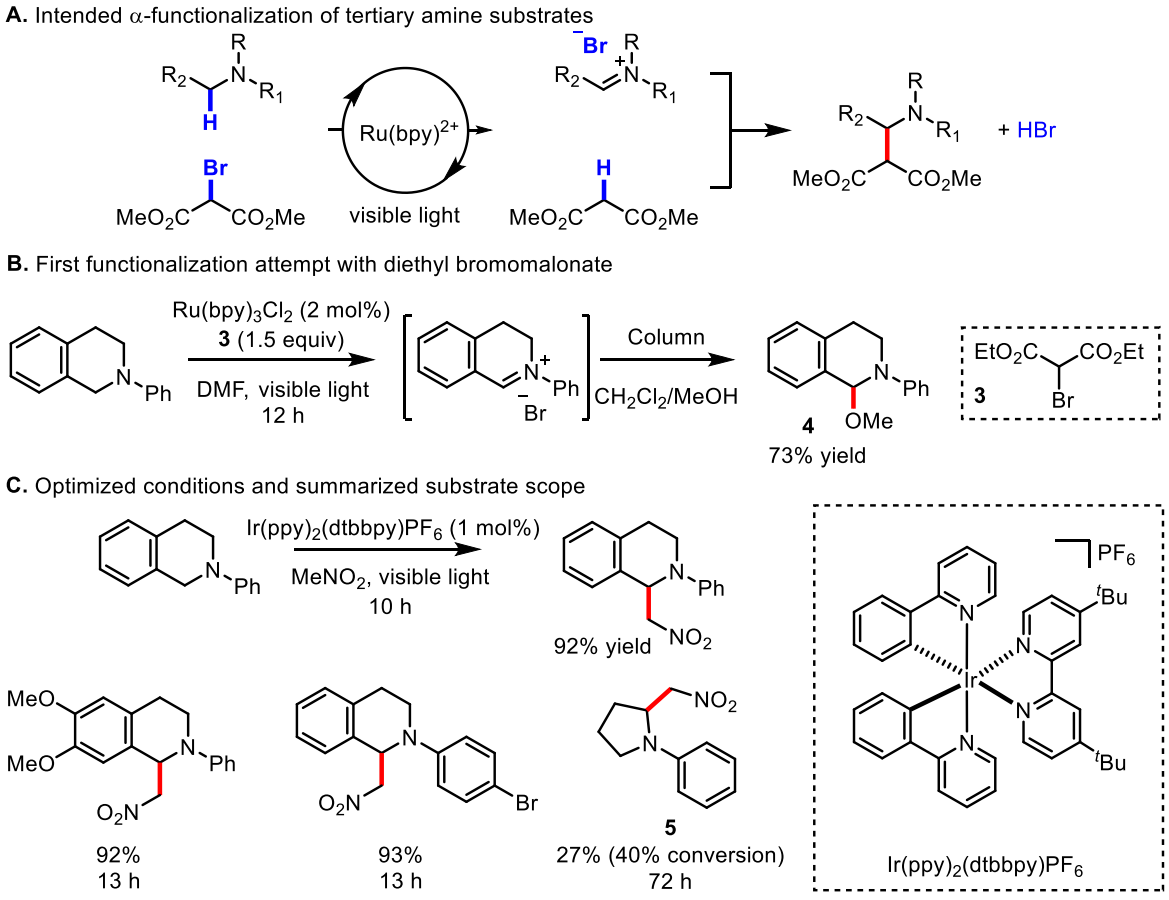

Figure 1.6 Oxidative tetrahydroisoquinoline functionalization.

Since the initial publication of these conditions, a wide array of methods has been developed for the diversification of the tetrahydroisoquinoline core, including the addition of myriad nucleophiles. Our lab has demonstrated the ability to nucleophilically cyanate, alkylate, and alkynylate *N*-aryl THIQs in good yield.[31] Other groups have demonstrated both intra- and intermolecular additions of nucleophiles through photochemical oxidation of the THIQ, and have demonstrated the addition of alcohols,[32,33] α-diazoacetates,[34] acrolein,[35] phosphonate esters,[36] ketones,[37] silyl enolethers,[38] and the Ruppert-Prakash reagent.[39]

Of particular mechanistic interest is the addition of enolized *tert*-butyl 2-oxobutanoate to the tetrahydroisoquinoline iminium ion (**Figure 1.7**), which under aerobic conditions in the presence of substoichiometric triflic acid results in a ring distortion cascade reaction.[40] The isoxazoline products of this reaction are produced in moderate yield but with high diastereoselectivity.

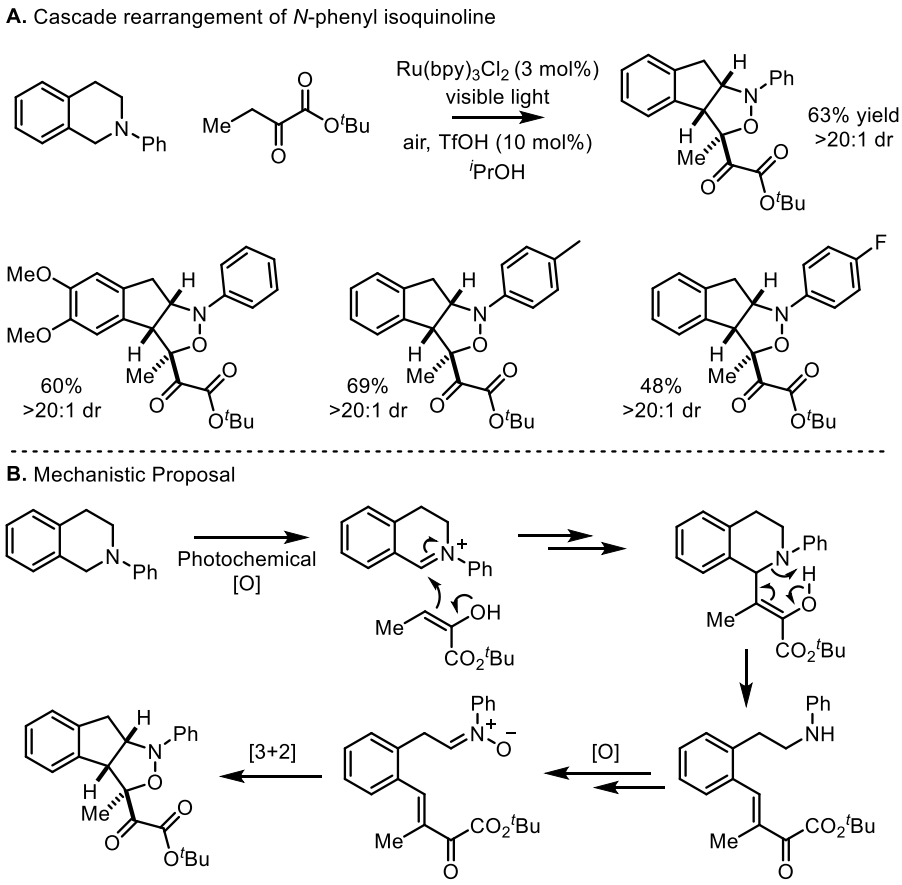

Figure 1.7 Cascade oxidative rearrangement of tetrahydroisoquinoline

Cycloadditions and Asymmetric Variants

A creative example of amine oxidation by Xiao and coworkers demonstrates the ability to promote a [3+2] cycloaddition, wherein the initial formation of the substrate iminium ion is followed by a facile deprotonation to provide an azomethine ylide for cycloaddition chemistry (**Fig 1.8**).[41] Upon initial photochemical aerobic oxidation of the THIQ substrate, a 1,3-dipole is accessed through a deprotonation of the exocyclic methylene, which then rapidly reacts with electron-poor dipolarophiles such as maleimides, nitrostyrenes, and propiolates. Due to the electron-rich nature of the initial pyrrolidine product, some over-oxidation to the corresponding pyrrole was observed. To simplify both the purification and analysis of the reaction mixtures, *N*-

bromosuccinimide (NBS) was added in a second step of the one-pot sequence, which fully aromatized each pyrrolidine to the corresponding pyrrole in high yield. A recent example of inverse electron-demand Aza-Diels-Alder reactivity with oxidized *N*-aryl tetrahydroisoquinolines has also been published.[42]

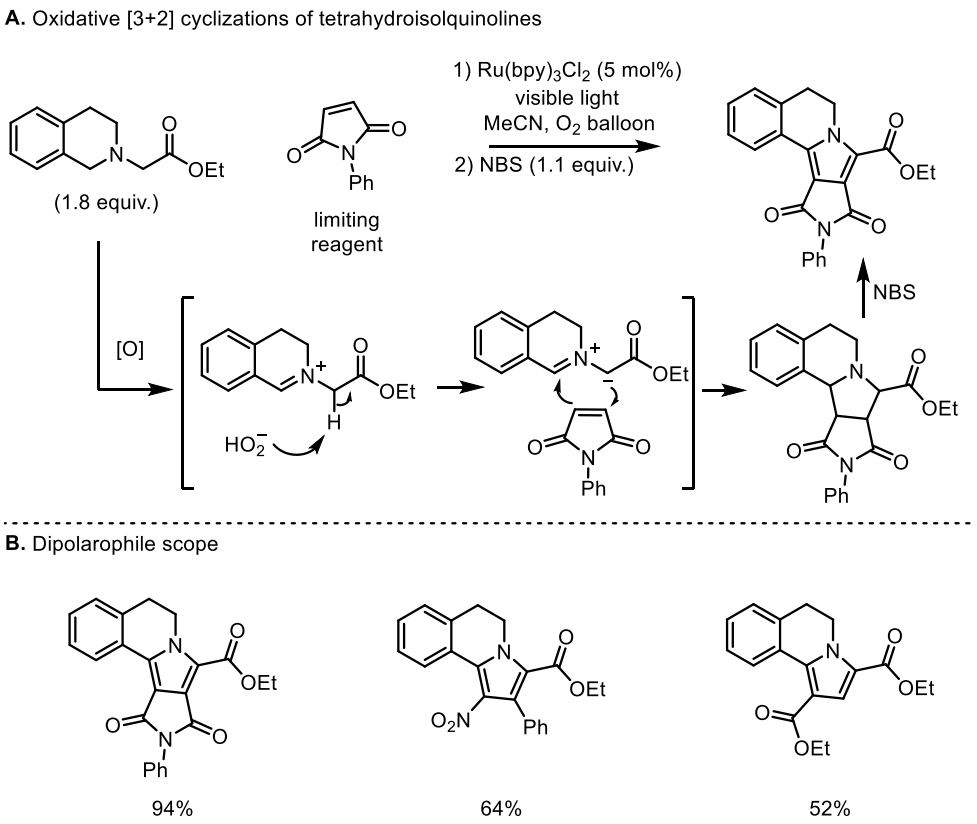

Figure 1.8 Oxidation/[3+2] cycloaddition of tetrahydroisoquinolines.

Asymmetric work by Rovis further cemented the compatibility of photoredox catalysis not only with a variety of nucleophiles but also with cooperative catalytic systems (**Figure 1.9**).[43] Following the screening of a number of conditions and various N-heterocyclic carbene (NHC) catalysts, the authors found conditions which promoted this oxidative process. Key to this chemistry was the inclusion of *m*-dinitrobenzene; when the nitroarene was excluded, only 13% yield of product was obtained, while with the additive the reaction yielded 81% product. Its role is hypothesized to involve the shuttling of electrons from the substrate to oxygen, as no reduced

nitrobenzene derivatives were detected in the reaction mixture. This is a rare example of the use of an oxidant for photoredox catalysis of which the reduction byproduct is seemingly innocent. The authors made clear that the use of alternative oxidants such as $BrCCl_3$ resulted in oxidative decomposition of the NHC catalyst **6**.

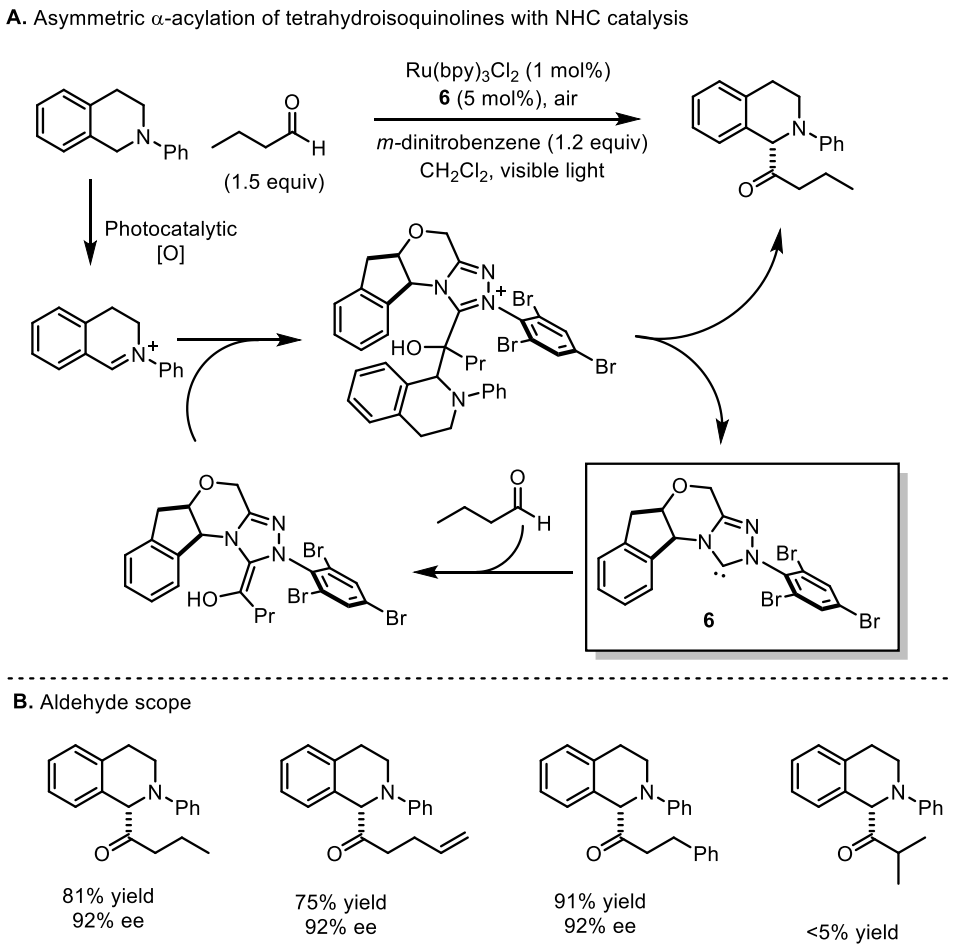

Figure 1.9 N-heterocyclic carbine catalysis for asymmetric α-amine acylation.

A further example of asymmetric additions to the oxidized tetrahydroisoquinoline cation was published by our group in collaboration with the Jacobsen lab, in which chiral thioureas were utilized as anion binding catalysts (**Fig. 1.10**).[44] A significant hurdle for the success of this methodology was the identification of a suitable solvent system, as photoredox catalysis is generally performed in polar solvents, which generally minimize enantioinduction in thiourea

catalysis. This problem was solved by running the photooxidation in acetonitrile before as solvent switch to methyl *tert*-butyl ether for the nucleophilic addition step. A series of β-amino esters were subsequently prepared with high enantiomeric excess (*ee*) and moderate yields.

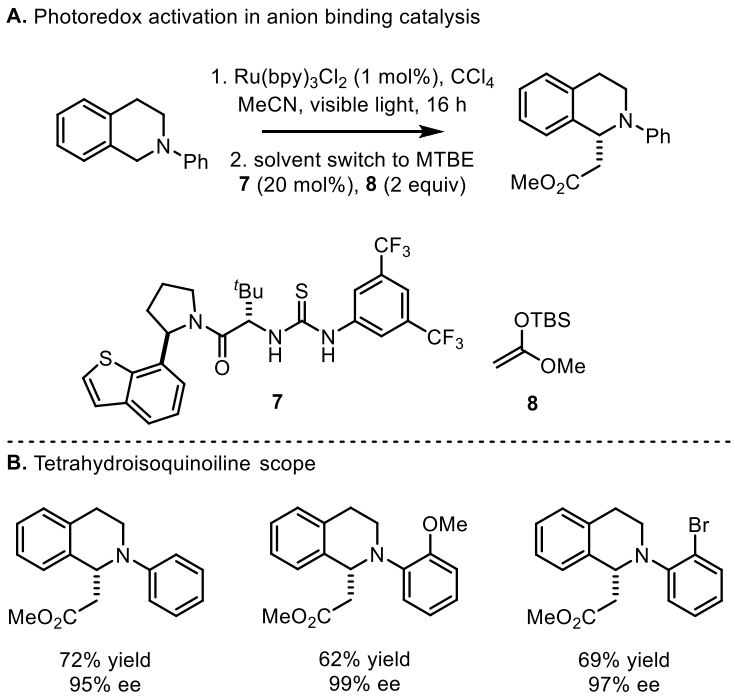

Figure 1.10 Anion binding catalysis and photooxidation for amine functionalization

Another example of asymmetric nucleophilic addition to tetrahydroisoquinoline was published by Xiao and coworkers, wherein the addition of acrolein and derivatives through a Morita-Baylis-Hillman protocol could be accomplished with 1,4-diazabicyclo[2.2.2]octane (DABCO) (**Fig. 1.11**).[35] Two asymmetric examples of this protocol were reported, using β-isocupreidine in 20 mol% to provide alkylated product in 82% yield and 83:17 enantiomeric ratio (*er*).

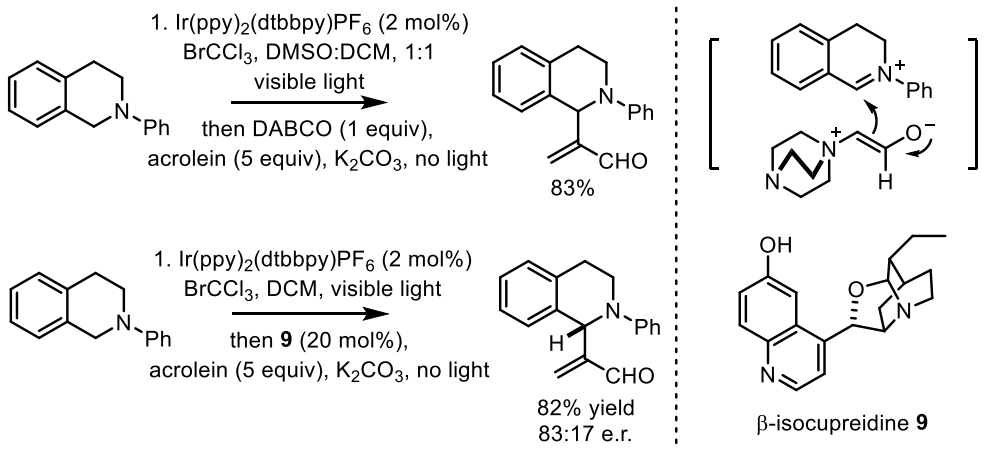

Figure 1.11 Nucleophilic catalysis for tetrahydroisoquinoline functionalization

While there is a significant amount of published work for the oxidation of tetrahydroisoquinolines, corresponding research towards the utilization of trialkylamine substrates as substrates has experienced moderately less success until recent years. In particular, the use of slightly altered substrates without benzylic activation such as *N*-phenylpyrrolidine often results in significantly decreased reaction efficiency reflected by decreased yields and increased reaction times. This may possibly arise from a lack of regioselectvity combined with the opportunity for subsequent reactivity such as enamine tautomerization and oxidation/addition events.

α-Amino Radical Formation

Initially, iminium ion formation with photoredox catalysis was much more thoroughly investigated than the utilization of the corresponding α-amino radicals. This is most likely due to the fairly negative reduction potentials of aminoalkyl radicals, which will quickly convert to the corresponding iminium ion under oxidative conditions.[45] The formation of these reactive intermediates can also theoretically be formed through the single-electron reduction of iminium ions, which may occur as a competing mechanistic pathway in some reactions. Their generation

and synthetic utility has progressed significantly in recent years, with many impressive published examples.

An early example of α-amino radical reactivity in the context of photoredox catalysis was published by Reiser and Pandey, who demonstrated a conjugate addition of an oxidized tetrahydroisoquinoline radical to a variety of enones (**Fig. 1.12A**).[46] This chemistry requires the exclusion of an oxidant, as the products are produced through a redox-neutral cycle. Lending credence to the formation of the radical intermediate, trace amounts of the dimerized product **10** were isolated after 7 days of reactivity (**Fig. 1.12B**). It is likely that the catalyst acts as a stoichiometric oxidant for this reaction, as two subsequent additions of 5 mol% were required for product formation. In a similar publication, Pandey also demonstrated the efficacy of amino-radical formation and utilization through the oxidation of 10-methyl-9,10-dihydroacridine **11**, demonstrating that the pK_a effects of amine oxidation are transmitted via conjugation (**Fig. 1.12C**).[47] The majority of tetrahydroisoquinoline oxidations result in the selective mono-functionalization of the substrate; however, the authors were able to bis-functionalize the dihydroacridine through a subsequent intramolecular cyclization step. The low conversion and long reaction times required for this intramolecular reaction further cement observations of selective mono-functionalization in the majority of isoquinoline functionalizations.

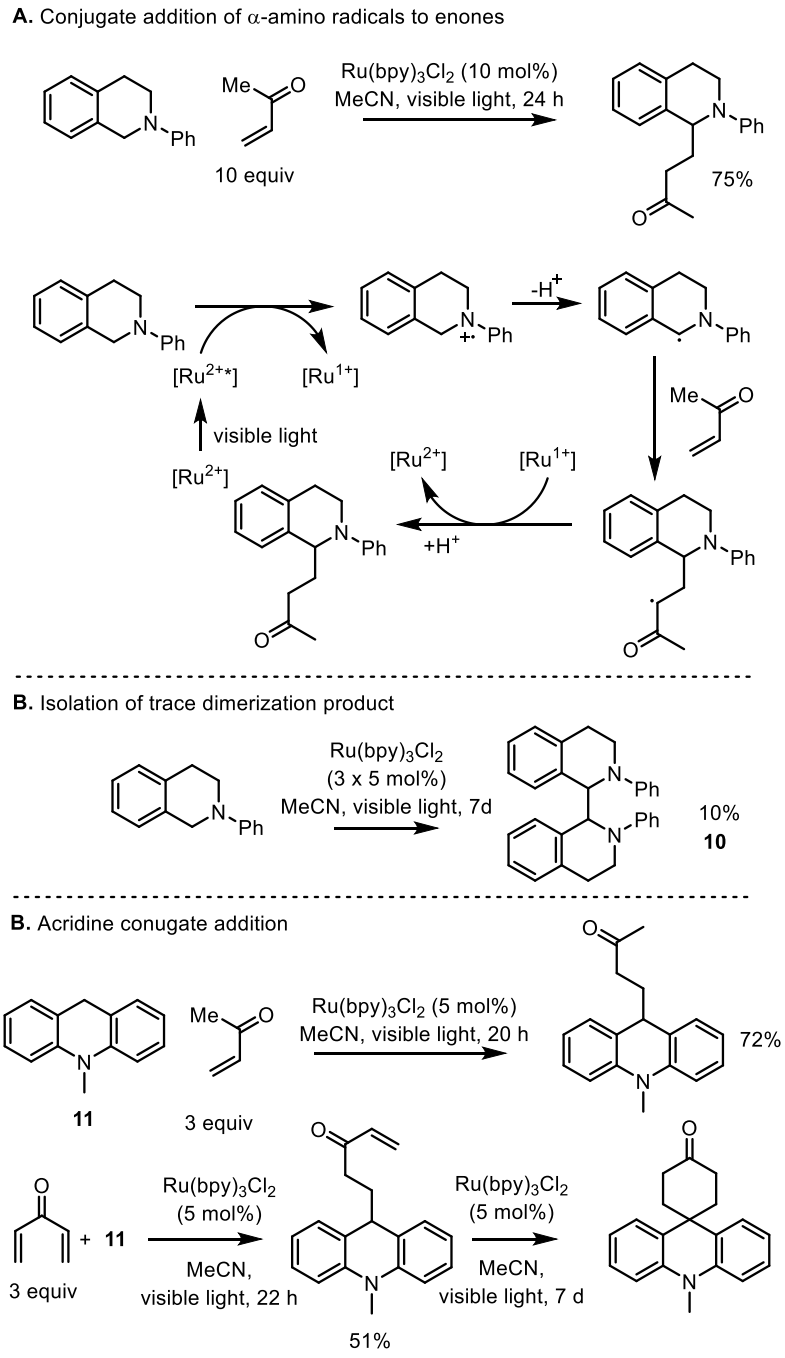

Figure 1.12 Conjugate addition of aminoradicals to methyl vinyl ketone

Aside from the highly activated benzylic C–H bonds previously mentioned, *N*-methyl aniline derivatives have been successfully utilized in a range of conjugate addition methods (**Fig 1.13**). Despite moderate amounts of methacrylate oligomerization, Xu and Li have successfully demonstrated conjugate addition of dimethylaniline to this material as well as a related Morita-

Baylis-Hillman adduct (**Fig 1.13A**).[48] Bian and Yu have demonstrated a cycloaddition strategy from this step, wherein the electron-poor radical formed upon conjugate addition of 4-methyl-*N*,*N*-dimethylaniline to *N*-phenylmaleimide is capable of cyclization back onto the electron-rich arene to form tetrahydroisoquinoline derivatives (**Fig. 1.13B**).[49] Similarly, Nishibayashi and coworkers have accomplished a highly-efficient conjugate addition using *N*-methyl-*N*-phenyl aniline (**Fig. 1.13C**).[50] Other work in this area by Curran and Reuping has demonstrated the ability of dimethyl anilines to undergo cyclizations with electron-poor alkenes.[51] There are several subsequent reports detailing this type of reactivity.[52,53]

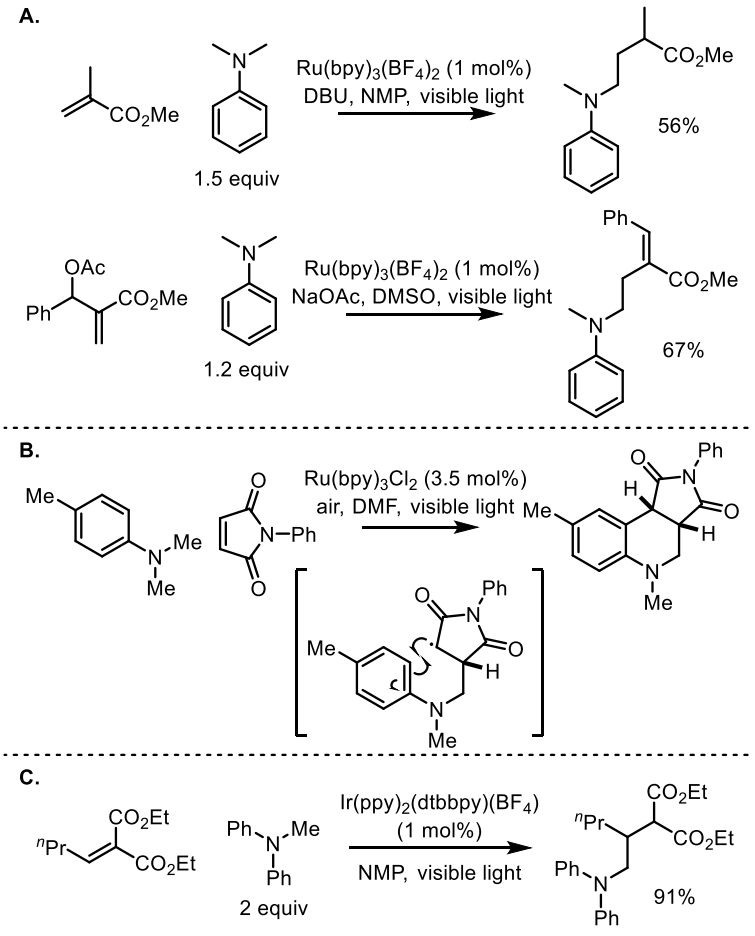

Figure 1.13 Conjugate addition of aniline-derived amino radicals

MacMillan and coworkers reported one of the more significant α-amino C–H functionalization reactions in a coupling with cyanoarenes (**Fig 1.14**).[54] This chemistry was significant for a number of reasons, not the least of which was that it was effective on amines which did not include anilines (*N*-alkyl pyrrolidines, for example). This reactivity was discovered *via* a high-throughput screening campaign, and a number of electron-poor cyanoarenes are capable of participating in the reaction. Interestingly, the reaction is mechanistically proposed to proceed through a radical-radical coupling mechanism, a mechanistic feature which is usually challenging to accomplish using photocatalysis. Primarily, this mechanism has been discounted for other systems due to the low probability of these transient species to encounter one another in solution—with low catalyst loadings, these species are only present in an estimated maximum of ~1 mole percent at any given time; however, the cyanoarene radical anion **12** is known to be persistent, causing it to increase in concentration to the point where radical-radical reactivity is much more likely. This methodology holds immediate relevance for the synthesis of select pharmaceuticals. The antibiotic Zyvox was derivatized effectively with this chemistry (**Fig 1.14**), and the authors mention that eight of the top selling drugs in 2008 possess an α-arylamine. Electron-deficient aryl chlorides are also effective coupling partners for this chemistry,[55] as well as vinyl sulfones.[56]

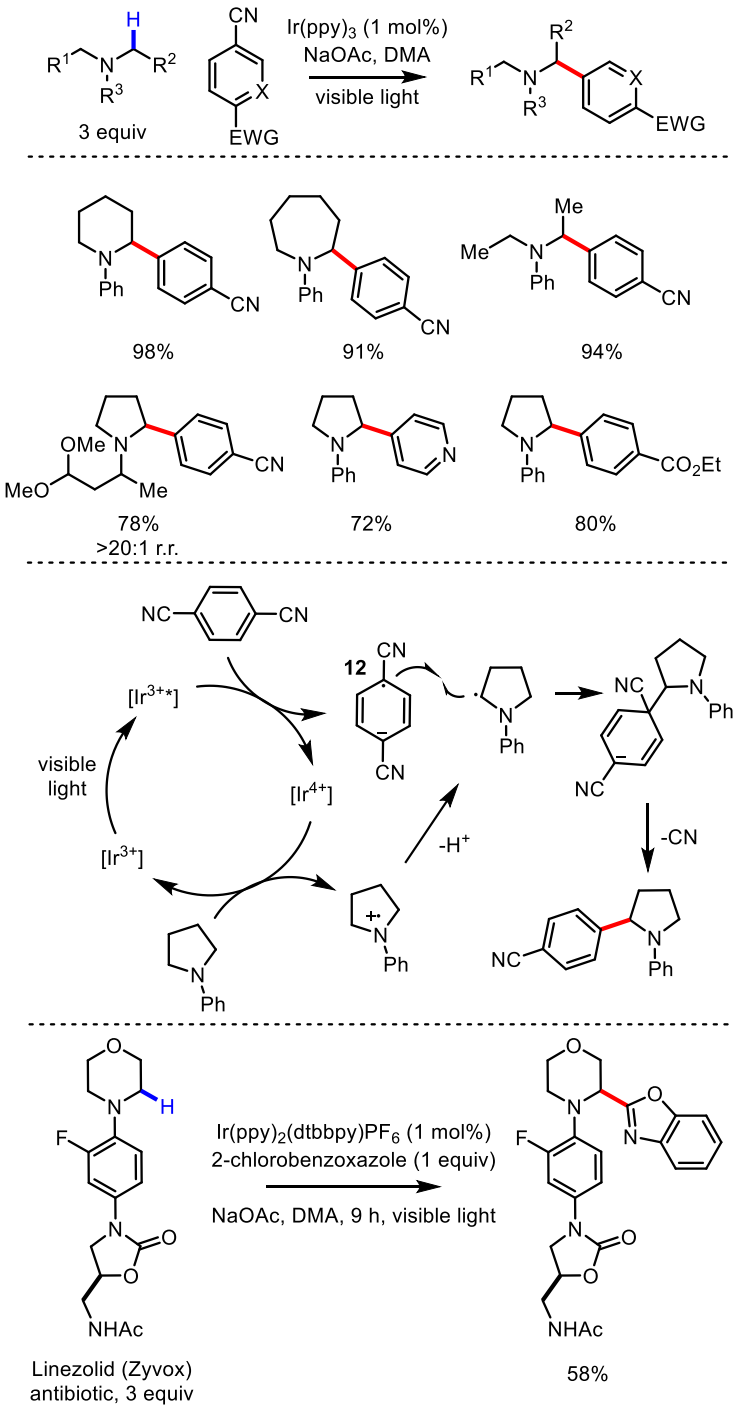

Figure 1.14 Photochemical α-arylation of tertiary amines

C–C Bond Functionalization

As mentioned above, the oxidation of amines to their radical cation results in a weakening of all bonds at the α-position, including C–C bonds. The degree of this effect is challenging to estimate, as the radical cation bond dissociation energy of the α-C–H bond is estimated using both the oxidation potential of the α-amino radical and the pKa of the parent C–H bond; the latter of these metrics is obviously not applicable for a C–C bond strength calculation. There is, however, experimental evidence to suggest that selectivity for C–C bond cleavage can be accomplished, and that this selectivity is dependent upon a number of factors. A few creative efforts have focused on the ability to cleave C–C bonds, but this process has empirically been demonstrated to be more synthetically challenging. While the associated bond strengths of unactivated sp^3–sp^3 C–C bonds are generally thought to be weaker (~90 kcal mol^{-1}) than that of an aliphatic C–H bond (~100 kcal mol^{-1}), the ability to cleave carbon-carbon bonds selectively using photoredox catalysis has been demonstrated in only a limited number of systems.

Zheng and co-workers reported in 2012 the ability to utilize *N*-cyclopropylanilines as reactants for [3+2] cycloaddition chemistry through photochemical oxidation of the substrate to the corresponding radical cation (**Fig. 1.15A**).[57] This dramatically weakens the bonds adjacent to nitrogen, and in this case selectively cleaves the C–C bond due to the strain energy of the cyclopropane ring.[58] Catalyst effectiveness for this chemistry trended with oxidizing ability, and $Ru(bpz)_3(PF_6)_2$ was the most effective in this way ($E_{1/2}^{+2*/+1}$ = + 1.45 V vs. SCE in MeCN).[59] Subsequent work from the Zheng lab has demonstrated the utility of cyclobutanes in this chemistry, which are known to fragment upon radical formation, albeit at a slower rate (**Fig.**

1.15B, 1.15C).[60] Additionally, Lu and coworkers have demonstrated the use of nitrocyclopropanes as reductively-activated coupling substrates for a similar fragmentation followed by [3+2] cycloaddition.[61] Yoon has also demonstrated the fragmentation of cyclopropanated styrenes with photoredox catalysis.[62]

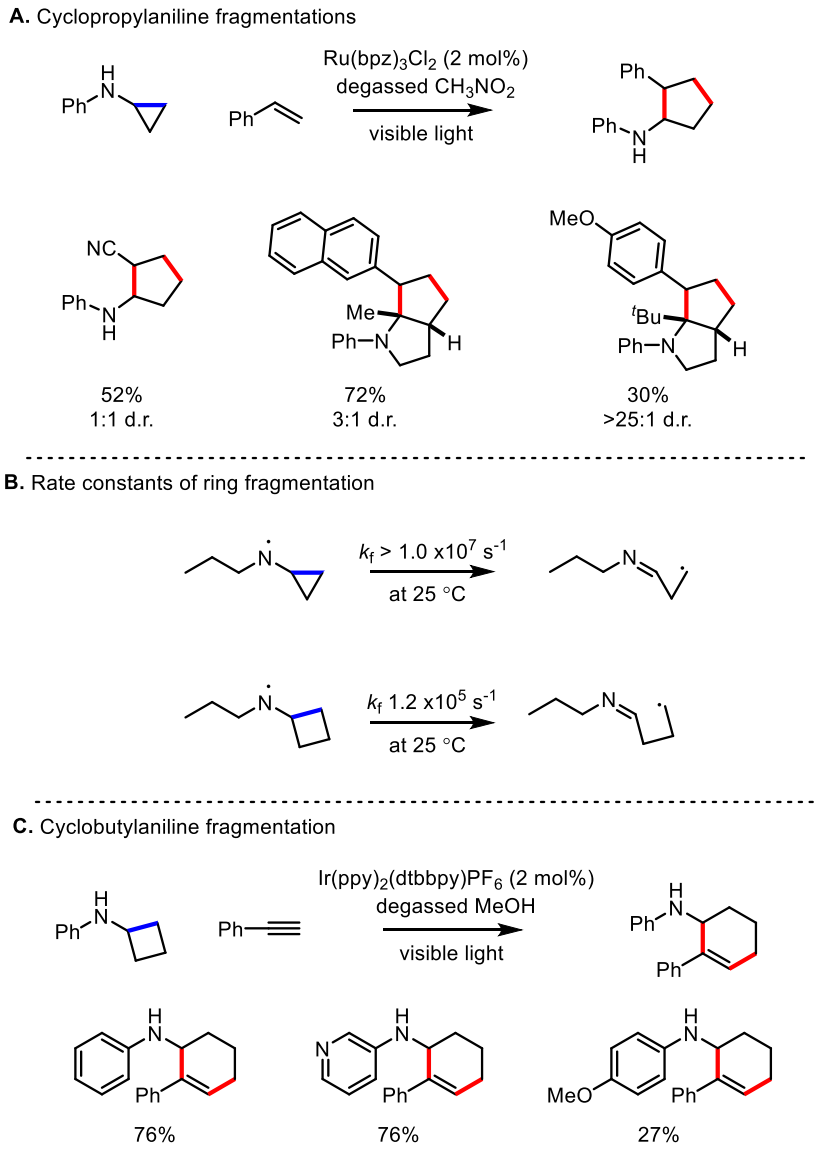

Figure 1.15 Intermolecular [3+2] cyclizations of *N*-cyclopropylamines

Aside from strain-driven bond fragmentation, entropic factors have also been demonstrated to provide selectivity for C–C over C–H bond cleavage. An early example of this

chemistry was published by Li, Wang, and coworkers, who showed that the photooxidation of tetramethylethene diamine (TMEDA) can result in the heterolytic cleavage of the radical cation to form both an aminoradical and iminium ion (**Figure 1.16**).[63] This fragmentation presumably requires the cation and radical stabilization afforded each product of bond cleavage.

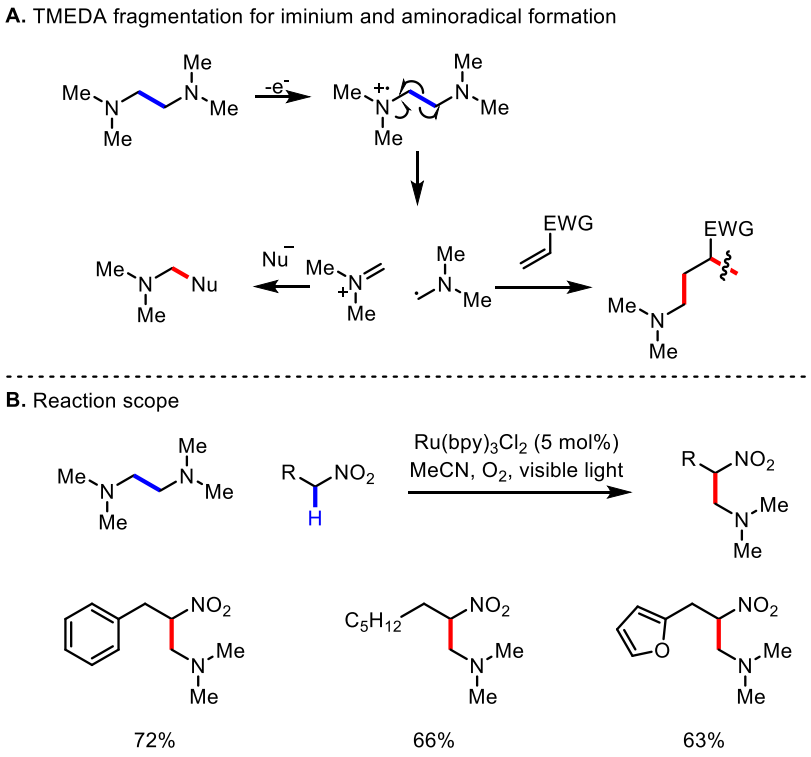

Figure 1.16 Carbon-carbon bond fragmentation of TMEDA

A further, more general approach to C–C bond fragmentation with photoredox catalysis is the single-electron oxidation of electron-rich carboxylates. The first example of this work was published by MacMillan and coworkers, and showcased the decarboxylation of amino acids to perform decarboxylative α-arylations of amines (**Fig. 1.17**).[64] As in the previous cases mentioned above, C–C bond cleavage is selective, however, for this chemistry oxidation most likely occurs on the carboxylate anion, resulting in complete regioselectivity for the reaction. Loss of CO_2 is entropically favored, and the products are produced in high yields.

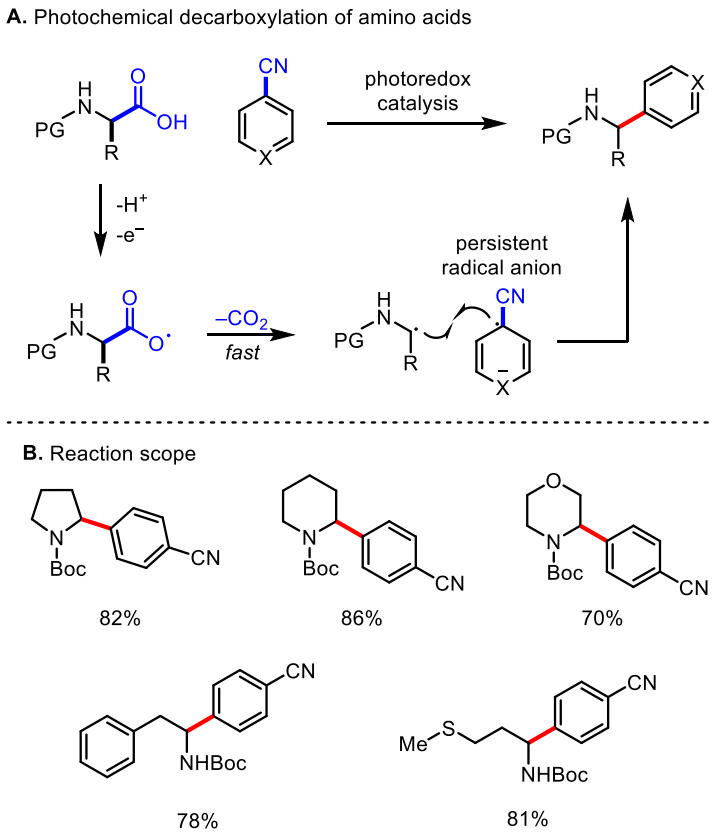

Figure 1.17 Decarboxylative α-arylation of amino acids

Conclusions and Future Prospects

The current state of research for photoredox catalysis is one of innovation and progress. While initial forays into this chemistry have been met with impressive returns for improved synthetic protocols, a thorough understanding of important mechanistic aspects has been developed. A wide array of tools which are used to study and apply these reactions have become common, including the measurement of quenching rates, redox potentials, quantum yield, and solution absorption spectra. Furthermore, flow processing techniques are slowly becoming adopted by industry, and promise to bring photoredox catalysis into the forefront of scalability and practicality for pharmaceutical manufacture. As the field progresses, the increased demand for green chemical processes, combined with a desire to expand the horizons of visible-light mediated processes, will likely result in additional developments in a few key areas.

Firstly, the use of organic dyes as photoredox catalysts has become an increasingly robust area of research. As the properties which dictate their behavior in solution become more and more well understood, the application of these dyes has expanded to the point of real possibility for pharmaceutical manufacture. While well-understood photochemical reactions can often be optimized to the point of minimal loadings of transition-metal catalyst, organic dyes may eventually act as a complete photosensitizer solution. However, the robust nature of iridium and ruthenium based catalysts remains a reliable staple of photoredox methodology, and further improvements to organic-dye photophysical properties will need to be made to address some of these issues. For example, eosin Y, fluorescein, and rose bengal each act as popular staples of the organic-dye photoredox literature; however, these dyes possess anionic functionalities which both complicate solvent selection and limit their utility in acidic media. Some more strongly-reducing, neutral photosensitizers have been reported in the literature; however, the most strongly reducing of these species requires near-UV irradiation, and also possesses utility in a limited pH range. Further developments in this area of research will be essential for a complete replacement of transition-metal based catalysts.

Another trend which is in focus is the use of first-row transition metals in place of the more-precious and less abundant iridium and ruthenium based complexes. In the design of transition metal photoactive complexes for organic synthesis, the toxicity, cost, and availability of the metal center are important factors. For photoredox methodologies to become more generally viable, the catalysts used must be readily available, non-toxic and relatively inexpensive, which has sparked interest in the use of first-row transition metals. The synthetic utility of these catalysts relies almost entirely upon their photophysical properties. In order for a chemical transformation (e.g. single-electron or energy transfer) to take place, contact must be made

between the photocatalyst in its excited state and a substrate of interest. Thus, the excited state lifetime of the complex and the efficiency with which the excited state is reached are key metrics in the design and choice of photocatalyst.

The factors that govern excited state lifetimes and electron transfer rates have largely been explained by energy gap law, which states that MLCT excited state lifetimes are dictated by the size of the energy gap between the excited and ground states, the degree of structural rigidity, and the extent of ligand delocalization of the excited electron.[65] Widely used heavy transition metal catalysts such as $Ru(bpy)_3^{2+}$ and $Ir(ppy)_2(dtbbpy)^+$ possess excited state lifetimes (τ) of 1100 ns and 550 ns, respectively (**Figure 1.18**).[2] Conversely, the excited state lifetimes of period 4 transition metals are generally much shorter, often hampering reaction efficiency. First row transition metals inherently have weaker $t_{2g} - e_g$ splitting (Δ_o), which in turn results in a smaller energy gap between the excited and ground states. For example, iron's weak ligand field prevents the population of a long lived ^{3}MLCT state, and instead populates a relatively low-energy and short lived ligand field state.[66] $Fe(bpy)_3^{2+}$ has an excited state lifetime of 810 ps,[67] and metalloporphyrins of magnesium and zinc display lifetimes ranging from 31 ps down to 8 ps.[68]

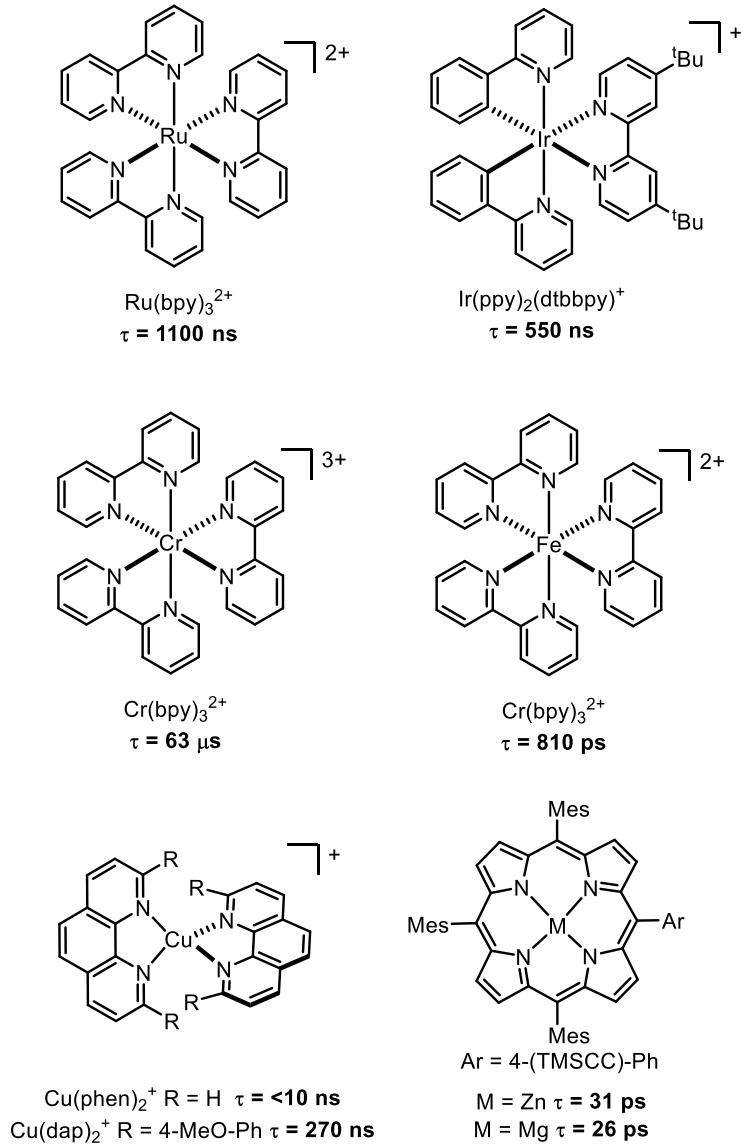

Figure 1.18 Excited-state lifetimes of first-row transition metal complexes

Excited state lifetimes can be altered through ligand tuning, and as such there are exceptions to the generalizations made about the first row transition metals. For example, while copper (I) bisphenanthroline [$Cu(phen)_2^+$] has an excited state lifetime of <10 ns,[69] $Cu(dap)_2^+$ (dap = 2,9-bis(*para*-anisyl)-1,10-phenanthroline) has an excited state lifetime of 270 ns and has been shown to effectively catalyze organic transformations.[70] It is worth noting that these complexes perform poorly in the presence of coordinating solvents and Lewis bases, which through coordination to

the Cu(II) center increase the non-radiative decay rate constant and shorten the excited state lifetime.[4] Additionally, the Cu(I) and Cu(II) oxidation states are structurally distinct, allowing for ligand sterics to bias oxidation state energetics.

Chromium-centered diimine complexes are another class of transition metal catalysts with long excited state lifetimes. $Cr(bpy)_3^{3+}$ is reported to display an incredibly long excited state lifetime of 63 μs, while its 1,10-phenanthroline analog $Cr(phen)_3^{3+}$ boasts an excited state lifetime of 360 μs.[71] The ($*Cr^{3+}/Cr^{2+}$) redox couple is more strongly oxidizing ($*E° = + 1.19$ V vs. SCE)[72] than the corresponding ($*Ru^{2+}/Ru^{+}$) couple ($*E° = + 0.84$ V vs. SCE);[73] however, the ground state redox couple (Cr^{2+}/Cr^{3+}) is reported to be only –0.26V, preventing the catalyst from acting as an efficient reductant.[71]

While longer excited state lifetimes are typically necessary for bimolecular electron transfer processes to outcompete decay pathways, this is not always the case. It has been shown that interfacial electron transfer to semiconductors such as TiO_2 can occur at 'ultrafast' rates that are competitive with any non-radiative decay to the ground state.[65] However, it remains to be concluded whether the passage of an electron from sensitizer to semiconductor in these systems represents an actual electron transfer reaction or a direct optical excitation.

Currently, the most synthetically useful photocatalysts are those with photophysical properties and electronic behavior which are well characterized. Ruthenium and iridium based photocatalysts remain ubiquitous in the literature despite their increased cost; this is a direct result of their superior photophysical properties and the breadth of literature precedent to date. Increased efficiency is needed for first-row transition metals to compete with the efficacy of these heavier, more expensive metals, but this is a barrier which may be overcome through further study.

Chapter 2: Synthesis of (–)-pseudotabersonine, (+)-coronaridine, and (–)-pseudovincadifformine

*Portions of this chapter have been published in 1) Beatty, J. W.; Stephenson, C. R. J. Amine functionalization via oxidative photoredox catalysis: Methodology development and complex molecule synthesis. *Acc. Chem. Res.* **2015**, *48*, 1474. 2) Beatty, J. W.; Stephenson, C. R. J. Synthesis of (–)-pseudotabersonine, (–)-pseudovincadifformine, and (+)-coronaridine enabled by photoredox catalysis in flow. *J. Am. Chem. Soc.* **2014**, *136*, 10270–10273.

Introduction:

Vinblastine and vincristine are bisindole alkaloids which are isolated from the leaves, roots, and stems of the plant *Catharanthus roseus*, found throughout North America.[74] These alkaloids hold global significance, as their chemotherapeutic properties have resulted in their clinical use in the treatment of both leukemia and non-Hodgkin's lymphoma; vinblastine is on the World Health Organization's "Model List of Essential Medicines,"[75] and a number of structurally related derivatives of these natural products have been studied extensively (**Fig. 2.1**).[76] These natural products are co-isolated with a number of other complex indole alkaloids, most significantly the more-abundant biosynthetic precursors of vinblastine, namely vindoline and catharanthine **13**. Despite the limited quantities of vinblastine which are available through isolation, the entirety of its clinical demand can be met through isolation from the plant source.[77]

Cell cultures of *Catharanthus roseus* can be engineered to contain up to ng L^{-1} quantities of the bisindole chemotherapeutic agents, while conversely catharanthine can be isolated in 50-100 mg L^{-1} quantities.[78]

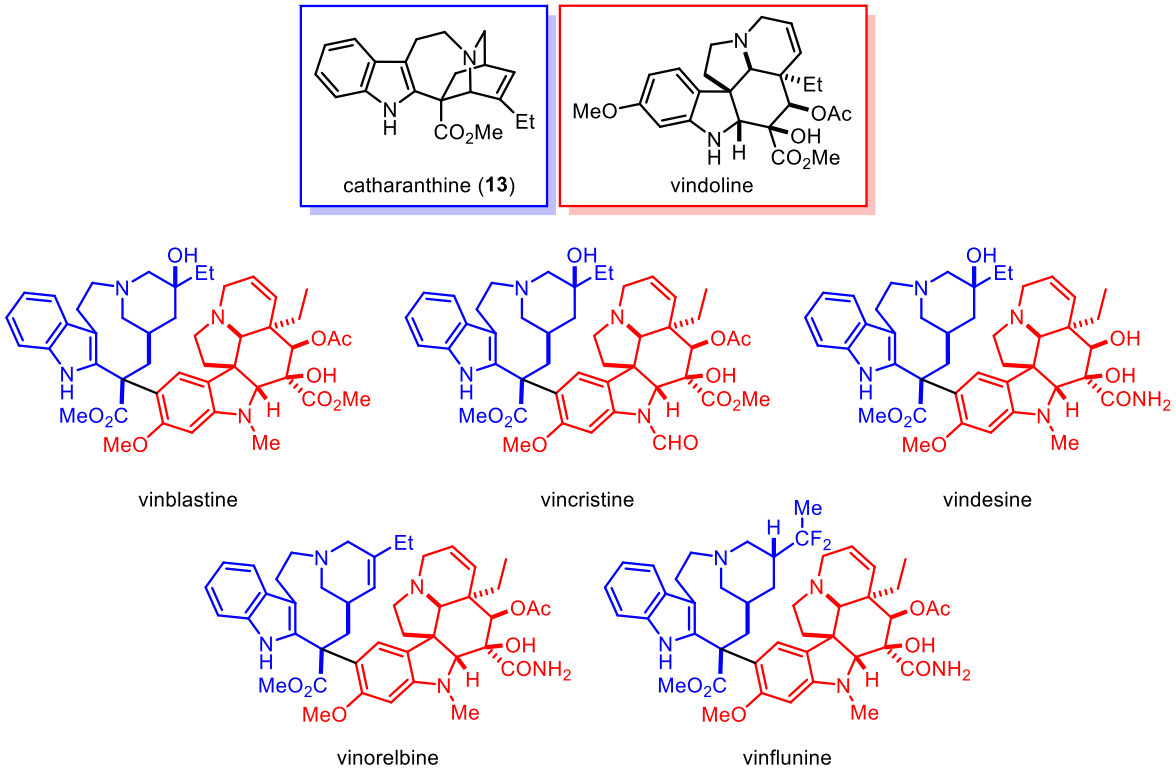

Figure 2.1 Chemotherapeutic bisindole alkaloids derived from catharanthine and vindoline

History of Catharanthine Fragmentation

As a consequence of the abundance of vindoline and catharanthine, coupled with the high importance of vinblastine and vincristine to clinical medicine, a number of efforts have been devoted to the total or semi-synthesis of vinblastine proceeding through these intermediates. Synthetic efforts towards the bisindole alkaloids in **Figure 2.1** are easily rationalized. Keuhne writes that "*[Vinblastine] and [vincristine] are said to be present in only minute amounts in Catharanthus roseus (L.) G . Don* ***(0.00025% of leaf dry weight)****, and their separation from*

other monomeric or binary alkaloids involves a complicated and tedious procedure based on their differential basicity followed by chromatography. Industrial production of [vinblastine] and [vincristine] has therefore been a serious problem, and consequently these drugs are among the most expensive on the pharmaceutical market."[79] As a consequence of these factors, various strategies for the synthesis of vinblastine have arisen, with key methodological focus on the formation of the key single bond connecting the two alkaloid subunits. Catharanthine itself possesses minimal biological activity,[80] and displays one-thousandth of the activity of either vinblastine or vincristine as an antimitotic agent.[81]

Biosynthetically, the production of vinblastine and structurally related natural products arises from an initial Pictet-Spengler reaction between tryptamine and secologanin (**Fig. 2.2**).[78] Plant feeding studies have confirmed the biosynthetic involvement of secologanin, and the resulting glucoside undergoes a series of rearrangements, likely proceeding through the natural products geissoschizine and stemmadenine. The common intermediate dehydrosecodine is postulated to undergo divergent Diels-Alder reaction pathways to form either catharanthine or the natural product tabersonine. Tabersonine possesses the key carbon framework present in vindoline, which is subsequently produced upon further oxygenation.

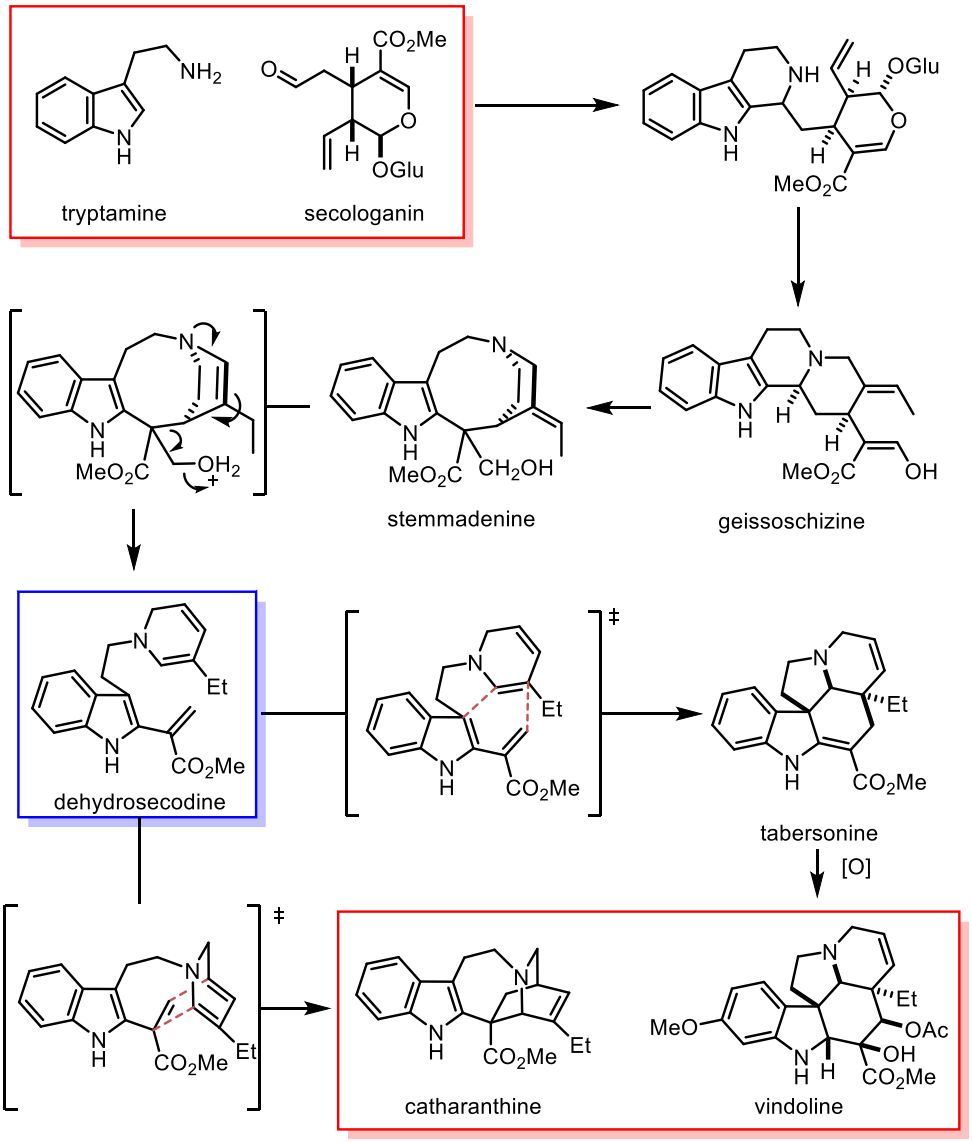

Figure 2.2 Divergent biosynthetic pathways for catharanthine and vindoline

The co-isolation of vindoline and catharanthine with vinblastine led to the proposal that the bisindole alkaloid was produced through a fragmentation and coupling of catharanthine with vindoline. Langlois and Potier were the first to demonstrate this reactivity was feasible through the use of a Polonovski-type fragmentation (later dubbed the Potier-Polonovski reaction) of the *N*-oxide of catharanthine in the presence of vindoline. (**Fig. 2.3**)[82] Although a number of two-step procedures for this coupling had previously been developed, this was the first laboratory

synthesis of vinblastine as all previous methods obtained the incorrect stereochemical outcome at the benzylic quaternary stereocenter. Later work, pioneered by Kutney[83] and improved by Boger,[77] has demonstrated that this type of oxidative coupling can be accomplished directly through the use of Fe(III) chloride in super-stoichiometric quantities.

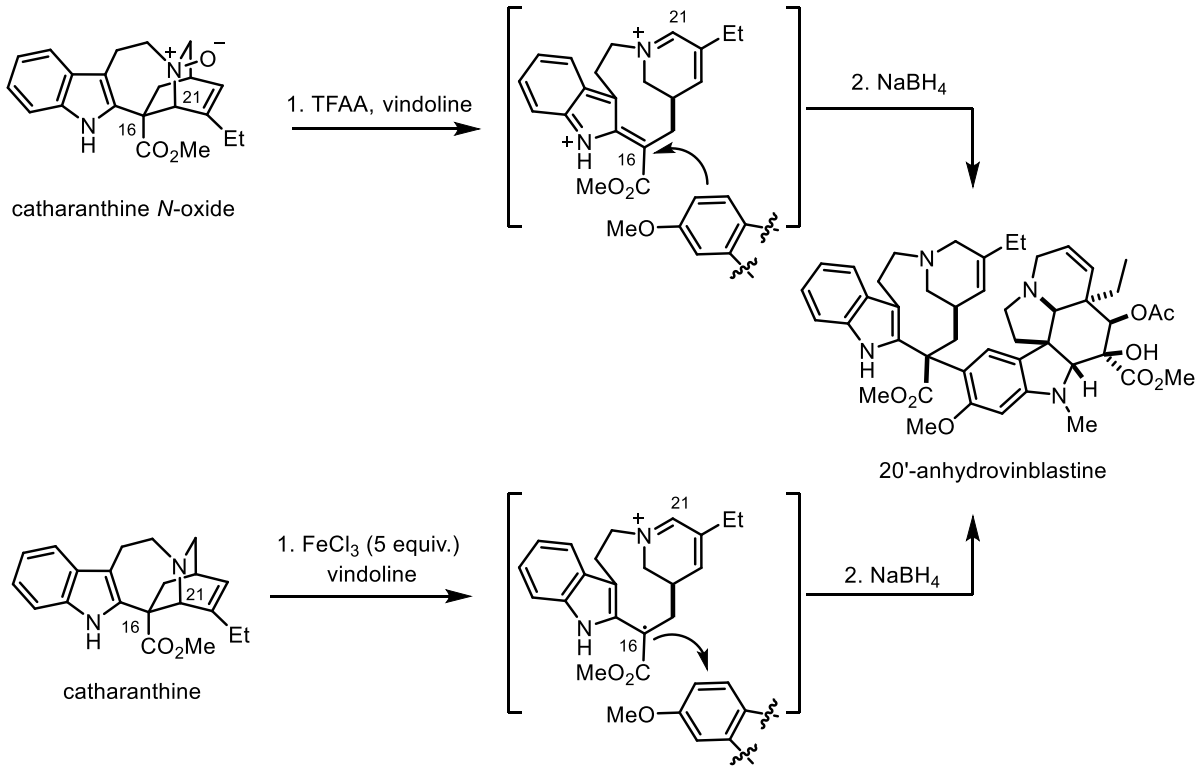

Figure 2.3 Biomimetic couplings of catharanthine and vindoline

This latter process is likely more reminiscent of the biosynthetic origin of vinblastine, and proceeds in high yields *via* proposed single-electron transfer mechanism. Specifically, the radical cation of catharanthine ($E_{1/2}^{ox}$ = +0.60 V vs. SCE in MeOH)[84] is formed upon single electron oxidation. This species can be drawn in two forms, with the radical cation localized on either the indole ring or localized on the nitrogen lone pair. The latter is reminiscent of the cyclopropylaniline fragmentation chemistry of Zheng,[57] and C16–C21 bond fragmentation can proceed directly through a β-scission even to form a ring-opened distonic radical cation. The

benzylic radical of this intermediate is capable of addition to the electron-rich 5-position of the aromatic ring of vindoline, which upon oxidative rearomatization followed by a sodium borohydride quench forms the natural product precursor 20'-anhydrovinblastine.

Aside from the oxidative strategies for catharanthine's coupling to vindoline, there are a number of reports of alternative strategies to accomplish this bond cleavage process, including electrochemical oxidation, as well as simple chemical oxidation or reduction. Furthermore there are a number of acid-mediated strategies that provide significant insight into the reactivity of the catharanthine scaffold. Tabakovic and coworkers have reported the electrochemical oxidation of catharanthine using a glassy carbon electrode in methanol in high yield (**Fig. 2.4**).[84] This chemistry presumably proceeds through a similar azafulvalene intermediate as that proposed for the Potier-Polonovski fragmentation. Similar results from Sundberg resulted in the isolation of a ring-opened methoxy aminal in much lower yield, an artifact of the poor stability of the aminal product.[85] These two examples demonstrate the generality of oxidative functionalization at the benzylic 2-position of the indole substrate.

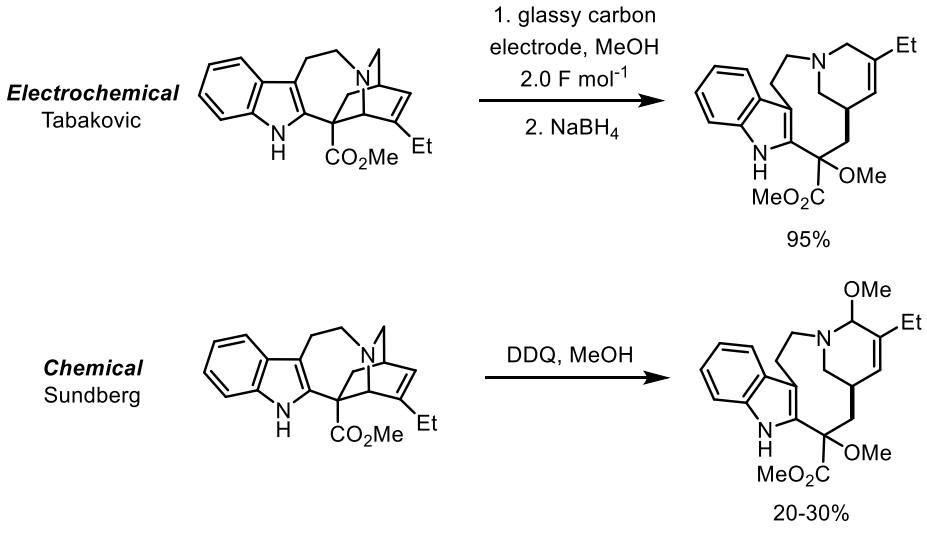

Figure 2.4 Oxidative strategies for catharanthine fragmentation

Alternative methods for catharanthine fragmentation consist of either acid or redox-promoted fragmentation of catharanthine to form cleavamine-type products with alternative functionalization at the benzylic 2-position. Specifically, Kutney and coworkers have developed a net-reductive fragmentation of catharanthine using zinc dust in neat acetic acid (**Figure 2.5**).[86] This reaction is thought to proceed via initial protonation of the indole 3-position of catharanthine, followed by a retro-Mannich ring opening to form the dihydropyridinium intermediate. Isomerization to rearomatize the indole ring and 4 e^- reduction of the pyridinium with zinc provides the ring-opened carbomethoxy dihydrocleavamine in 23% yield.

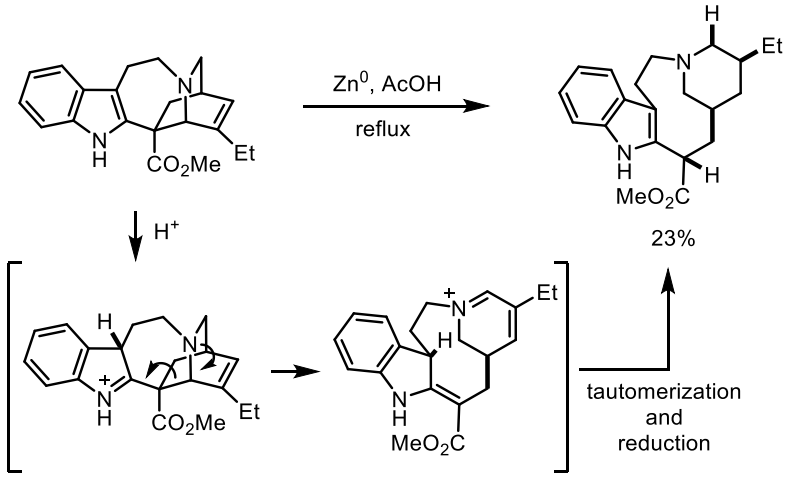

Figure 2.5 Reductive fragmentation of catharanthine

Pioneering photochemical studies by Sundberg demonstrated the feasibility of catharanthine fragmentation using a number of photosensitizers using both UV and visible light.[87] While no yields were reported in their initial communication, the concept was nevertheless demonstrated that a redox-neutral fragmentation of catharanthine is possible under photochemical conditions. Furthermore, the authors identified the essential combination of trimethylsilyl cyanide and methanol, which was later used by Ferroud and coworkers.[88]

A final examination of catharanthine fragmentation reactivity is in the realm of high-temperature acid-promoted isomerization. In the mid 1960's Gormann, Neuss, and Cone reported the acid-mediated rearrangement of catharanthine and dihydrocatharanthine to indoline-type products (**Fig. 2.6**).[89] Specifically, upon heating a solution of 5.5 grams of catharanthine in glacial acetic acid for 16 hours resulted in a mixture of rearranged products containing the isomerized vinylogous carbamate of type **13**. Subsequent reports by Brown investigated this transformation, of which the products had since been identified as tabersonine **13** and pseudotabersonine **14**.[90] It should be noted that the literature contains multiple names for these materials, wherein pseudotabersonine (also written Ψ-tabersonine) is also called pseudocatharanthine. While devoid of chiral-HPLC analysis of these transformations, the authors correctly surmised from optical rotation measurements that the pseudotabersonine produced from the rearrangement of enantiopure (–)-catharanthine in refluxing acetic acid had undergone significant enantio-erosion to produce material that had undergone roughly 90% racemization.

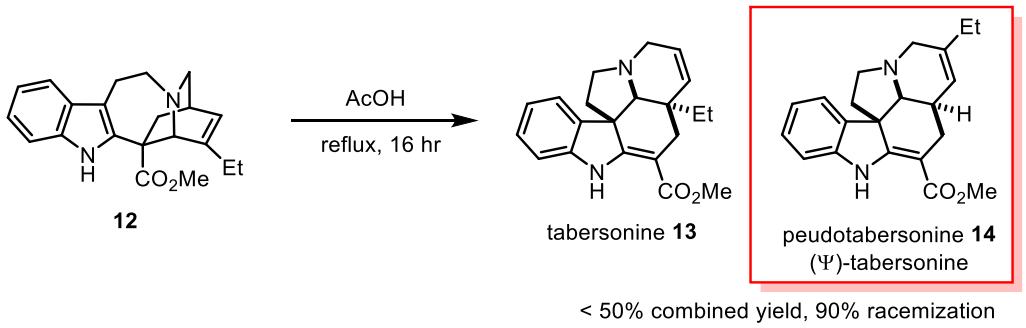

Figure 2.6 Isomerization of catharanthine to tabersonine derivatives

De Novo Syntheses of Pseudotabersonine

Aside from the isomerization of catharanthine to pseudotabersonine in this fashion, only a few total syntheses of pseudotabersonine have been reported in the literature. The first synthesis of pseudotabersonine was published by Carroll and Greico in 1993, with the goal of

testing previously proposed biosynthetic hypotheses involving the intermediacy of dehydrosecodine.[91] The synthesis commences from oxindole (**Fig. 2.7**), with a rapid 5-step sequence to access a spirocyclic intermediate capable of fragmenting to form dehydrosecodine transiently in the reaction solution. The synthesis was completed in a final 3 steps due to difficulties oxidizing the formyl group to the methyl ester in the natural product.

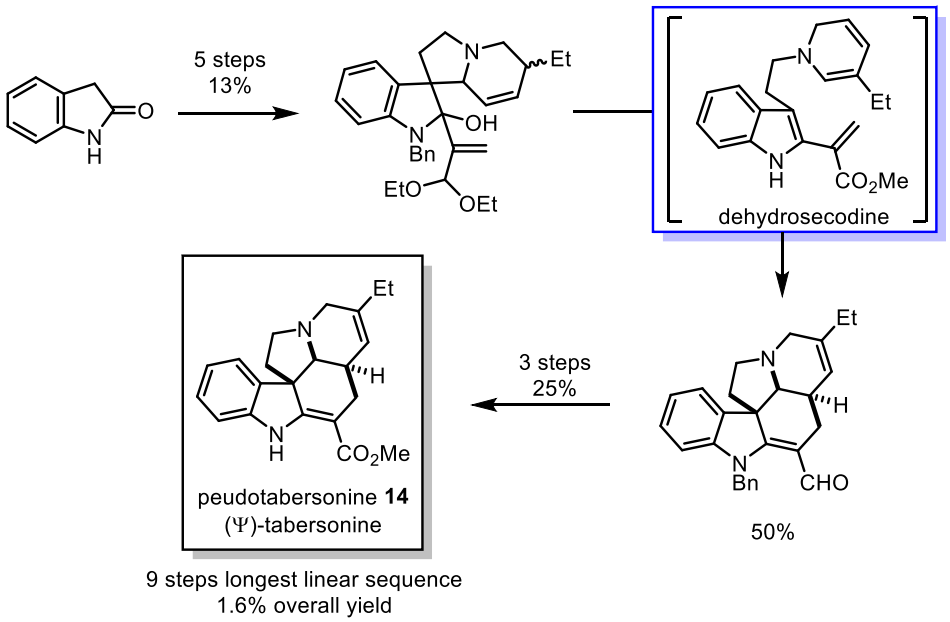

Figure 2.7 Greico's total synthesis of (±)-pseudotabersonine

More recently the Martin lab reported the total synthesis of pseudotabersonine through a ring-closing metathesis cascade strategy (**Figure 2.8**).[92] This synthesis provided the natural product in racemic form in 11 steps and 5% overall yield, and also provided the diastereomer, 14-*epi*-pseudotabersonine (not shown) in 8% overall yield.

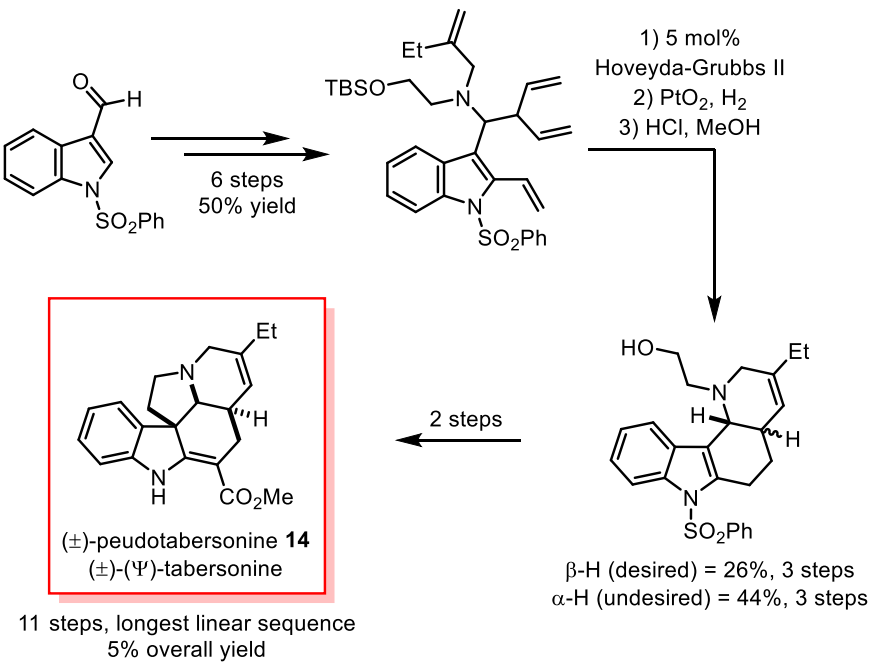

Figure 2.8 Martin's total synthesis of (±)-pseudotabersonine

Fragmentation of catharanthine using photoredox catalysis

Optimization of Catharanthine Fragmentation in Batch

The precedent concerning catharanthine fragmentation, particularly under photolytic conditions, inspired us to investigate this transformation using photoredox catalysis. Particularly, the investigation of this fragmentation process provided what we identified as significant opportunity to investigate the factors which contribute to C–C functionalization of amines as opposed to the more common and ubiquitous α-amine C–H functionalization. Due to the commercial importance of vinblastine and vincristine, catharanthine is available for purchase in multi-gram quantities, and the tartrate salt was purchased initially in 5 gram quantities at roughly $80/gram. As the oxidation of catharanthine is more feasible from the corresponding free-base ($E_{ox}^{1/2}$ = 0.60 V vs. SCE in MeCN),[84] this complex starting material was subjected to basic workup before direct utilization of the free amine. The free base of catharanthine is

unfortunately unstable to extended exposure to ambient conditions. Even when stored in the freezer the amorphous white solid slowly colorizes into various brown decomposition products. As such, it was prudent to store the starting material as the tartrate salt, and a pre-treatment workup of the material with base was performed before each use.

The solvent and nucleophile combination reported by Sundberg was found to be optimal for this chemistry, and provided the aminonitrile **15** (**Table 2.1**).[87] Usage of potassium cyanide (KCN) or sodium cyanide (NaCN) in place of TMSCN resulted in longer reaction times with lower yields, with the reaction profile being further complicated by the limited solubility of the cyanide salt. Improved results were obtained through grinding solid KCN in a mortar and pestle before use; however, TMSCN remained the optimal nucleophile. A screening of polypyridyl metal photocatalysts revealed that the polyfluorinated photocatalyst $Ir(dF(CF_3)ppy)(dtbbpy)PF_6$ performed best, although our understanding of why this catalyst was the optimal choice remains empirical (**Table 2.1**). Optimization reactions were performed on 0.1 mmol scale in 1 ml of MeOH. The optimized result provided the desired ring-opened product as a single diastereomer in 93% yield after 3 hours. If the reaction was left to run longer than three hours, or if the reaction temperature was allowed to get too high (due to closer than optimal light source placement) a white solid crashed out of solution. This white solid was found to be product, and subsequently it was found that recrystallization from methanol provided the purest form of product material. Basic workup provided material that was >90% pure by NMR, but possessed yellow impurities that are presumably caused by catalyst contamination. Purification could also be performed using column chromatography to recover roughly 70-80% of the crude material; it is likely that the sub-optimal recovery of material from column chromatography is a result of material instability to silica gel, as TLC analysis of the reaction mixture often provided an array

of product spots more in keeping with decomposition than the crude HNMR of the reaction. Control reactions excluding light (**Table 2.1**, entry 4) and photocatalyst (entry 5) provided no conversion of starting material.

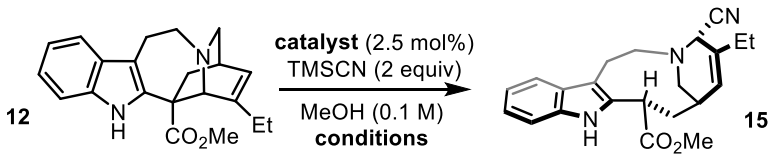

Entry	Photocatalyst	Conditions	Yield
1	$Ru(bpy)_3Cl_2$	blue LEDs	83%
2	$Ir(ppy)_2(dtbbpy)PF_6$	blue LEDs	80%
3	$Ir(dF(CF_3)ppy)_2(dtbbpy)PF_6$	blue LEDs	93%
4	$Ir(dF(CF_3)ppy)_2(dtbbpy)PF_6$	no light	N.R.
5	none	blue LEDs	N.R.

Table 2.1 Catalyst screen for catharanthine fragmentation

Mechanistically, this fragmentation process is thought to proceed through direct oxidation of catharanthine through reductive quenching of the photocatalyst excited state to form the catharanthine radical cation (**Fig. 2.9**). The catharanthine radical cation is known to undergo facile fragmentation (*vide supra*) to provide the ring-opened distonic radical cation **17**. Subsequent nucleophilic trapping of this intermediate is thought to precede single-electron reduction of the subsequent amino-nitrile **18** at the benzylic position, followed by diastereoselective protonation to yield the ring-opened product **15**. This proposed order of steps is partially based upon the finding that when the reaction was run without TMSCN, unreacted starting material was recovered in excellent condition. As it is expected that the cyanide anion is innocent during the fragmentation event itself, it likely serves as a trap for ring-opened material, which would otherwise be capable of efficiently reverting to catharanthine.

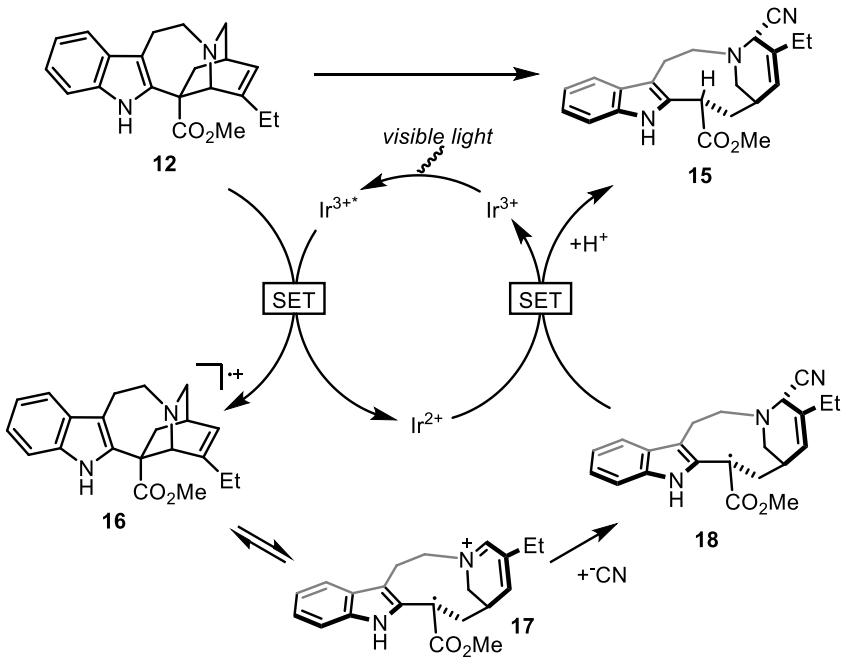

Figure 2.9 Mechanistic considerations for catharanthine fragmentation

An additional consideration for the fragmentation mechanism is the possibility of oxidation on a moiety other than nitrogen. Boger and coworkers have published impressive studies on tetrahydrocarbazole derivatives such as **19** (**Figure 2.10**), which can undergo benzylic functionalization in the presence of $FeCl_3$, mimicking the fragmentation/coupling conditions which they had previously applied to catharanthine and vindoline.[93] This is suggestive of an oxidation of the indole itself, wherein the fragmentation of the radical cation occurs in a two-electron push from the isoquinuclidine nitrogen. Ultimately, the oxidation of catharanthine could occur on either of these positions, as each provides an identical intermediate upon C16–C21 fragmentation.

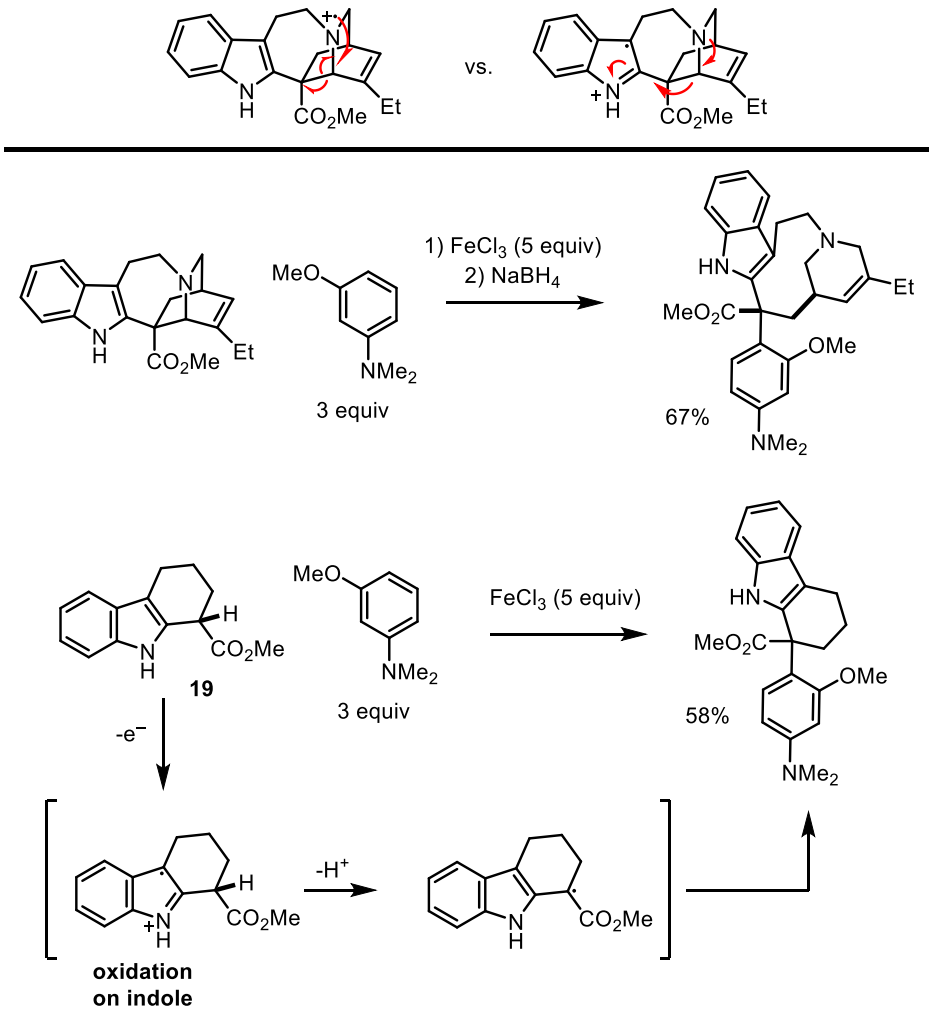

Figure 2.10 Competing sites of oxidation on catharanthine

Catharanthine Fragmentation in Flow

In order to investigate further synthetic utility of the fragmentation product, we began to consider alternatives for scale-up other than batch reactivity. While the limits of batch scalability for this process were never tested, we turned to testing the reaction in flow with the aim of improving material throughput.[94] On hand we had a 1.34 ml internal volume flow reactor (**Fig. 2.11**), which consisted of three glass test tubes wrapped with 0.76 mm internal diameter PFE tubing. Using a 34 W blue LED wafer connected to a heat sink, investigation of flow

conditions began with determining suitable residence time for the reaction. Beginning with long residence times to ensure conversion (42 minutes), the flow rate of the reaction was incrementally increased until incomplete conversion was observed for a single run. This was observed at a 1.5 minute residence time, so in order to provide a small margin of error between runs the residence time was elongated to 2 minutes. On the standard 0.1 mmol scale, this results in a total reaction time of only 3.5 minutes—a dramatic improvement over the previous 3 hour time requirement—with a yield of 96% (**Fig. 2.12**). A control reaction without photocatalyst revealed that there was no background reaction when the flow apparatus was used.

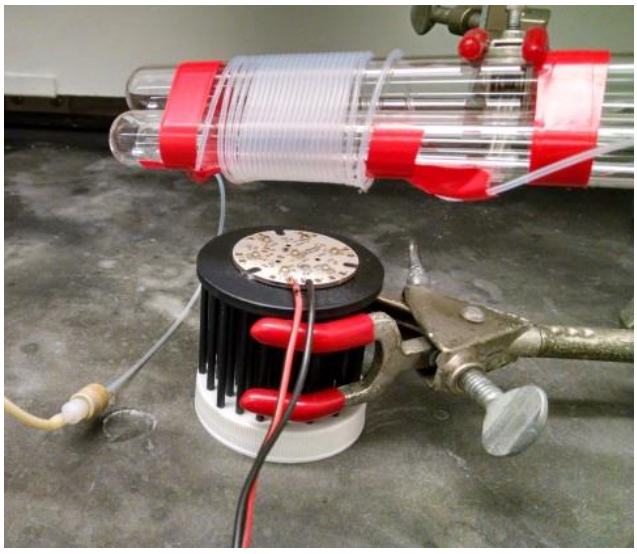

Figure 2.11 Flow reactor and puck LED

Unfortunately, the translation of these encouraging results into a readily scalable method was met with unforeseen complications. When the reaction was run for extended periods of time, crystallization of material occurred at inconsistent times ranging from 10-30 minutes into a reaction run. The back-pressure caused in this manner invariably resulted in the peristaltic pump tubing being forced off of its fitting, and un-monitored the reaction would flow onto the floor of the hood. The crystals causing these issues were again found to be product, while further

experimentation showed that alteration of solvent composition to increase product solubility was very detrimental to product yield.

Crystallization was occurring initially at the outlet of the reactor, and these crystals seeded the reactor for crystallization earlier in the reaction flow. Fortunately, this issue could be circumvented entirely through immersion of the outlet in ethyl acetate or dichloromethane. This solution was suitable to a point, but remained slightly labor-intensive, as on sufficient scale this solution needed to be monitored for crystal formation and was switched out if they were observed. A more general and scalable solution was found in the continuous inflow of dichloromethane or ethyl acetate into the reaction flow just after the irradiated portion of the tubing. This was sufficient to assist in the production of 2 grams of material in 88% yield with a total reaction time of 1.5 hours (**Fig. 2.12**).

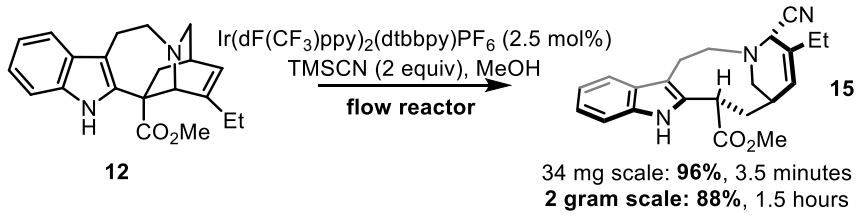

Figure 2.12 Optimized fragmentation of catharanthine in flow

Nucleophilic Diversification of the Fragmentation Product

With the capability of producing the ring-opened aminonitrile product on sufficient scale for further synthetic work, we were intrigued by the possibilities of both natural product synthesis as well as natural-product diversification, as our material closely resembled closely the upper portion of vinblastine and vincristine. These many possibilities led us to preliminarily investigate the addition of nucleophiles to the electrophilic position at C–21, which is by far the most sensitive and reactive functionality in the substrate. The goal of this work was to

investigate the reactivity of the substrate, as well as potentially evaluate structure-activity-relationships at this position.

Treatment of the α-amino nitrile with methanolic hydrochloric acid promotes ionization and formation of the dihydropyridinium ion (**Fig. 2.13**). This species is observable by HNMR, and the ionized nature of this species is supported by the sufficiently high resonance of the iminium C-H bond (δ 10.26, $CDCl_3$). Attempted malonations of this pre-activated intermediate were unsuccessful, as were similar attempts in the Friedel-Crafts reaction of 1,3,5-trimethoxybenzene and indole. An initial hit for the addition of a nucleophile to the iminium ion was found in the aza-Henry reaction through treatment of the dihydropyridinium ion with triethylamine in nitromethane. The resulting addition product was isolated by flash chromatography in 20% yield as a single diastereomer, the nucleophilic addition being presumably highly diastereoselective due to the bowl-shaped conformation of the substrate. While this material could be fully characterized, its stability at room temperature was minimal, and the material rapidly decomposed (yellow colorization upon decomposition) within one hour at room temperature.

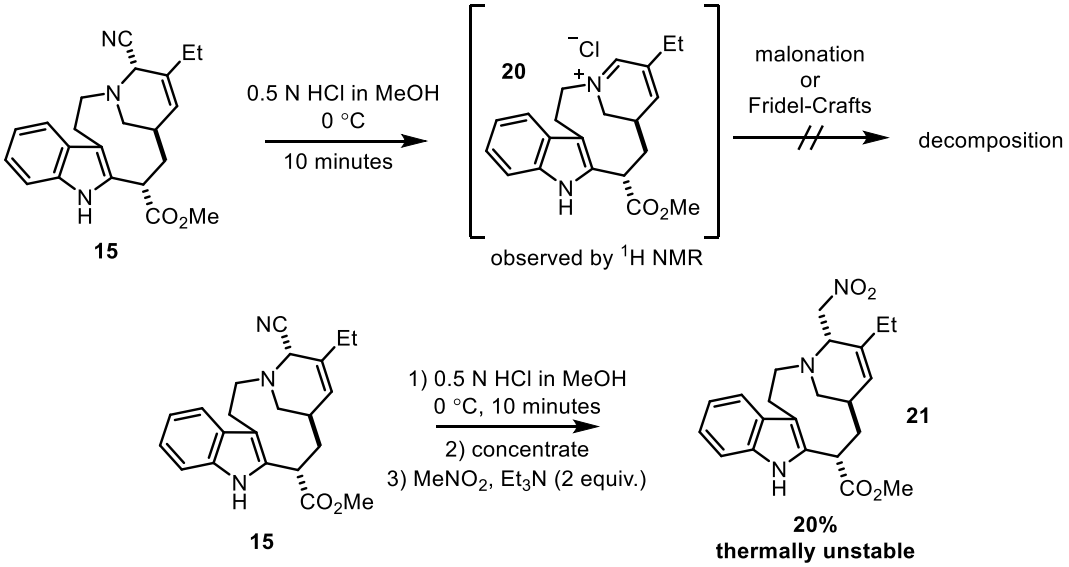

Figure 2.13 Acidic activation of the aminonitrile and nitromethane addition

The instability of this addition product combined with our failure to add similar carbon-centered nucleophiles led us to suspect that retro-addition process was actually quite facile, and we sought to investigate the addition of unstable carbon-centered nucleophiles to prevent this degradation process. Fortunately, the addition of Grignard reagents to α-amino nitriles has been well investigated, and has been named the Bruylants reaction after its discoverer.[95] Sundberg and coworkers have studied in detail the addition of nucleophiles to very similar α-β-unsaturated substrates, and found that the use of the aminonitrile substrate provided superior selectivity for 1,2 addition over 1,4 addition of nucleophiles.[96]

Our investigation into the suitability of the fragmentation product as a substrate for the Bruylants reaction progressed initially with treatment of the substrate **15** with 1 equivalent of methylmagnesium bromide at -78 degrees. This resulted in a mixture of products, with minor selectivity for the desired mono-addition product **22** over a triple-addition tertiary alcohol product (**Fig. 2.14**). This selectivity could not be suitably improved through alteration of temperature, and we turned our attention to the addition of zinc reagents to the substrate.

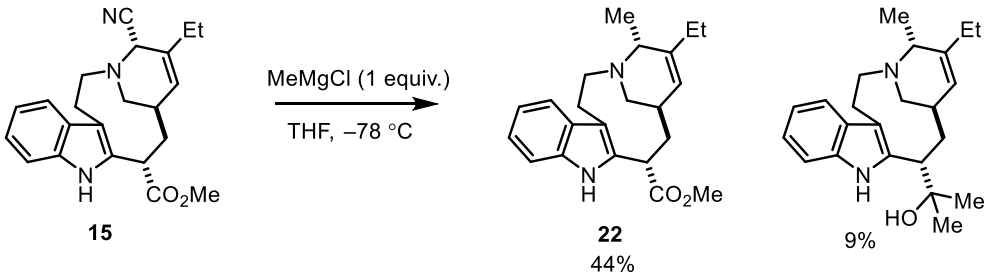

Figure 2.14 Grignard addition to the fragmentation product

The use of alkyl zinc reagents satisfactorily prevented undesired addition to the methyl ester moiety (**Table 2.2**). We found that mono-alkyl zinc reagents were slightly less efficient nucleophiles for the production of the desired alkylation products than the corresponding dialkyl

zinc reagents, and subsequently we investigated the addition of a range of dialkyl zinc nucleophiles to the substrate. These zinc reagents were formed through a number of methods; for non-commercially available versions, transmetallation from the corresponding Grignard reagents onto dry $ZnCl_2$ was effective. In many cases the Grignard was made from the corresponding aryl iodide or bromide.

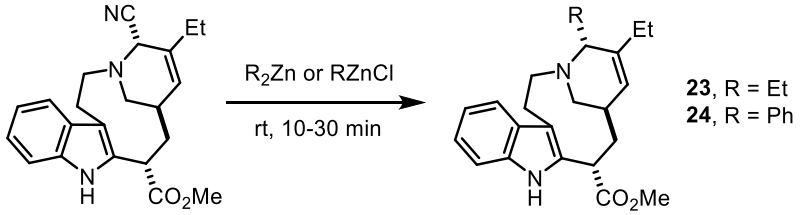

entry	reagents	equivalents	Product	% yield
1	$EtZnCl/MgCl_2$	1.1	**23**	19
2	$EtZnCl/MgCl_2$	2.0	**23**	70
3	Et_2Zn	2.0	**23**	88
4	$PhZnCl/MgX_2$	1.1	**24**	34
5	Ph_2Zn/MgX_2	2.0	**24**	63

Table 2.2 Efficacy of Monoalkylzinc vs. Dialkylzinc Reagents

The range of alkylated products produced can be found in **Figure 2.15**. This methodology was tolerant of all hybridizations of the C-centered anion, including sp, sp^2, and sp^3 hybridized nucleophiles. Unfortunately, the corresponding products were in the majority of cases found to be unusually unstable under an aerobic atmosphere at room temperature. For proper characterization, the materials had to be immediately placed under an inert atmosphere, and basified (filtered through K_2CO_3) degassed deuterated chloroform was required for minimal decomposition in the NMR tube.

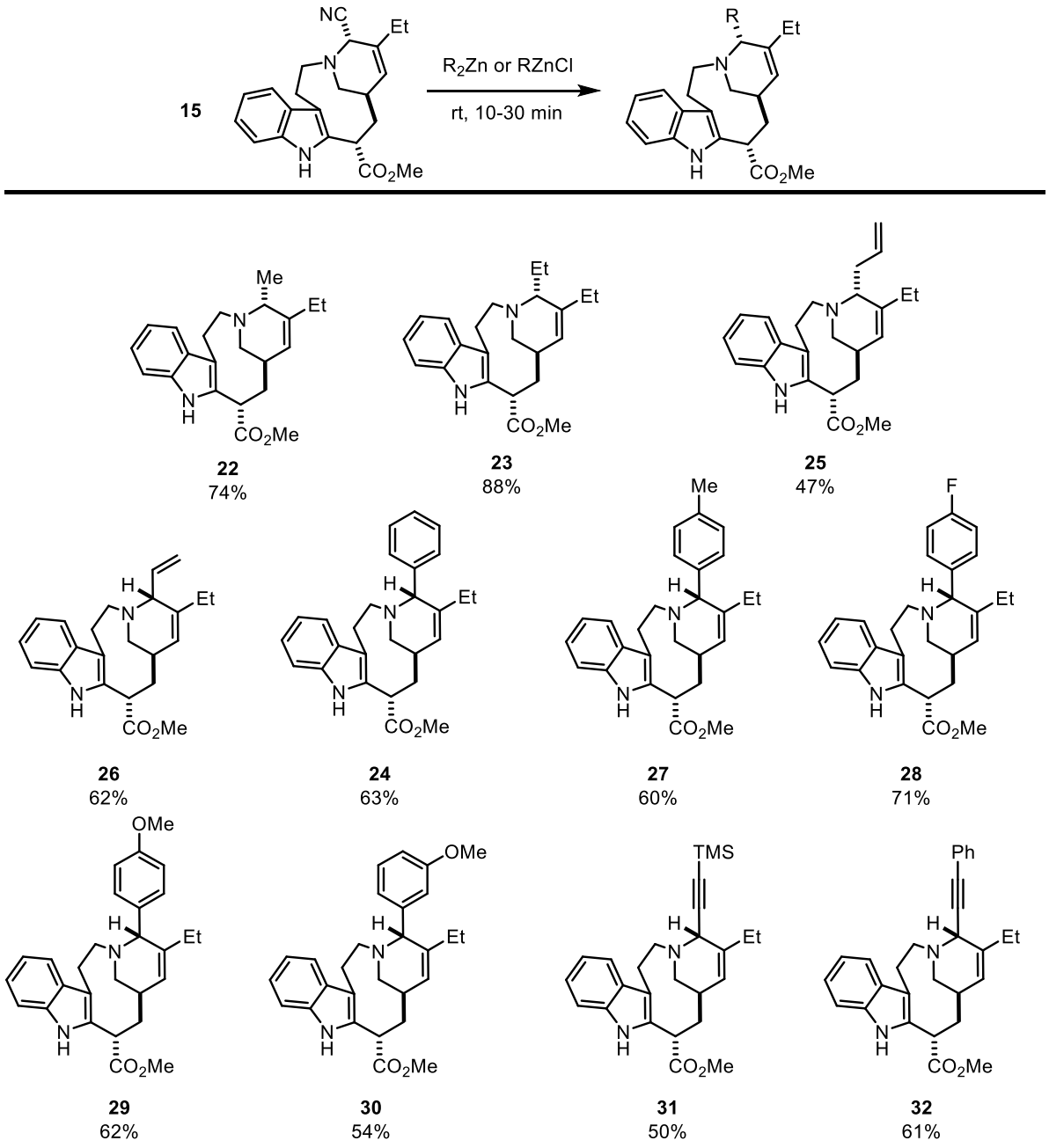

Figure 2.15 Alkylation and formation of velbanamine derivatives

While these samples were sent out to collaborators for characterization, no data was ultimately generated for their biological activity, and they were likely too unstable for subsequent utility in biological systems. Literature precedent supports this phenomenon, as the natural product anhydrovinblastine (**Fig. 2.3**, *vide supra*) is known to be highly unstable in

relation to vinblastine (**Fig. 2.1**). In the crystal structure of vinblastine,[97] a hydrogen bonding interaction is observed between the C-22 OH group and the piperidine nitrogen—a phenomenon which is likely responsible for the decreased basicity of vinblastine in relation to its dehydrated precursor.[98] This difference in basicity is almost certainly correlated with oxidation potential, and the dehydrated products are consequently more likely to be sensitive to oxidative decomposition. Anhydrovinblastine is known to be "rapidly oxidized to leurosine in air if it is not stored in an inert atmosphere, and the oxidation is even faster in solution; as much as 40% of leurosine can be obtained after only 72 hr at room temperature."[99] These impractical physical properties have prevented further study.

Semi-synthesis of Pseudotabersonine, Coronaridine, and Pseudovincadifformine

Subsequent to the production of the unstable velbanamine analogues, we turned our attention to the synthesis of indole terpene natural products which contained structural similarities to the cyanocleavamine **15** (**Fig. 2.16**). The relationship between catharanthine and tabersonine has already been mentioned; these natural products are accessed through the common biosynthetic precursor dehydrosecodine (**Fig. 2.2**). There are also other natural products which have been accessed through the acidic rearrangement of catharanthine, including pseudotabersonine (aka pseudocatharanthine, **Fig. 2.16**). The defining difference between tabersonine and pseudotabersonine is the regioisomeric placement of the ethyl group, and while the majority of alkaloids isolated from *Catharanthus roseus* possess the regioisomeric ethyl placement corresponding to that found in tabersonine, there are a large number of alkaloids which also possess the Ψ connectivity (**Fig. 2.16**).

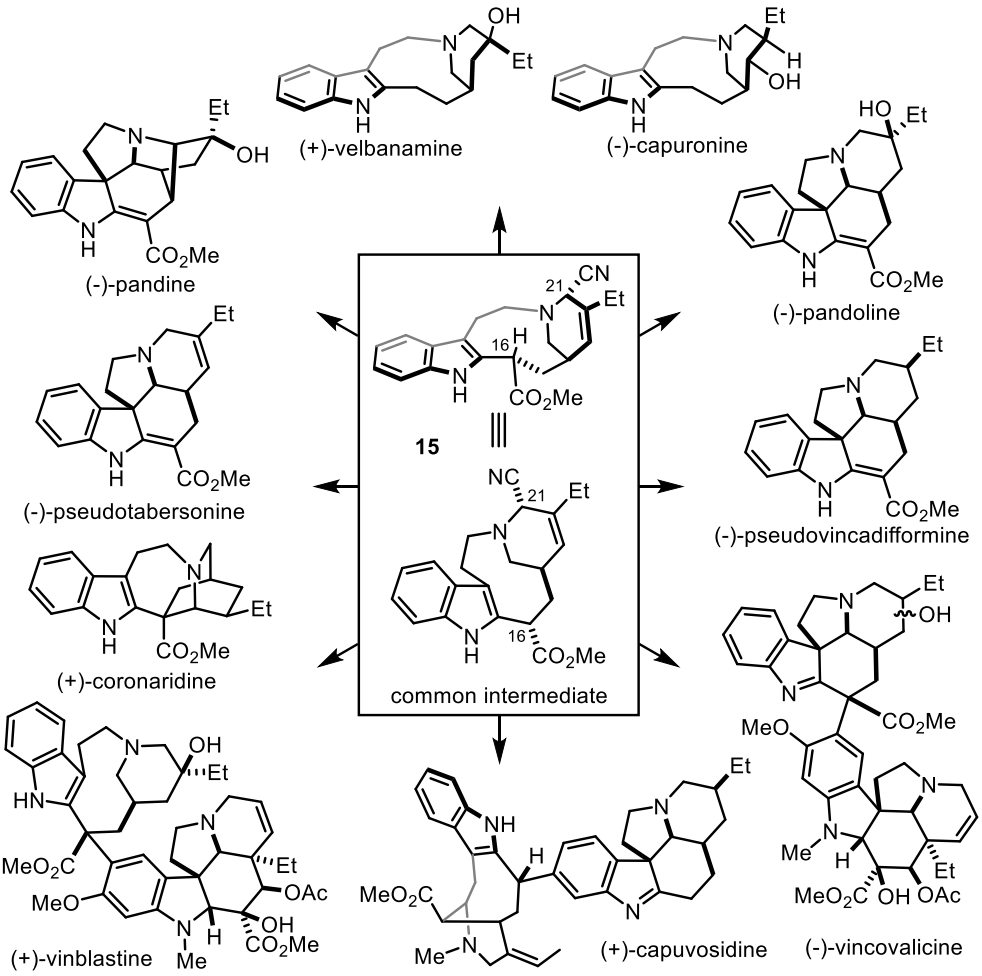

Figure 2.16 Possible natural product targets from the fragmentation product

We were specifically intrigued by the biosynthetic relationships presented in the literature between catharantine and tabersonine (the precursor of vindoline), and attempted to access tabersonine directly from the fragmentation product. In our previous studies for the nucleophilic diversification of the fragmentation product, we had found that acidic treatment of the amino nitrile produced the dihydropyridinium ion **20** (**Fig. 2.17**). We further hypothesized that heating this intermediate might promote C-C bond cleavage to provide transiently dehydrosecodine, which could undergo an intramolecular Diels-Alder cyclization to form tabersonine.

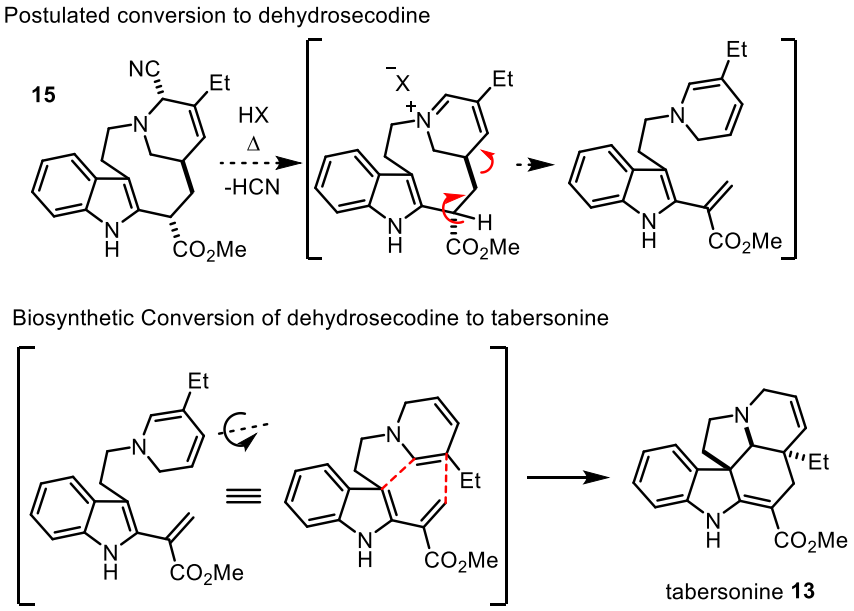

Figure 2.17 Proposed conversion of the cyanocleavamine to tabersonine

This idea was flawed for a number of reasons, one of which is that dehydrosecodine is capable of divergent Diels-Alder reactivity to produce catharanthine as well—clearly an undesired outcome. Furthermore, the proposed elimination reaction produces a planar intermediate, destroying any possibility of enantio-retention through the process. Serendipitously, upon heating the fragmentation product to reflux in toluene for one hour in the presence of a small amount of benzoic acid resulted in formation of three distinct products (**Fig. 2.18**), chief among which was the natural product pseudotabersonine isolated in 13% yield. The other two products were identified as redox disproportionation products, with the tertiary amine **33** the product of starting material reduction and the aminonitrile **34** an equivalent of product oxidation.

Optimization of this process for the formation of pseudotabersonine was accomplished through the addition of a stoichiometric amount of acid, this time in the form of trifluoroacetic acid. This was postulated to prevent intermolecular hydride transfer between substrates, as presumably the ability to donate a hydride equivalent (or even a single electron) is predicated on

the presence of sufficient electronic density (i.e. free amine). Furthermore, the low mass balance of our initial result demonstrated that decomposition was occurring, which presumably was due to oxidative decomposition as we had seen previously. Excitingly, upon changing these variables the rearrangement to pseudotabersonine proceeded efficiently in 90% yield (**Fig. 2.18B**).

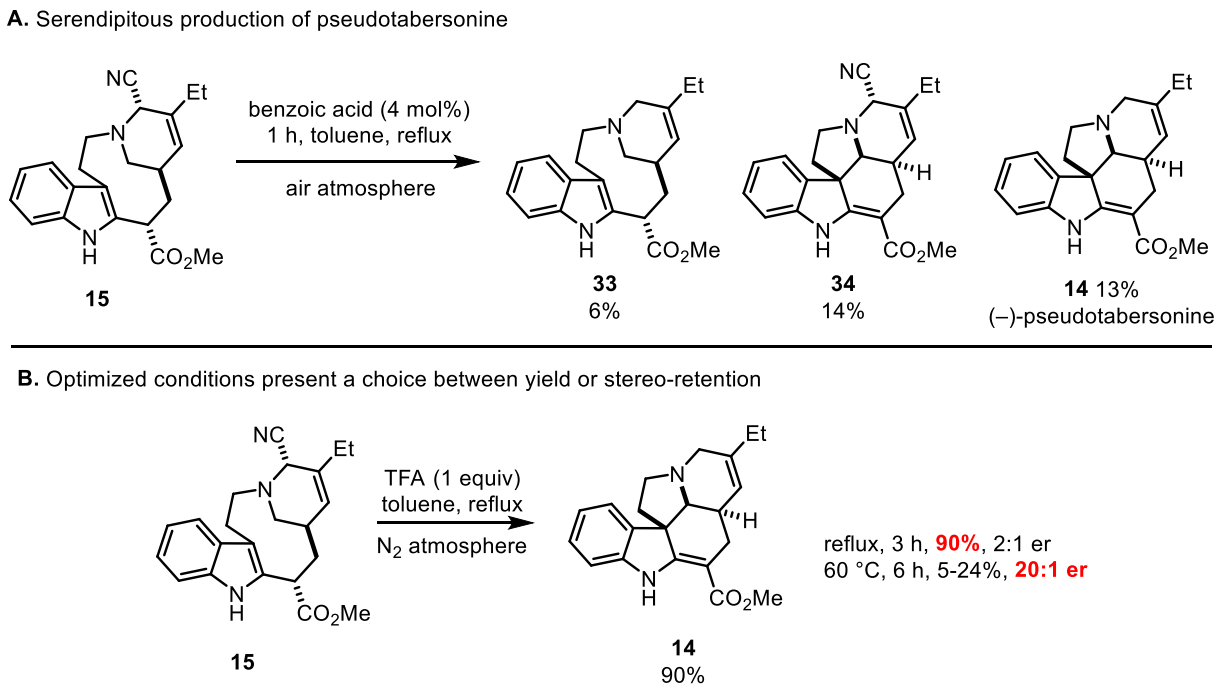

Figure 2.18 First hit and optimized conditions for the pseudotabersonine rearrangement

Unfortunately the material produced had a low optical rotation, and upon chiral HPLC analysis we determined the reaction to proceed in only 2:1 er. Further experimentation with temperature demonstrated that the enantiopurity of the reaction could be improved through lowering temperature; however, while this resulted in a 20:1 er, the reaction yields were inconsistent and low (5-24%, **Fig. 2.18B**). While an opportunity for further optimization of this process presents itself in the form of chiral anion catalysis, we foresee the ease of execution of such a process to be unlikely due to the high-temperatures required for the rearrangement.

Mechanistically, the rearrangement is thought to begin with dihydropyridinium ion formation (**Fig. 2.19**), followed by iminium isomerization to the internal position before transannular cyclization of the indole onto the newly-formed iminium ion. This mechanism satisfies a number of experimental observations, as both postulated iminium ion intermediates are capable of undergoing epimerization at the methine ring juncture. This stereocenter is thought to be stereocontrolling for the entire transformation, as all other stereocenters in the starting material are destroyed in the process.

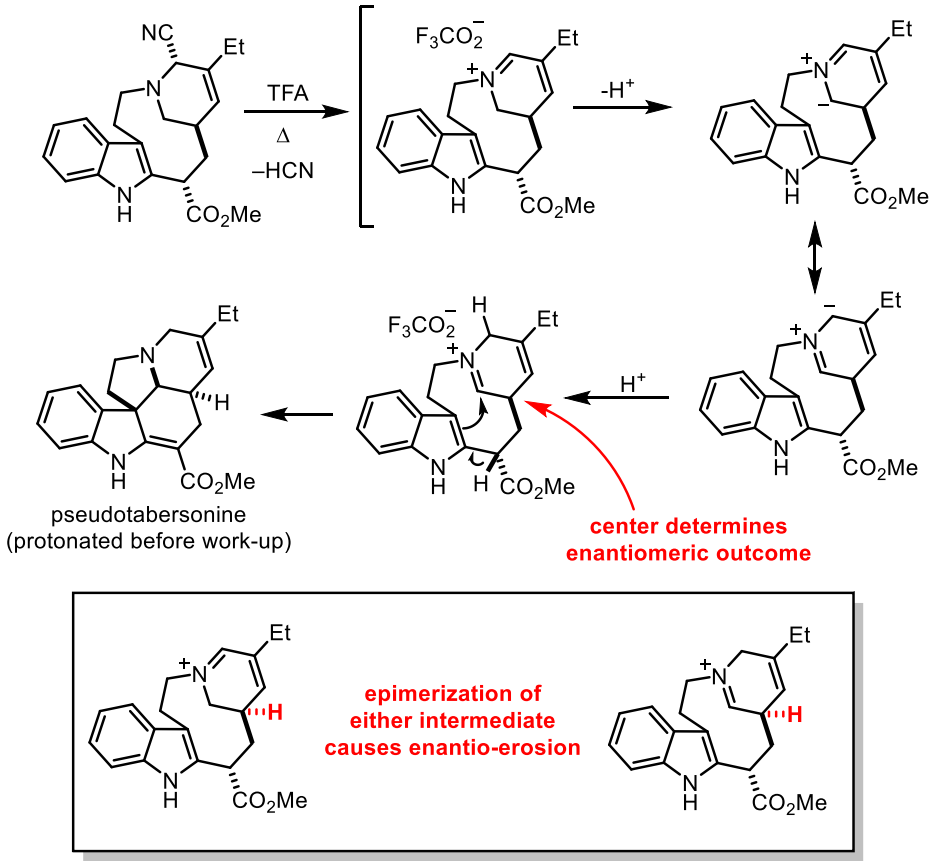

Figure 2.19 Mechanistic proposal for pseudotabersonine formation

The byproducts **33** and **34** isolated from the rearrangement reaction using substoichiometric acid were intriguing as well. We postulate that these products arise from a redox-disproportionation event (**Fig. 2.20**), as **33** is a reduction product and **34** is an oxidized

version of pseudotabersonine. The ability for these products to actively contribute in the transformation was confirmed through a simple experiment; combining the materials in a 1:1 ratio and heating to reflux in toluene (optimized conditions), the natural product was produced in 65% isolated yield, which unambiguously demonstrates that both of these materials can be funneled together to form product. It is possible that this process occurs through direct hydride transfer between the two species, as this process has been documented under acidic conditions in several instances.[100,101]

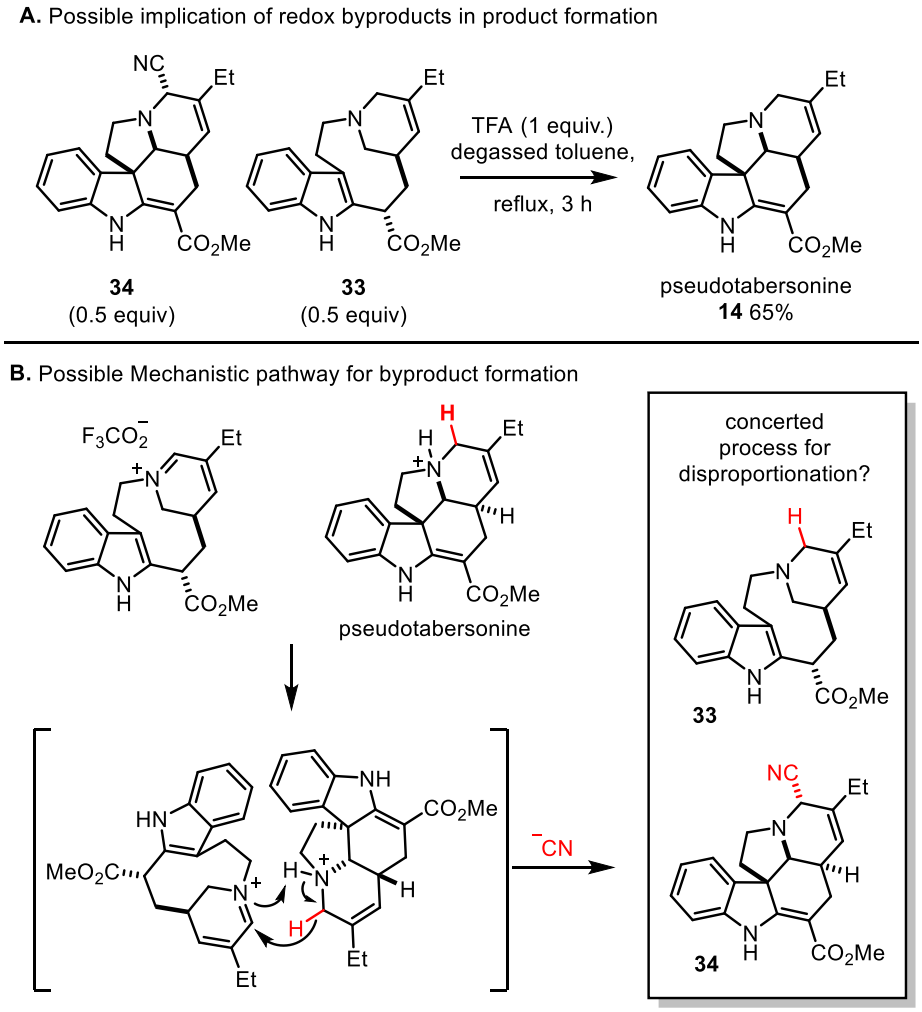

Figure 2.20 Redox disproportionation in the pseudotabersonine rearrangement

With these results in hand, we turned our attention to the synthesis of the structurally related natural product pseudovincadifformine (**Fig. 2.21**). While this natural product is merely a hydrogenated analog of pseudotabersonine, we had no desire to perform the direct hydrogenation of our enantiomerically impure material. Instead, intrigued by acid-promoted iminium isomerization chemistry seen in the formation of pseudotabersonine, we were curious as to whether we could probe the mechanism and evaluate its scope at the same time. Specifically, we thought it possible that the initial dihyropyridinium ion (**Fig. 2.19**) could be responsible for the majority of the racemization observed, and that upon formation of the internal iminium ion transannular cyclization may out-compete further tautomerization/racemization (**Fig. 2.21A**).

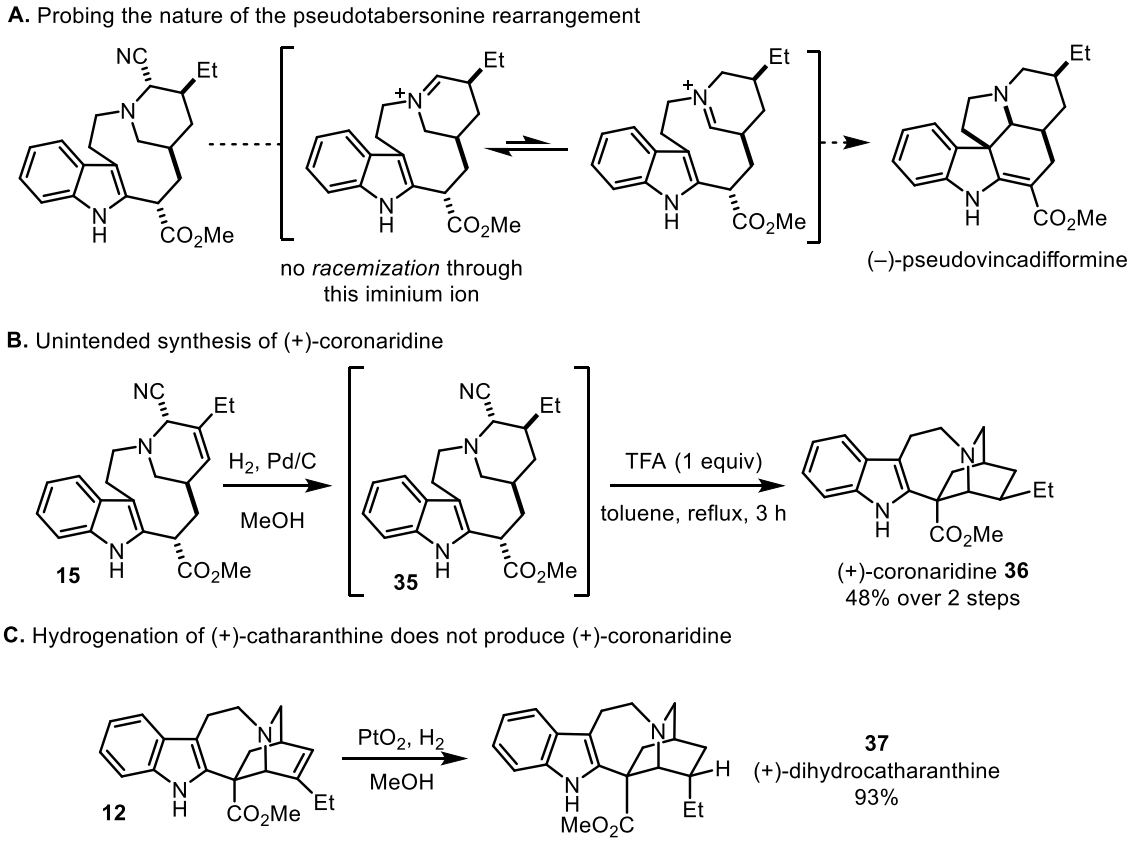

Figure 2.21 Synthesis of (+)-coronaridine through a mechanistic probe

To access pseudovincadifformine, hydrogenation of the tri-substituted double bond would eliminate the possibility of vinylogous epimerization from the initial iminium ion (**Fig.**

2.21B). This was accomplished successfully using 10% palladium ion carbon under an atmosphere of hydrogen gas in methanol. The product **35** of this hydrogenation was unstable to TLC reaction analysis, and consequently the reaction was monitored by HNMR, which revealed that optimal reaction time on a 20 mg scale is 25 minutes. If the reaction is left longer than this amount of time, reductive de-cyanation is observed as a major process for product decomposition, and epimerization of the ethyl group also occurs, presumably *via* the intermediacy of the iminium ion. The product aminonitrile was found to be unstable to column chromatography, so it was carried forward without purification.

The hydrogenated material was directly subjected to the optimized isomerization conditions that were used for the production of pseudotabersonine; interestingly, instead of isolating the desired product pseudovincadifformine, a hydrogenated product of catharanthine was isolated, namely the natural product coronaridine **36** (**Fig 2.21B**). On first approximation this result was disappointing, as it did not produce the desired reactivity; however, further investigation revealed that this material is not readily accessible from catharanthine, as the direct hydrogenation of the natural product results in the opposite, axial ethyl diastereomer **37** (dubbed "dihydrocatharanthine," **Fig. 2.21C**).[102] Literature precedent for the formation of coronaridine is sparse, and the reported conditions do not provide selectivity for the natural product.[103] Consequently, to our knowledge the synthesis of coronaridine described here represents the highest-yielding preparation of this material reported in the literature.

Upon the failure of this approach to the synthesis of pseudovincadifformine, we settled upon a reduction-oxidation approach which finally yielded the natural product. Upon diastereoselective hydrogenation of the aminonitrile double bond, followed by a sodium borohydride quench, the tertiary amine **38** was formed in high yield (**Fig. 2.22**). Our goal of

oxidatively forming the internal iminium ion for cyclization had been accomplished previously by Kutney and coworkers, although the previous strategy entailed the use of superstoichiometric amounts of $Hg(OAc)_2$—an environmentally detrimental protocol. Our strategy would improve the environmental impact of this type of oxidative cyclization, and further would be a unique example of photocatalysis in terms of complex amine oxidation. As is outline in Chapter 1, the majority of examples pertaining to trialkylamine oxidation utilize the amine as a sacrificial additive. Conversely, examples using the amine as a more-precious substrate have resulted in the majority of examples possessing pre-activation of the substrate through the inclusion of regiochemical bias (i.e. tetrahydroisoquinoline). We set out to perform this oxidation chemistry fully aware of the limitations in the previous examples.

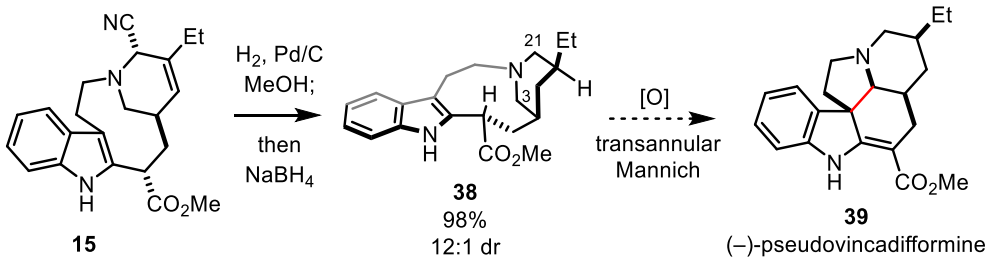

Figure 2.22 Proposed synthesis of (–)-pseudovincadifformine

We were bolstered by an accidental result which resulted from a hydrogenation experiment gone awry. In one exploratory instance, hydrogenation of the cycanocleavamine intermediate on small scale was allowed to proceed overnight to see the effects of prolonged hydrogenation on the diastereoselectivity and chemoselectivity (k_{rel} double bond hydrogenation >> k_{rel} iminium reduction) of the transformation. Interestingly, upon loss of all hydrogen atmosphere from the reaction balloon overnight, the presence of oxygen allowed for the formation of a minute quantity of pseudovincadifformine directly from the fragmentation product in one step (not shown).

Attempts to perform this chemistry using photocatalysis first were met with decomposition using aerobic conditions, but subsequent attempts to use organic oxidants were met with successive success (**Table 2.3**). Bromochloroform provided the natural product in 22% yield, and subsequent optimization resulted in optimal conditions using diethyl bromomethylmalonate **40** in three equivalents in a flow reactor. These conditions provided the natural product in 58% yield and 8:1 d.r.

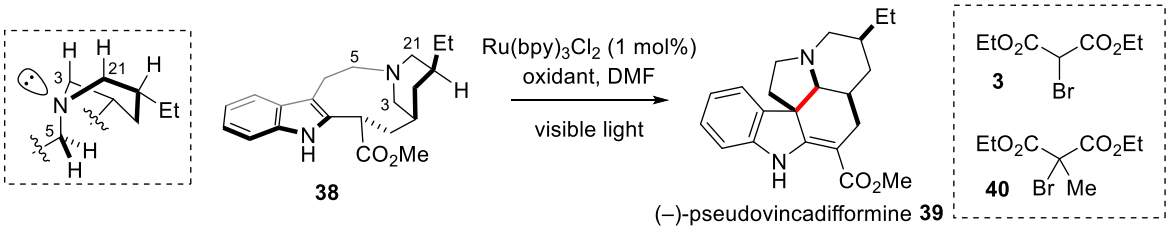

entry	oxidant	yield
1	air	0%
2	$BrCCl_3$ (3 equiv)	22%
3	**3** (3 equiv)	**34%**
4	**40** (3 equiv)	39%
5[a]	**40** (3 equiv)	58%

[a] Flow reactor, t_R = 5 min

Table 2.3 Oxidant screening for the formation of (–)-pseudovincadifformine

As mentioned in Chapter 1, the oxidation of tertiary amines is often met with limited selectivity. While this example does not substantially improve upon previous results in the realm, there are a number of stereoelectronic aspects to the described reaction which may contribute to its success. Mechanistically, it is proposed that the tertiary amine substrate reductively quenches the photocatalyst by a single electron, to both form the $[Ru]^{+1}$ species and the corresponding amine radical cation (**Fig. 2.23**). Further reduction of the organic oxidant (in

this case the bromomalonate) by $[Ru]^{+1}$ results in a free radical species. The amine radical cation possesses significantly weakened α-C–H bonds, which can either undergo deprotonation followed by oxidation to form the iminium ion, or alternatively can participate as a hydrogen atom donor in the presence of an appropriate free-radical.

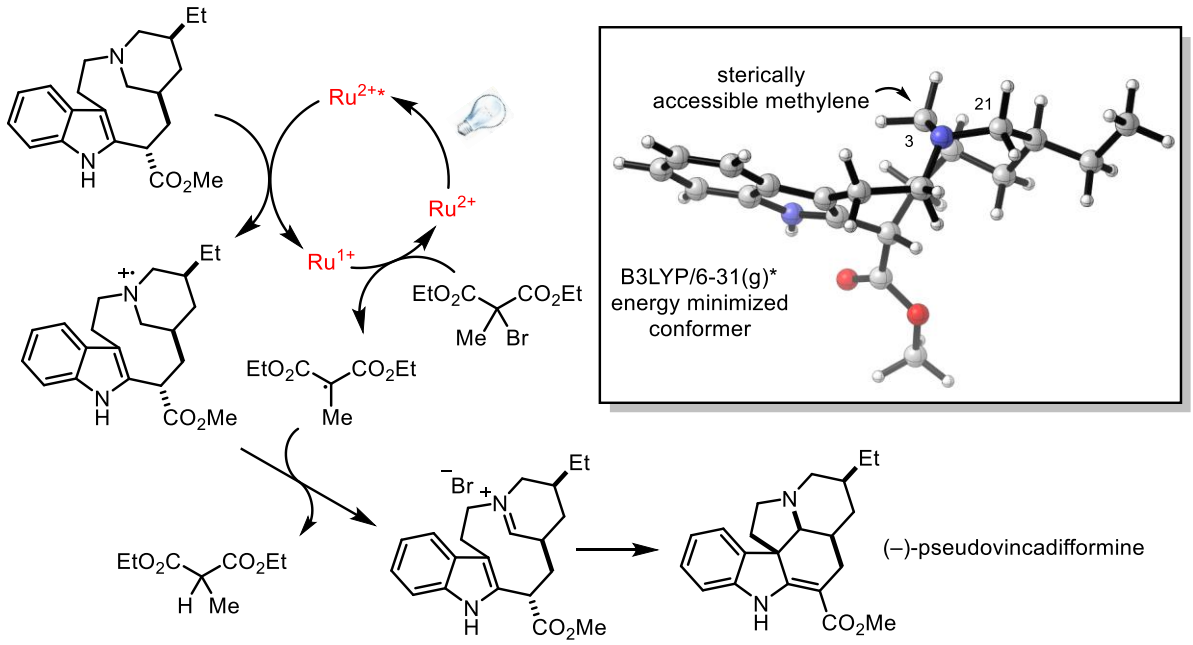

Figure 2.23 Mechanism of oxidative cyclization

While **Figure 2.23** depicts the mechanism as proceeding *via* hydrogen atom abstraction, statistically it may be more likely that the radical cation undergoes deprotonation followed by oxidation. This is because the lifetimes of each of the radical species in the proposed C–H abstraction step are presumably very short, and the corresponding concentration of each reactive species would likely not exceed 1 mol% at any given time (i.e. organic radical lifetime being shorter than a complete catalytic cycle). Consequently the statistical likelihood of radical-radical disproportionation is low, and alternative mechanisms may be at work.

While this analysis may be correct, the selectivity observed in this reaction does correspond with steric restraints imposed by the organic oxidants used. The more sterically

encumbered oxidants provided higher yields (**Table 2.3**), which suggest a possible intermolecular selectivity which results in more prominent functionalization of the less sterically encumbered α-amino methylene. Three-dimensional analysis of the piperidine ring of the substrate reveals that only two of the three positions adjacent to the nitrogen provide acceptable overlap with the nitrogen P-orbital for productive functionalization to occur (C3 and C21, **Table 2.3**). Furthermore, a three-dimensional depiction of the substrate reveals that C3 is less sterically-encumbered than may be suggested by its two-dimensional drawing (**Fig. 2.23**). These factors may combine to explain some of the selectivity observed.

Generality of the catharanthine fragmentation

Upon synthesis of (–)-pseudovincadifformine, (+)-coronaridine, and (–)-pseudotabersonine, we set out to evaluate the generality of the C–C bond fragmentation chemistry. We opted for a dual approach through both computation and experiment, both in order to ensure data accuracy as well as because we had obtained access to each of the hydrogenated derivatives of catharanthine. To investigate the strain energy released upon carbon-carbon bond cleavage, we began to investigate the process using homodesmotic equations for the energy estimation.[104]

Homodesmotic reactions occupy an optimized location in theoretical space, wherein the error in estimation is minimal for the amount of computational resources required for geometry optimization. Specifically, in this approach the total energies of energy-minimized geometries of both starting materials and products are compared to each other through a series of thermochemical correction factors. Homodesmotic reactions, according to Wheeler et al., require that "(a) equal numbers of each type of carbon-carbon bond (Csp^3–Csp^3, Csp^3–Csp^2, Csp^3–Csp,

Csp^2–Csp^2, Csp^2–Csp, Csp–Csp, Csp^2=Csp^2, Csp=Csp, Csp=Csp, Csp≡Csp) [*are present*] in reactants and products, and (b) equal numbers of each type of carbon atom (sp3, sp2, sp) with zero, one, two, and three hydrogens [*are*] attached in reactants and products."[104]

Because of the need for a balanced equation in terms of both types of atoms (hybridization preserved) and types of bonds, a number of "strain free" reference molecules must be used. As an illustrative example, consider the strain energy of a cyclopropane ring (**Fig. 2.24**). The strain energy is the amount of energy resulting from the ring conformation of the substrate, which includes both non-optimal bond angles enforced on each atom, as well as eclipsing interactions of vicinal bonds. In order to isolate the energy corresponding to these factors from the irrelevant energy value of the C–C bond energy, the homodesmotic reaction of cyclopropane with ethane to form n-pentane provides direct insight into the strain of the substrate. Ethane is used as a "strain-free" reference molecule in accordance with the guidelines put forth by Schleyer and coworkers.[105]

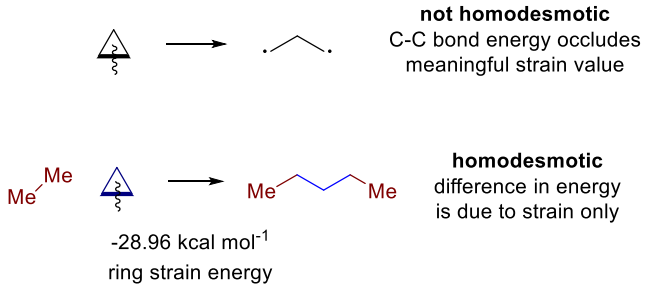

Figure 2.24 Homodesmotic ring strain of cyclopropane

The strain energy of catharanthine and its analogues is considerably more complicated, as the ring-opened products are not straight chain alkanes but complex tetracyclic cyclophanes. As a consequence, the introduction of ethane across the C16-C21 bond would introduce additional strain that is irrelevant to the reaction in question. Consequently, to ensure minimal energy distortion due to steric clashing around the ring-opening sites, hydrogen atoms were added across

each broken carbon-carbon bond (**Fig. 2.25**). All methyl, methine, and quaternary carbon substituents balance out on each side of the reaction and are incorporated in "strain free" thermochemical standards as put forth by Schleyer.[104] To balance the number of methylenes on both sides of each reaction, a methylene correction term, as reported by Khoury and coworkers was incorporated.[106] This term is abbreviated *E(CH$_2$)* and is the (B3LYP/6-31G*) optimized energy difference between n-pentane and n-butane.

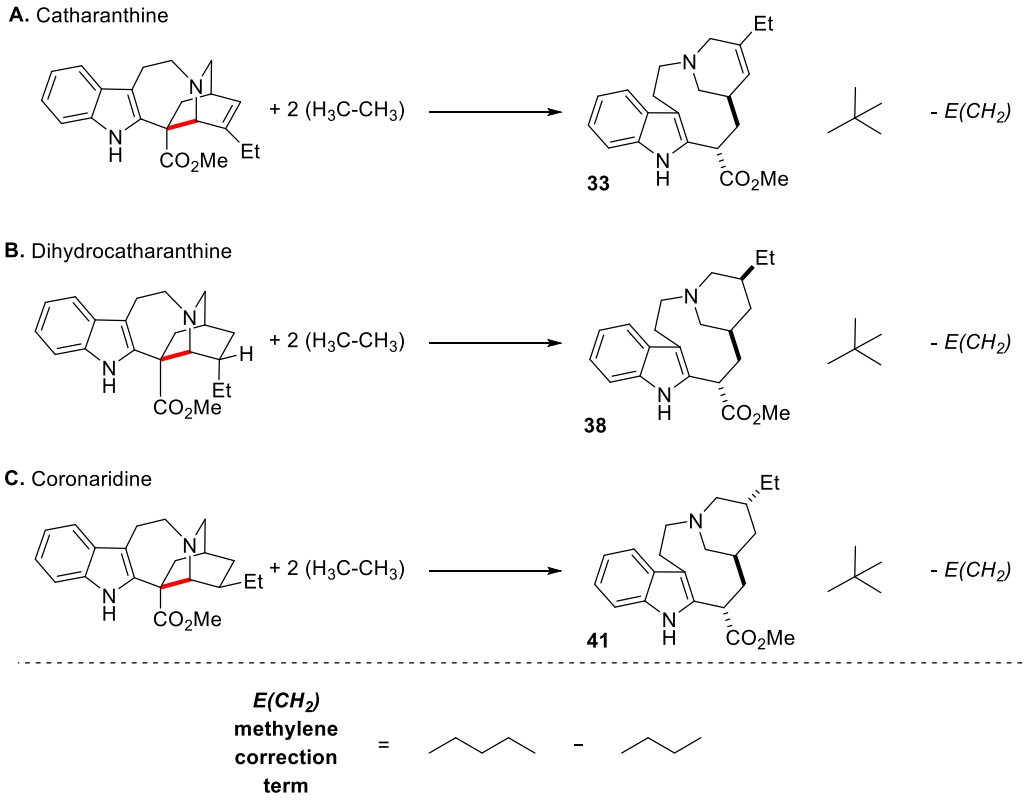

Figure 2.25 Homodesmotic fragmentation of catharanthine analogs

The Gaussian 09 program was used to optimize structures at the (B3LYP/6-31G*) level of theory.[107] Structures were minimized with no symmetry restrictions, and vibrational modes were generated simultaneously to ensure the absence of imaginary frequencies corresponding to unstable structures or transition states. Homodesmotic cleavage of catharanthine as well as the two hydrogenated diastereomers—dihydrocatharanthine and coronaridine—revealed large

differences in strain energy depending upon the degree of substrate unsaturation (**Fig. 2.26**). Catharanthine exhibits roughly 4.2 kcal mol^{-1} of strain release whereas the hydrogenated derivatives are roughly energy-neutral upon fragmentation. The energy-minimized conformations of ring-opened **38** and **41** revealed that the ethyl configuration of the ring-opened material may dictate a different piperidine ring conformation in the ring-opened form. Specifically, the β-configuration of the ethyl group would be axially disposed for the chair conformation of the piperidine ring. Consequently, the ring is in a lower energy boat conformation.

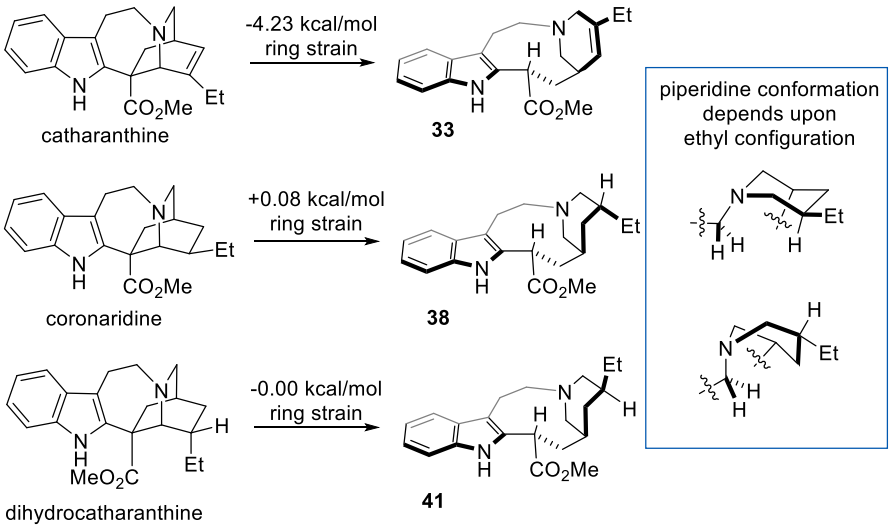

Figure 2.26 Strain release energies of catharanthine analogs

Experimentally, the hydrogenated catharanthine analogs behave consistently with these calculations (**Fig. 2.26**). To promote fragmentation of the hydrogenated analogs, more forcing conditions were required, which entailed longer residence times (42 min vs. 2 min, >20x increase) and higher reaction temperatures (50 °C vs. 35 °C). In addition, the reaction selectivity was much worse, where the fragmentation products are only obtained in 25-37% yield. Side-products from the reaction included α-cyanation of the substrate tertiary amine. These results are

indicative of reactivity trends which had already been suspected; in the absence of sufficient strain energy, C–H functionalization is the preferred pathway over C–C fragmentation.

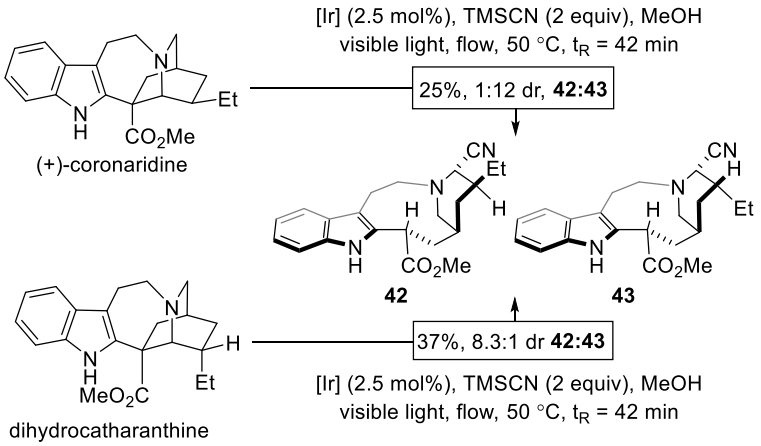

Figure 2.26 Fragmentation of hydrogenated catharantine analogs

Conclusions

This work has demonstrated the utility of photoredox catalysis in the arena of complex molecule synthesis, and in particular has served as a demonstration of the utility of flow chemistry for scalable photochemical transformations. The syntheses of (–)-pseudovincadifformine, (+)-coronaridine, and (–)-pseudotabersonine presented here represent to our knowledge the highest-yielding preparations of each material to date, in 55%, 46%, and 86% overall yield, respectively (**Fig. 2.27**). The synthesis of (–)-pseudovincadifformine utilized visible-light photoredox catalysis in flow for two out of the three total steps for its preparation. In addition, the synthesis of a number of analogous structures including dihydrocatharanthine has enabled the elucidation of factors determining the efficiency of C–C bond fragmentation in these complex structures. This work has demonstrated the utility of photoredox catalysis to replace toxic reagents such as $Hg(OAc)_2$ in complex synthetic contexts.

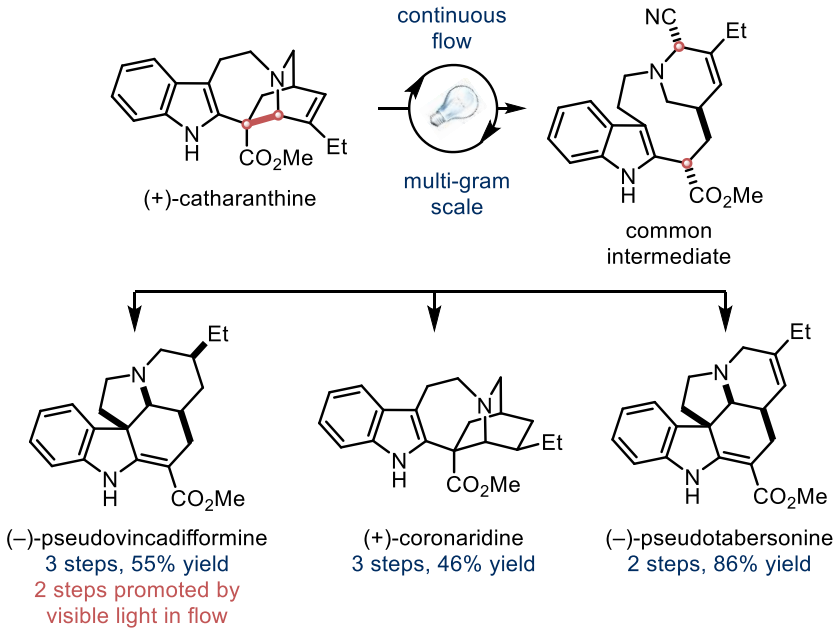

Figure 2.27 Overall yields and step-counts

Experimental

General Information:

Chemicals were either used as received or purified according to *Purification of Common Laboratory Chemicals*. Catharanthine was obtained as a tartrate salt from both Ontario Chemicals, Inc. and Arking Pharma Scientific, Inc. and was free-based within two hours prior to use through workup with ethyl acetate and saturated sodium bicarbonate. All reactions were performed using common dry, inert atmosphere techniques. Reactions were monitored by TLC and visualized by a dual short wave/long wave UV lamp and stained with an ethanolic solution of potassium permanganate or p-anisaldehyde. Column flash chromatography was performed using 230-400 mesh silica gel. NMR spectra were recorded on Varian Unity Plus 400, Varian MR400, Varian vnmrs 500, Varian Inova 500, Varian Mercury 500, and Varian vnmrs 700 spectrometers. Chemical shifts for ^{1}H NMR were reported as δ, parts per million, relative to the signal of $CHCl_3$ at 7.26 ppm. Chemical shifts for ^{13}C NMR were reported as δ, parts per million, relative to the center line signal of the CDCl3 triplet at 77.0 ppm. The abbreviations s, br. s, d, dd, br. d, ddd, t, q, br. q, qi, m, and br. m stand for the resonance multiplicity singlet, broad singlet, doublet, doublet of doublets, broad doublet, doublet of doublet of doublets, triplet, quartet, broad quartet, quintet, multiplet and broad multiplet, respectively. IR spectra were recorded either on an Avatar 360 FT-IR or Perkin-Elmer Spectrum BX FT-IR spectrometer. Mass spectra were recorded at the Mass Spectrometry Facility at the Department of Chemistry if the University of Michigan in Ann Arbor, MI on an Agilent Q-TOF HPLC-MS with ESI high resolution mass spectrometer. The enantiomeric purity of relevant samples was determined by chiral HPLC analysis performed on a Shimadzu system using a CHIRALPAK AD-H column from Daicel Chemical Ind., Ltd. with iPrOH/hexane as the eluent. Concentration refers to removal of solvent under reduced pressure (house vacuum at ca. 20 mmHg).

Batch Reaction Apparatus:

Photoredox catalyzed reactions were carried out under visible light irradiation by a commercially available 2W blue LED strip in a circle around and approximately 4 cm from the reaction flask. For optimized conditions, when the reaction was left for 6 hours a precipitate of product formed in the reaction (pictured).

Batch Fragmentation Procedure:

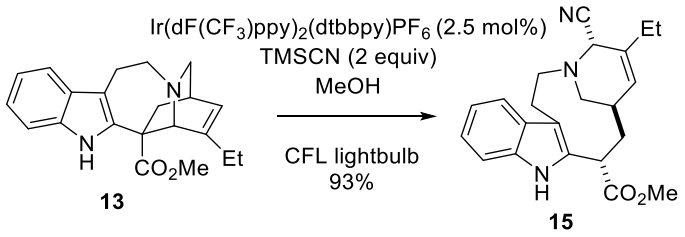

A flame dried 5 ml round bottom flask was charged with freshly free-based catharanthine (0.1 mmol, 33.6 mg, 1 equiv), $Ir(dF(CF_3)ppy)_2(dtbbpy)PF_6$ (0.0025 mmol, 2.8 mg, 2.5 mol%), and methanol (1 ml, 0.1 M). The resulting solution was degassed *via* the freeze pump-thaw method (3 cycles) and the flask was back-filled with argon. Trimethylsilylcyanide (0.2 mmol, 25 µl, 2 equiv) was then added *via* micro syringe. The flask was then irradiated by a 2W blue LED strip under an atmosphere of nitrogen and stirred for three hours. Upon consumption of starting

material by TLC, the reaction was removed from the light source and quenched with sat. $NaHCO_3$ (5 ml). The layers were separated and the aqueous layer was extracted with EtOAc (x3). The combined organic layers were washed with brine and dried (Na_2SO_4) before concentrating. Internal standard solution was prepared by mixing 216 µl (2 mmol) of 2,5-dimethylfuran in $CDCl_3$ prepared in a 10 ml volumetric flask. The crude residue was dissolved in 500 µl (0.1 mmol) of internal standard solution and diluted to a final volume of 1 ml for ^{1}HNMR analysis. The reaction yields a pale yellow amorphous solid (93% yield vs. internal standard), which can be further purified through rinsing with ice cold methanol to yield the pure product as a white crystalline solid.

(4S,7R,9S)-methyl 4-cyano-5-ethyl-2,4,7,8,9,10-hexahydro-1H-3,7-methano[1]azacycloundecino[5,4-b]indole-9-carboxylate (15)[88]

IR (neat): 3377, 2924, 1723, 1460, 1434, 1248m 1163, 844, 737 cm^{-1};

^{1}H NMR ($CDCl_3$, 500 MHz): δ 8.61 (br. s, 1H), 7.51 (d, *J* = 7.6 Hz, 1H), 7.34 (d, *J* = 7.6 Hz, 1H), 7.18 (dd, *J* = 7.6, 7.4 Hz, 1H) 7.11 (dd, *J* = 7.6, 7.4 Hz, 1H), 5.54 (d, *J* = 4.1 Hz, 1H), 4.78 (d, *J* = 10.3 Hz, 1H), 4.13 (s, 1H), 3.67 (s, 3H), 2.99-2.93 (m, overlap, 2H), 2.89-2.83 (m, 1H), 2.75 (dd, *J* = 12.6, 3.5 Hz, 1H), 2.53 (m, 1H), 2.42-2.34 (m, overlap, 2H), 2.29-2.16 (m, overlap, 3H), 2.10 (d, *J* = 14.4 Hz, 1H), 1.17 (t, *J* = 7.3 Hz, 3H)

^{13}C NMR ($CDCl_3$, 175 MHz): δ 175.0, 136.0, 135.8, 133.9, 127.6, 126.4, 122.0, 119.3, 118.2, 117.8, 110.9, 110.7, 55.7, 52.3, 51.8, 49.4, 38.3, 37.4, 33.7, 26.2, 25.8, 12.0

HRMS (ESI) *m/z* calculated for $C_{21}H_{25}N_2O_2^+$ ($[M\text{-}CN]^+$) 337.1911, found 337.1916

$[\alpha]_D^{26}$ = -43 (c 1.0, $CHCl_3$)

Fragmentation Optimization and Control Experiments:

Reaction optimization reactions were conducted using the batch procedures outlined above. $Ir(dF(CF_3)ppy)_2(dtbbpy)PF_6$ was found to perform superiorly to both $Ru(bpy)_3Cl_2$ and $Ir(ppy)_2(dtbbpy)PF_6$. Thorough exclusion of light resulted in no observable reactivity, and there was no background reaction observed when the reaction was run with light irradiation but without photocatalyst. As the flow reaction utilizes a 5.88 W LED as opposed to the 14W CFL used for batch reactions, photocatalyst was also excluded from the flow reaction but again no light-driven background reaction was observed. Yields are NMR yields vs. 2,5-dimethylfuran as the internal standard.

Flow Fragmentation Procedure:

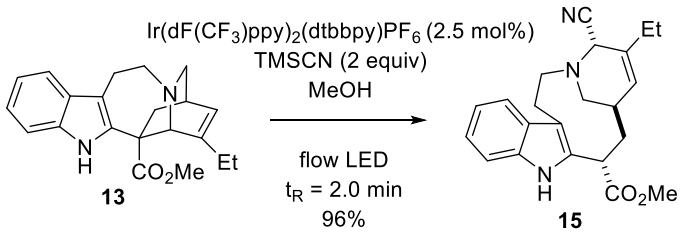

To a flame dried 5 ml round bottom flask equipped with a rubber septum and magnetic stir bar was added catharanthine (0.25 mmol, 1.0 equiv, 84 mg), $Ir(dF(CF_3)ppy)_2(dtbbpy)PF_6$ 5 (0.006 mmol, 0.025 equiv, 7.0 mg) and methanol (2.5 ml). The resultant mixture was degassed *via* the freeze pump-thaw method (3 cycles) and the flask back-filled with argon. TMSCN (0.5 mmol, 2.0 equiv, 63 µl) was subsequently added to the degassed solution. The reaction mixture was then pumped through the photoreactor at a flow rate of 670 µl/min to achieve a residence time of 2.0 minutes and collected in a 25 ml round bottom flask. After 3.0 minutes the needle was taken out of the feeder solution, resulting in an overall reaction scale of 0.20 mmol. The reaction mixture was poured into a separatory funnel containing saturated $NaHCO_3$. The resulting solution was extracted with EtOAc (x3). The combined organic layers were washed with brine,

dried (Na_2SO_4) and concentrated to provide a yellow amorphous solid. Yield (96% by NMR) was determined as outlined in the batch procedure.

Flow Fragmentation Procedure (2 gram scale):

To a flame dried 100 ml round bottom flask equipped with a rubber septum and magnetic stir bar was added catharanthine (6.02 mmol, 1.0 equiv, 2.025 g), $Ir(dF(CF_3)ppy)_2(dtbbpy)PF_6$ 5 (0.150 mmol, 0.025 equiv, 147 mg) and methanol (60.2 ml). The resultant mixture was degassed *via* the freeze pump-thaw method (3 cycles) and the flask back-filled with argon. TMSCN (12.04 mmol, 2.0 equiv, 1.51 ml) was subsequently added to the degassed solution. The reaction mixture was then pumped through the photoreactor at a flow rate of 670 μl/min to achieve a residence time of 2.0 minutes and flowed into a 500 ml Erlenmeyer flask containing 300 ml of ethyl acetate. The reactor tubing was submerged beneath the surface of the solvent in the collection flask to ensure that no crystallization occurred in the tubing due to evaporation of solvent upon elution. Care should be taken to ensure that no crystals form in the collection flask, and if they do the solution should be replaces immediately with fresh ethyl acetate. As the reaction progressed, white crystals began to form in feeder solution. Upon full uptake of the reaction solution, an additional 2 ml of methanol were added to rinse any residue through the reactor, but was insufficient to dissolve all remaining material. The reaction mixture was poured into a separatory funnel containing saturated $NaHCO_3$. The resulting solution was extracted with EtOAc (x3). The combined organic layers were washed with brine, dried (Na_2SO_4) and concentrated to provide a yellow amorphous solid. Yield (88% by NMR) was determined vs. 2,5-dimethylfuran as the internal standard.

General Procedure for the Addition of R_2Zn Reagents:

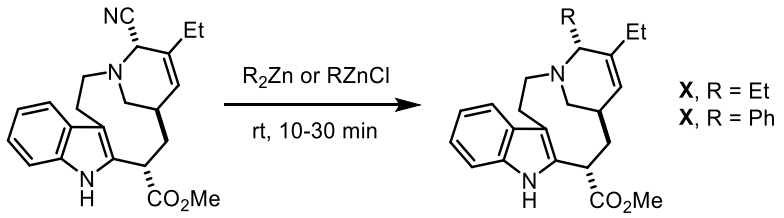

A 5 ml flame dried round bottom flask was equipped with a rubber septum and magnetic stir bar and charged with alpha amino nitrile **15** (0.1 mmol, 1.0 equiv, 36.4 mg) and dry THF (1.0 ml). The flask was evacuated and backfilled with argon. To this solution at room temperature was added drop wise 0.8 ml of a 0.25M solution of R_2Zn in THF (0.2 mmol, 2.0 equiv). The reaction was allowed to stir for 10 minutes before quenching with deionized water (1.0 ml). The resulting biphasic mixture was extracted with EtOAc (x3) and the combined organic layers were washed with brine, dried (Na_2SO_4) and concentrated. The residue was purified by chromatography on silica gel, using the solvent system indicated, to afford the desired alkylation product.

(4R,7R,9S)-methyl 4,5-diethyl-2,4,7,8,9,10-hexahydro-1H-3,7-methano[1]azacycloundecino[5,4-b]indole-9-carboxylate (23)

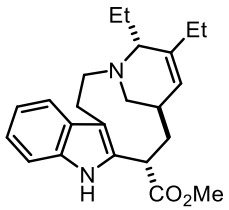

The general procedure afforded **23** (88%) as a white solid after purification by chromatography on SiO_2 (19:1, hexanes/EtOAc).

R_f (4:1 hexanes/EtOAc): 0.49;

IR (neat): 3389, 2962, 2926, 2873, 1719, 1462, 1434, 1336, 1248, 1159, 1094, 1012, 933, 740 cm^{-1};

^1H NMR ($CDCl_3$, 500 MHz): δ 8.55 (br. s, 1H), 7.50 (d, *J* = 7.6 Hz, 1H), 7.33 (d, *J* = 7.7 Hz, 1H), 7.16 (dd, *J* = 7.7, 7.3 Hz, 1H), 7.09 (dd, *J* = 7.6, 7.3 Hz, 1H) 5.25 (d, *J* = 4.2 Hz, 1H), 4.91 (d, *J* = 9.8 Hz, 1H), 3.68 (s, 3H), 3.17 (dd, *J* = 5.3, 5.3 Hz, 1H), 3.10 (ddd, *J* = 13.8, 3.2, 2.6 Hz, 1H), 2.99 (dd, *J* = 12.5, 4.6 Hz, 1H), 2.85-2.74 (m, overlap, 2H), 2.50 (ddd, *J* = 13.8, 11.6, 2.6 Hz, 1H), 2.34-2.28 (m, 1H), 2.20-2.03 (m, overlap, 5H), 1.67-1.60 (m, overlap, 2H), 1.13 (t, *J* = 7.5 Hz, 3H), 1.0 (t, *J* = 7.7, 3H);

^{13}C NMR ($CDCl_3$, 125 MHz): δ 175.7, 145.9, 135.8, 134.3, 127.8, 121.5, 121.5, 118.9, 118.2, 111.9, 110.6, 60.9, 52.1, 51.8, 47.5, 38.8, 37.8, 34.3, 27.5, 26.5, 23.3, 13.2, 12.9;

HRMS (ESI) *m/z* calculated for $C_{23}H_{31}N_2O_2^+$ ($[M+H]^+$) 367.2386, found 367.2384 ;

$[\alpha]_D^{26}$ = +0.7 (c 0.83, CH_2Cl_2)

(4S,7R,9S)-methyl 5-ethyl-4-phenyl-2,4,7,8,9,10-hexahydro-1H-3,7-methano[1]azacycloundecino[5,4-b]indole-9-carboxylate (24)

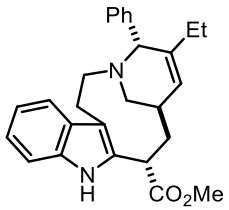

The general procedure afforded **24** (63%) as a white solid after purification by chromatography on SiO_2 (19:1, hexanes/EtOAc).

R_f (9:1 hexanes/EtOAc): 0.31;

IR (neat): 3363, 3023, 2925, 2850, 1719, 1462, 1248, 1171, 739 cm^{-1};

^1H NMR ($CDCl_3$, 500 MHz): δ 8.50 (br. s, 1H), 7.35 (d, *J* = 8.1 Hz, 1H), 7.24 (d, *J* = 7.6 Hz, 2H), 7.20-7.15 (overlap, 3H), 7.04 (dd, *J* = 7.4 Hz, 1H), 6.96 (dd, *J* = 7.6, 7.4 Hz, 1H), 5.49 (d, *J* = 5.1 Hz, 1H), 4.95 (d, *J* = 9.0 Hz, 1H), 4.17 (s, 1H), 3.60 (s, 3H), 2.98-2.91 (m, overlap, 2H), 2.84-2.74 (m, overlap, 2H), 2.31 (m, 1H), 2.23 (br. m, 1H), 2.08 (d, *J* = 13.9 Hz, 1H), 2.03 (d, *J* = 12.5 Hz, 1H), 1.91 (ddd, *J* = 13.9, 11.7, 2.0 Hz, 1H), 1.80 (q, *J* = 7.4 Hz, 2H), 0.95 (t, *J* = 7.4 Hz, 3H);

^{13}C NMR ($CDCl_3$, 125 MHz): δ 175.7, 142.5, 138.9, 135.7, 134.3, 129.1, 127.9, 127.9, 127.1, 123.2, 121.5, 118.9, 118.2, 112.1, 110.5, 64.0, 52.1, 50.0, 47.3, 38.8, 38.2, 34.2, 27.1, 25.6, 12.5;

HRMS (ESI) *m/z* calculated for $C_{27}H_{31}N_2O_2^+$ ($[M+H]^+$) 415.2386, found 415.2375;

$[\alpha]_D^{26}$ = +9.6 (c 0.47, CH_2Cl_2)

(4R,7R,9S)-methyl 5-ethyl-4-methyl-2,4,7,8,9,10-hexahydro-1H-3,7-methano[1]azacycloundecino[5,4-b]indole-9-carboxylate (22)

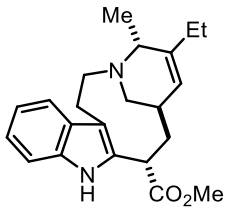

The general procedure afforded **22** (74%) as a white solid after purification by chromatography on SiO_2 (9:1 hexanes/EtOAc).

R_f (4:1 hexanes/EtOAc): 0.40;

IR (neat): 3380, 2963, 2925, 2873, 1728, 1462, 1163, 742 cm^{-1};

^1H NMR ($CDCl_3$, 500 MHz): δ 8.56 (br. s, 1H), 7.51 (d, *J* = 7.7 Hz, 1H), 7.33 (d, *J* = 7.6 Hz, 1H), 7.15 (dd, *J* = 7.7, 7.4 Hz, 1H), 7.09 (dd, *J* = 7.6, 7.4 Hz, 1H), 5.25 (d, *J* = 4.6 Hz, 1H), 5.07 (d, *J* = 9.8 Hz, 1H), 3.67 (s, 3H), 3.3 (q, *J* = 6.4 Hz, 1H), 2.89-2.76 (m, overlap, 4H), 2.36-2.29 (m, overlap, 2H), 2.11-2.02 (m, overlap, 5H), 1.10 (t, *J* = 7.3 Hz, 3H), 1.0 (d, *J* = 6.4 Hz, 3H);

^{13}C NMR ($CDCl_3$, 125 MHz): δ 175.8, 146.2, 135.8, 134.5, 127.9, 121.5, 121.4, 118.9, 118.2, 111.7, 110.5, 55.4, 52.1, 50.5, 46.4, 38.7, 38.2, 34.6, 26.8, 26.4, 12.8, 11.0;

HRMS (ESI) *m/z* calculated for $C_{22}H_{29}N_2O_2^+$ ($[M+H]^+$) 353.2229, found 353.2234 ;

$[\alpha]_D^{26}$ = -2.2 (c 0.45, CH_2Cl_2)

(4R,7R,9S)-methyl 5-ethyl-4-vinyl-2,4,7,8,9,10-hexahydro-1H-3,7-methano[1]azacycloundecino[5,4-b]indole-9-carboxylate (26)

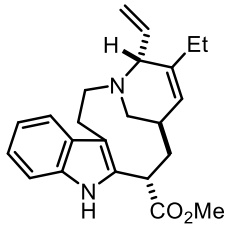

The general procedure afforded **26** (62%) as a white solid after purification by chromatography on SiO_2 (19:1 hexanes/EtOAc).

R_f (4:1 hexanes/EtOAc): 0.45;

IR (neat): 3384, 2963, 2922, 2853, 1717, 1462, 1247, 1159, 739 cm^{-1};

^1H NMR ($CDCl_3$, 500 MHz): δ 8.57 (br. s, 1H), 7.51 (d, *J* = 8.0 Hz, 1H), 7.34 (d, *J* = 7.8 Hz, 1H), 7.16 (ddd, *J* = 8.0, 7.0, 1.2 Hz, 1H), 7.10 (ddd, *J* = 7.8, 7.0, 1.2 Hz, 1H), 5.79 (ddd, *J* = 17.1, 10.0, 8.6 Hz, 1H), 5.41 (d, *J* = 4.9 Hz, 1H), 5.21 (dd, *J* = 10.0, 2.2 Hz, 1H), 5.13 (ddd, *J* = 17.1, 2.2, 0.7 Hz, 1H), 5.04 (d, *J* = 9.8 Hz, 1H), 3.69 (s, 3H), 3.56 (d, *J* = 8.6 Hz, 1H), 2.95-2.77 (m, overlap, 4H), 2.37 (ddd, *J* = 14.2, 10.0, 6.1 Hz, 1H), 2.30 (ddd, *J* = 13.9, 11.8, 2.2 Hz, 1H), 2.19-2.02 (m, 5H), 1.11 (t, *J* = 7.5 Hz, 3H);

^{13}C NMR ($CDCl_3$, 125 MHz): δ 175.7, 142.5, 135.8, 134.7, 134.3, 127.9, 122.8, 121.5, 118.9, 118.2, 117.1, 111.9, 110.6, 64.1, 52.1, 50.5, 48.0, 38.4, 38.2, 34.5, 26.6, 26.1, 12.7;

HRMS (ESI) *m/z* calculated for $C_{23}H_{29}N_2O_2^+$ ($[M+H]^+$) 365.2229, found 365.2234;

$[\alpha]_D^{26}$ = +26.5 (c 0.37, CH_2Cl_2)

(4R,7R,9S)-methyl 4-allyl-5-ethyl-2,4,7,8,9,10-hexahydro-1H-3,7-methano[1]azacycloundecino[5,4-b]indole-9-carboxylate (25)

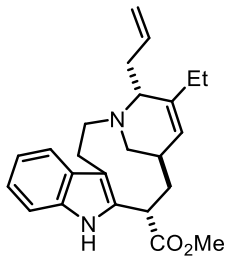

The general procedure afforded **25** (47%) as a white solid after purification by chromatography on SiO_2 (92:8 hexanes/Et_2O).

R_f (4:1 hexanes/Et_2O): 0.62;

IR (neat): 3386, 3055, 2962, 2924, 2850, 1718, 1462, 1434, 1159, 741 cm^{-1};

^1H NMR ($CDCl_3$, 500 MHz): δ 8.58 (br. s, 1H), 7.51 (d, *J* = 7.7 Hz, 1H), 7.34 (d, *J* = 7.8 Hz, 1H), 7.17 (ddd, *J* = 7.7, 7.4, 1.2 Hz, 1H), 7.10 (ddd, *J* = 7.8, 7.4, 1.2 Hz, 1H), 5.97 (dddd, *J* = 17.1, 1.0, 7.4, 7.4, 1H), 5.29 (d, *J* = 4.6 Hz, 1H), 5.06 (ddd, *J* = 17.1, 1.7, 1.7 Hz, 1H), 4.98 (ddd, *J* = 10.0, 1.0, 1.0 Hz, 1H), 4.94 (d, *J* = 9.5 Hz, 1H), 3.68 (s, 3H), 3.35 (dd, *J* = 5.4, 5.4 Hz, 1H), 3.08 (ddd, *J* = 13.8, 3.4, 3.4 Hz, 1H), 3.02 (dd, *J* = 12.5, 4.4 Hz, 1H), 2.88-2.75 (m, overlap, 2H), 2.49-2.30 (m, overlap, 4H), 2.20-2.05 (m, overlap, 5H), 1.13 (t, *J* = 7.3 Hz, 3H);

^{13}C NMR ($CDCl_3$, 125 MHz): δ 175.6, 145.4, 138.0, 135.8, 134.3, 127.8, 122.0, 121.5, 118.9, 118.2, 115.6, 111.8, 110.6, 60.3, 52.1, 51.9, 47.5, 38.7, 37.9, 34.7, 34.3, 27.3, 26.4, 12.8;

HRMS (ESI) *m/z* calculated for $C_{24}H_{31}N_2O_2^+$ ($[M+H]^+$) 379.2386, found 379.2390 ;

$[\alpha]_D^{26}$ = +5.2 (c 0.37, CH_2Cl_2)

(4S,7R,9S)-methyl 5-ethyl-4-(4-fluorophenyl)-2,4,7,8,9,10-hexahydro-1H-3,7-methano[1]azacycloundecino[5,4-b]indole-9-carboxylate (28)

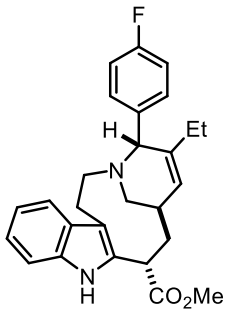

The general procedure afforded **28** (71%) as a white solid (rapidly colorizes on contact with air) after purification by chromatography on SiO_2 (19:1, hexanes/EtOAc).

R_f (9:1 hexanes/EtOAc): 0.26;

IR (neat): 3378, 2963, 2926, 2851, 1718, 1601, 1502, 1462, 1435, 1222, 1158, 736 cm^{-1};

^1H NMR ($CDCl_3$, 500 MHz): δ 8.57 (br. s, 1H), 7.45 (d, *J* = 7.8 Hz, 1H), 7.33 (d, *J* = 8.1 Hz, 1H) 7.23 (m, 2H), 7.14 (ddd, *J* = 8.1, 7.5 , 1.2 Hz, 1H), 7.06 (ddd, *J* = 7.8, 7.5, 0.7 Hz, 1H), 7.02 (m, 2H), 5.59 (d, *J* = 5.1 Hz, 1H), 5.01 (d, *J* = 9.5 Hz, 1H), 4.25 (s, 1H), 3.70 (s, 3H), 3.02 (ddd, *J* = 14.1, 3.0, 3.0 Hz, 1H), 2.97 (dd, *J* = 12.5, 3.9 Hz, 1H), 2.92-2.84 (m, overlap, 2H), 2.42 (ddd, *J* = 14.1, 9.7, 6.1 Hz, 1H), 2.32 (br. s, 1H), 2.16 (d, *J* = 13.9 Hz, 1H), 2.12 (d, *J* = 12.5 Hz, 1H) 2.00 (ddd, *J* = 13.9, 11.3, 2.4 Hz, 1H), 1.90 (q, *J* = 7.4 Hz, 2H), 1.06 (t, *J* = 7.4 Hz, 3H);

^{13}C NMR ($CDCl_3$, 125 MHz): δ 175.6, 162.1 (d, *J* = 245.2 Hz), 142.4, 135.8, 134.7, 134.3, 130.4 (d, *J* = 7.9 Hz), 127.8, 123.4, 121.6, 119.0, 118.2, 114.8 (d, *J* = 20.9), 112.0, 110.6, 63.3, 52.2, 50.0, 47.1, 38.7, 38.2, 47.1, 38.7, 38.2, 34.1, 27.0, 25.6, 12.5;

HRMS (ESI) *m/z* calculated for $C_{27}H_{25}FN_2O_2^+$ ($[M+H]^+$) 433.2291, found 433.2272;

$[\alpha]_D^{26}$ = +6.2 (c 0.50, CH_2Cl_2)

(4S,7R,9S)-methyl 5-ethyl-4-(4-methoxyphenyl)-2,4,7,8,9,10-hexahydro-1H-3,7-methano[1]azacycloundecino[5,4-b]indole-9-carboxylate (29)

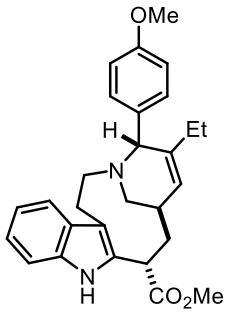

The general procedure afforded **29** (62%) as a white solid after purification by chromatography on SiO_2 (9:1, hexanes/EtOAc).

R_f (9:1 hexanes/EtOAc): 0.24;

IR (neat): 3385, 2959, 2926, 2841, 2720, 1607, 1506, 1462, 1250, 1174, 736 cm^{-1};

^1H NMR ($CDCl_3$, 500 MHz): δ 8.58 (br. s, 1H), 7.45 (d, *J* = 7.6 Hz, 1H), 7.33 (d, *J* = 7.6 Hz, 1H), 7.18 (d, *J* = 8.6 Hz, 2H), 7.14 (dd, *J* = 7.6, 7.2 Hz, 1H), 7.06 (dd, *J* = 7.6, 7.2 Hz, 1H), 6.87 (d, *J* = 8.6 Hz, 2H), 5.57 (d, *J* = 5.1 Hz, 1H), 5.05 (d, *J* = 9.5 Hz, 1H), 4.22 (s, 1H), 3.81 (s, 3H), 3.70 (s, 3H), 3.04 (ddd, *J* = 14.0, 3.1, 3.1 Hz, 1H), 2.99 (dd, *J* = 12.5, 4.2 Hz, 1H), 2.93-2.83 (m, overlap, 2H), 2.39 (ddd, *J* = 14.2, 9.8, 6.4 Hz, 1H), 2.31 (br. s, 1H), 2.16 (d, *J* = 13.9 Hz, 1H), 2.10 (d, *J* = 12.5 Hz, 1H), 2.00 (ddd, *J* = 13.9, 11.5, 2.4 Hz, 1H), 1.90 (q, *J* = 7.6 Hz, 2H), 1.04 (t, *J* = 7.6 Hz, 3H);

^{13}C NMR ($CDCl_3$, 125 MHz): δ 175.7, 158.7, 142.8, 135.7, 134.3, 131.2, 130.1, 127.9, 123.0, 121.5, 118.9, 118.2, 113.3, 112.1, 110.5, 63.3, 55.2, 52.1, 50.0, 47.3, 38.8, 38.2, 34.2, 27.1, 25.7, 12.6;

HRMS (ESI) *m/z* calculated for $C_{28}H_{33}N_2O_3^+$ ($[M+H]^+$) 445.2491, found 445.2489;

$[\alpha]_D^{26}$ = +7.2 (c 0.76, CH_2Cl_2)

(4S,7R,9S)-methyl 5-ethyl-4-(3-methoxyphenyl)-2,4,7,8,9,10-hexahydro-1H-3,7-methano[1]azacycloundecino[5,4-b]indole-9-carboxylate (30)

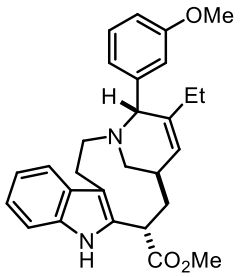

The general procedure afforded **30** (54%) as a white solid after purification by chromatography on SiO_2 (1:1, hexanes/CH_2Cl_2).

R_f (4:1 hexanes/EtOAc): 0.57;

IR (neat): 3375, 2925, 2854, 1718, 1597, 1581, 1461, 1434, 1250, 1159, 738 cm^{-1};

^1H NMR ($CDCl_3$, 500 MHz): δ 8.59 (br. s, 1H), 7.45 (d, *J* = 7.7 Hz, 1H), 7.35 (d, *J* = 7.2 Hz, 1H), 7.26 (dd, *J* = 7.8, 7.8 Hz, 1H), 7.16 (ddd, *J* = 7.8, 7.2, 1.1 Hz, 1H), 7.06 (ddd, *J* = 7.8, 7.7, 1.0 Hz, 1H), 6.87-6.81 (m, 3H), 5.59 (d, *J* = 5.4 Hz, 1H), 5.02 (d, *J* = 9.3 Hz, 1H), 4.24 (s, 1H), 3.82 (s, 3H), 3.70 (s, 3H), 3.10-3.04 (m, overlap, 2H), 2.93-2.83 (m, overlap, 2H), 2.40 (ddd, *J* = 14.2, 9.8, 6.1 Hz, 1H), 2.34 (br. s, 1H), 2.18-2.12 (m, overlap, 2H), 2.03 (ddd, *J* = 14.0, 11.4, 2.4 Hz, 1H), 1.92 (q, *J* = 7.6 Hz, 2H), 1.06 (t, *J* = 7.6 Hz, 3H);

^{13}C NMR ($CDCl_3$, 125 MHz): δ 175.7, 159.4, 142.4, 140.7, 135.7, 134.3, 128.8, 127.9, 123.2, 121.7, 121.5, 118.9, 118.2, 115.2, 112.0, 111.8, 110.5, 63.9, 55.2, 52.1, 50.0, 47.4, 38.8, 38.2, 34.1, 27.1, 25.6, 12.6;

HRMS (ESI) *m/z* calculated for $C_{28}H_{33}N_2O_3^+$ ($[M+H]^+$) 445.2491, found 445.2485;

$[\alpha]_D^{26}$ = +13.1 (c 0.93, CH_2Cl_2)

(4S,7R,9S)-methyl 5-ethyl-4-(phenylethynyl)-2,4,7,8,9,10-hexahydro-1H-3,7-methano[1]azacycloundecino[5,4-b]indole-9-carboxylate (32)

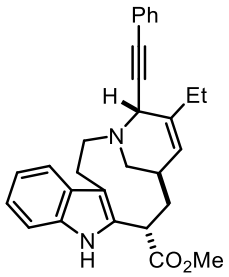

The general procedure afforded **32** (50%) as a white solid after purification by chromatography on SiO_2 (19:1 hexanes/EtOAc).

R_f (4:1 hexanes/Et_2O): 0.52;

IR (neat): 3387, 3054, 2964, 2924, 2850, 1718, 1462, 1247, 1160, 740 cm^{-1};

^1H NMR ($CDCl_3$, 500 MHz): δ 8.58 (br. s, 1H), 7.52 (d, *J* = 7.8 Hz, 1H), 7.41-7.39 (m, 2H), 7.35 (ddd, *J* = 8.0, 1.0, 0.9 Hz, 1H), 7.29-7.26 (m, 3H), 7.17 (ddd, *J* = 8.0, 7.0, 1.2 Hz, 1H), 7.11 (ddd, *J* = 7.8, 7.0, 1.0 Hz, 1H), 5.39 (d, *J* = 4.9 Hz, 1H), 5.07 (d, *J* = 9.8 Hz, 1H), 4.20 (s, 1H), 3.69 (s, 3H), 3.04 (ddd, *J* = 13.9, 4.2, 2.9 Hz, 1H), 2.98-2.86 (m, overlap, 2H), 2.47-2.20 (m, overlap, 6H), 2.12 (d, *J* = 13.9 Hz, 1H), 1.19 (t, *J* = 7.5 Hz, 3H);

^{13}C NMR ($CDCl_3$, 125 MHz): δ 175.6, 141.1, 135.8, 134.3, 131.7, 128.2, 127.9, 127.8, 123.4, 121.6, 119.0, 118.2, 111.6, 110.6, 88.1, 83.7, 55.0, 52.1, 51.6, 48.8, 38.5, 38.1, 34.2, 26.7, 26.1, 12.4;

HRMS (ESI) *m/z* calculated for $C_{29}H_{31}N_2O_2^+$ ($[M+H]^+$) 439.2386, found 439.2406;

$[\alpha]_D^{26}$ = -51.5 (c 0.81, CH_2Cl_2)

(4S,7R,9S)-methyl 5-ethyl-4-((trimethylsilyl)ethynyl)-2,4,7,8,9,10-hexahydro-1H-3,7-methano[1]azacycloundecino[5,4-b]indole-9-carboxylate (30)

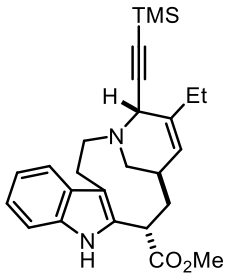

The general procedure afforded **30** (61%) as a white solid after purification by chromatography on SiO_2 (CH_2Cl_2).

R_f (4:1 hexanes/EtOAc): 0.47;

IR (neat): 3386, 2962, 2926, 2852, 2155, 1718, 1462, 1434, 1337, 1249, 1159, 824, 739 cm^{-1};

^1H NMR ($CDCl_3$, 500 MHz): δ 8.58 (br. s, 1H), 7.53 (d, *J* = 7.7 Hz, 1H), 7.35 (d, *J* = 7.7 Hz, 1H), 7.17 (dd, *J* = 7.7, 7.5 Hz, 1H), 7.11 (dd, *J* = 7.7, 7.5 Hz, 1H), 5.35 (d, *J* = 4.2 Hz, 1H), 5.03 (d, *J* = 10.0 Hz, 1H), 3.98 (s, 1H), 3.68 (s, 3H), 2.97-2.92 (m, overlap, 2H), 2.86-2.80 (m, overlap, 2H), 2.39-2.34 (m, overlap, 2H), 2.27-2.07 (m, overlap, 5H) 1.15 (t, *J* = 7.3 Hz, 3H), 0.17 (s, 9H);

^{13}C NMR ($CDCl_3$, 125 MHz): δ 175.3, 140.7, 135.5, 134.1, 127.6, 122.9, 121.4, 118.8, 118.0, 111.4, 110.4, 104.4, 87.4, 55.0, 51.9, 51.2, 48.3, 38.3, 37.8, 33.9, 26.4, 25.8, 12.2, 0.0;

HRMS (ESI) *m/z* calculated for $C_{26}H_{35}N_2O_2Si^+$ ($[M+H]^+$) 435.2468, found 435.2470 ;

$[\alpha]_D^{26}$ = -23.8 (c 0.32, CH_2Cl_2)

(4S,7R,9S)-methyl 5-ethyl-4-(p-tolyl)-2,4,7,8,9,10-hexahydro-1H-3,7-methano[1]azacycloundecino[5,4-b]indole-9-carboxylate (27)

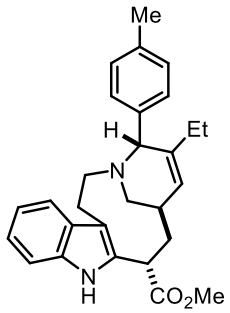

The general procedure afforded **27** (60%) as a white solid after purification by chromatography on SiO_2 (CH_2Cl_2).

R_f (20% EtOAc in hexanes): 0.53;

IR (neat): 3382, 2923, 2858, 1718, 1515, 1462, 1435, 1335, 1250, 1161, 739 cm^{-1};

^1H NMR ($CDCl_3$, 500 MHz): δ 8.57 (br. s, 1H), 7.44 (d, *J* = 7.9 Hz, 1H), 7.33 (d, *J* = 8.1 Hz, 1H), 7.15-7.12 (m, overlap, 5H), 7.06 (ddd, *J* = 7.9, 7.0, 1.2 Hz, 1H), 5.57 (d, *J* = 5.4 Hz, 1H), 5.04 (d, *J* = 9.3 Hz, 1H), 4.23 (s, 1H), 3.70 (s, 3H), 3.07-3.00 (m, overlap, 2H), 2.92-2.82 (m, overlap, 2H), 2.42-2.29 (m, overlap, 5H), 2.16 (d, *J* = 13.9 Hz, 1H), 2.11 (d, *J* = 12.7 Hz, 1H), 2.00 (ddd, *J* = 14.2, 11.5, 2.4 Hz, 1H), 1.89 (q, *J* = 7.4 Hz, 2H), 1.04 (t, *J* = 7.4 Hz, 3H);

^{13}C NMR ($CDCl_3$, 125 MHz): δ 175.7, 142.7, 136.6, 135.9, 135.7, 134.3, 129.0, 128.7, 127.9, 123.0, 121.5, 118.9, 118.2, 112.1, 110.5, 63.6, 52.1, 50.0, 47.3, 38.8, 38.2, 34.2, 27.1, 25.6, 21.1, 12.5;

HRMS (ESI) *m/z* calculated for $C_{28}H_{33}N_2O_2^+$ ($[M+H]^+$) 429.2542, found 429.2541 ;

$[\alpha]_D^{26}$ = +3.9 (c 0.82, CH_2Cl_2)

Procedure for the formation of (–)-pseudotabersonine:

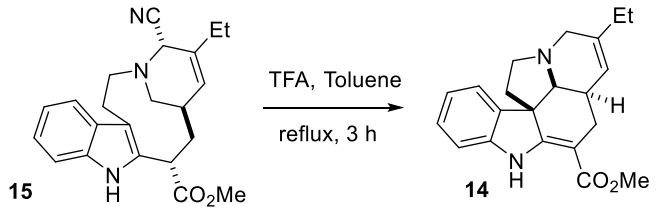

To a flame dried 2-dram vial with a stir bar was added starting material **15** (0.1 mmol, 36.4 mg) and dry toluene (2.0 ml, 0.05M). The solution of starting material was degassed *via* three cycles of freeze pump thaw under a nitrogen atmosphere. Trifluoroacetic acid (0.1 mmol, 8 μl) was added and the reaction was heated to reflux under nitrogen with a stream of air concentrated on the outside of the upper half of the vial to ensure condensation. Reaction progress was monitored by TLC, but the consumption of starting material is difficult to follow due to proposed stoichiometric ionization to the iminium ion. After three hours, the reaction had formed one major spot off the baseline with 20% EtOAc in hexanes as the TLC mobile phase. The reaction was diluted with ethyl acetate and poured into saturated sodium bicarbonate. The organic phase was separated, and the aqueous phase was extracted three times with ethyl acetate. The combined organic layers were washed with brine, dried over sodium sulfate, and concentrated to provide a crude yellow oil. Purification on SiO_2 with 5% EtOAc in hexanes provided (–)-pseudotabersonine **14** (30.3 mg, 90%) as an amorphous solid.

(–)-pseudotabersonine (14)[92,108]

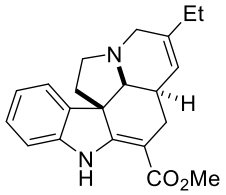

R_f (20% EtOAc in hexanes): 0.53;

IR (neat): 3362, 3052, 2960, 2874, 1728, 1672, 1606, 1477, 1464, 1435, 1238, 1201, 1117, 735 cm^{-1};

^{1}H NMR ($CDCl_3$, 500 MHz): δ 8.99 (br. s, 1 H), 7.31 (d, *J* = 7.1 Hz, 1H), 7.16 (dd, *J* = 7.6, 7.5 Hz, 1H), 6.89 (dd, *J* = 7.5, 7.1 Hz, 1H), 6.83 (d, *J* = 7.6 Hz, 1H), 5.52 (d, *J* = 4.1 Hz, 1H), 3.78 (s, 3H), 3.37 (d, *J* = 16.5 Hz, 1H), 3.28 (d, *J* = 16.5 Hz, 1H), 3.05-3.02 (m, overlap, 2H), 2.82-2.78 (m, 1H), 2.68 (d, *J* = 14.8, 3.1 Hz, 1H), 2.16 (dd, *J* = 14.8, 11.5 Hz, 1H), 2.10-2.04 (m, overlap, 3H), 1.91 (ddd, *J* = 11.5, 4.9, 1.5 Hz, 1H), 1.77 (br. s, 1H), 1.07 (t, *J* = 7.4 Hz, 3H);

^{13}C NMR ($CDCl_3$, 175 MHz): δ 168.7, 165.9, 143.6, 139.3, 138.0, 127.7, 121.8, 121.4, 120.6, 109.1, 95.5, 65.2, 55.5, 53.2, 51.0, 51.0, 44.4, 36.8, 27.8, 26.3, 12.5;

HRMS (ESI) *m/z* calculated for $C_{21}H_{25}N_2O_2^+$ ($[M+H]^+$) 337.1911, found 337.1913

$[\alpha]_D^{26}$ = -171.6 (c 1.0, MeOH) lit.[108] $[\alpha]_D^{26}$ = +320 (MeOH)

Carbomethoxy cleavamine (33)[88]

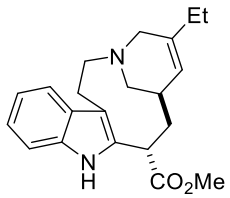

^{1}H NMR ($CDCl_3$, 500 MHz): δ 8.58 (br. s, 1H), 7.52 (d, *J* = 7.6 Hz, 1H), 7.34 (d, *J* = 8.0 Hz, 1H), 7.16 (dd, *J* = 8.0, 7.7 Hz, 1H), 7.10 (dd, *J* = 7.7, 7.6 Hz, 1H), 5.30 (d, *J* = 5.4 Hz, 1H), 5.18 (d, *J* = 10.3 Hz, 1H), 3.67 (s, 3H), 3.18 (d, *J* = 15.5 Hz, 1H), 3.09 (d, *J* = 15.5 Hz, 1H), 2.92-2.83 (m, overlap, 2H), 2.74 (ddd, *J* = 13.6, 3.0, 3.0 Hz, 1H), 2.42-2.32 (m, overlap, 4H), 2.19 (br. s, 1H), 2.11-2.05 (m, overlap, 3H), 1.09 (t, *J* = 7.6 Hz, 3H)

21-cyanopseudotabersonine (34)

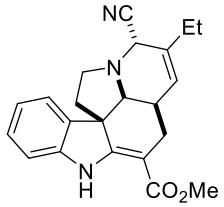

IR (neat): 3367, 2924, 2853, 1731, 1677, 1608, 1465, 1239, 1203, 748 cm^{-1};

^{1}H NMR ($CDCl_3$, 500 MHz): δ 8.92 (br. s, 1H), 7.33 (d, 7.5 Hz, 1H), 7.16 (ddd, *J* = 7.7, 7.6, 1.2 Hz, 1H), 6.90 (ddd, *J* = 7.6, 7.5, 0.9 Hz, 1H), 6.82 (d, *J* = 7.7 Hz, 1H), 5.71 (dd, *J* = 5.3, 1.5 Hz, 1H), 4.33 (s, 1H), 3.76 (s, 3H), 3.38 (d, *J* = 3.6 Hz, 1H), 3.07-3.01 (m, overlap, 2H), 2.66 (ddd, *J* = 14.9, 3.6, 1.4 Hz, 1H), 2.29-2.24 (m, 1H), 2.16-2.10 (m, overlap, 2H), 2.04 (ddd, *J* = 11.7, 11.5, 6.6 Hz, 1H), 1.90 (dd, *J* = 11.7, 3.7 Hz, 1H), 1.84 (br. m., 1H), 1.12 (t, *J* = 7.4, 3H);

^{13}C NMR ($CDCl_3$, 175 MHz): δ 168.5, 165.4, 143.5, 137.0, 135.0, 128.3, 126.4, 122.2, 121.2, 116.5, 109.5, 95.5, 60.9, 54.7, 53.6, 51.2, 48.4, 43.9, 37.4, 26.4, 24.7, 12.2;

HRMS (ESI) *m/z* calculated for $C_{22}H_{24}N_3O_2^+$ ($[M+H]^+$) 362.1881, found 362.1863

$[\alpha]_D^{26}$ = -25.2 (c 0.19, $CHCl_3$)

Formation of pseudotabersonine from 33 and 34

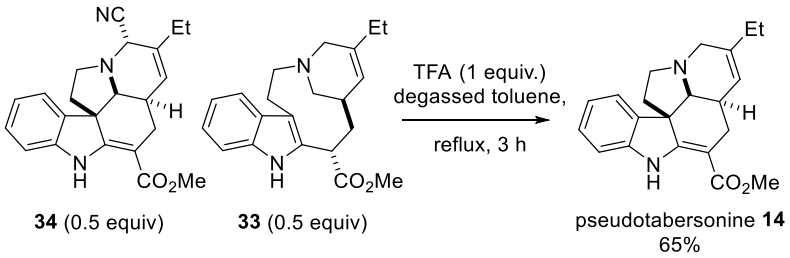

Cyanated pseudotabersonine **34** (18.1 mg, 0.05 mmol, 0.5 equiv) and reduced fragmentation product **33** (16.9 mg, 0.05 mmol, 0.5 equiv) were combined in a 2 dram vial equipped with a stir bar and a septum screw top. Toluene (2 ml) was added to the vial and the solution was degassed *via* the freeze-pump-thaw method (3 cycles) and the vial was back-filled with nitrogen. TFA (7.6 µl, 0.1 mmol, 1 equiv) was added to the reaction and the vial was placed on a pre-equilibrated heating block set to 120 °C. Upon TFA addition the reaction turned a slightly yellow-brown color, and some precipitate could be observed. A slow stream of air was directed at the top of the sealed vial to facilitate solvent condensation. The reaction was stirred for 3 hours at reflux, after which the reaction mixture was diluted with ethyl acetate and poured into saturated sodium bicarbonate. The combined organic layers were washed with brine, dried over sodium sulfate, and concentrated to provide a crude yellow oil. Purification on SiO_2 with 5% EtOAc in hexanes provided pseudotabersonine **14** (22.0 mg, 65% yield) as an amorphous solid.

Preparation of Near-Racemic pseudotabersonine for HPLC Reference:

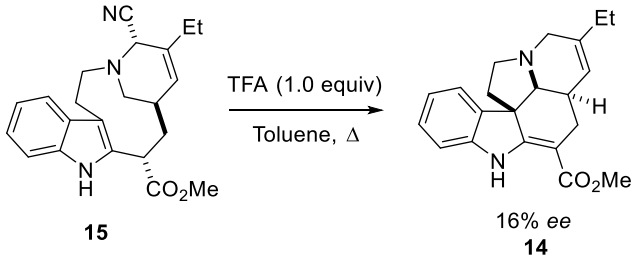

15 16% *ee*
14

Crude, solid α-aminonitrile **15** from the flow fragmentation procedure was placed on filter paper in a Buchner funnel inserted in a side-arm Erlenmeyer flask attached to house vacuum. The solid was washed with ice-cold methanol until the faint-yellow color was removed from the sample. The solution of filtrate was concentrated to a yellow foam constituted by the α-aminonitrile **15** with impurities. This impure material (457 mg, ~1.26 mmol) was suspended in anhydrous toluene (25 ml, 0.05M) in a flame-dried 50 ml round-bottom flask attached to a reflux condenser and degassed *via* the freeze pump-thaw method (3 cycles) and the flask back-filled with nitrogen. To the solution was added trifluoroacetic acid (96 µl, 1.26 mmol, 1.0 equiv) and the reaction was placed on a heating block pre-equilibrated to 135 degrees. The reaction was stirred for 14 hours under nitrogen. Upon completion, the reaction was diluted with ethyl acetate and poured into saturated aqueous sodium bicarbonate solution. The organic phase was removed and the aqueous phase was washed with ethyl acetate (x3). The combined organic phase was washed with brine and dried over sodium sulfate before concentrating. Purification on SiO_2 with 5% EtOAc in hexanes provided pure pseudotabersonine **14** (43.0 mg, 10% yield, 16% *ee*, $[\alpha]_D^{26}$ = -63.1 (c 1.0, MeOH)) along with a number of mixed fractions.

Synthesis of (+)-coronaridine:

Hydrogenation of 15 to generate 35:

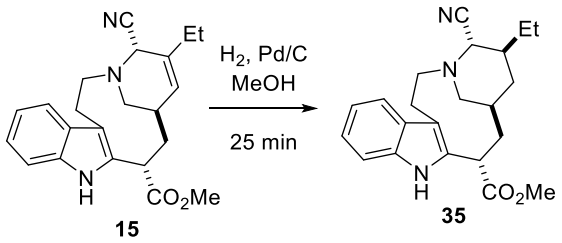

Fragmentation product **15** (50.0 mg, 0.14 mmol) was placed in a 10 ml round-bottom flask with 10% palladium on carbon (20 mg). The flask was evacuated and back-filled with nitrogen three times, after which methanol was added to the flask (2 ml). Hydrogen was bubbled through the reaction from a balloon for 25 minutes, venting the flask with a needle through the septum. After 25 minutes the reaction mixture was promptly filtered through celite with ethyl acetate, and the filtrate was concentrated to yield chromatographically unstable **35** as the major product. Reaction time had been determined previously by taking aliquots for HNMR analysis, as the reaction is unable to be monitored by TLC. Longer reaction times result in de-cyanation of the product, as well as epimerization of the ethyl group. The product was found to be unstable to purification on silica gel, and so the crude material was brought on to the next step without purification.

Conversion of 35 to (+)-coronaridine:

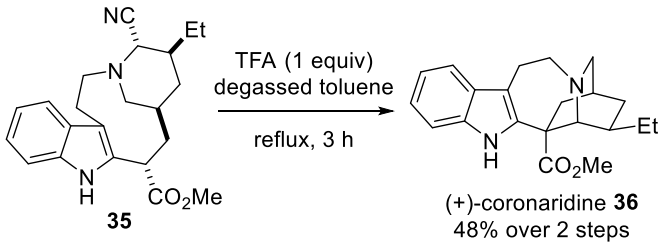

Crude hydrogenation product **35** (0.14 mmol) was placed in a 2 dram vial equipped with a stir bar and a septum screw top. Toluene (2.75 ml) was added to the vial and the solution was degassed *via* the freeze-pump-thaw method (3 cycles) and the vial was back-filled with nitrogen. TFA (10.5 μl, 0.14 mmol, 1 equiv) was added to the reaction and the vial was placed on a pre-equilibrated heating block set to 120 °C. Upon TFA addition the reaction turned a slightly yellow-brown color, and some precipitate could be observed. A slow stream of air was directed at the top of the sealed vial to facilitate solvent condensation. The reaction was stirred for 3 hours at reflux, after which the reaction mixture was diluted with ethyl acetate and poured into saturated sodium bicarbonate. The combined organic layers were washed with brine, dried over sodium sulfate, and concentrated to provide a crude yellow oil. Purification of the crude material on SiO_2 with 5% EtOAc in hexanes provided (+)-coronaridine **36** (22.0 mg, 48% yield) as an amorphous solid. Treatment with ethereal HCl provided the hydrochloride salt.

(+)-coronaridine (36)[109,110]

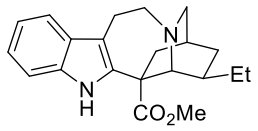

R_f (freebase, 25% EtOAc in hexanes): 0.50;

IR (freebase, neat): 3375, 2951, 2926, 2856, 1709, 1459, 1434, 1250, 739 cm^{-1};

^{1}H NMR (HCl, CD_3OD, 700 MHz): 7.48 (d, *J* = 8.0 Hz, 1H), 7.33 (d, *J* = 8.0 Hz, 1H), 7.12 (ddd, *J* = 8.0, 8.0, 0.9 Hz, 1H), 7.05 (ddd, *J* = 8.0, 8.0, 0.7 Hz, 1H), 4.58 (s, 1H), 4.05 (ddd, *J* = 12.9, 5.3, 3.8 Hz, 1H), 3.76 (s, 3H), 3.52 (ddd, *J* = 16.5, 11.5, 5.3 Hz, 1H) 3.47 (ddd, *J* = 11.5, 4.2, 2.4 Hz, 1H), 3.41 (ddd, *J* = 12.9, 12.8, 4.6 Hz, 1H), 3.24 (ddd, *J* = 16.5, 4.3, 4.2 Hz, 1H), 3.89 (br. d, *J* = 11.6 Hz, 1H), 2.73 (ddd, *J* = 14.0, 1.7, 1.7 Hz, 1H), 2.39 (ddd, *J* = 14.0, 4.6, 2.0 Hz, 1H), 2.21 (br. d, *J* = 3.8 Hz, 1H), 2.09 (m, 1H), 1.81-1.67 (m, overlap, 3H), 1.37 (dd, *J* = 13.9, 8.4 Hz, 1H), 1.03 (t, *J* = 7.2 Hz);

^{13}C NMR (free base, $CDCl_3$, 175 MHz): δ 175.7, 136.6, 135.4, 128.8, 121.9, 119.2, 118.4, 110.31, 110.30, 57.5, 55.1, 53.1, 52.6, 51.5, 39.1, 36.5, 32.0, 27.4, 26.7, 22.1, 11.6;

HRMS (ESI) *m/z* calculated for $C_{21}H_{27}N_2O_2^+$ ($[M+H]^+$) 339.2067, found 339.2068

$[\alpha]_D^{26}$ = +6.0 (HCl salt c 1.0 MeOH) lit.[109] $[\alpha]_D^{26}$ = -8.5 (HCl salt c 1.0 $CHCl_3$)

Synthesis of dihydrocatharanthine 37:[102]

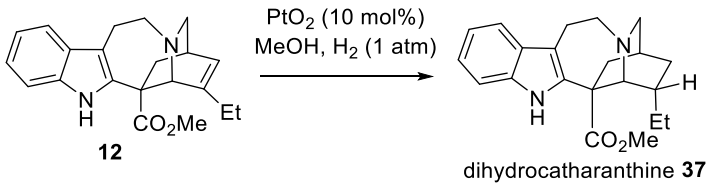

Freshly free-based catharanthine **12** (42.8 mg, 0.13 mmol, 1.0 equiv) was placed in a 10 ml round-bottom flask and PtO_2 (2.9 mg, 0.013 mmol, 0.1 equiv) was added. The flask was evacuated and backfilled three times with nitrogen gas before methanol (2.5 ml) was added. The solution was sparged for 5 minutes from a hydrogen balloon. During this time, the suspended PtO_2 turned from brown to black. The reaction was complete by TLC after 24 hours. The reaction mixture was filtered through celite with ethyl acetate and concentrated to yield pure dihydrocatharanthine **37** as a white foam (40.2 mg, 93% yield)

Dihydrocatharanthine (37)[102]

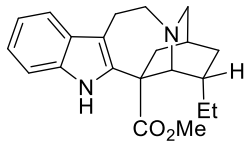

R_f (40% EtOAc in hexanes, 5 drops Et_3N/10 ml): 0.61;

IR (neat): 3372, 2928, 2857, 1706, 1460, 1433, 1250, 1172, 740 cm^{-1};

^1H NMR ($CDCl_3$, 500 MHz): δ 7.76 (br. s, 1H), 7.50 (d, *J* = 7.5 Hz, 1H), 7.25 (d, *J* = 7.7 Hz, 1H), 7.16 (dd, *J* = 7.7, 7.4, 1H), 7.11 (dd, *J* = 7.5, 7.4 Hz, 1H), 3.82 (br. s, 1H), 3.67 (s, 3H), 3.60-3.56 (m, 1H), 3.18-3.12 (m, overlap, 2H), 3.10-3.05 (m, overlap, 2H), 2.83 (d, *J* = 8.9 Hz, 1H), 2.65 (d, *J* = 13.1 Hz, 1H), 2.11 (br. s, 1H), 1.99-1.93 (m, overlap, 3H), 1.37 (ddd, *J* = 12.9, 7.1, 5.2 Hz, 1H), 1.18 (d, *J* = 11.2 Hz, 1H), 1.05 (ddd, *J* = 12.9, 10.7, 7.1 Hz, 1H), 0.93 (t, *J* = 7.1 Hz, 3H);

^{13}C NMR ($CDCl_3$, 175 MHz): δ 175.6, 137.1, 135.3, 128.5, 121.9, 119.2, 118.4, 110.40, 110.35, 56.3, 53.1, 52.4, 52.2, 51.3, 43.9, 37.1, 31.5, 27.34, 27.30, 21.7, 12.6;

HRMS (ESI) *m/z* calculated for $C_{21}H_{27}N_2O_2^+$ ($[M+H]^+$) 339.2067, found 339.2056

$[\alpha]_D^{26}$ = +37 (c 1.0 $CHCl_3$) lit. $[\alpha]_D^{26}$ = +33 (c 1.0 $CHCl_3$)[102]

Synthesis of pseudovincadifformine 39:

Hydrogenation of 15 to generate 38:[111]

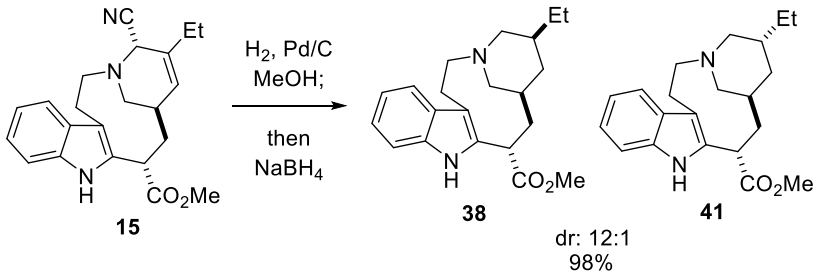

Fragmentation product **15** (430 mg, 1.16 mmol) was placed in a 25 ml pear-shaped flask with 10% palladium on carbon (252 mg, 20 mol%). The flask was evacuated and back-filled with nitrogen three times, after which methanol was added to the flask (16 ml). Hydrogen was bubbled through the reaction from a balloon for 25 minutes, venting the flask with a needle through the septum. After 25 minutes the reaction mixture was cooled to zero degrees and $NaBH_4$ (179 mg, 4.0 equiv) was added in one portion. The reaction was allowed to stir for ten minutes at zero degrees before it was run through a column of celite, washed through with ethyl acetate, and concentrated to form a light yellow amorphous solid. This material was pure by HNMR (395 mg, 98% yield). Purification on silica gel (5% EtOAc in hexanes to 30% EtOAc in hexanes to 100% EtOAc) resulted in decolorization of the material with a significant loss in yield (126 mg recovered, 31% yield) possibly due to oxidative decomposition.

methyl (5S,7S,9S)-5-ethyl-1,4,5,6,7,8,9,10-octahydro-2H-3,7-methano[1]azacycloundecino[5,4-b]indole-9-carboxylate (**38)**

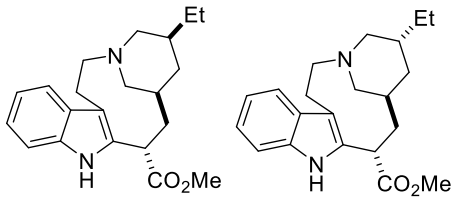

dr: 12:1

IR (neat): 3381, 2917, 1723, 1461, 1433, 1251, 1158, 738 cm^{-1};

^{1}H NMR ($CDCl_3$, 500 MHz, mixture of diastereomers): 8.64 (br. s, 1H), 8.59 (br. s, 0.14H), 7.50 (app. d, overlap, 1.2H), 7.35 (app. d, overlap, 1.2H), 7.16 (app. t, overlap, 1.3H), 7.09 (app. t, overlap, 1.2H), 5.55 (d, 11.7 Hz, 0.08 H), 5.09 (d, *J* = 10.3 Hz, 1H), 3.72 (s, overlap, 3.6), 2.92-2.87 (m, overlap, 2.5H), 2.68 (dd, *J* = 9.0, 9.0 Hz, 1H), 2.54-2.47 (m, overlap, 2.2H), 2.35-2.26 (m, overlap, 2.5H), 2.26-2.11 (m, overlap, 1.34H), 2.07 (app. d, overlap, 1.2H), 1.87-1.81 (m, overlap, 1.87-1.80, 2.5H), 1.55-1.48 (m, overlap, 2.2H), 1.37-1.28 (m, overlap, 4H), 0.91 (app. t, overlap, 3.4 H);

^{13}C NMR ($CDCl_3$, 175 MHz): δ 175.5, 135.9, 133.9, 127.7, 121.5, 119.0, 118.2, 111.9, 110.6, 59.0, 52.1, 51.8, 51.2, 38.6, 37.6, 34.8, 32.1, 31.0, 28.7, 26.5, 11.7;

HRMS (ESI) *m/z* calculated for $C_{21}H_{27}N_2O_2^+$ ($[M+H]^+$) 341.2224, found 341.2225

$[\alpha]_D^{26}$ = -84.46 (c 1.0, $CHCl_3$)

Conversion of 38 to (–)-pseudovincadifformine:

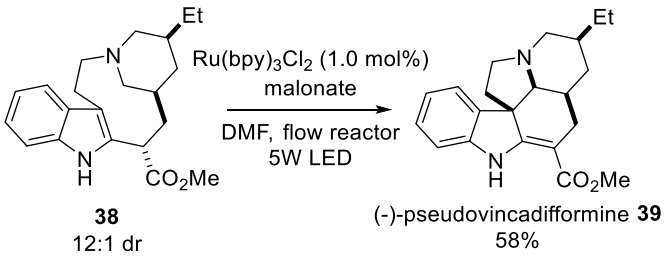

Tertiary amine **38** (34 mg, 0.1 mmol) and $Ru(bpy)_3Cl_2$ (0.6 mg, 1 mol%) were placed in a 2-dram vial equipped with a septum and dissolved in dry DMF (1.0 ml). This solution was degassed *via* the freeze-pump-thaw method (x3) and backfilled with nitrogen. Diethyl 2-bromo-2-methylmalonate (57.3 µl, 75.9 mg, 0.3 mmol, 3 equiv) was added to the solution. A flow photoreactor with a 670 µl internal volume was placed ~1 cm from the LED light source and allowed to warm to 50-55 ˚C. The reaction mixture was then flowed through the reactor at a rate of 134 µl/min (5 minute residence time). Upon complete uptake of the reaction mixture by the pump (nitrogen is beginning to be pumped through the reactor tubing), an additional 0.5 ml of DMF was added to the reactor input flask to minimize transfer loss. Upon complete elution of all solvent, the reaction was diluted with ethyl acetate and partitioned with water. 2 ml of triethylamine were added to the separatory funnel, and the mixture was extracted with ethyl acetate (x3). The combined organic phases were washed with brine before drying over sodium sulfate and concentrating. Purification on SiO_2 under nitrogen with nitrogen-sparged solvent (5% EtOAc in hexanes) provided (–)-pseudovincadifformine **39** (19.5 mg, 58% yield) as an amorphous solid.

(–)-pseudovincadifformine (39)[112]

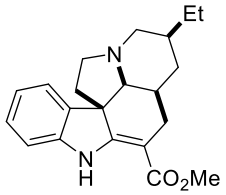

IR (neat): 3367, 2927, 2779, 1675, 1608, 1465, 1436, 1241, 1199, 1119, 743 cm^{-1};

^{1}H NMR ($CDCl_3$, 500 MHz): δ 8.94 (br. s), 7.24 (d, *J* = 7.3 Hz, 1H), 7.15 (ddd, *J* = 7.7, 7.5, 1.0 Hz, 1H), 6.88 (dd, *J* = 7.5, 7.3 Hz, 1H), 6.81 (d, *J* = 7.7 Hz, 1H), 3.77 (s, 3H), 3.00 (d, *J* = 4.1 Hz, 1H), 2.92 (dd, *J* = 8.4, 6.2 Hz, 1H), 2.84 (d, *J* = 5.8 Hz, 2H), 2.69 (ddd, *J* = 11.4, 8.5, 4.3 Hz, 1H), 2.54 (dd, *J* = 14.6, 2.9 Hz, 1H), 2.30 (dd, *J* = 14.6, 11.7 Hz, 1H), 2.02 (ddd, *J* = 11.5, 11.5, 6.2 Hz, 1H), 1.81-1.76 (m, overlap, 2H), 1.66-1.62 (br. m, 1H), 1.54-1.45 (m, overlap, 2H), 1.43-1.38 (m, overlap, 2H), 0.93 (t, *J* = 7.4 Hz, 3H);

^{13}C NMR ($CDCl_3$, 175 MHz): δ 168.6, 165.8, 143.5, 137.9, 127.6, 121.8, 120.4, 109.1, 96.1, 66.0, 55.2, 54.9, 51.4, 50.9, 44.2, 36.2, 35.5, 32.5, 28.7, 26.5, 12.4;

HRMS (ESI) *m/z* calculated for $C_{21}H_{27}N_2O_2^+$ ($[M+H]^+$) 339.2067, found 339.2076

$[\alpha]_D^{26}$ = -460 (c 0.24, EtOH) lit. $[\alpha]_D^{26}$ = -506 (c 0.62 EtOH)

Fragmentation of dihydrocatharanthine 37:

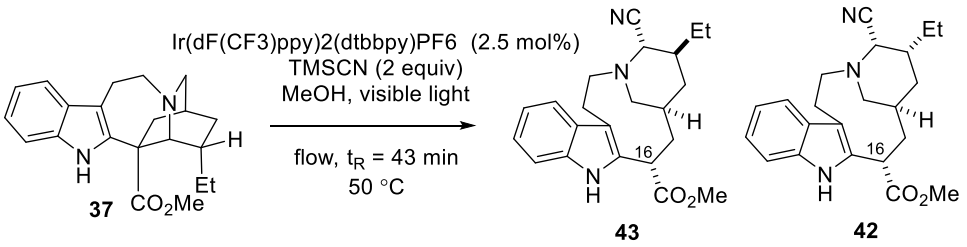

The flow reaction apparatus was set up with the reactor ~1.0 cm away from the LED puck. A thermometer was placed inside one of the test tubes to accurately measure the internal reaction temperature, and the temperature was regulated to 50 °C using a slow stream of air directed at the reactor. Dihydrocatharanthine **37** (33.9 mg, 0.1 mmol, 1.0 equiv) was placed in a 5ml round-bottom flask. $Ir(dF(CF_3)ppy)_2(dtbbpy)PF_6$ (2.8 mg, 2.5 mol%) was then added to the flask before the addition of methanol (1.0 ml). The resulting solution was degassed *via* the freeze-pump-thaw method (3 cycles) and the flask was backfilled with nitrogen. TMSCN (25 μl, 0.2 mmol, 2.0 equiv) was added to the solution. The reaction mixture was then pumped through the photoreactor at a flow rate of 32.2 μl/min (t_R = 43 minutes) and collected in a 25 ml round bottom flask. Upon complete uptake of the reaction solution an additional 0.5 ml of methanol was added to the reaction flask to rinse any residue through the reactor. Upon elution the reaction mixture was poured into a separatory funnel containing a mixture of saturated $NaHCO_3$ and water. The resulting solution was extracted with EtOAc (x3). The combined organic layers were washed with brine, dried (Na_2SO_4) and concentrated. Crude ^{1}HNMR analysis in $CDCl_3$ revealed two distinct doublets (δ 4.77 and δ 5.20, **42** and **43** respectively) corresponding to the C16 benzylic methine (see above) present in the ring opened products. Yields were determined for each residence time by ^{1}HNMR with diethyl phenylmalonate as an internal standard.

t_R = 42 minutes 8.3:1 dr **42**:**43**, 37% yield.

All attempts to isolate α-aminonitrile **42** or **43** through column chromatography on both SiO_2 and neutral Al_2O_3 were met with decomposition. Further confirmation of the structure of **42** was obtained through further reductive decyanation of the product to compound **38** with sodium borohydride in a manner identical to the procedure described for the coronaridine fragmentation products.

Fragmentation of coronaridine 36:

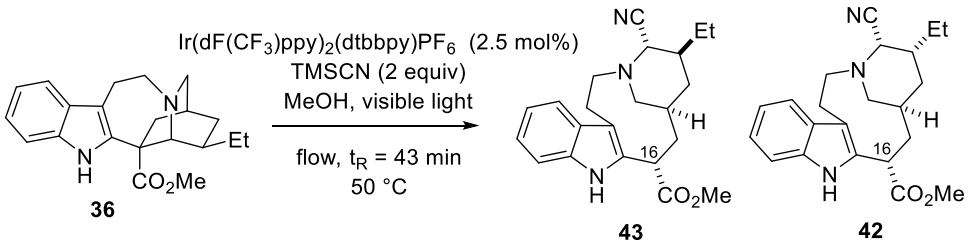

The flow reaction apparatus was set up with the reactor ~1.0 cm away from the LED puck. A thermometer was placed inside one of the test tubes to accurately measure the internal reaction temperature, and the temperature was regulated to 50 °C using a slow stream of air directed at the reactor. Coronaridine **36** (33.9 mg, 0.1 mmol, 1.0 equiv) was placed in a 5ml round-bottom flask. $Ir(dF(CF_3)ppy)_2(dtbbpy)PF_6$ (2.8 mg, 2.5 mol%) was then added to the flask before the addition of methanol (1.0 ml). The resulting solution was degassed *via* the freeze-pump-thaw method (3 cycles) and the flask was backfilled with nitrogen. TMSCN (25 μl, 0.2 mmol, 2.0 equiv) was added to the solution. The reaction mixture was then pumped through the photoreactor at a flow rate of 32.2 μl/min (t_R = 43 minutes) and collected in a 25 ml round bottom flask. Upon complete uptake of the reaction solution an additional 0.5 ml of methanol was added to the reaction flask to rinse any residue through the reactor. Upon elution the reaction mixture was poured into a separatory funnel containing a mixture of saturated $NaHCO_3$ and water. The resulting solution was extracted with EtOAc (x3). The combined organic layers were washed with brine, dried (Na_2SO_4) and concentrated. Crude ^{1}HNMR analysis in $CDCl_3$ revealed two distinct doublets (δ 4.77 and δ 5.20, **42** and **43** respectively) characteristic of the C16 benzylic methine (see above) present in the ring opened products. Yields were determined for each residence time by ^{1}HNMR with diethylphenyl malonate as an internal standard.

t_R = 42 minutes 1:12 dr **42**:**43**, 25% yield.

Further confirmation of the structure of **42** was obtained through further reduction of the product to the known compound **38**.

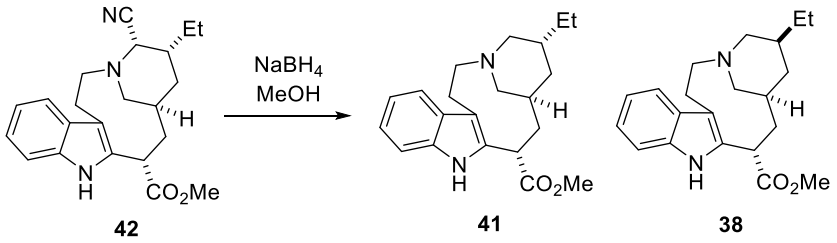

42 **41** **38**

The above fragmentation protocol was repeated on a 0.25 mmol scale without the final addition of the diethyl phenyl malonate as an internal standard. The crude reaction mixture was dissolved in 2.5 ml of methanol and cooled to zero degrees in an ice bath. Sodium borohydride (37.7 mg, 1.0 mmol, 4.0 equiv) was added in one portion and the reaction was allowed to stir for 20 minutes at zero degrees, at which point the reaction was removed from the ice bath and stirred for an additional 20 minutes. The reaction mixture was poured into saturated sodium bicarbonate, and the resulting solution was extracted with ethyl acetate (x3). The organic phases were combined and washed with brine before drying over sodium sulfate and concentrating.

The crude reaction mixture was purified on silica gel with a gradient of 100% hexanes to 20% ethyl acetate 80% hexanes to yield known compound **41** (16.1 mg, 19% yield, 6:1 dr **41**:**38**, 2 steps).

methyl (5R,7S,9S)-5-ethyl-1,4,5,6,7,8,9,10-octahydro-2H-3,7-methano[1]azacycloundecino[5,4-b]indole-9-carboxylate (41)

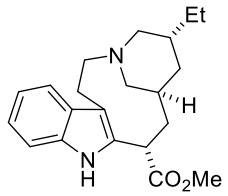

IR (neat): 3381, 2917, 1716, 1460, 1433, 1335, 1258, 1154, 909, 739 cm^{-1};

^{1}H NMR ($CDCl_3$, 700 MHz, 6:1 mixture of diastereomers with integrals normalized for the major isomer): δ 8.64 (br. s, 0.17H), 8.59 (br. s, 1H), 7.51 (app d, overlap, *J* = 8.0 Hz, 1.09H), 7.34 (app ddd, overlap, *J* = 8.0, 0.8, 0.8 Hz, 1.03H), 7.15 (app ddd, overlap, *J* = 8.1, 7.0, 1.1 Hz, 1.08H), 7.09 (app ddd, overlap, *J* = 7.9, 6.9, 1.0 Hz, 1.08H), 5.55 (dd, *J* = 12.1, 1.7 Hz, 1H), 5.09 (d, *J* = 10.8 Hz, 0.16H), 3.72 (s, 0.34 H), 3.71 (s, 3H), 3.05 (dd, *J* = 10.6, 4.4 Hz, 1H), 2.92-2.90 (m, overlap, 0.35H), 2.89-2.86 (m, overlap, 1.93H), 2.67 (dd, *J* = 8.9, 8.9 Hz, 0.18H), 2.64-2.61 (m, overlap, 1.03H), 2.57-2.47 (m, overlap, 1.41H), 2.31 (app ddd, overlap, *J* = 13.5, 9.4, 5.1 Hz, 1.26H), 2.26 (app dd, overlap, *J* = 11.8, 1.9 Hz, 1.05H), 2.18 (dd, *J* = 12.8, 6.1 Hz, 0.2H), 2.14-2.06 (m, overlap, 2.29H), 1.98 (d, *J* = 14.6 Hz, 1H), 1.88-1.79 (m, overlap, 2.34H), 1.66 (ddd, *J* = 12.9, 4.3, 1.9 Hz, 1H), 1.53 (m, overlap, 0.34H), 1.36-1.33 (m, overlap, 0.41H), 1.22-1.15 (m, overlap, 2H), 1.07 (app ddd, overlap, *J* = 12.9, 12.9, 4.9 Hz, 1.11H), 0.95 (t, *J* = 7.5 Hz, 3H), 0.91 (t, *J* = 7.3 Hz, 0.54H);

^{13}C NMR ($CDCl_3$, 175 MHz): δ 175.7, 135.8, 133.9, 127.8, 121.4, 118.9, 118.2, 111.6, 110.6, 60.7, 55.9, 54.1, 52.1, 42.0, 40.4, 39.2, 36.1, 31.1, 27.8, 26.5, 11.4;

HRMS (ESI) *m/z* calculated for $C_{21}H_{28}N_2O_2^+$ ($[M+H]^+$) 341.2224, found 341.2232

$[\alpha]_D^{26}$ = -6.5 (c 0.81, $CHCl_3$)

Computational Studies

The Gaussian 09 program was used to optimize structures at the (B3LYP/6-31G*) level of theory. Structures were minimized with no symmetry restrictions, and vibrational modes were generated simultaneously to ensure the absence of imaginary frequencies corresponding to unstable structures or transition states.

Homodesmotic Reactions

The homodesmotic reactions used to evaluate ring strain for this work are listed below and were balanced in accordance with the standardized definition of homodesmotic reactions (RC4) proposed by Wheeler *et al*.[104]

To ensure minimal energy distortion due to steric clashing around the ring-opening sites, hydrogen atoms were added across each broken carbon-carbon bond. All methyl, methine, and quaternary carbon substituents balance out on each side of the reaction and are incorporated in "strain-free" reference molecules in accordance with the guidelines put forth by Schleyer and coworkers.[105] To balance the number of methylenes on both sides of each reaction, a methylene correction term, as reported by Khoury and coworkers,[106] was incorporated. This term is abbreviated $E(CH_2)$ and is the (B3LYP/6-31G*) optimized energy difference between n-pentane and n-butane. The balanced equations are below:

A. Catharanthine

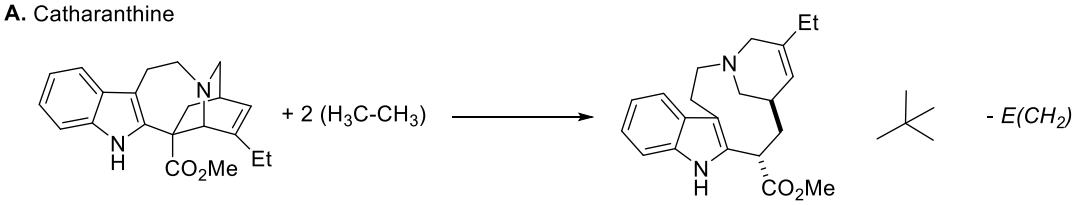

B. Dihydrocatharanthine

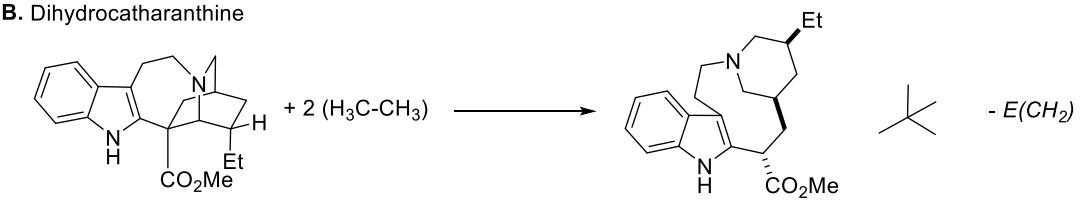

C. Coronaridine

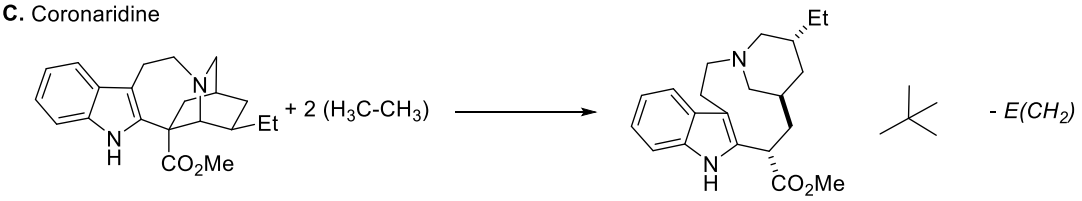

Computed Total Energies:

Total energies of all reference compounds (B3LYP/6-31G*)

Structure	Total Energy (Hartrees) B3LYP/6-31G*
Ethane	-79.83041744
isobutane	-158.4588127
n-butane	-158.4580421
n-pentane	-197.7717819
neopentane	-197.7729563
E(CH2)	-39.31373986

Total energies of all bicyclic compounds (B3LYP/6-31G*)

Structure	Total Energy (Hartrees) B3LYP/6-31G*
12	-1074.622737
33	-1075.833776
37	-1075.846281
38	-1077.052450
36	-1075.854670
41	-1077.057331

Strain release energies (kcal/mol) of structures **1**, **10**, and **4**

in accordance with their homodesmotic reactions reported in Scheme S1

Structure	Strain Release Energy (kcal/mol)
12	-4.23
37	-0.00
36	+0.08

Cartesian Coordinates for all Energy Minimized Structures:

Structure 12

catharanthine

OPT FREQ B3LYP/6-31G(d) temperature=300.0 geom=(connectivity)

C	0.60834400	0.35105900	0.53573900
C	1.60148600	-0.45423600	-0.38893200
C	2.07364000	-1.12167400	2.00481600
C	0.90941000	-0.09878800	2.01339000
H	1.16215900	0.77198300	2.62289500
H	0.01546900	-0.55772700	2.44852700
H	2.30403900	-1.43977400	3.02640800
H	1.42035100	-0.20062200	-1.43447900
C	1.62068200	-2.34171800	1.16181800
H	2.36711300	-3.14879700	1.21231100
H	0.68660100	-2.73447100	1.59403400
N	1.43816700	-1.90099000	-0.22653700
C	3.02711900	-0.12327800	0.04533400
C	3.25754900	-0.48369100	1.31443300
H	4.21818700	-0.36536600	1.81124100
C	4.03725800	0.43895000	-0.91673100
H	3.63596600	1.34686600	-1.38604300
H	4.93480100	0.73810200	-0.35998800
C	4.43306100	-0.55790100	-2.02244100
H	5.15196100	-0.10338900	-2.71393200
H	4.88916600	-1.45576800	-1.59227700
H	3.56214100	-0.87690200	-2.60563500
C	0.83837900	1.86382700	0.38513600
O	0.64285500	2.68614800	1.26024100

O	1.20069400	2.20978900	-0.86578400
C	1.33578600	3.62219100	-1.10653900
H	1.64702500	3.71054500	-2.14745400
H	0.37975100	4.12764100	-0.94742700
H	2.08480700	4.05516100	-0.43933100
C	-0.85690800	0.10938300	0.19125600
C	-1.54078100	-1.00434000	-0.26015400
N	-1.77218200	1.13334800	0.42996800
C	-2.93858900	-0.64095900	-0.29803800
C	-3.04750900	0.70152700	0.14775200
H	-1.53088100	2.00494400	0.87996600
C	-1.05174000	-2.40220200	-0.53219200
H	-1.19461500	-3.01485400	0.37179600
H	-1.69537400	-2.86669800	-1.29215700
C	0.40183700	-2.54346700	-1.01625900
H	0.63794900	-3.61531800	-1.08264800
H	0.48049300	-2.14363600	-2.03537200
C	-4.10943300	-1.32975800	-0.66038200
C	-5.33290600	-0.67652400	-0.57210300
H	-6.24344200	-1.20112000	-0.84915000
C	-5.41515300	0.65841800	-0.12614900
H	-6.38587900	1.14305700	-0.06570200
C	-4.27479100	1.36610200	0.23770200
H	-4.33602500	2.39528100	0.58215400
H	-4.06249800	-2.36066700	-1.00214400

Structure 33

ring-opened catharanthine

OPT FREQ B3LYP/6-31G(d) temperature=300.0 geom=(connectivity)

C	0.29229000	0.82985200	0.27552900
C	2.69182800	-1.99387000	-0.51004700
C	1.71758300	-0.65283800	1.93078100
C	0.80423400	0.59120000	1.74909000
H	1.36429500	1.46971900	2.09458200
H	-0.06801100	0.50605300	2.40710800
H	1.80857900	-0.80213100	3.01761300
H	2.77329200	-1.76774900	-1.58237000
C	1.12198800	-1.93250000	1.31989200
H	1.61103000	-2.82274800	1.76194100
H	0.05830100	-1.99583300	1.55700900
N	1.30395600	-1.86336200	-0.12226900
C	3.57698900	-1.04882200	0.27923200
C	3.10586800	-0.43616800	1.37333700
H	3.74884300	0.26139600	1.91198500

C	4.97833000	-0.82519400	-0.24153200
H	5.58693400	-0.36924200	0.54873500
H	5.44530400	-1.79422200	-0.47312400
C	5.03157400	0.06751300	-1.49599400
H	6.06787300	0.23013000	-1.81363000
H	4.49455100	-0.38192100	-2.33890200
H	4.57435400	1.04221400	-1.29353000
C	0.46780400	2.30906600	-0.04079800
O	-0.28599800	3.21879800	0.26287600
O	1.64177700	2.52882900	-0.66498600
C	1.95290900	3.90702000	-0.93758200
H	2.92181900	3.89231900	-1.43705200
H	1.19201600	4.35030500	-1.58478200
H	2.00683000	4.47970900	-0.00797100
C	-1.12707200	0.34102300	0.05787200
C	-1.67209300	-0.87964200	-0.32608800
N	-2.16093700	1.22729700	0.33609300
C	-3.10878400	-0.70169700	-0.29520800
C	-3.37504100	0.63148600	0.10742700
H	-1.98073500	2.20960300	0.50543800
C	-4.19421300	-1.55297400	-0.57069200
C	-5.48838100	-1.05844500	-0.45813200
H	-6.33264500	-1.70851000	-0.67237800
C	-5.72642200	0.27578300	-0.06951900
H	-6.74888700	0.63585600	0.00812500
C	-4.67456700	1.13802200	0.21834200
H	-4.85452600	2.16602100	0.52215200
H	-4.02984700	-2.58501300	-0.87034200
H	3.07293100	-3.03393300	-0.39247200
H	0.95344600	0.27781800	-0.38707400
C	-1.12372600	-2.26440300	-0.61185700
H	-1.71525500	-2.69023200	-1.43384200
H	-1.35966400	-2.90894300	0.24914400
C	0.34180300	-2.49515300	-1.00209100
H	0.51815900	-2.09157300	-2.00923500
H	0.48624200	-3.59320900	-1.07878800

Structure 37

dihydrocatharanthine

OPT FREQ B3LYP/6-31G(d) temperature=300.0 geom=(connectivity)

C	0.65860300	0.21571300	0.34169200
C	1.53066500	-0.63038800	-0.64890000
C	1.87219600	-1.56318600	1.69352100
C	1.03454400	-0.27154300	1.78745000

H	1.59797400	0.50924000	2.30799600
H	0.12351700	-0.44866500	2.36768800
H	1.98580800	-1.99719500	2.69402400
H	1.36572400	-0.27940800	-1.66961100
C	1.15681200	-2.57522800	0.78046700
H	1.66536400	-3.55141700	0.80957600
H	0.13356100	-2.73488500	1.15982800
N	1.16777300	-2.04619000	-0.58985500
C	3.05203700	-0.58438400	-0.31405300
C	3.24764900	-1.22043000	1.09844400
H	3.87009100	-2.12097600	1.04053900
C	3.76183800	0.77257200	-0.47288600
H	3.45940100	1.23051500	-1.42292900
H	3.45487800	1.46520700	0.32227800
C	5.29080400	0.64169300	-0.44901400
H	5.77214900	1.61924000	-0.56629200
H	5.64738500	0.20996700	0.49334100
H	5.64248500	-0.00427000	-1.26294200
C	0.91192300	1.72442300	0.18113800
O	0.98463900	2.52405100	1.09579800
O	0.95168500	2.09223700	-1.11385400
C	1.08693900	3.50256500	-1.35845900
H	1.10063200	3.60893200	-2.44323500
H	0.24138300	4.04655200	-0.92962200
H	2.01472100	3.88006200	-0.92116400
C	-0.84508900	0.06123900	0.11210600
C	-1.65503500	-0.91159900	-0.44532800
N	-1.65860500	1.06836300	0.63847500
C	-3.01931900	-0.47195100	-0.25456800
C	-2.98383000	0.76909000	0.42945800
H	-1.30872300	1.86166500	1.15652000
C	-1.33340100	-2.26353300	-1.02250200
H	-1.60371000	-3.03031700	-0.28004000
H	-1.99223100	-2.46009300	-1.88025000
C	0.11510000	-2.49330100	-1.48458200
H	0.24795900	-3.56930000	-1.67117200
H	0.27617600	-1.98995800	-2.44550000
C	-4.26695600	-1.02224300	-0.59497400
C	-5.42498300	-0.33175600	-0.25636400
H	-6.39468900	-0.74814200	-0.51567000
C	-5.36367000	0.90299800	0.42084800
H	-6.28525300	1.42033600	0.67369200
C	-4.14377900	1.47112900	0.77226600
H	-4.09512200	2.42232400	1.29613700
H	-4.32883400	-1.97476300	-1.11510900
H	3.49169400	-1.25993900	-1.05741800

H	3.76461200	-0.52151500	1.76888600

Structure 38

ring-opened dihydrocatharanthine

OPT FREQ B3LYP/6-31G(d) temperature=300.0 geom=(connectivity)

C	-0.15908100	1.37225700	-0.00241800
C	3.17650100	-1.92279900	-0.13029400
C	1.70938700	0.17302900	1.45452900
C	0.61862500	1.26365200	1.35404200
H	1.10739400	2.22774200	1.55389000
H	-0.12191400	1.12332100	2.14998200
H	2.03166000	0.20709300	2.50639900
H	3.47649500	-2.00233500	-1.18203300
C	1.24729500	-1.29725300	1.17889700
H	1.66110700	-1.93729800	1.96998000
H	0.16281300	-1.39094200	1.24662000
C	3.90645200	-0.70970700	0.52793700
C	2.95585700	0.49593400	0.60365100
H	3.47898600	1.36129200	1.03254300
C	5.22420400	-0.36457000	-0.18570400
H	5.00395900	-0.08534700	-1.22693500
H	5.65718800	0.53007800	0.28387700
C	6.26610000	-1.49010100	-0.16654400
H	7.19391100	-1.17599400	-0.65795500
H	6.51570900	-1.77854000	0.86218200
H	5.90792000	-2.38755700	-0.68373700
C	-0.61315300	2.82149200	-0.14305500
O	-1.55176000	3.33413500	0.44031100
O	0.20440800	3.51238400	-0.95875100
C	-0.09333200	4.91430800	-1.09923300
H	0.66185700	5.30393100	-1.78190400
H	-1.09549700	5.05139500	-1.51269700
H	-0.03465100	5.41643200	-0.13019700
C	-1.31872000	0.40714100	-0.09686200
C	-1.42060900	-0.85894000	-0.64216700
N	-2.51270900	0.73370600	0.53575900
C	-2.76234100	-1.31314600	-0.35647200
C	-3.42042100	-0.28427700	0.36821700
H	-2.69801900	1.67115300	0.86922400
C	-0.43809700	-1.71131300	-1.41258900
H	-0.58846400	-2.75851300	-1.11788300
H	-0.70201400	-1.66611900	-2.48084200
C	1.07326200	-1.43989300	-1.32915800
H	1.53361900	-2.04064900	-2.12290100

H	1.28069700	-0.39073200	-1.60686600
C	-3.46826600	-2.49329200	-0.65037100
C	-4.78758000	-2.61342100	-0.23109200
H	-5.34243400	-3.52075300	-0.45469000
C	-5.42321800	-1.57395000	0.47903700
H	-6.45703500	-1.69493200	0.79150600
C	-4.75006900	-0.39756700	0.78856000
H	-5.23767200	0.40347800	1.33809600
H	-2.99269500	-3.30014900	-1.20219500
H	4.15893100	-0.98569800	1.56441700
H	2.66903700	0.79120600	-0.41471600
H	0.53083200	1.18839100	-0.82457500
H	3.50895700	-2.84990900	0.35997300
N	1.70862000	-1.86909300	-0.08354700

Structure 36

Coronaridine

OPT FREQ B3LYP/6-31G(d) temperature=300.0 geom=(connectivity)

C	0.55199700	0.43848300	0.43166700
C	1.54692900	-0.35860900	-0.47352400
C	1.90886100	-1.10805600	1.92919800
C	0.91792300	0.07371400	1.92077800
H	1.35368100	0.94344700	2.42251500
H	0.00909400	-0.18878000	2.47130500
H	2.04079200	-1.46856200	2.95621600
H	1.38135300	-0.09060200	-1.51864000
C	1.34333100	-2.24491900	1.06017600
H	1.94553200	-3.15906800	1.17424500
H	0.32303900	-2.48433000	1.40357500
N	1.37187400	-1.80302600	-0.34114600
C	3.00240000	-0.01406600	-0.05982500
C	3.25541700	-0.66067600	1.33464500
H	3.91567700	-1.53225600	1.23755000
C	0.69155000	1.95421500	0.20565200
O	0.51262700	2.80109300	1.06161300
O	0.96160400	2.26281500	-1.07679700
C	1.01538300	3.66761200	-1.38273000
H	1.24821300	3.72412200	-2.44610200
H	0.05207400	4.13993500	-1.17394700
H	1.79070900	4.15931400	-0.79001400
C	-0.91172200	0.12275300	0.14272100
C	-1.57578200	-0.96736800	-0.39127300
N	-1.85597100	1.06534500	0.55226600
C	-2.98799200	-0.66904900	-0.30618400

C	-3.12607400	0.60955400	0.29147000
H	-1.61823500	1.92825500	1.02062400
C	-1.07638100	-2.31166000	-0.85248400
H	-1.29950600	-3.05052400	-0.06730400
H	-1.66739500	-2.63912200	-1.71955300
C	0.40960600	-2.41900700	-1.24048700
H	0.65879800	-3.48554200	-1.34038500
H	0.56312800	-1.97044300	-2.22917300
C	-4.14754300	-1.37296300	-0.67475900
C	-5.39049000	-0.79351700	-0.44787500
H	-6.29306700	-1.32920300	-0.72960100
C	-5.50178100	0.48088000	0.14455200
H	-6.48678300	0.90875400	0.31069500
C	-4.37289500	1.20049900	0.52082200
H	-4.45727700	2.18251000	0.97916300
H	-4.07646500	-2.35743900	-1.13022700
H	3.75670300	0.04356800	2.00909600
H	3.08087000	1.07806500	0.03563400
C	4.01593400	-0.45220300	-1.12754400
H	3.72924500	-0.00545400	-2.09023300
H	3.93870100	-1.53926800	-1.25485200
C	5.46239500	-0.05773800	-0.80856800
H	6.14181600	-0.37788100	-1.60678900
H	5.56413700	1.02994700	-0.70284100
H	5.81360400	-0.51421800	0.12411200

Structure 41

ring-opened coronaridine

C	0.20510200	0.90967600	0.18429000
C	2.73666700	-1.77842400	-0.45784400
C	1.59880300	-0.55143600	1.96121500
C	0.77870700	0.73194000	1.64626100
H	1.41597100	1.59338500	1.88645800
H	-0.07440200	0.78920100	2.33161000
H	1.50993000	-0.69512500	3.04753800
H	2.85244600	-1.76948200	-1.54754400
C	1.04846200	-1.81338300	1.27636100
H	1.51422600	-2.71341500	1.72848900
H	-0.02676500	-1.88838900	1.44726200
N	1.31834200	-1.71524700	-0.14996600
C	3.47858800	-0.57716500	0.16325200
C	3.11087000	-0.45061800	1.65436500
H	3.51932100	0.48548700	2.05976300
C	5.00464900	-0.66920400	-0.01584600
H	5.46848100	0.15554600	0.54310000

H	5.36638000	-1.59453700	0.45652100
C	5.48589200	-0.61515400	-1.47113000
H	6.58062300	-0.61992600	-1.52207400
H	5.12871000	-1.47152100	-2.05410200
H	5.13397900	0.29621100	-1.97046300
C	0.28592600	2.39478800	-0.14258100
O	-0.50827100	3.26252700	0.17767100
O	1.43078000	2.67522400	-0.79885100
C	1.66237800	4.06709800	-1.08280600
H	2.61686700	4.10105000	-1.60834000
H	0.86192300	4.46691500	-1.71011600
H	1.71129600	4.64494200	-0.15613900
C	-1.19164100	0.34530200	0.01472400
C	-1.68081900	-0.88916500	-0.39569600
N	-2.26225100	1.16106700	0.36515100
C	-3.12291400	-0.79550400	-0.30879600
C	-3.44878000	0.50482200	0.15280100
H	-2.13401700	2.15171300	0.53309200
C	-4.16667900	-1.69830100	-0.57983900
C	-5.48202800	-1.28385100	-0.40569700
H	-6.29535300	-1.97331900	-0.61635000
C	-5.78101400	0.01971300	0.04041300
H	-6.81882100	0.31719700	0.16517300
C	-4.77016400	0.93067900	0.32601500
H	-4.99750600	1.93485800	0.67442600
H	-3.95365400	-2.70701700	-0.92477300
H	3.19495300	-2.72439100	-0.09526200
H	0.86456900	0.38909600	-0.50116500
C	-1.06365900	-2.22678900	-0.75598400
H	-1.60220000	-2.62048200	-1.62940200
H	-1.30829700	-2.93410900	0.05142900
C	0.42790700	-2.37224600	-1.08768800
H	0.62610400	-1.93498000	-2.07635300
H	0.62967100	-3.45907900	-1.18458500
H	3.61256300	-1.26566600	2.19922800
H	3.13278700	0.32642300	-0.35902100

Chiral HPLC traces of (-)-pseudotabersonine: near-racemic sample

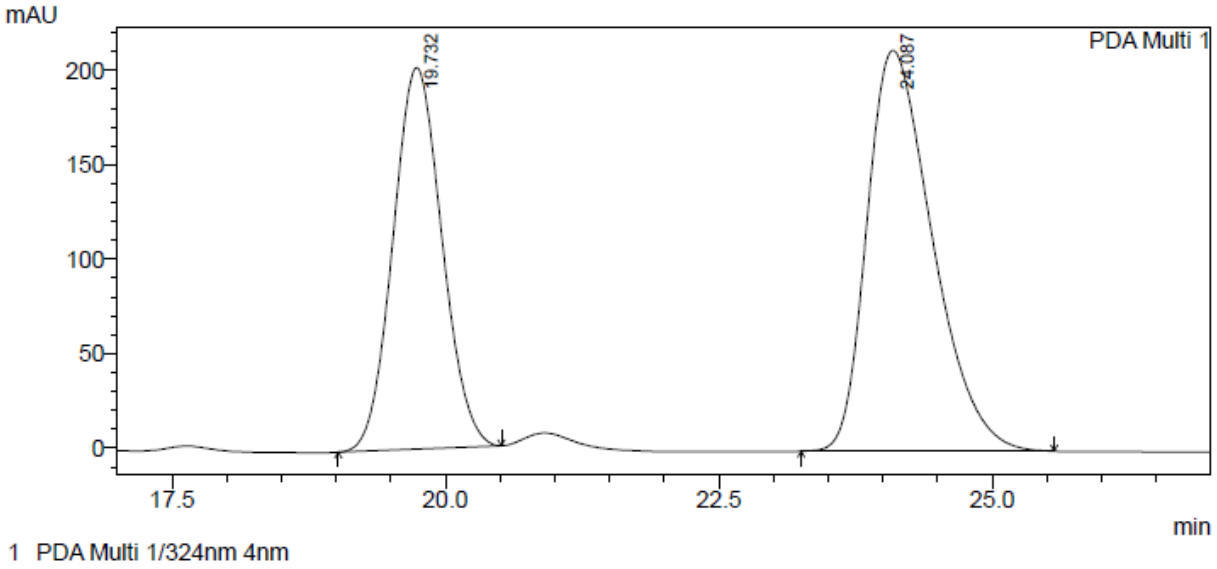

1 PDA Multi 1/324nm 4nm

PeakTable

PDA Ch1 324nm 4nm

Peak#	Ret. Time	Area	Height	Area %	Height %
1	19.732	6294034	201956	41.623	48.759
2	24.087	8827423	212235	58.377	51.241
Total		15121457	414191	100.000	100.000

Sample from rearrangement at reflux:

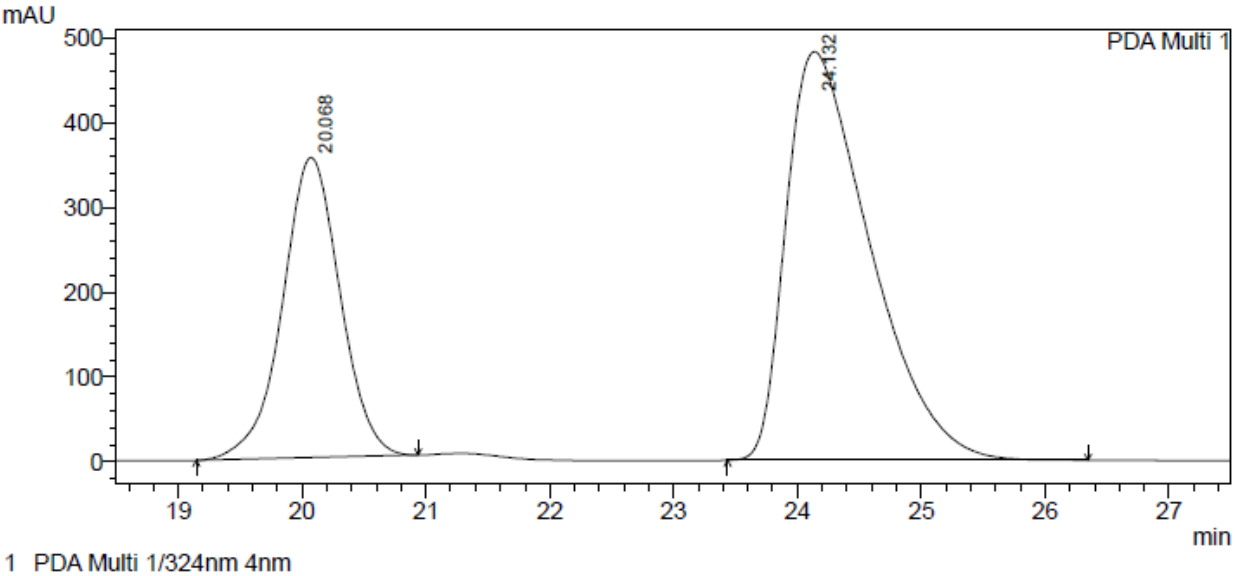

1 PDA Multi 1/324nm 4nm

PeakTable

PDA Ch1 324nm 4nm

Peak#	Ret. Time	Area	Height	Area %	Height %
1	20.068	11461227	353915	33.549	42.358
2	24.132	22701577	481610	66.451	57.642
Total		34162804	835525	100.000	

Sample from rearrangement at 60 °C:

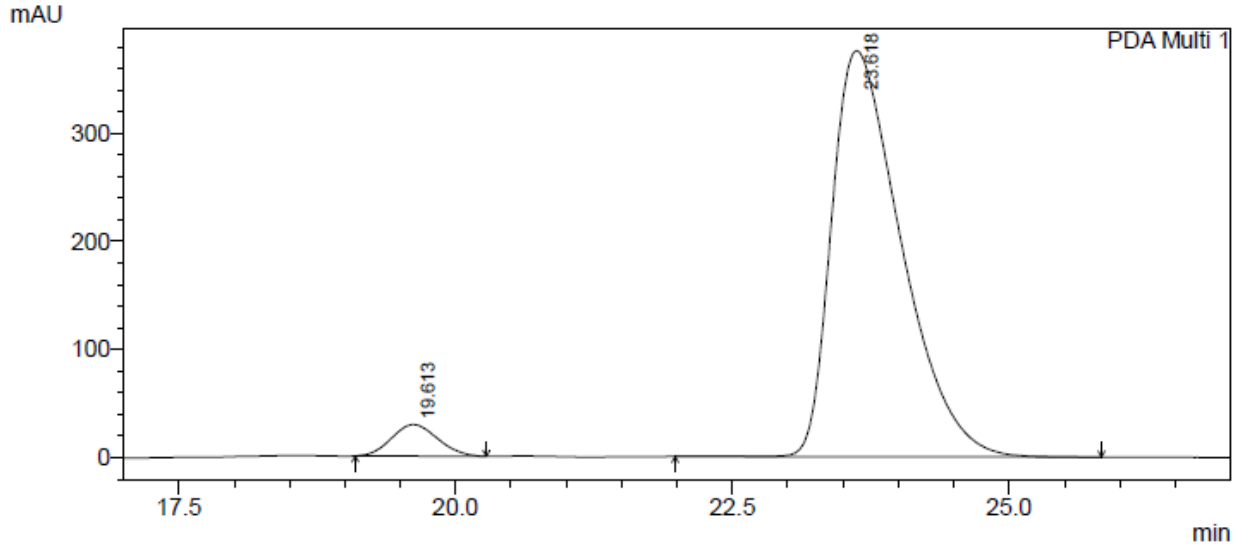

1 PDA Multi 1/324nm 4nm

PeakTable

PDA Ch1 324nm 4nm

Peak#	Ret. Time	Area	Height	Area %	Height %
1	19.613	842630	29134	4.867	7.200
2	23.618	16470181	375490	95.133	92.800
Total		17312812	404624	100.000	100.000

Chapter 3: Strategies and Reagents for the Trifluoromethylation of Aromatics

*Portions of this chapter have been published in Beatty, J. W.; Douglas, J. J.; Cole, K. P.; Stephenson, C. R. J. A Scalable and Operationally Simple Trifluoromethylation. *Nat. Commun.* **2015**, *6*, 7919.

Introduction

The incorporation of fluorine atoms into organic molecules dramatically improves their resistance to oxidative metabolism and can significantly alter the physicochemical profile of a drug candidate. Fluorine also imparts many beneficial properties for commercial applications of specialty materials; for example, perfluorooctanoic acid and its analogs have been used broadly to impart water, oil, and soil resistant properties to a wide array of products including paints, outerwear, carpeting, and even hydraulic fluids.[113] Perhaps the most well-known fluorinated commercial material is Teflon®, which is produced through the polymerization of tetrafluoroethylene and is used in non-stick pans and as a repellant coating.

In the context of small molecule drug and agrochemical design, the incorporation of fluorine has resulted in a large portion of fluorinated top-selling drugs (up to 20%) and agrochemicals (up to 30%).[114,115,116,117] Fluorine atoms can be found in over 200 approved pharmaceuticals to date, showcasing the undeniable impact which organo-fluorine chemistry has had on the pharmaceutical industry (**Fig. 3.1**).[118] Fluorine's inductive effects protect nearby positions from oxidative metabolism, and can furthermore alter conformational biases of molecules through selective contributions to C–F σ* orbitals.[119] These conformational biases can potentially decrease the free-energy of a binding event, and consequently can be beneficial for

protein-binding kinetics and thermodynamics. Additionally, fluorine groups can behave as bioisosteres in lieu of more reactive functionalities. The C–F bond is similar in length to the C–O bond[114] and the trifluoromethyl group has been used successfully as an isostere of the carbonyl group.[120]

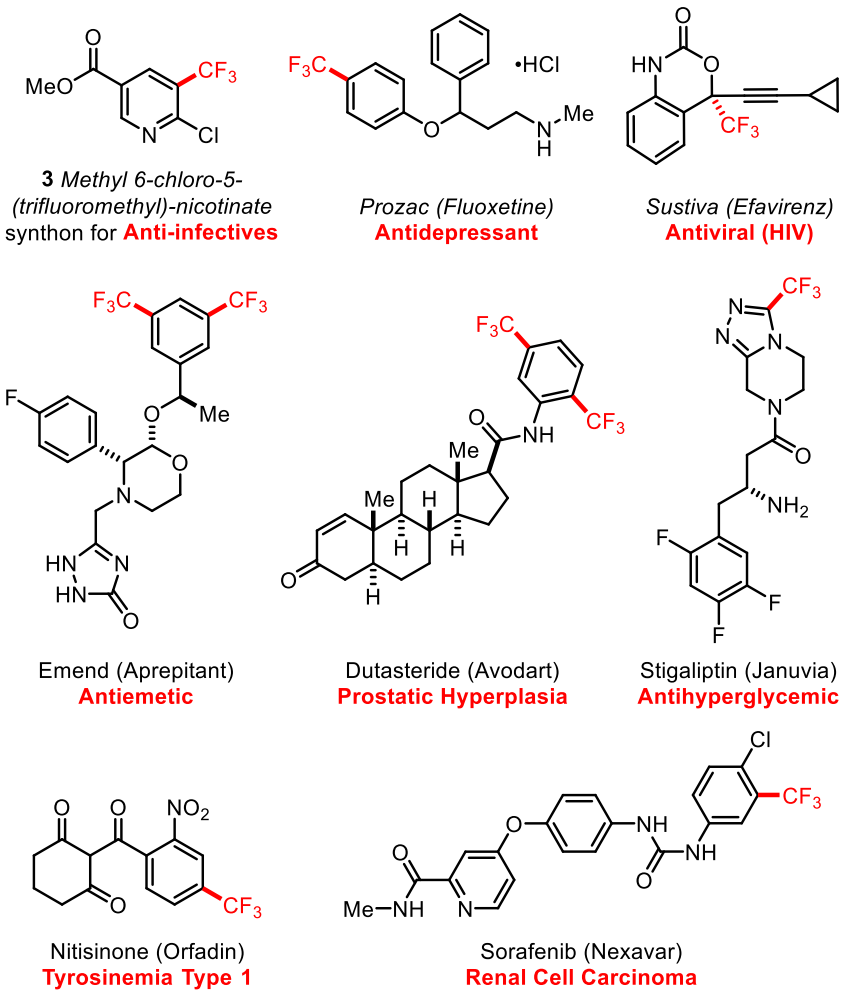

Figure 3.1 Pharmaceuticals containing the trifluoromethyl group

Lipophilicity trends with the density of fluorine incorporation, and as such it may be incorporated in varying quantities to more selectively tune the pharmacokinetic profile of a given molecule. Nonetheless, despite the prospect of such controlled drug and material design, the properties which render fluorinated compounds so inert to metabolism and so dramatically change the polarity and solubility profile of these compounds also interfere with their ease of

synthesis and production. This has resulted in the slow development of various methods for fluorine incorporation. The synthetic challenge of fluorine incorporation in some cases could limit the number of fluorinated analogs which are synthetically accessible for a given drug discovery campaign.

Simple trifluoromethylated arenes are produced industrially on significant scale through a two-step process from methylated arenes. This process consists of an initial benzylic chlorination step, which forms the corresponding benzotrichloride. Subsequent fluoride-chloride exchange is accomplished through heating in the presence of anhydrous hydrogen fluoride.[121] While this process is highly efficient and inexpensive to employ, the scope of this chemistry is limited to oxidatively and thermally stable substrates. Additionally, this chemistry is impractical on small-scale application.

CF_3 Reagents and Sources

Given the challenges associated with direct C–F bond formation, it is highly desirable to employ reagents which already possess the C–F bond. As the trifluoromethyl group has grown in popularity and utility, a wide array of reagents prepossessing C–F bonds have been developed in order to enable the direct synthesis of CF_3 containing molecules. As a general principal, the design of trifluoromethylating reagents has been focused on the formation of weak F_3C–X bonds to improve reactivity and enable mild conditions for reagent use. In many cases this results in reagent syntheses which require multiple steps, although virtually every trifluoromethylating reagent is now commercially available.

While the breadth of effective trifluoromethylation reagents is impressive, the relative cost and availability of these reagents varies greatly with complexity and molecular weight–a

feature which is largely ignored in the context of academic methodology development. Conversely, in consideration of scalable, financially feasible, and industrially relevant trifluoromethylation methodologies, reagent choice is far more limited. Factors of cost and availability are, to a rough approximation, directly attributable to the limited number of chemicals which are used as original CF_3 sources. In other words, every CF_3-containing reagent is synthesized from a limited number of source materials, and the number of steps required for reagent preparation from these source materials simultaneously inflates reagent price and decreases availability.

Bromotrifluoromethane ($BrCF_3$) is a well-known promoter of ozone-depletion with a half-life of 110 years in the troposphere and is the most commonly utilized fluorinated material for reagent synthesis (**Fig. 3.2**, top).[122] $BrCF_3$ is produced from fluoroform (HCF_3), a greenhouse gas (atmospheric lifetime = 254 yrs),[123] and the two constitute the original source of CF_3 for a large number of reagents including CF_3I,[124] $TMSCF_3$,[125] Umemoto's reagent **43,**[126,127] and Togni's reagent **44.**[128] Alternative CF_3 reagents are obtained as derivatives of triflic or trifluoroacetic acid, which are produced avoiding the use of environmentally harmful gases directly through the electrochemical fluorination of either methanesulfonyl fluoride or acetyl fluoride, respectively.

In the process of reagent choice and comparison, a number of factors must be considered. One important factor is ease of handling. While gases are quite challenging to handle on small scale, in an industrial setting the handling of gasses is inconsequential and routine. CF_3I, for example, is a gas at room temperature, and several methods of metering the stoichiometry of this reagent have been used. One common method is the preparation of a saturated solution of the reagent, the concentration of which is then back-calculated based on changes in the solution's

mass.[129] This method inherently wastes the reagent, as the saturated solution is prepared through bubbling of the gas through solvent. Another alternative to this method is the preparation of halogen-bonding complexes,[130] which can significantly improve the practicality of using CF_3 on small scale; however, this entails an additional step of preparation, and these solutions are currently quite expensive (tetramethyl guanidine (TMG)•CF_3I complex, Sigma Aldrich 4/2016, \$212 for 5 mL = \$8,833 mol^{-1}) when compared to CF_3I itself (CF_3I, Sigma Aldrich 4/2014, \$578 for 100 g = \$1,132 mol^{-1}). Other means of controlling stoichiometry can be used industrially and in flow, which is covered later in this chapter. Reagent volatility is, in summary, a surmountable challenge which serves as a larger barrier for small-scale laboratory applications and becomes inconsequential on large industrial scale.

Another practical consideration of reagent choice is the factor of cost. The issue of reagent expense varies in importance based upon the context of application. For example, reagent cost is an insignificant factor in most medicinal chemistry applications, where time is the most important commodity. The sulfinate reagents CF_3SO_2Na[131] and $Zn(SO_2CF_3)_2$[132] in particular have garnered significant popularity for medicinal chemistry in industry; however, it should be mentioned that beyond their cost and limited availability, the use of these reagents requires an excess of both sulfinate (2-6 equiv.) and *tert*-butyl hydroperoxide (3-10 equiv.), and occasionally requires multiple additions of reagent.[133,134]

On large scale, reagent cost intuitively becomes much more important, although for some drug synthesis programs it may still be insignificant. For example, the material cost of a synthetic route is most important for the production of drugs where the dosage is high, and the margin of profit is low. However, if there is a context in which the pricing of a drug is not reflective of its material cost, then reagent cost will be more insignificant. In a very similar vein,

reagent sourcing becomes very significant on scale. For example, Umemoto's reagent **43** (**Fig. 3.2**) is only offered in 1 gram quantities on Sigma Aldrich, and this is likely reflective of the difficulty of its synthesis. The expense of this reagent has completely avoided its use on significant production scale. Large scale pricing of many common CF_3 reagents was obtained and is summarized in **Figure 3.3**.

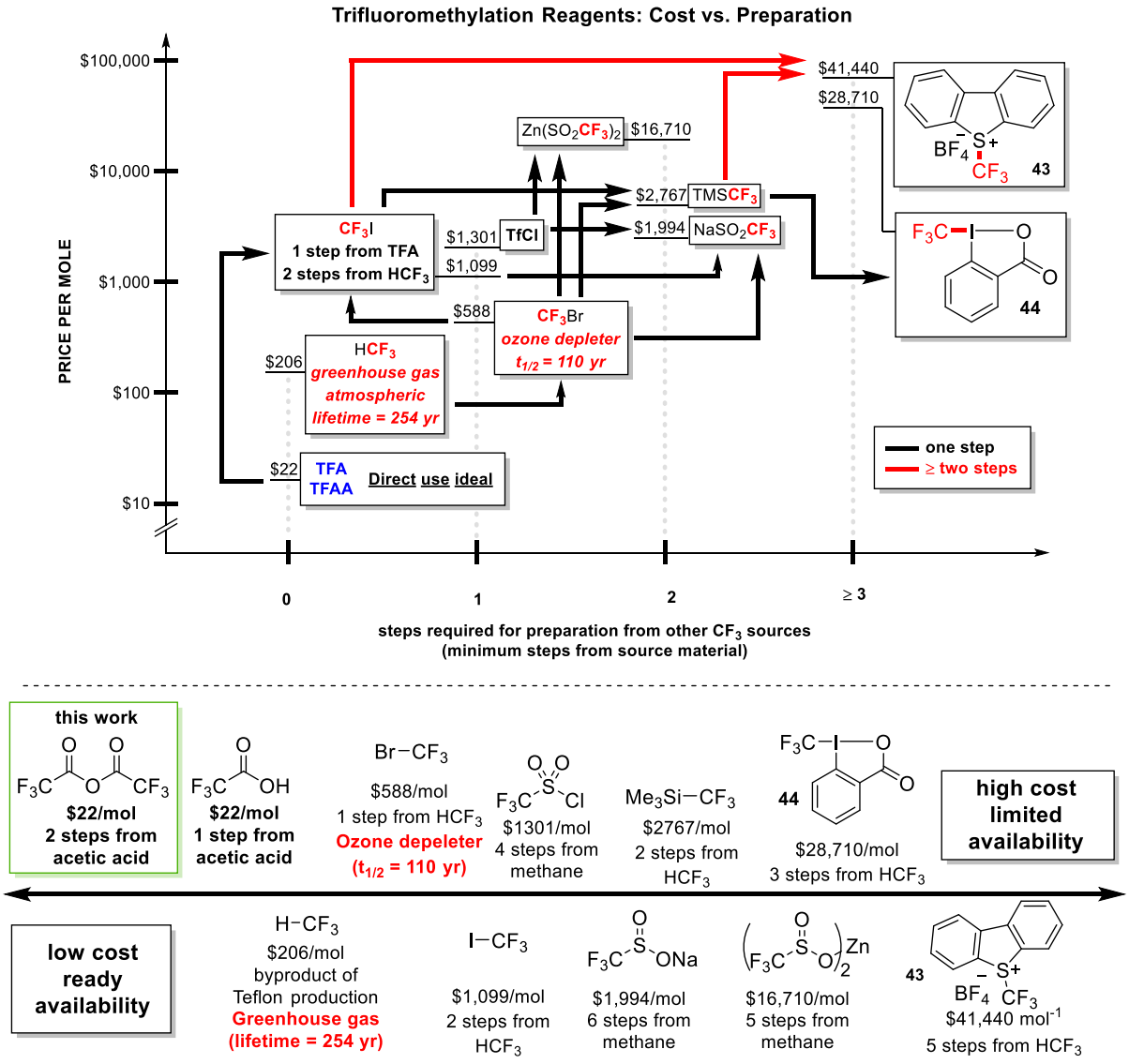

Figure 3.2 CF_3 reagent preparation and cost.

Prices are from the Sigma Aldrich catalog, 2016, and extrapolated to a per-mole basis from the largest quantity available.

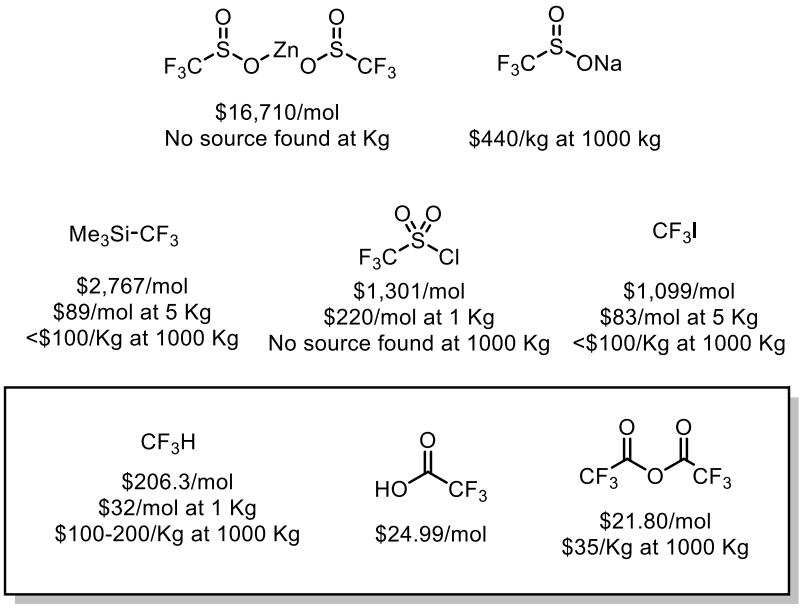

Figure 3.3 Large scale pricing of CF_3 sources.

Prices based on sources available to Eli Lilly and Co. for moderate scale 0.5-5 Kg and projected estimates at larger scale (1000 Kg).

As a consequence of the many factors of reagent sourcing, cost, and difficulty of reagent preparation, the use of CF_3 source materials such as HCF_3, TFA, and TFAA should be aggressively pursued. While HCF_3 is a greenhouse gas, its role as a byproduct of Teflon® production has resulted in a significant need for methods utilizing this material. TFA and TFAA are slightly less desirable in this way, as their consumption does not provide some additional environmental benefit; however, the extremely low cost of these materials has resulted in the publication of several significant methods for its use as a CF_3 source.

Trifluoromethylation using TFAA

Within this context, the use of trifluoroacetic acid and its derivatives is highly desirable for the development of trifluoromethylation chemistry. The earliest published example of CF_3 radical production was accomplished by Swartz through the Kolbe electrolysis of trifluoroacetic acid in 1933.[135] This reaction resulted in the dimerization of CF_3 radicals to form C_2F_6, along with other products.[136] Since this time, a number of efforts have been made to utilize TFA as a synthetically useful CF_3 source, although several challenges remain.

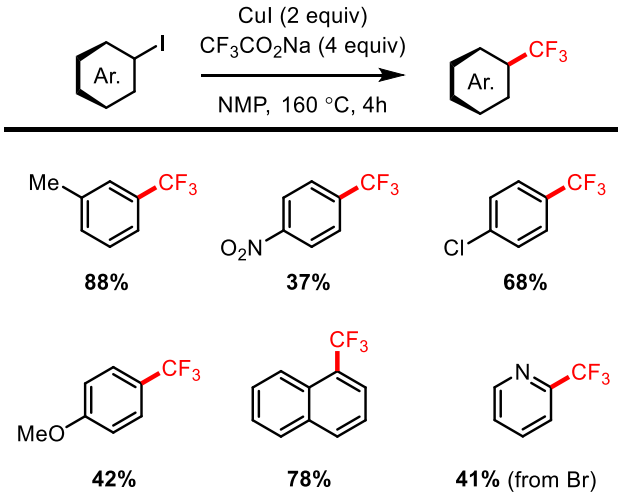

Figure 3.4 Matsui's trifluoromethylation of aryl halides with CF_3CO_2Na

One the earliest example of using trifluoroacetate for the trifluoromethylation of aryl halides was published by Matsui and coworkers in 1981.[137] This work demonstrated the feasibility of the decarboxylation of sodium trifluoroacetate in the presence of copper, which the authors observed began to occur at temperatures around 140 ˚C (**Fig. 3.4**). Performing these reaction at 160 ˚C in the presence of two equivalents of copper iodide, moderate to excellent yields were obtained. Lending further credibility to the environmental benefits of using TFA derivatives over alternative reagents, this work was first presented as an alternative to bis(trifluoromethyl)mercury, which was used as a CF_3 source for transmetallation onto super

stoichiometric copper.[138] Subsequent papers detailing the use of sodium trifluoroacetate attribute the use of excess acetate to large quantities of fluoroform formation.[139] A much more recent example of this chemistry accomplishes the decarboxylation of sodium trifluoroacetate at slightly diminished temperature (130 °C), with substoichiometric amounts of copper (20 mol%) and silver (60 mol%).[140] Buchwald and coworkers have also demonstrated this process to be quite efficient for a flow protocol operating between 200 and 210 °C, which results in a much faster decarboxylation event (**Fig. 3.5**).[141] While it is common for this type of reactivity to require the acetate salts, Langlois and coworkers have reported the use of methyl trifluoroacetate in the presence of CuI and CsF; however, this work likely proceeds through similar pathways to the alternative methods using the trifluoroacetate salts, as Krapcho demethylation of the reagent is accomplished by the CsF at 70 ˚C.[142]

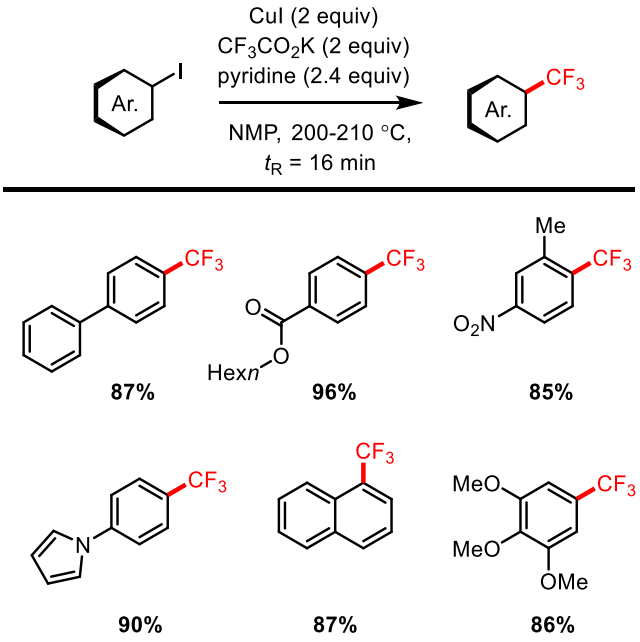

Figure 3.5 Buchwald's trifluoromethylation in flow

For the trifluoromethylation of aryl halides, a practical improvement can be made through the use of methyl chlorodifluoroacetate (MCDFA) in the place of trifluoroacetate, as the

decarboxylation of this material has been shown to occur at significantly lower and more practical temperatures. Chen and coworkers have reported the trifluoromethylation of a range of aryl, allyl, and vinyl, and benzyl halides using MCDFA, which they report can undergo productive decarboxylation in the presence of KF and CuI at temperatures ranging from 100-120 ˚C (**Fig. 3.6**).[143] The decarboxylation of the reagent results in the chlorodifluoromethly anion, which is very short lived and undergoes *ipso* elimination to provide the dilfuorocarbene. Fluoride anion is essential to this process, and adds to the carbene to form the trifluoromethyl anion, which is stabilized by coordination to copper.

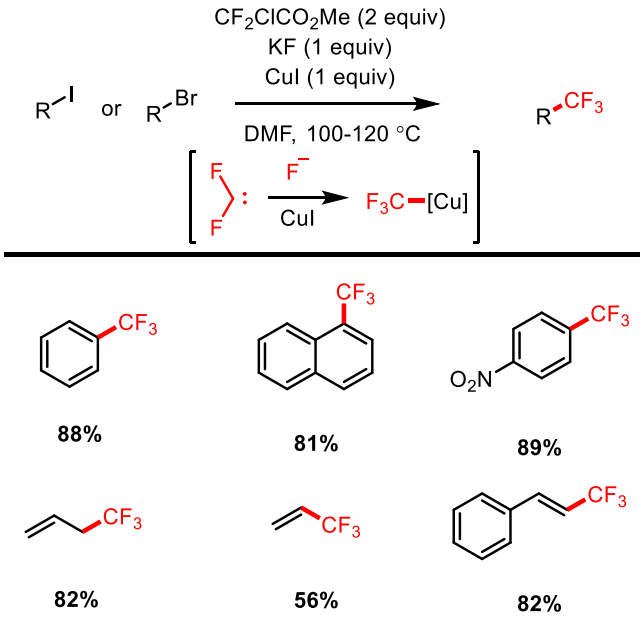

Figure 3.6 Trifluoromethylation with MCDFA

As MCDFA is roughly 85% more inexpensive than Ruppert's reagent, which is the traditional source of the CF_3 anion, it has been used in large-scale application by Boehringer-Ingelheim for the production of a trifluoromethyl pyridine synthon (**Fig. 3.7**).[144] One challenge associated with this process was the formation of chain-elongation products such as **45**, which arise from the oligomerization of the difluoromethyl carbine species in solution. While MCDFA was used in this context successfully, this side pathway was significant when copper was used in

substoichiometric amounts, and consequently the optimized conditions still utilized 1.5 equivalents of copper. Nevertheless, MCDFA has been clearly demonstrated to be useful on scale, and its availability and cost are clear benefits in this case.

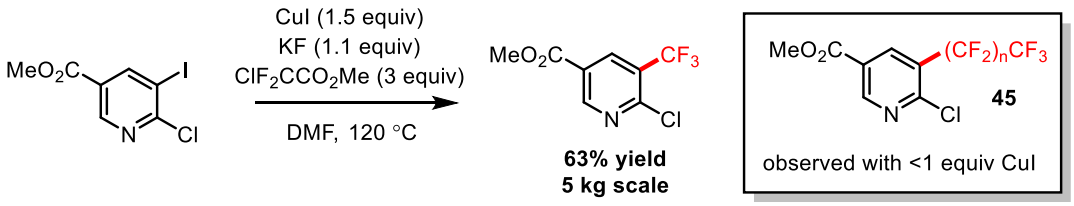

Figure 3.7 Trifluoromethylation with MCDFA on 5 kg scale

Aside from copper-mediated trifluoromethylations of aryl halides, TFA derivatives have for the most part been used as radical CF_3 sources. This mechanistic pathway has several benefits, perhaps the most significant of which is the direct functionalization of C–H bonds of the substrate of choice. This minimizes pre-functionalization steps, and can generally result in high regiochemical selectivity based on arene electronics. Additionally, the use of the CF_3 radical does not require the use of a transition metal catalyst such as copper, and the intermediacy of the CF_3 radical bypasses the CF_3 anion and associated carbene formation. A wide array of methods has been developed for the radical decarboxylation of TFA, which proceeds through the carboxylate radical (**Fig. 3.8A**). While the first example of TFA decarboxylation was electrochemical, this oxidative decarboxylation has not been widely adopted due to the forcing electrochemical conditions required. The oxidation of sodium trifluoroacetate requires potentials more positive than + 2.4 V in MeCN vs. SCE, which are strong enough potentials to oxidize most solvents. Furthermore, this is just the *onset potential*, which means that it is the mildest possible potential at which an electrochemical signal can be obtained, which implies slow reactivity. Trevin and coworkers have demonstrated that this chemistry is still feasibly performed on electron-poor arenes such as benzonitrile (**Fig. 3.8B**),

albeit in moderate yields.[145] This chemistry results in a significant amount of background decomposition of the substrate, which is already fairly electron poor in relation to many of the substrates described above. An additional drawback lies in the experimental execution, which although highly scalable results in corrosion of the anode.

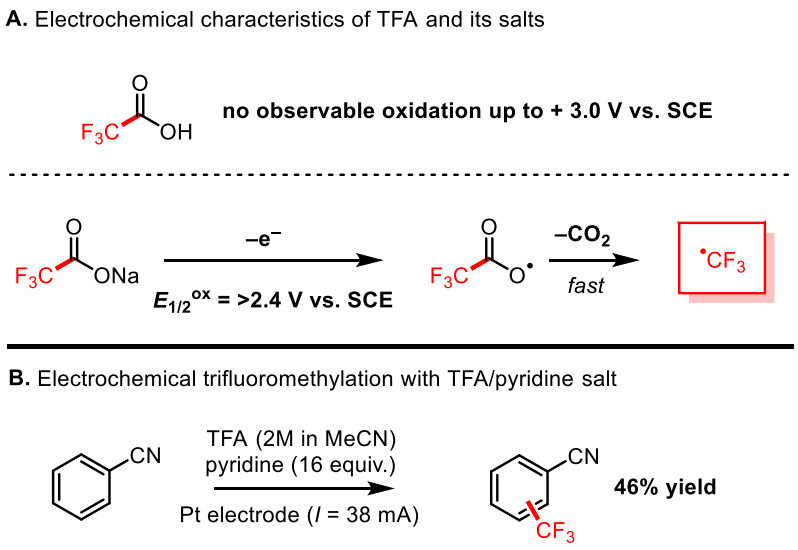

Figure 3.8 Electrochemical trifluoromethylation through oxidation of TFA salts

In addition to the electrochemical decarboxylation of TFA and its salts, there are a number of published methods for the chemical oxidation of trifluoroacetate. One of the older methods for this reaction involves the use of XeF_2, which is a very strong oxidant.[146] However, this method has been demonstrated to be compatible with a wider array of electron-rich substrates than the direct Kolbe electrolysis of TFA, as a few examples of moderately electron-rich substrates have been demonstrated (**Fig. 3.9**). Unfortunately, the general trend remains in that sufficiently electron-rich substrates are not broadly employed, and the yields of the most electron-rich examples are stunted compared to less reactive substrates. Despite these limitations, the use of XeF_2 is operationally simple, and the reactions must be cooled to room temperature rather than heated. This chemistry was also found to be effective with perfluoroalkyl acids for pentafluoroethylation and heptafluoropropylation.

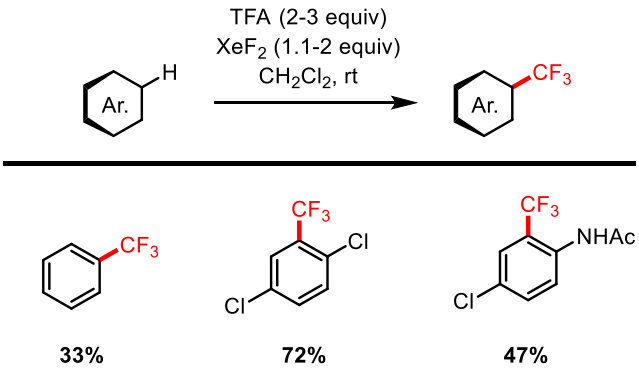

Figure 3.9 XeF_2 for the decarboxylation of TFA

Trifluoroacetate can also be activated for photochemical decarboxylation using anatase TiO_2 powder in combination with silver trifluoroacetate.[147] This chemistry also presents several undesirable features in that silver trifluoroacetate is used in 4-fold excess relative to the substrate of choice. Furthermore, chemical yields for the described process are low to moderate, with the highest yields being observed for simple substrates such as benzene and naphthalene (both 50%). While performed at room temperature, the described method utilizes UV light (500 W Hg lamp) and is conducted in a quartz tube for 24 hours. It is hesitantly speculated that the interaction of the UV light directly with substrate or product may be resulting in the low yields observed, but it is also likely that that oxidative nature of the conditions contributes to substrate degradation. A more recent non-photochemical example of silver-promoted decarboxylation has resulted in moderately higher yields, but these improvements are limited to sufficiently electron-poor substrates (**Fig. 3.10**).[148]

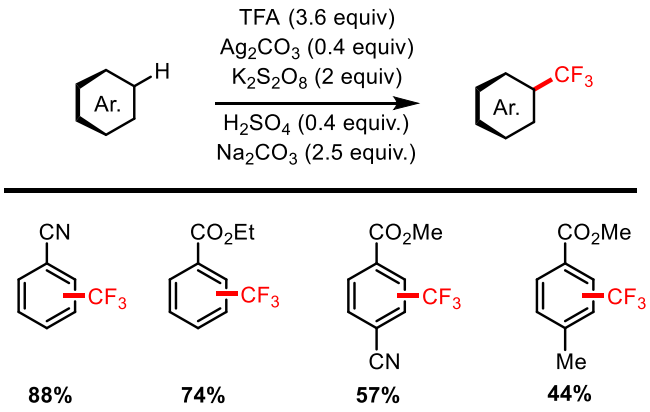

Figure 3.10 Silver and persulfate for CF_3 radical generation

Aside from the various one-electron oxidation processes for TFA decarboxylation, an alternative and mild method was published by Sawada and Nakayama in 1990 using hydrogen peroxide to form a bis(trifluoroacetyl) peroxide reagent (**Fig. 3.11**).[149] This method is remarkable in the sense that it expanded the scope of heterocycles to those which are much more electron-rich than previously demonstrated to be possible through the direct singe-electron oxidation of TFA. While the yields are moderate to good, this chemistry is performed in Freon 113, a solvent also known as 1,1,2-trichloro-1,2,2-trifluoroethane which is a potent ozone-depleting agent. The bis(trifluoroacetyl)peroxide reagent is produced through mixing TFAA with hydrogen peroxide in Freon in the presence of sodium carbonate and sodium chloride. The organic layer ends up containing the peroxide in roughly 30% assay yield. Despite the impressive yields of trifluoromethylated products, the method is arguably not scalable both due to solvent choice as well as the thermal instability of the peroxide reagent.

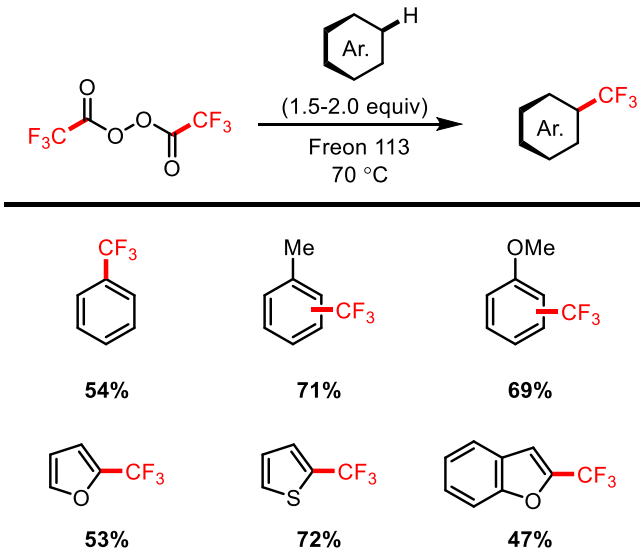

Figure 3.11 Bis(trifluoroacetyl)peroxide as a CF_3 source

Of the methods for CF_3 incorporation using TFA as the CF_3 source, the copper mediated trifluoromethylation of aryl halides has arguably seen the most utility; however, the thermal requirements for this type of reactivity limits the substrate scope in some instances, and the requirement for halogenation of the substrate may not be ideal in every circumstance; furthermore, the intermediacy of the CF_3 anion sometimes results in complex reaction mixtures arising from the formation of the difluorocarbene. Over the years, a wide array of methods for the decarboxylation of TFA derivatives at lower temperature have been reported, most significantly the use of MCDFA and perhaps the bis(trifluoroacetyl)peroxide. Further developments in these areas are required to realize the full utility of TFA as the ideal CF_3 source.

Radical Trifluoromethylation with Photoredox Catalysis

Radical arene and alkene functionalization are central modes of reactivity for photoredox catalysis, as the use of redox-active catalysts readily provides access to odd-electron radical species in solution. As a consequence, a wide array of activated alkyl halides are accessible to reduction by a photoexcited catalyst, and trifluoromethyl iodide (CF_3I) has become the staple

source of CF_3 for radical trifluoromethylations with photoredox catalysis. While the majority of examples do fall under the use of CF_3I, in recent years a wide array of methods for radical trifluoromethylations have been developed using a number of the reagents outlined above. This area has been reviewed by Koike and Akita;[150] below is a brief overview of these different methods, and the contexts in which each CF_3 source reacts within visible-light catalysis.

Trifluoromethyl Iodide

The first trifluoromethylations reaction with photoredox catalysis was published by MacMillan and coworkers in 2009, and detailed the enantioselective α-trifluoromethylation of aldehydes.[151] This reactivity was accomplished through the use of a chiral amine catalyst in 20 mol%, along with $Ir(ppy)_2(dtbbpy)PF_6$ in 0.5 mol% loading (**Fig. 3.12**). This chemistry is proposed to proceed through a reductive quenching cycle of the catalyst, where a sacrificial amount of enamine initiates the reaction through reduction of the catalyst excited state. The reduced catalyst (Ir^{2+}) is a sufficiently good reductant ($E_{1/2}^{red}$ = –1.51 V vs. SCE in MeCN)[152] to donate an electron to CF_3I ($E_{1/2}^{red}$ = –1.22 V vs. SCE in DMF),[153] which subsequently fragments to for the CF_3 radical. This reactivity is general to CF_3I in photoredox catalysis, where it is rare for it to act directly as an oxidative quencher. CF_3 radical then adds in an enantioselective fashion to the electronically-matched enamine intermediate, which provides highly enantio enriched products. An array of steric bulk and substitution patterns are accommodated in this chemistry. Further work by the MacMillan group has demonstrated the compatibility of this chemistry with enol silanes, which is a racemic variant of this chemistry.[154]

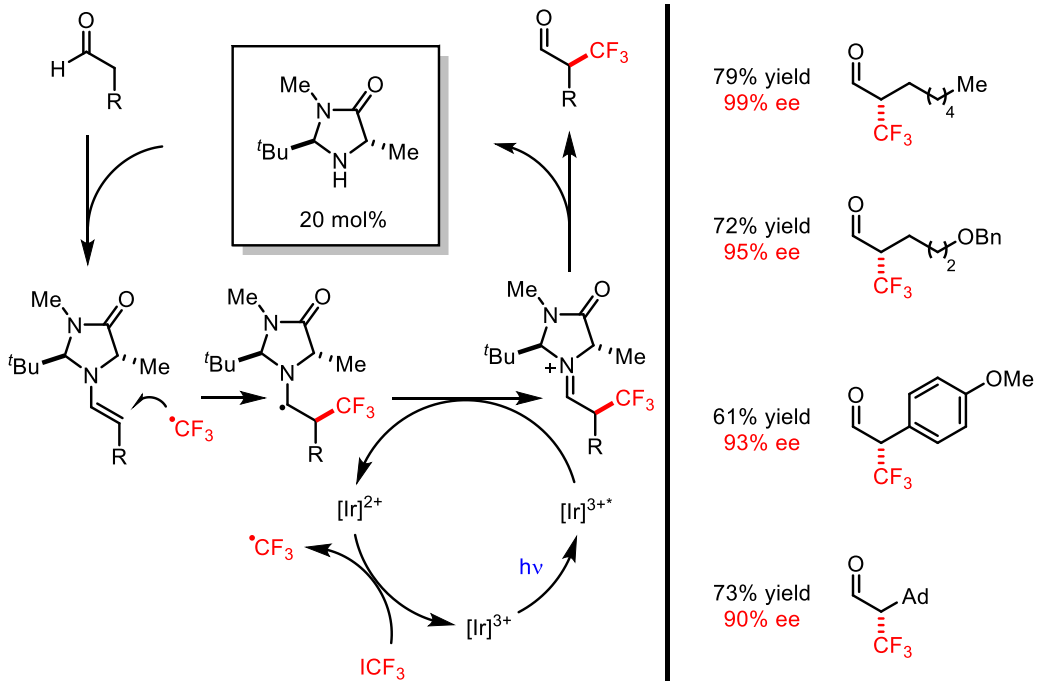

Figure 3.12 Enantioselective α-trifluoromethylation

Trifluoromethyl iodide has been utilized in a number of additional examples, including two iterations published by our research group on the atom transfer radical addition of organohalides across aliphatic alkenes.[155, 156] An additional example along these lines has been published wherein the product secondary iodide can be eliminated to provide vinyl CF_3 products from CF_3I.[157] The most significant improvement on these methods has been published by Sanford and Ye, wherein the CF_3 radical can be harnessed for the copper-catalyzed trifluoromethylation of aryl boronic acids (**Fig. 3.13**).[129] This chemistry also leverages two coinciding catalytic cycles, wherein the photoredox reactivity of $Ru(bpy)_3Cl_2$ interacts directly with a copper-catalyzed cross coupling reaction. A wide range of trifluoromethylated arenes could be synthesized in this manner. Interestingly, this chemistry is performed at elevated temperatures (60 ˚C), which in general coincides with shortened excited state lifetimes for photoexcited catalysts; however, clearly this limitation is not yet debilitating at these temperatures.

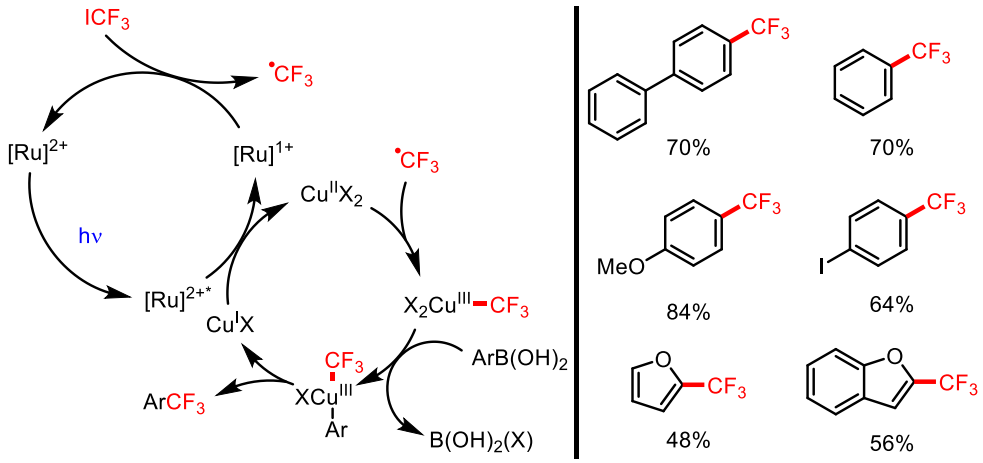

Figure 3.13 Trifluoromethylation of aryl boronic acids

Trifluoromethanesulfonyl chloride

MacMillan has also published a seminal radical trifluoromethylation of arenes and heterocycles using trifluoromethanesulfonyl chloride (CF_3SO_2Cl).[158] This reagent is reductively activated at mild potentials, and quenching studies have confirmed its ability to be reduced directly by the $Ru(phen)_3Cl_2$ photocatalyst. Single-electron reduction results in a fragmentation through loss of chloride anion and SO_2 gas, forming the CF_3 radical. This radical then is capable of addition to a range of arenes and heterocycles in good yields (**Fig. 3.14**). Dolbier and coworkers have also demonstrated the utility of CF_3SO_2Cl as a CF_3 radical source for cyclizations of *N*-aryl acrylamides, which essentially works in an identical catalytic fashion.[159]

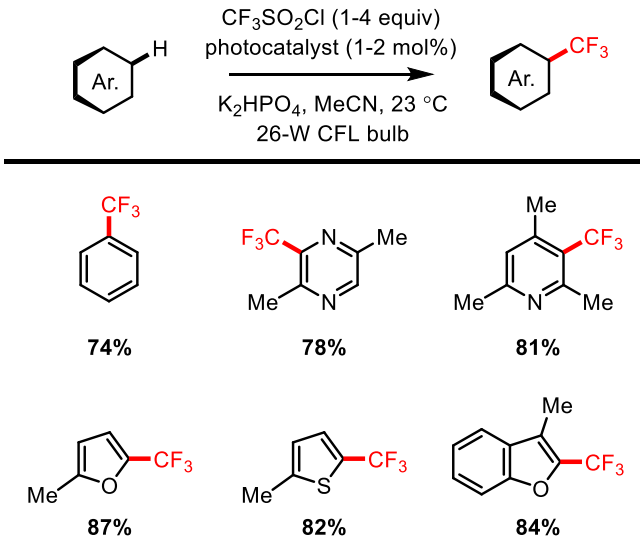

Figure 3.14 Trifluoromethylation of arenes with CF_3SO_2Cl

Umemoto's and Togni's Reagent

Reductive formation of the CF_3 radical has also been accomplished using Umemoto's reagent (*S*-(trifluoromethyl)dibenzothiophenium triflate) by Koike and Akita (**Fig. 3.15**).[160] This work proceeds through direct oxidative quenching of the photocatalyst, which in this instance was *fac*-Ir(ppy)$_3$. This highly reducing catalyst is more than capable of reducing Umemoto's reagent, which can undergo reduction at –0.75 V vs. Fc in MeCN (Fc = SCE + 0.38 V). Subsequent addition of the CF_3 radical to a styrenyl alkene provides a highly electron-rich radical that can be oxidized by the photocatalyst to the corresponding cation, which is then trapped by an alcohol to form the oxytrifluoromethylated products. The substrate scope of alkene was somewhat limited in this chemistry by the requirement of cation stability, and all the demonstrated examples were either styrenes or enol ethers.

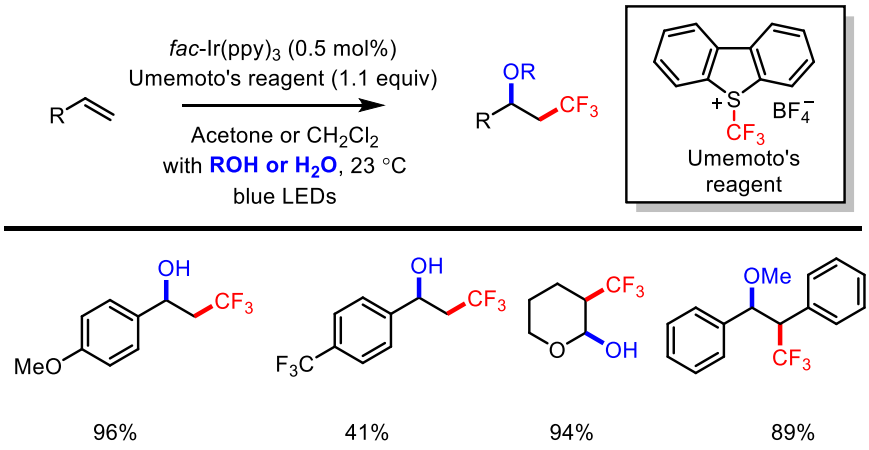

Figure 3.15 Oxytrifluoromethylation of alkenes with Umemoto's reagent

While the first iteration of their work in this arena accomplished the oxytrifluoromethylation of alkenes, subsequent publications detail various controlled reaction pathways for the intermediate carbocation; these include nucleophilic trapping with a variety of chemical species such as nitriles,[161] DMSO,[162] amides,[163] and triflates,[164] as well as elimination to the corresponding CF_3 alkenes through both deprotonation[165] and loss of BF_3.[166] Umemoto's reagent has also been used for the radical trifluoromethylation of alkenes followed by oxidative cyclization of hydrazones to form pyrazoline and isoxazolines by Xiao and coworkers.[167]

Togni's reagent has been utilized in a similar manner to Umemoto's reagent, although the reduction of Togni's reagent (–1.34 V vs. Fc and –1.49 V vs. Fc for the carbonyl and dimethyl variants respectively) is slightly more challenging than the reduction of Umemoto's reagent. These reagents have been used by Gouverneur and coworkers for the trifluoromethylation of allyl silanes,[168] as well as by Scaiano for the trifluoromethylation of alkenes and alkynes.[169] Togni's reagent has also been used for the radical C–H trifluoromethylation of free anilines.[170]

Sodium Trifluoromethanesulfinate

In a conceptually alternative approach, Nicewicz and coworkers have utilized sodium trifluoromethanesulfinate (Langlois' reagent) for the trifluoromethylation of alkenes.[171] This

work is significant in that the formation of the CF_3 radical requires a single-electron oxidation of the reagent, which produces an intermediate catalyst species which can only behave as a reductant. Consequently, the authors corrected the catalytic cycle for this chemistry by utilizing a hydrogen-atom donor in the form of thiophenol, which can transfer a hydrogen atom to the electron rich intermediate **46** (**Fig 3.16**). Reduction of the thiyl radical with the photocatalyst subsequently produces the ground-state photocatalyst, which can then re-enter the catalytic cycle. It should be noted that this chemistry could be accomplished without the addition of hydrogen-atom donor, but reaction times were significantly prolonged (>48 hr).

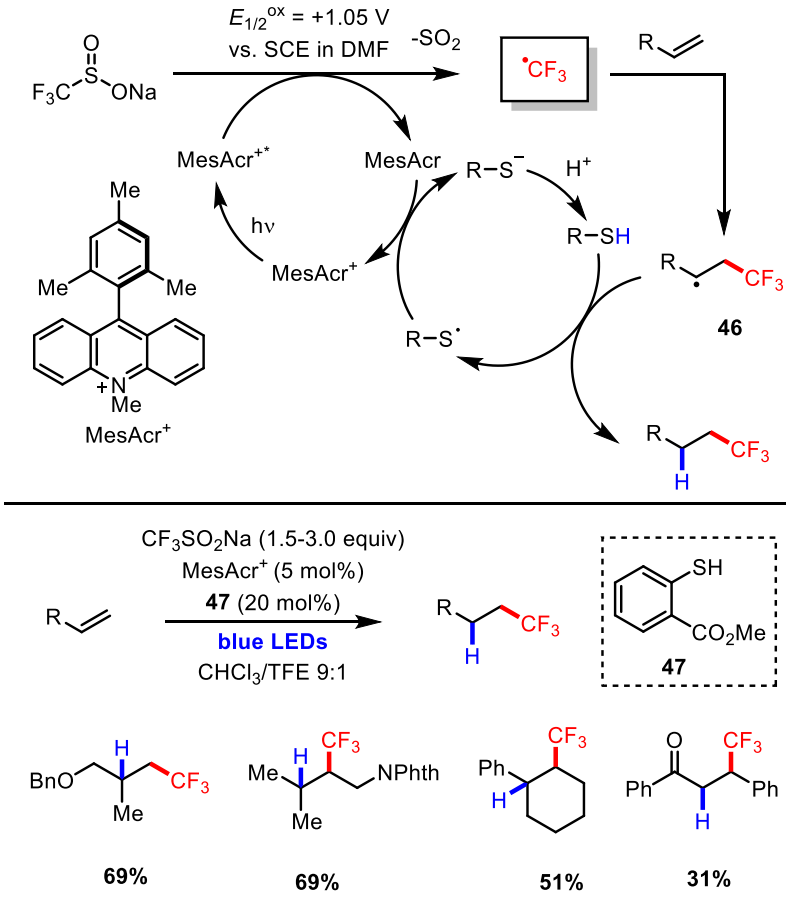

Figure 3.16 Hydrotrifluoromethylation with sodium trifluoromethanesulfinate

Photochemical Trifluoromethylations in Flow

While for industrial purposes the use of gaseous reagents is not a challenge, the most significant challenge in the use of gaseous CF_3I on laboratory scale is the ability to accurately control the stoichiometry of this reagent. Generally, methods to measure out this material have involved the preparation of a saturated solution by bubbling the gas through solvent.[129] This inherently wastes the gas—clearly undesirable—and furthermore results in estimations of stoichiometry rather than absolute measurements. As a solution to this issue, the use of a flow system can greatly improve the control of stoichiometry through the use of a mass-flow controller, which has been utilized by Noël and coworkers to great effect (**Fig. 3.17**).[172] Using $Ru(bpy)_3Cl_2$ as the photocatalyst, along with TMEDA as a reductive quencher and base, the authors were able to efficiently trifluoromethylate an array of pyrrole and indole substrates while accurately controlling the stoichiometry of CF_3I in the system. The trifluoromethylation of 3-methylindole was conducted on a 1.31 g scale to provide 2-trifluoromethyl-3-methylindole in 95% yield in this manner. Noël has also published an example of this reaction setup applied towards the trifluoromethylation of thiophenols.[173] Kappe and coworkers have also demonstrated the use of TfCl as a CF_3 source in flow, wherein the formation of silyl enol ethers in flow is followed by a photochemical trifluoromethylation with TfCl and eosin Y.[174]

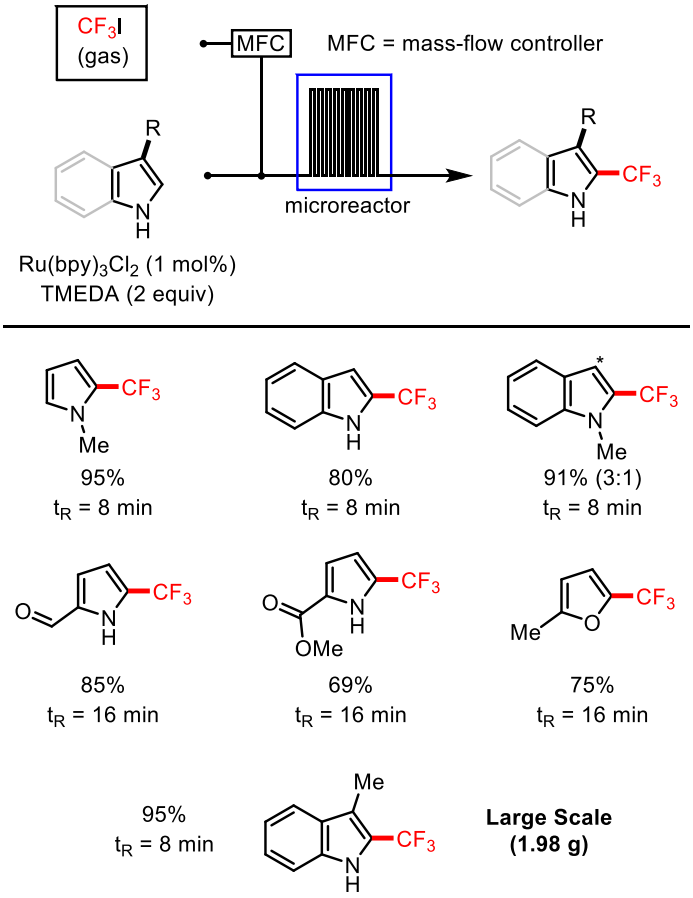

Figure 3.17 Trifluoromethylation in flow with a mass-flow controller

Conclusions

Photoredox catalysis has been shown to be remarkably effective for the trifluoromethylation of a variety of substrates. While CF_3I has by far been the most commonly used CF_3 source in this way, a wide array of reagents have been put to use through single-electron transfer to or from a photocatalyst. While this range of reagents is promising, each has drawbacks, and further work must be done to improve the utility of photoredox catalysis in this arena. For example, prior to our work in this area, no examples of photoredox catalysis existed for the use of TFA, TFAA, or HCF_3 in a radical trifluoromethylation reaction. This is a significant challenge which must be addressed. Furthermore, while photoredox catalysis is touted as an environmentally friendly alternative to traditional chemical methods, there is a distinct lack

of examples for the large-scale application of these methods. For example, to our knowledge, the trifluoromethylation of 3-methylindole by Noël (**Fig. 3.17**) to produce nearly two grams of product is the largest published example of a trifluoromethylation reaction using photoredox catalysis. The next chapter outlines our efforts to both improve the scalability and limit the expense of these transformations through the use of TFAA as a CF_3 source.

Chapter 4: Photochemical Perfluoroalkylations with Pyridine *N*-Oxides

*Portions of this chapter have been published in Beatty, J. W.; Douglas, J. J.; Cole, K. P.; Stephenson, C. R. J. A Scalable and Operationally Simple Trifluoromethylation. *Nat. Commun.* **2015**, *6*, 7919.

Introduction

Considering the literature precedent available for trifluoromethylation with photoredox catalysis, as well as precedent concerning TFA decarboxylation, we identified a clear need for further chemical development in this area. Specifically, the limitations of decarboxylative methods with photoredox catalysis led us to consider options for improving the scope of this chemistry to more electron-poor substrates. Additionally, we considered the decarboxylation of a TFA derivative to be a key testing ground for this concept, wherein TFA represented one of the most challenging substrates for decarboxylation.

With these goals in mind, a few literature reports were particularly inspirational in the ultimate design of our reaction system. First, we considered work by Barton and Zard, which utilized a thiohydroxamic acid as an activating group[175] for the decarboxylation of TFAA (**Fig. 4.1**).[176] Mixing the thiopyridone, TFAA, and DMAP together at room temperature, the authors demonstrated the *S*-trifluoromethylation of 2-thiopyridine in 96% yield after irradiating the reaction solution for 15 minutes with a 300W lamp. This chemistry could be extended to higher-order analogs including perfluoroethyl, perfluorobutyl, and perfluoroheptyl groups, all of which were observed to add back to the thiopyridone upon irradiation. Strikingly, the CF_3 radical generated under these reaction conditions could not be utilized for addition across even primary

alkenes. For higher-order fluoroalkyl radicals such as the perfluorobutyl radical, alkenes could be trapped by the intermediate fluorinated radical, but the alkene had to be used in solvent quantities. Even with this considerable stoichiometric bias, the major byproducts in all cases were the result of thiopyridine alkylation.

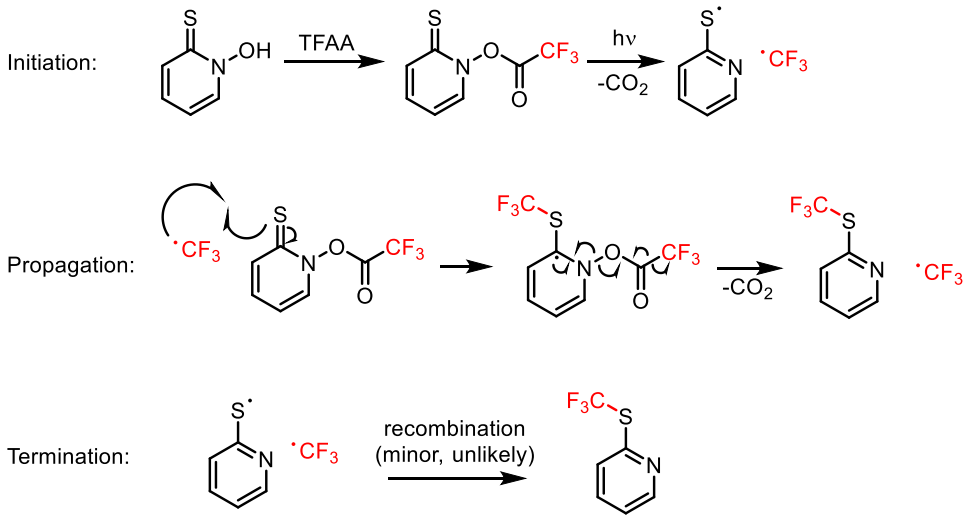

Figure 4.1 The Barton decarboxylation preferentially forms CF_3-thiopyridines

This chemistry is striking for a number of reasons. Firstly, the decarboxylation of TFAA was accomplished under mild photolytic conditions (albeit with UV light) and high yield of products were generally obtained. In a similar vein to the work by Sawada, a weak heteroatom-heteroatom bond (in this case S–O) could result in formation of the carboxylate radical under mild conditions; however, the use of peroxides is fairly hazardous, especially on scale, and the use of the thiohydroxamic acid which Barton has pioneered is much more desirable in this aspect. This chemistry was also striking in the difficulty which the authors encountered when attempting to utilize the CF_3 radical for addition to pi-systems other than the thiopyridine. This is most likely due to electronic effects, which result in the selective addition of electron-poor radicals to electron rich systems.[177] This is also true for the inverse electronic regime, wherein an electron-rich radical will preferentially add to an electron-poor pi-system. In consideration of

these factors, it became clear to us that if we were to use an additive to alter the redox-properties of TFA or TFAA, it would need to possess an electron-poor pi system in order to discourage non-productive CF_3 reactivity with its activating group.

An additional example which inspired this work was published by Oda and Okada in 1991, which accomplished the decarboxylation of a number of carboxylic acids through the initial acylation of *N*-hydroxy phthalimide (**Fig. 4.2**).[178] This work accomplished the decarboxylation of three different carboxylate substrates, each of which formed an electron-rich radical upon decarboxylation, which then was harnessed in an addition to an enolate coupling partner. This work demonstrated that decarboxylation of an alkyl carboxylic acid can be accomplished through a reductive mechanism—a process which we were keen to emulate. Sanford has demonstrated that the use of *N*-hydroxyphthalimide in conjunction with TFAA does not result in the formation of the CF_3 radical, but results in the formation of trifluoroacetate and the phthalimide radical upon single-electron reduction.[179] This suggested that an alternative activation group would be necessary for the development of radical trifluoromethylation chemistry.

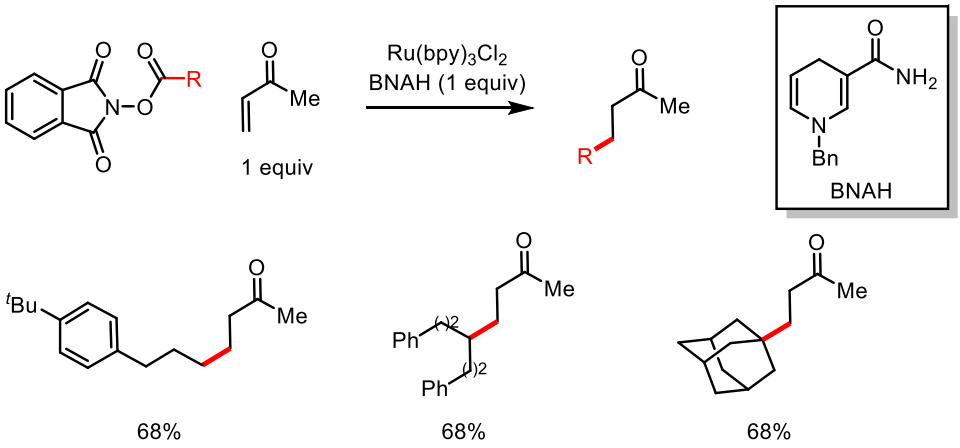

Figure 4.2 Decarboxylation of *N*-acyloxyphthalimides

Reaction Design and Scope

In the context of these publications, we decided to investigate the use of a chemical additive to tune the redox behavior of TFAA to within a more feasible electrochemical window for reaction with $Ru(bpy)_3Cl_2$ (**Fig. 4.3**). $Ru(bpy)_3Cl_2$ possesses electrochemical reactivity between –1.33 V to +1.28 V vs. SCE in MeCN, and has clearly been demonstrated to be capable of both reductive and oxidative electrochemical events. As such, we decided to approach this chemistry with a combination of lessons learned from the literature (*vide supra*, Introduction). Specifically, we wanted to use an electron-poor compound which would not readily undergo trifluoromethylation in the presence of more electron-rich pi systems. This was specifically intended to avoid the difficulties encountered in the Barton chemistry, wherein the majority of CF_3 radical added back to the thiopyridone redox activator. As the majority of trifluoromethylation chemistry using TFA derivatives is performed on electron-poor substrates, we considered this to be a key design feature in order to expand the utility of this CF_3 source.

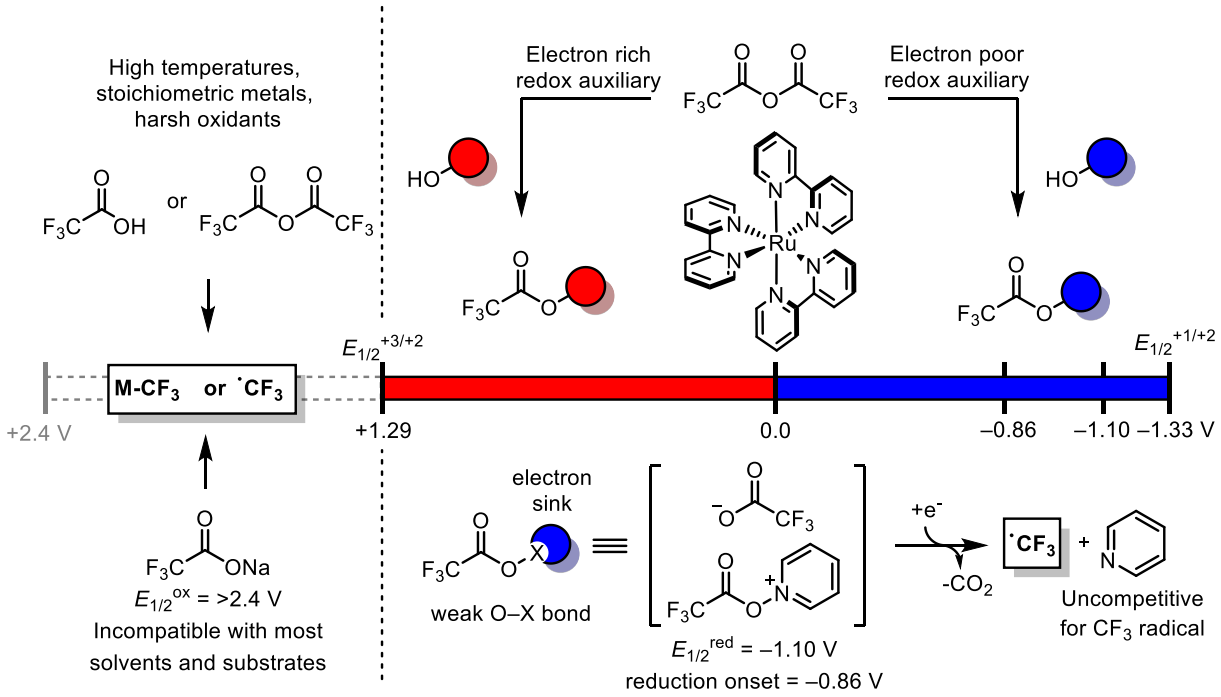

Figure 4.3 Reaction design for TFAA decarboxylation

In addition to the requirement for an electron-poor chemical additive, we required a reagent which possessed a weak heteroatom-heteroatom bond for fragmentation; furthermore, this reagent could not be a peroxide due to safety concerns. As a consequence, we turned our attention to the use of pyridine *N*-oxide and its derivatives as an activating reagent for TFAA reduction. This choice met all of our requirements, as pyridine *N*-oxide is inexpensive ($40-$70 kg^{-1} on 1,000 kg scale), possesses a weak N–O bond, and presents a cationic pi-system upon acylation. Furthermore, the reduction of the acylated adduct provides pyridine as a byproduct of the reaction, which then can act as a necessary base for further C–H functionalization by the concomitantly formed CF_3 radical.

Initially, we approached the optimization of this reaction by examining three simple electron rich substrates, including 1,4-dimethoxy benzene, mesitylene, and 4-chloroanisole (**Table 4.1**). We had several initial procedural concerns, and made an initial effort to simplify

reaction setup as much as possible. Primarily, it was suspected that the hygroscopic nature of pyridine *N*-oxide might interfere with reaction efficiency, as water is incompatible with TFAA. Our pyridine *N*-oxide in the closet has absorbed so much water that it had turned into a liquid (it is deliquescent), but in control reactions comparing dry and lyophilized PNO to this hydrated version showed minimal differences (entries 1-2). Yields were very substrate dependent, with mesitylene (entry 3) providing higher yields than either of the other two substrates. For 4-chloro anisole, degassing the reaction was found to provide insignificant improvement in product yield (entries 8-9), and so for this work, the reactions were not degassed at all. Later, we found that for some substrates such as mesitylene, yields go up 5-10% in the absence of oxygen, and our fully optimized conditions eventually consisted of a degassing step.

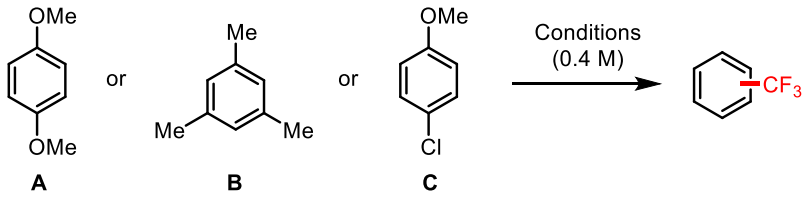

Entry	Substrate[a]	Solvent	Catalyst (1 mol%)	pyridine-*N*-oxide (equiv.)	TFAA (equiv.)	Time (h)	Yield (%)[b]
1	**A**	CH_2Cl_2	$Ir(ppy)_2(dtbbpy)PF_6$	2[c]	2	24	39%
2	**A**	CH_2Cl_2	$Ir(ppy)_2(dtbbpy)PF_6$	2	2	24	39%
3	**B**	CH_2Cl_2	$Ir(ppy)_2(dtbbpy)PF_6$	2	2	12	62% (56:6)[d]
4	**C**	CH_2Cl_2	$Ir(ppy)_2(dtbbpy)PF_6$	2	4	24	33% (2:1)[e]
5	**C**	CH_2Cl_2	$Ir(ppy)_2(dtbbpy)PF_6$	2	4	24	37% (2:1)[e]
6	**C**	CH_2Cl_2	$Ru(phen)_3Cl_2$	2	4	24	15%
7	**C**	CH_2Cl_2	$Ru(bpy)_3Cl_2$	2	4	24	38% (2:1)[e]
8	**C**	CH_2Cl_2	$Ru(bpy)_3Cl_2$	1	1.1	15	33%
9[f]	**C**	CH_2Cl_2	$Ru(bpy)_3Cl_2$	1	1.1	15	34%
11	**C**	MeCN	$Ru(bpy)_3Cl_2$	2	4	15	42% (2:1)[e]
12	**C**	MeCN	$Ru(bpy)_3Cl_2$	2	4	45	55% (2:1)[e]
13	**C**	MeCN	$Ru(bpy)_3Cl_2$	4	8	15	51% (2:1)[e]
14	**B**	MeCN	$Ir(ppy)_2(dtbbpy)PF_6$	1	1.1	15	48% (45:3)[d]
15	**B**	MeCN	$Ir(dF(CF3)ppy)_2(dtbbpy)PF_6$	1	1.1	15	32% (31:1)[d]
16	**B**	MeCN	$Ru(bpy)_3Cl_2$	1	1.1	15	52% (48:4)[d]
17	**B**	MeCN	9-Mesityl-10-methylacridinium	1	1.1	15	7%
18	**B**	MeCN	Eosin Y (5 mol%)	1	1.1	15	0%
19	**B**	CH_2Cl_2	$Ru(bpy)_3Cl_2$	1	1.1	15	50% (47:3)[d]
20	**B**	DMF	$Ru(bpy)_3Cl_2$	1	1.1	15	25%
21	**B**	MeCN	$Ru(bpy)_3Cl_2$ (0.1 mol%)	1	1.1	15	51% (48:4)[d]
22	**B**	MeCN	none	1	1.1	15	0%
23[g]	**B**	MeCN	$Ru(bpy)_3Cl_2$	1	1.1	15	0%
24	**B**	MeCN	$Ru(bpy)_3Cl_2$	none	1.1	15	0%
25	**B**	MeCN	$Ru(bpy)_3Cl_2$	2	2.1	15	**69% (59:10)**[d]
26	**B**	MeCN	$Ru(bpy)_3Cl_2$	3	3.1	15	71% (49:22)[d]

[a]Run on 0.8 mmol scale. [b]F NMR yields vs. 1 equivalent of trifluorotoluene as internal standard. [c]Dry, lyophilized pyridine-*N*-oxide used. [d]Mono-:di-functionalized product ratio. [e]Regioisomeric ratio. [f]Degassed (freeze-pump-thaw x 3) [g]Light excluded.

Table 4.1 Optimization of the PNO trifluoromethylation

Further optimization revealed several things. While the initial reaction hit was performed in dichloromethane, the use of higher equivalents of the PNO/TFAA reagent combination did not

result in better yields (ex. entries 7-8). Closer inspection revealed that this effect was due to an insolubility of the reagent combination, which resulted in an oiling-out of the reagent on the bottom of the vial. This residue was clear and difficult to see without close inspection. Fortunately, the use of MeCN as solvent allowed for multiple equivalents of reagent to be used in a fully soluble state, and subsequent reactions were mostly run in MeCN. Entries 11-13 detail this effect, wherein the use of two reagent equivalents required a full 45 hours to reach reaction completion, while doubling the equivalents of PNO used resulted in similar yields but after only a third of the time.

A catalyst screen (entries 12-18) revealed that $Ru(bpy)_3Cl_2$ provided the highest yields for this reaction. The use of 9-mesityl-10-methylacridinium (Fukuzumi's catalyst)[180] predictably did not provide high yields of product, as it is a strong oxidant while this chemistry requires an initial reduction event. Similarly, Eosin Y was incompatible with the reaction conditions, as it contains a number of anionic oxygens which are readily acylated upon addition of TFAA. This was accompanied by a dramatic loss of color from the solution. Re-testing our solvent choice (entries 19-21), we found that MeCN behaved similarly to CH_2Cl_2, and proceeded with MeCN as our solvent of choice, both due to its improved ability to solubilize the reagent as well as the industrial preference to avoid the use of dichloromethane.

Several control experiments were then run with mesitylene as the substrate. The exclusion of light (entry 23) provided no detectable product formation, and the exclusion of pyridine *N*-oxide (entry 24) also gave 0% yield of the desired product. Increasing the equivalents of the reagent provided higher yields of product, but with significantly diminishing returns (entries 25 and 26). Furthermore, the use of these conditions resulted in the formation of more bis-functionalized product, which is merely a function of the higher yields. Because there were

higher levels of mono-functionalized material present later in the reaction, CF_3 radical formed at this late stage would have a stoichiometric bias for the already-functionalized material despite the altered electronics.

With these results in hand, we set out to explore the substrate scope of the reaction. Inherently, this work is designed to provide access only to the trifluoromethylation of electron-rich substrates, as the transition to electron-poor substrates would be expected to competitively functionalize the pyridine redox-auxiliary. As expected, the attempted trifluoromethylation of a range of electron-poor substrates did not provide appreciable yields of the desired products (**Fig. 4.4**). Even pyridines substituted at the 3 and 4 positions with methoxy groups were unreactive under the reaction conditions, and insignificant amounts of trifluoromethylated reagent were observed. As a general principal, sufficiently electron-poor substrates contributed to lower conversion of the reagent, a phenomenon which may be attributable to more difficulty in the aromatization process.

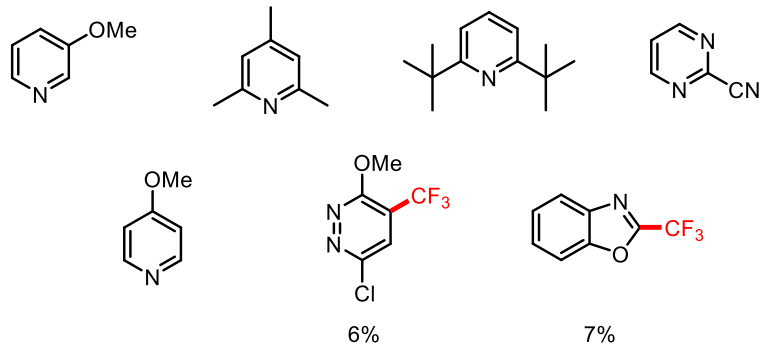

Figure 4.4 Electron-poor substrates incompatible with the methodology

Despite the lack of reactivity for electron-poor substrates, a wide array of electron-rich substrates were reactive under the reaction conditions. Simple substituted arenes such as 1,4-dimethoxy benzene, methyl benzoate, and methyl *p*-anisate were trifluoromethylated in moderate yields (**Figure 4.5A**). Benzene was also a decent substrate for the reaction, although its

functionalization served as a proof-of concept more than an actually useful application due to the large availability of benzotrifluoride. In a demonstration that the electron-poor heterocycles above in **Figure 4.4** were unreactive due to electronic factors, 4,6-dimethoxypyriimidine could be functionalized in moderate yields with this chemistry.

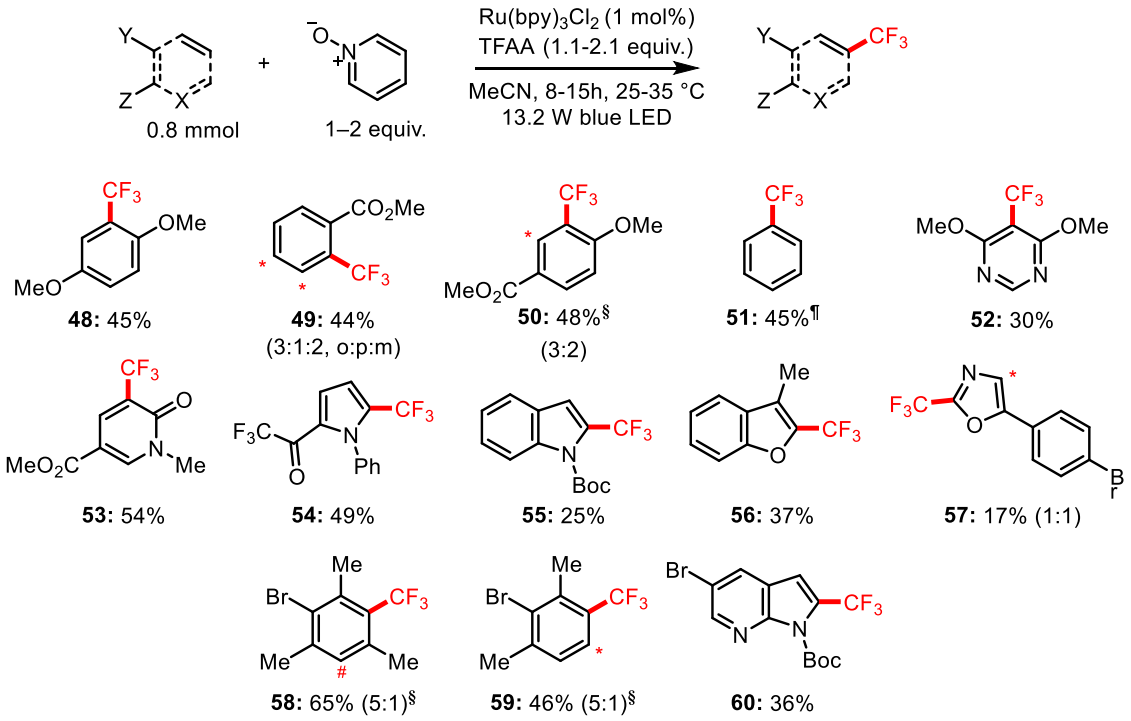

Figure 4.5 Trifluoromethylation of various substrates with TFAA

A number of electron-rich heterocycles could also be functionalized. Pyridones served as good substrates, where the position *ortho* to the oxygenated position was the most electron-rich and consequently functionalized selectively. A range of 5-membered heterocycles provided moderate to good yields for this chemistry, with pyrrole derivatives generally performing best. Indoles were surprisingly poor substrates, and we later learned that this is likely due to their low ionization potential. Brominated arenes were also well tolerated (**Fig. 4.5B**).

Before evaluating the scalability of this reaction, a few things should be mentioned. Firstly, this reaction is moderately incompatible with free heteroatom functional groups containing O–H or N–H bonds, as these groups are readily acylated by TFAA. For example, *N*-Boc aniline is not a good substrate for the reaction; despite its electron-density, the free N–H group is readily acylated by TFAA, which in turn deactivates the aryl ring to further reaction with the electron-rich trifluoromethyl radical. Even when an excess equivalent of TFAA is used, this substrate is unreactive under the reaction conditions. As a consequence, acylatable groups are likely only compatible if they are removed from the pi-system in question, and their presence may add additional synthetic steps for the removal of the trifluoroacetate group upon reaction completion.

Another substrate limitation is that there is a threshold limit for electron-density for the substrates. For example, mixing *N*-phenyl pyrrole with TFAA results in the Friedel-Crafts acylation of the heterocycle; this results in a roughly 9:1 ratio of acetyl pyrroles functionalized at the 2 and 3 positions, respectively. While the product 2-trifluoroacetyl *N*-phenyl pyrrole is itself a good substrate for this trifluoromethylations chemistry (**Fig. 4.5A**), the lack of regioselectivity in the acylation reaction limits the utility and yields obtained from a 1-pot acylation/trifluoromethylations process. Similarly, *N*-methyl indole is too electron-rich for the reaction conditions and undergoes Friedel-Crafts acylation at the 3-position.

Alkenes were found to be good substrates for the trifluoromethylation reaction, as they are more reactive to the addition of the CF_3 radical than pyridine; however, a few considerations currently constrain the scope of this chemistry. Generally, styrenes are the only alkenes which are suitable substrates for this chemistry, which has provided significant mechanistic insight into the reaction mechanism. The photocatalyst is thought to readily oxidize the intermediate radical

to its corresponding cation, as it is highly unlikely for trifluoroacetate to add to this position in any role other than as a nucleophile. Further evidence for this mechanism is provided by solvent choice. When performed in acetonitrile, these reactions also provide varied amounts of the Ritter product, which results from nucleophilic trapping of the cation by solvent. This reaction pathway may be avoided by using CH_2Cl_2 as a solvent instead. The products of atom transfer onto styrenes can be utilized in two different manners. Firstly, upon the addition of methanol to the crude reaction mixture and stirring for one hour, the trifluoroacetate can be methanolyzed to form benzylic alcohol products. Likewise, the product of the ATRA reaction can be subjected to strong base such as DBU to promote elimination to the styrene product. Each of these transformations can be conducted in a one-pot manner, and are quite efficient.

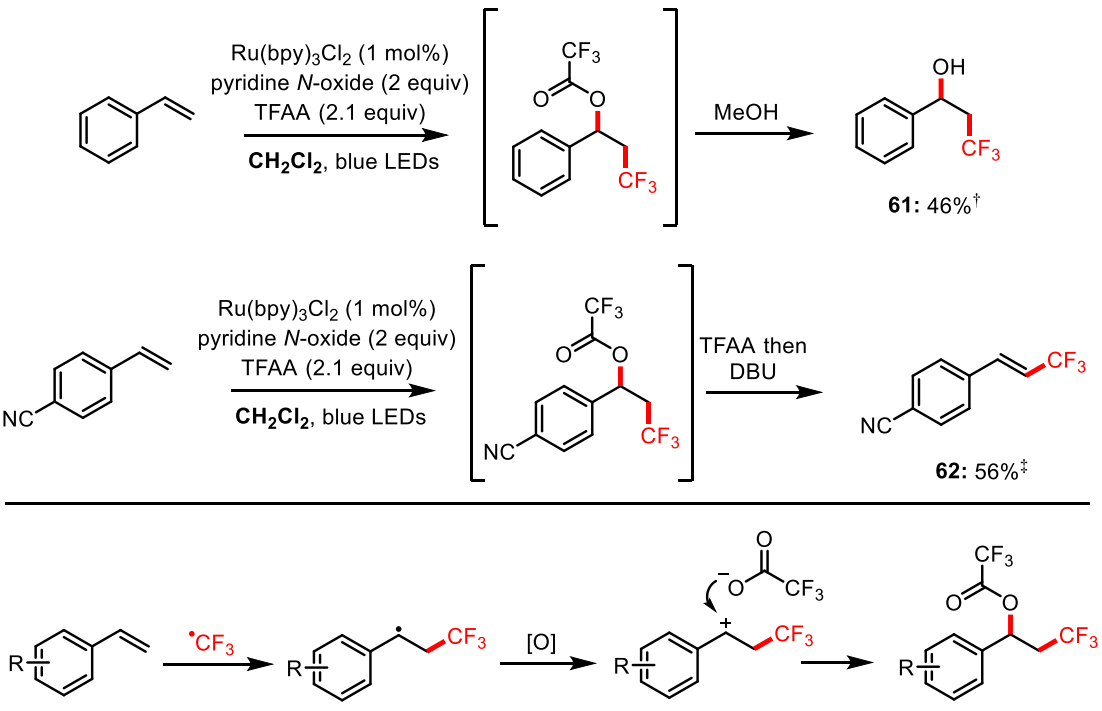

Figure 4.6 Trifluoromethylation of styrenes with TFAA

When primary alkenes are used which are out of conjugation with a pi-system, the resultant radical likely cannot undergo efficient oxidation by the photocatalyst, as no atom transfer radical addition (ATRA) products are observed under these conditions. (**Fig. 4.7A**). The resultant radical of alkene addition is nucleophilic in character, and can add back to the pyridine in solution in a fairly selective fashion. This reactivity has been observed by Baran and coworkers in their sodium trifluoromethanesulfinate chemistry, as *tert*-butyl-hydroperoxide contains a small amount of isobutylene as a stabilizer, which the CF_3 radical adds to in minor quantities.[134] A sole exception to the styrene scope is the use of *N*-phenyl acrylamides such as **63**, which upon addition of the CF_3 radical can undergo intramolecular cyclization onto the electron-rich arene to provide oxindole products in moderate yields (**Figure 4.7B)**.

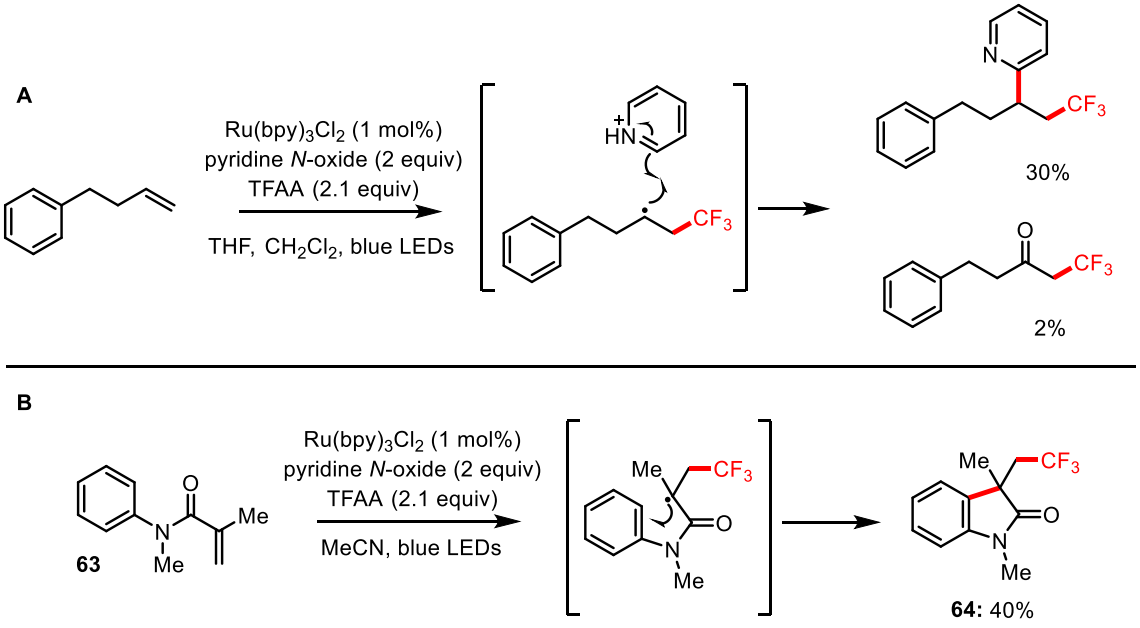

Figure 4.7 Alkene trifluoromethylations of non-styrenyl substrates

We have also demonstrated the utility of this chemistry in the synthesis of a chloropyridine intermediate which is of interest to Boehringer Ingelheim for the synthesis of anti-infective drugs (**Fig. 4.8**). A recent report concerning the synthesis of this material on scale

detailed the importance of CF_3 source selection, and discussed the relative difficulties of choosing a feasibly scalable route to this material.[144] In particular, the authors noted that for trifluoromethylations on large scale "[a]pplications of Ruppert's reagent (R_3SiCF_3, R = alkyl) are most prominent. However, the large-scale availability of CF_3SiMe_3 and higher alkyl variants is still limited, and their cost can be prohibitive for use in commercial pharmaceutical manufacture." For the author's production of the chloropyridine on scale, they developed instead a methodology utilizing MCDFA as a CF_3 source in the presence of superstoichiometric CuI. The optimized route for this chemistry was performed on a 7.0 kg scale, which required 6.65 kg of CuI. While the scale was impressive, the removal of copper was problematic, and additional workup steps were required for its safe removal. In the context of this chemistry, we sought to examine the utility of our trifluoromethylation methodology. We trifluoromethylated the pyridone **65** in 54% yield, and then subjected it to a chlorination/demethylation reaction which provided the desired synthon in 47% yield. While these yields are lower than those reported in the large scale copper trifluoromethylation (63% isolated), this demonstrates the use of minimal amounts of transition metal (0.1 mol% Ru vs. 120 mol% Cu) and uses TFAA directly.

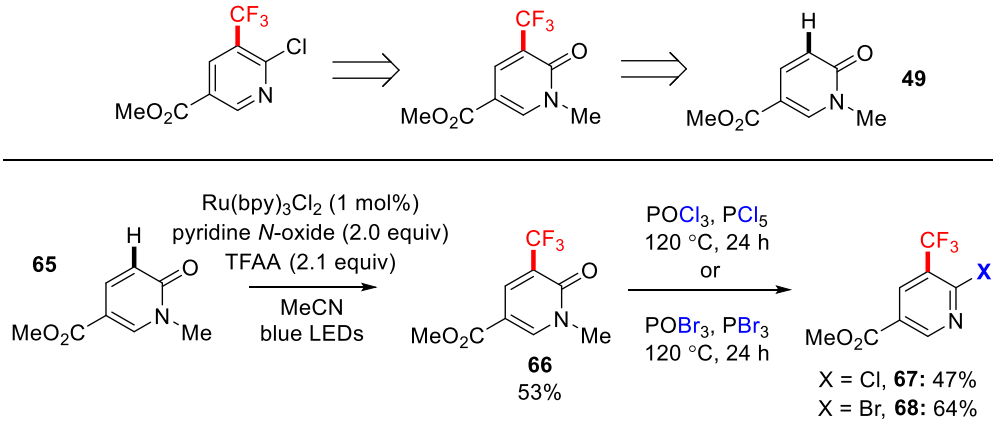

Figure 4.8 Synthesis of a pharmaceutically relevant chloropyridine

We then investigated the scalability of this chemistry in multiple stages. While every reaction for substrate scope was carried out on a 0.8 mmol scale, we transitioned to a 5 gram scale in batch for a number of representative substrates. **Figure 4.9** displays the substrates which were trifluoromethylated on this scale. Generally, minimal losses in yield were observed between the 0.8 mmol and 5 gram scales, preliminarily confirming the scalability of this chemistry. Reaction scale-up to produce MIDA boronate **73** and the brominated indole **74**, proceeded smoothly, and these structures were readily cross-coupled to provide a doubly-trifluoromethylated product.

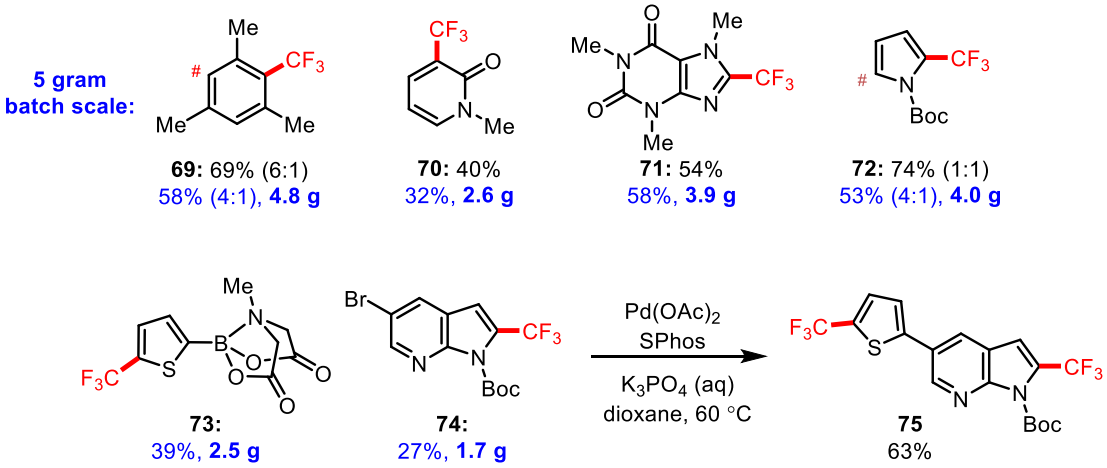

Figure 4.9 Scale up to 5-gram batch reactions

Having observed moderate scalability, we then pushed the limits of this reaction further in the scale-up of the trifluoromethylation of *N*-Boc pyrrole. We chose this substrate as an ideal example, as it is neither oxidatively nor thermally stable, and represents a substrate class which has traditionally been inaccessible to ready functionalization with TFA derivatives by any means. In an 18.3 gram batch reaction, we were able to trifluoromethylate *N*-Boc pyrrole in 57% isolated yield with a 5:1 ration of mono:bis functionalization, which was a yield comparable to what was obtained on a 0.8 mmol and 5.0 gram scale (**Fig. 4.10**). Further attempts to scale this chemistry were initially met with difficulty; we performed a trifluoromethylation of 100 gram

scale in batch, which required the use of a 3 L round bottom flask and an overhead mechanical stirrer. This reaction used 1.0 liters of MeCN, 453 mg of $Ru(bpy)_3Cl_2$, 115 grams of pyridine *N*-oxide, and 267 grams of TFAA. Unfortunately, on this scale reaction times were notably longer, and the reaction stalled at 35% yield of product (33% mono, 2% bis by FNMR assay). While the yields for this process were low, the overall cost of reagents (academic vendor pricing) was calculated to be less than $150.

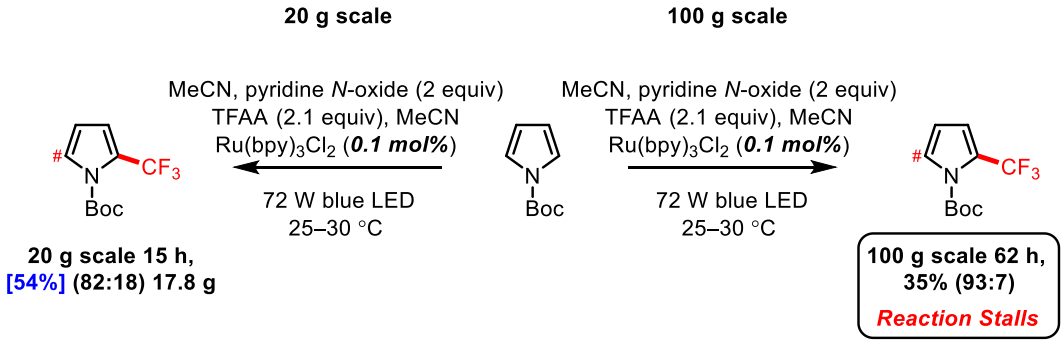

Figure 4.10 Batch scale-up of the trifluoromethylation

Scale-Up in Flow

The difficulty of performing this reaction on larger scale suggested that light penetration was an issue for adequate reactivity in this type of reactor. A number of factors including reaction concentration, catalyst loading, and light intensity will affect the distance of light penetration into solution. These effects can be simplified and visualized for any light of a given intensity, wherein the percent of light absorbance can be plotted against the path length in solution according to Beer's law.[94] Using the extinction coefficient of $Ru(bpy)_3Cl_2$ at 452 nm (ε = 1300 M^{-1} cm^{-1})[3] it is possible to plot the absorbance of the solution with path length for a known concentration of the photocatalyst. Using Beer's law in the form of:

$$A = \varepsilon l c$$

where ***A*** is absorbance, ***ε*** is the extinction coefficient, ***l*** is path length, and ***c*** is concentration, it is possible to obtain a linear dependence of absorbance upon path length. Absorbance can be mathematically converted into percent absorbance (***%A***) by assuming that:

$$\%A = 1 - \%T$$

$$\%T = 10^{-A}$$

$$\%A = 1 - \ 10^{-A}$$

Where ***%T*** represents the percent of light transmitted. As a consequence of this, plotting the following relationship demonstrates the percent of light transmitted with distance at a given concentration:

$$\%A = 1 - \ 10^{-\varepsilon \, l \, c}$$

For example, assuming a reaction concentration of 0.1 M, with a photocatalyst loading of 1.0 mol%, the concentration of $Ru(bpy)_3Cl_2$ in solution is 1.0 $x10^{-3}$ M. For a solution of this concentration, over 95% of the incident light is absorbed by the solution in under 1.0 mm (**Fig. 4.11,** blue line). If the reaction solution is concentrated by a factor of 4 to 0.4 M (the concentration of the trifluoromethylation protocol) while maintaining the 1.0 mol% catalyst loading, over 99% of the incident light is absorbed within the first 0.5 mm (**Fig. 4.11,** red line). The path length is significantly lengthened if the catalyst loading is decreased by a factor of 10 to 0.1 mol%, which would result in roughly 95% absorbance of light in the first 2.5 mm of solution (**Fig. 4.11,** green line). These curves adequately rationalize the lack of reactivity observed on the 100 gram batch trifluoromethylation reaction, as light penetration into solution only irradiates roughly the outer 3 mm of the flask, which as a percentage of the overall volume of the flask is very small.

The use of alternative photocatalysts can result in vastly different light penetration profiles. For example, the organic dyes Fluorescein and Eosin Y possess very high extinction coefficients (92000 M^{-1} cm^{-1} at 499 nm and 112000 M^{-1} cm^{-1} at 526 nm, respectively),[181] and consequently display abbreviated path-lengths at these wavelengths (**Fig. 4.12**). The high absorbance of these organic dyes is not a general rule, however, as Fukuzumi's catalyst (Mes-Acr^{+}) has a lower extinction coefficient (5500 M^{-1} cm^{-1} at 500 nm)[182] than common polypyridyl metal photocatalyst such as $Ru(bpy)_3Cl_2$ or $Ir(ppy)_3$ (7200 M^{-1} cm^{-1} at 375 nm).[183]

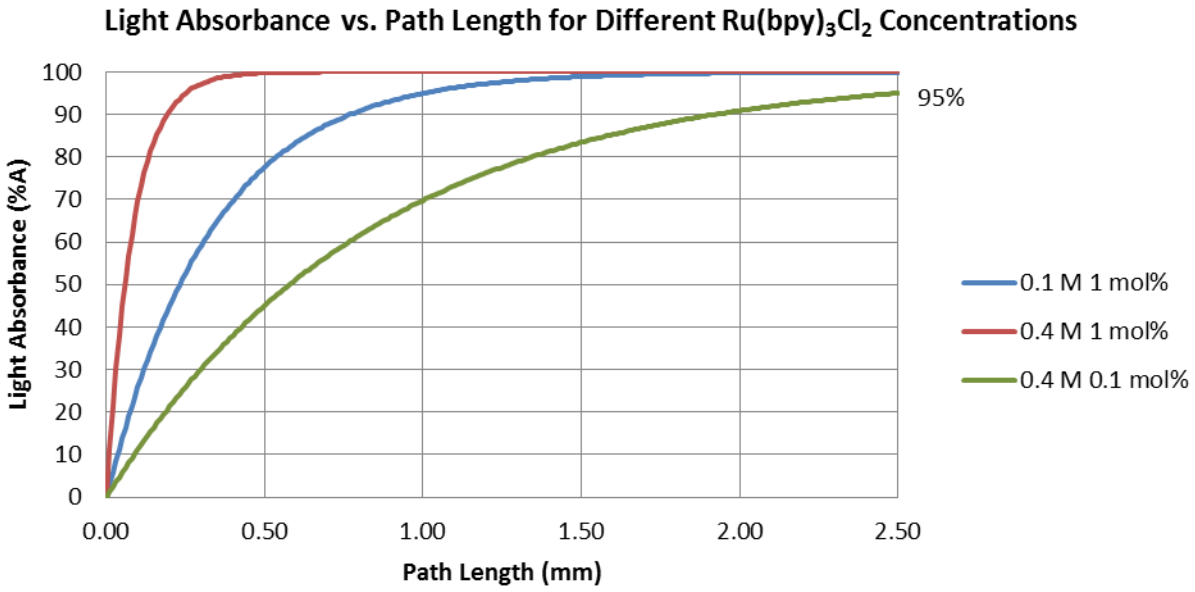

Figure 4.11 Light absorbance vs. path length for varied $Ru(bpy)_3Cl_2$ concentrations

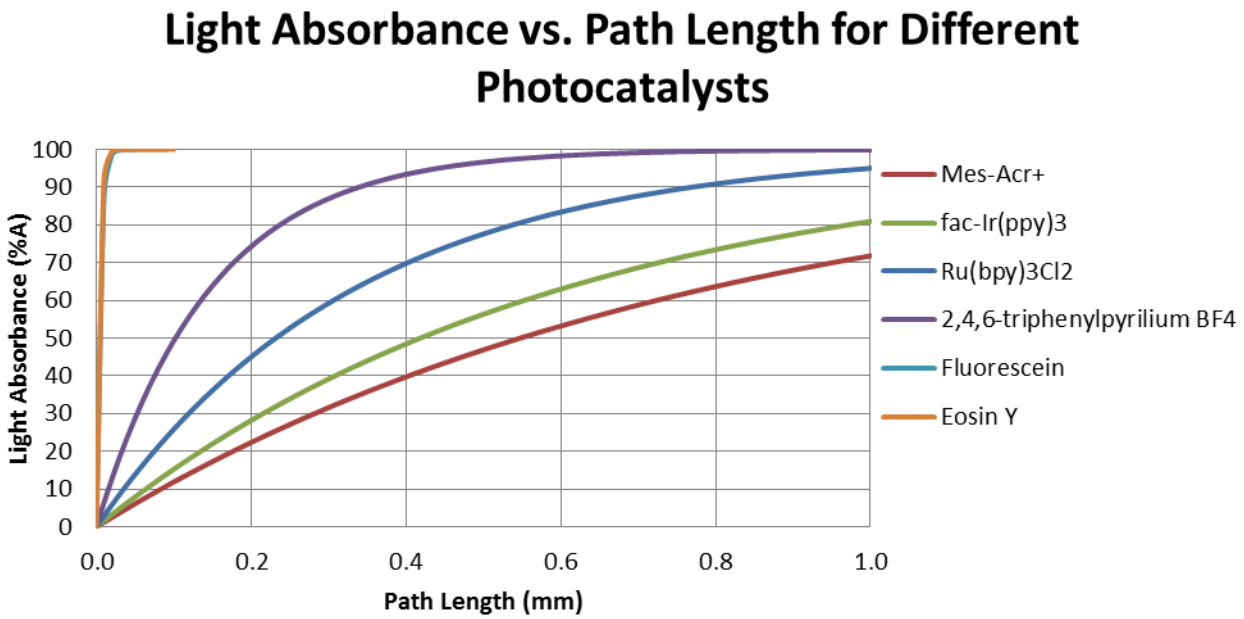

Fig 4.12 Effect of extinction coefficient on path length

As a solution to the limited light penetration into solutions of $Ru(bpy)_3Cl_2$, we turned to performing our trifluoromethylation reaction in flow in order to improve levels of catalyst activation (**Fig. 4.13**). Using a flow reactor with a 10 ml internal volume, we were able to trifluoromethylate 20.0 grams of *N*-Boc pyrrole over a period of 6 hours in 77% yield (46% mono, 31% bis). While not yet validation that this chemistry can be run on 100 gram scale or greater, this yield was significantly higher than that of the analogous batch reaction (57%), and furthermore was indicative that this reactivity can be achieved in a much faster manner (3.33 grams per hour).

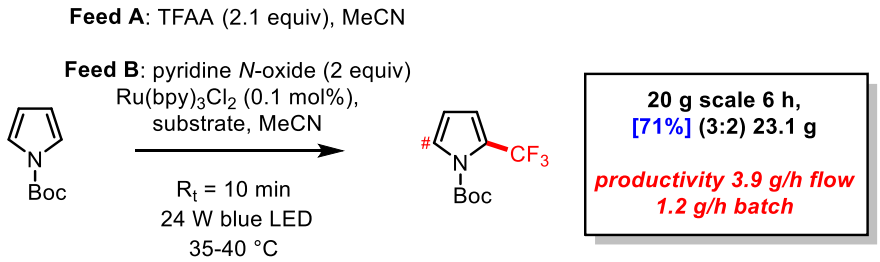

Figure 4.13 Flow apparatus for medium scale trifluoromethylation

We have further investigated the scalability of this chemistry on a 1.2 kg scale, which is to our knowledge a larger scale radical trifluoromethylation than any reported in the literature. This work required a significant amount of engineering, as the photochemical reactor was built from scratch. To ensure catalyst and substrate stability before material entered the reaction vessel, two separate solutions were used, one containing photocatalyst, pyridine *N*-oxide, and our substrate pyrrole, while the other contained TFAA, both solutions being made up in MeCN. The reactor consisted of an initial length of wider 3/8" diameter tubing, which served as a mixing zone for the reactants after they were combined but before they entered the irradiated vessel (**Fig. 4.14**). After exiting this stretch of tubing, the solution entered the reactor, which was submerged in water and temperature controlled with a glycol cooling loop. The reactor itself was constructed out of 1/8" PFA tubing which was 250 feet long and possessed and internal volume of 151 mL. Three blue aquadock® lights were used as the light source, which were placed in the center of the coiled reactor. The outside of the reactor was surrounded with an aluminum drum, which served to reflect unused light back at the photoreactor.

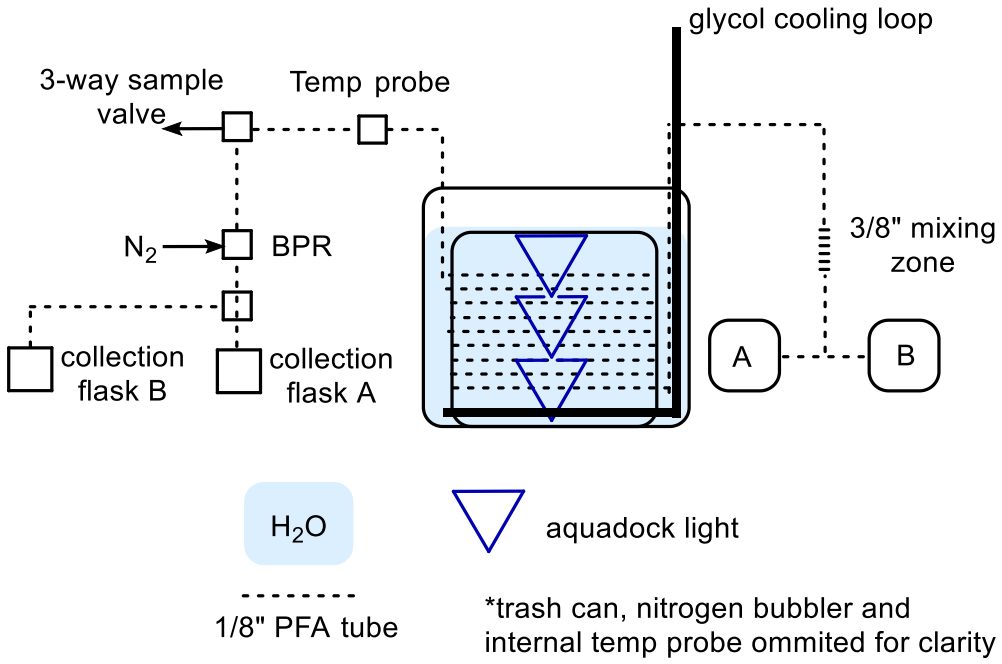

Figure 4.14 Schematic of large-scale flow reactor

Using methyl *N*-Boc-pyrrole-2-carboxylate as the substrate with 0.1 mol% $Ru(bpy)_3Cl_2$, 2 equivalents of PNO and 2.1 equivalents of TFAA, the reaction was optimized to a 30 minute residence time with an overall flow rate of 5.03 mL min^{-1}. Roughly half a kilogram of material was consumed in the optimization process. Under optimized conditions, 1.2 kilograms of the pyrrole were functionalized in 60-65% assay yield, producing 948 grams of a crude oil with 81% purity (**Fig. 4.15**). The purification process required the removal of the Boc group with TFA, which resulted in a 77% yield of the deprotected pyrrole in 98% purity after recrystallization.

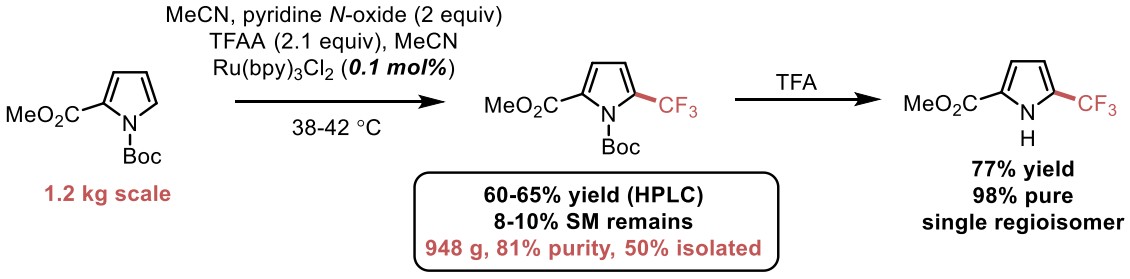

Figure 4.15 Trifluoromethylation on 1.2 kilogram scale

The scaled-up procedure took roughly 48 hours to go to completion under these conditions, and displayed consistent performance over time (**Fig. 4.16**). Gaps in data represent operation overnight, as the reaction was continuously operated during this time. Due to limitations of volume for the two 2.0 L feed bottles, the reaction was prepared in 4 separate batches. Overall, 3.92 grams of $Ru(bpy)_3Cl_2 \cdot 6H_2O$ were used in the process, as well as 992 grams of pyridine *N*-oxide and 2.30 kilograms of TFAA.

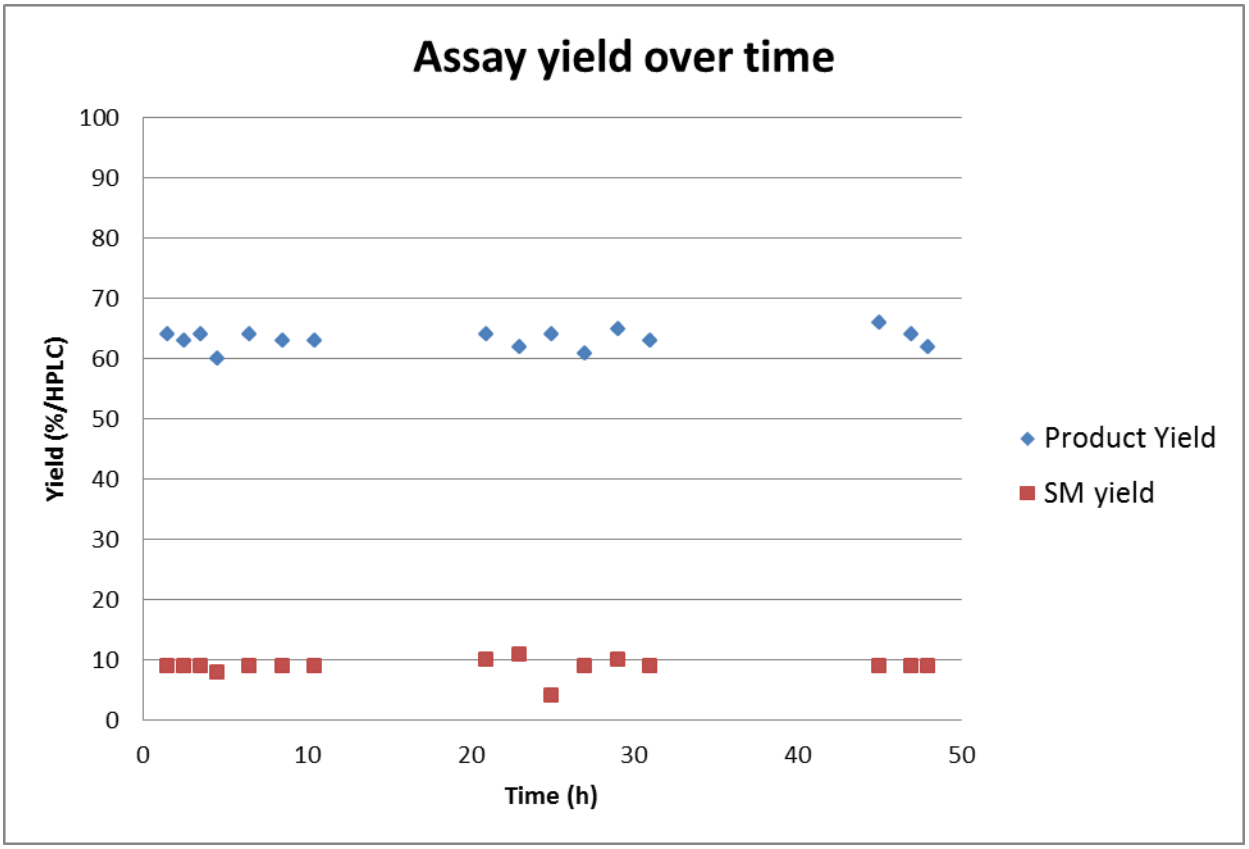

Figure 4.15 Kilogram scale reaction assay yield over time

Investigation of Alternative Pyridine *N*-Oxides and Radical Precursors

With clear demonstration of the scalability of this method, we turned to the investigation of alternative *N*-oxide derivatives in order to fully understand the tenability of the reaction. Due to the proposed mechanistic role of the *N*-oxide as a photo-quencher upon acylation, we expected

that substitution of the pyridine ring would result in altered electronics and consequently altered reaction kinetics (**Table 4.2**). A number of pyridine *N*-oxide derivatives including electron poor (entries 2-4) and electron rich analogs (entries 5-8) resulted in lower yields than pyridine itself.

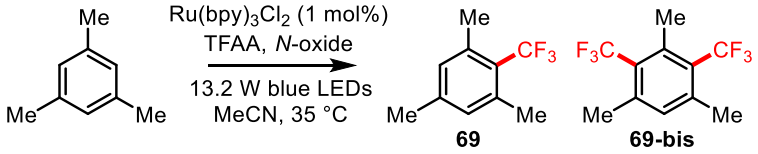

Entry[a]	*N*-oxide	Equiv.[b]	Yield **69**[c]	Yield **69-bis**[c]
1	pyridine	1	44%	< 5%
2	4-Cl-pyridine	1	16%	n.d.
3	4-CN-pyridine	1	25%	< 5%
4	4-NO2-pyridine	1	n.d.	n.d.
5	4-tBu-pyridine	1	27%	n.d.
6	3,5-dimethylpyridine	1	< 10%	n.d.
7	4-MeO-pyridine	1	< 10%	n.d.
8	quinoline	1	n.d.	n.d.
9	4-Ph-pyridine	1	54%	< 5%
10	2-Ph-pyridine	1	24%	< 5%
11	2,2'-bipyridine	1	45%	< 5%
12	2,2'-bipyridine *bis* oxide	0.5[d]	29%	< 5%
13[i]	pyridine	1	n.d.	n.d.
14[i]	4-Ph-pyridine	1	< 10%	n.d.
15	pyridine	2	47%	< 5%
16	4-Ph-pyridine	2	59%	16%
17[e]	pyridine	2	57%	12%
18[e]	4-Ph-pyridine	2	62%	16%
19[e,f]	pyridine	2	57%	6%
20[e,f]	4-Ph-pyridine	2	65%	14%
21[e,i]	4-Ph-pyridine	1	40%	< 5%
22[e,i]	4-Ph-pyridine	2	55%	< 5%
23[e,f,h]	4-Ph-pyridine	1	n.d.	n.d.
24[e,f,j]	4-Ph-pyridine	1	74%	< 5%

[a]Optimization reactions performed on 0.8 mmol scale in 2.0 ml of MeCN, 12 h reaction time. [b]For every X equiv of *N*-oxide, X.1 equiv. of TFAA were used. [c]Yields obtained vs. trifluorotoluene as internal standard. [d]1.1 equiv. TFAA. [e]Degassed. [f]0.1 mol% $Ru(bpy)_3Cl_2$. [g]4.0 ml of MeCN. [h]Light excluded. [i]No catalyst. [j]10.0 equiv. mesitylene. n.d. = not detected.

Table 4.2 Screening and control reactions for varied *N*-oxide structure

Fortunately, switching to 4-phenylpyridine *N*-oxide (PPNO) resulted in slightly higher yields of product (54% vs. 45%, entry 9), but alternative biaryl *N*-oxides did not demonstrate the same efficiency (entries 10-12). Control reactions without photocatalyst at this point of optimization confirmed that catalyst is needed for the reaction (entries 13-14), and increasing loadings to 2 equivalents of *N*-oxide showed that PPNO maintains higher efficiencies than PNO at these higher loadings (15-16). Degassing of the reaction did show minor improvements in reaction efficiency (entries17-18), and lower catalyst loadings at 0.1 mol% maintained these yields (entries 19-20).

Oddly, control reactions in the absence of oxygen revealed significant background reactivity in the absence of photocatalyst (entries 21-22 vs. entries 12-14). We have since identified the source of this reactivity, and it is discussed later in this chapter. Exclusion of light from the degassed reaction provided no observable product (entry 23). It was also demonstrated that the formation of bis-functionalized mesitylene was a function of stoichiometry, as the use of excess mesitylene (10 equiv) resulted in minimal amounts of bis-functionalized material (entry 24).

Having demonstrated that PPNO provides better yields for the trifluoromethylation of mesitylene, we sought to evaluate the generality of this improvement. Using this reagent, yields roughly 10-20% higher than those obtained with PNO were observed for a range of electron-rich substrates including arenes and heteroarenes (**Fig. 4.16**). Yields averaged between 55% and 80%, and were best when the substrates were five-membered heterocyclic compounds. Indoles were not compatible with this chemistry, and it is likely that they are oxidized directly by the reagent through a complexation event (discussed below). Yields did not improve significantly for 6-membered heterocycles, but for a wide array of electron-rich substrates the reaction was

improved significantly. It was found that by varying the equivalents of reagent, *N*-Boc-pyrrole could be selectively trifluoromethylated once (1 equiv., 6:1 mono:bis) or twice (3 equiv., 1:8 mono:bis).

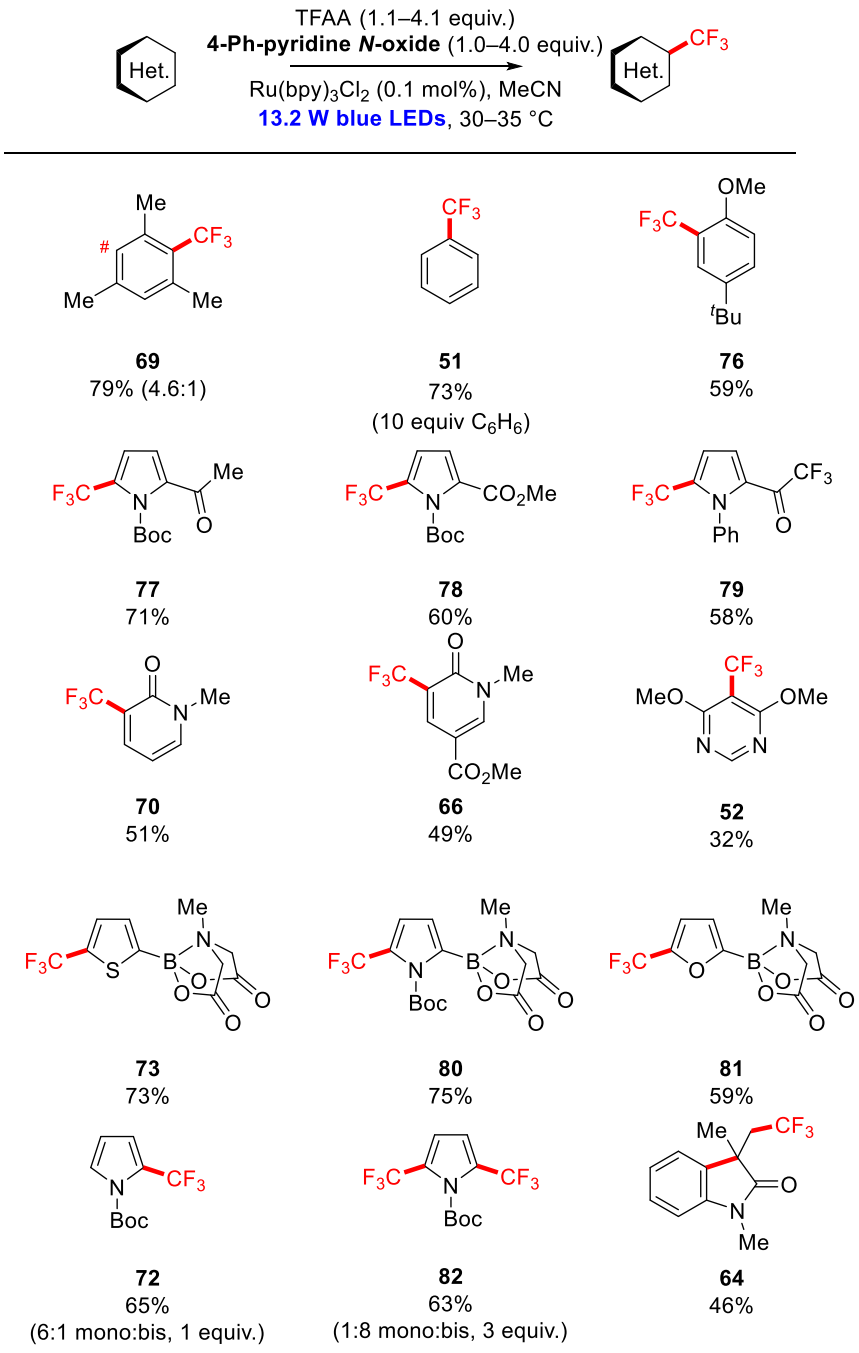

Figure 4.16 Substrate scope with 4-Ph-pyridine *N*-oxide

Further exploring the generality of the fluoroalkylation chemistry, we next turned to the use of pentafluoropropionic anhydride (**Fig. 4.17**). This chemistry presumably operates quite similarly to the trifluoromethylation conditions; however, slightly higher yields were obtained for the substrates tested, suggesting that this process is slightly more efficient. It is currently not entirely understood why this is the case, although the perfluoropropyl, perfluoroethyl, and trifluoromethyl radicals have each been kinetically studied and demonstrate varied kinetic profiles, which may have a significant effect in this system.[136]

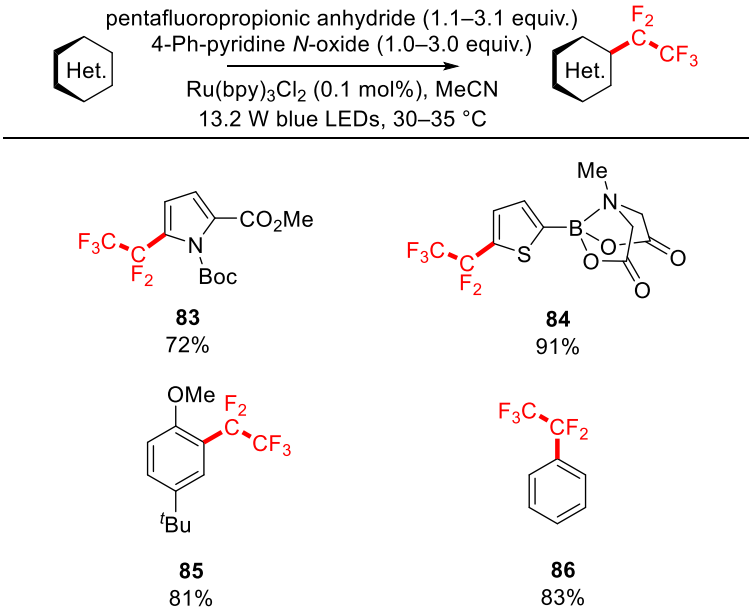

Figure 4.17 Photochemical perfluoroethylation of representative substrates

Perfluoropropylations were also performed, using two difference C_3F_7 sources including the anhydride and acid chloride (**Fig. 4.18**). As the molecular weight of the alkylating reagent goes up, the use of an anhydride is obviously undesirable as half of the reagent is wasted. In this case, the use of the acid chloride worked almost as well as the anhydride, with the major differences likely attributable to the differing solubility of the different salts formed. While this similarity is expected to be a general trend, the use of higher-order perfluoroalkyl acid chlorides has not been tested. Additionally, the use of lower-molecular weight acid chlorides is no

practical, as both perfluoropropionyl chloride and trifluoroacetyl chloride are gasses at room temperature.

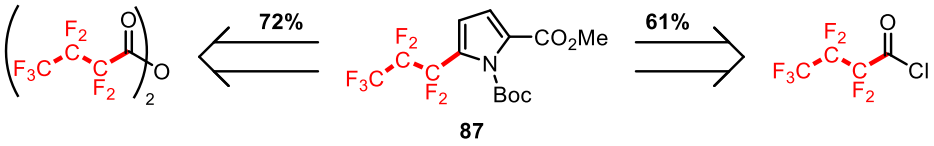

87

Figure 4.18 Perfluoropropylation works with acid chloride or anhydride

Several alternative acid chlorides and anhydrides have been evaluated in the context of this chemistry; however, the timing of their development lags behind those results reported here, and cannot be included in this thesis.

Mechanistic Insights

In our initial report of this chemistry, the mechanistic picture was fairly simple, with a proposed catalytic cycle which is consistent with many such mechanisms supported in the literature. Preliminary quenching studies demonstrated that the pyridine *N*-oxide/TFAA adduct is a fluorescence quencher of $Ru(bpy)_3Cl_2$ (**Fig. 4.19**), although these measurements were taken without prior degassing. This preliminary quenching data suggested that either energy-transfer or electron-transfer events were occurring between the excited state of the photocatalyst and the acylated PNO species, while neither PNO or TFAA could individually take part in this reactivity.

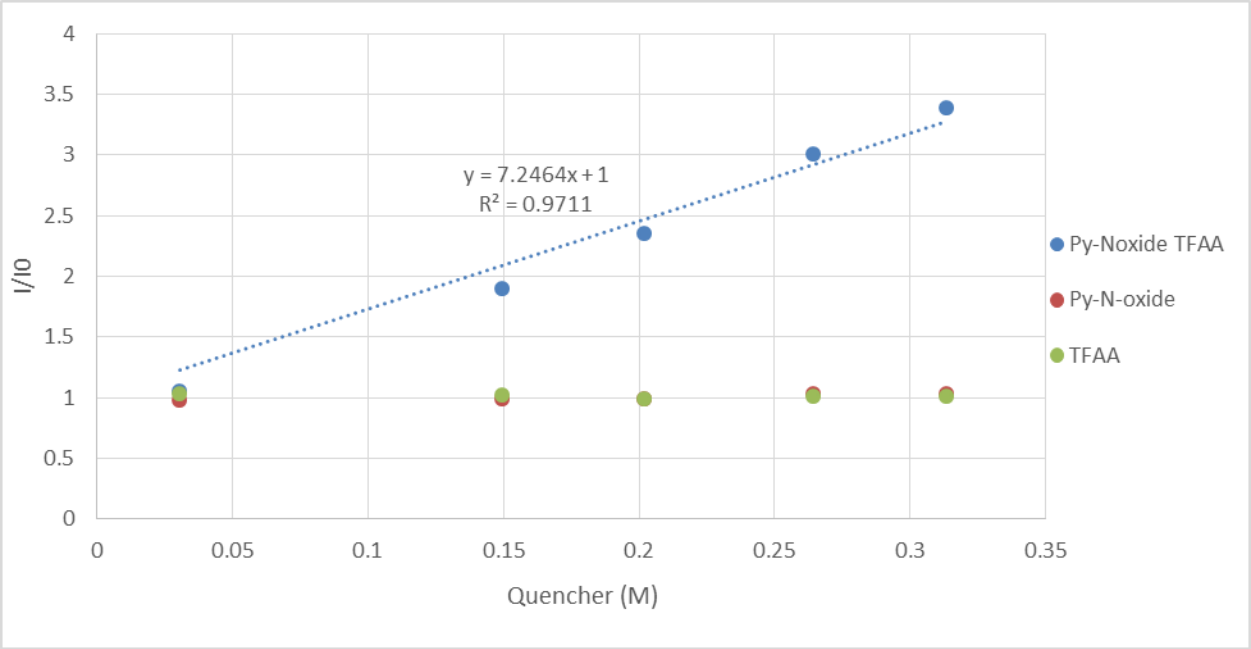

Figure 4.19 Quenching data in the presence of oxygen

Following this experiment, we turned our attention to evaluating the reduction potential of the PNO/TFAA adduct. We surprisingly found that attempts to measure the reduction potential of this species by cyclic voltammetry (CV) were inconsistent and dependent upon the sweep-rate of the measurement. Similar difficulties have been encountered in the literature for this type of measurement, the most similar being the measurement of the reduction potential of *N*-methoxy pyridinium salts.[184] While these measurements were inconsistent, we measured a reduction at roughly –1.21 V vs. SCE in MeCN, with an onset reduction observable at –0.8 V vs. SCE.

Suggestions by Professors Bart Bartlett and Nate Szymczak pointed us towards the use of differential pulsed voltammetry (DPV), which eliminates the observed variability of CV measurements for irreversible processes. Subsequent evaluation of the electrochemical behavior of the PNO/TFAA adduct by DPV revealed a reproducible reduction with a peak at –1.10 V vs. SCE in MeCN and an onset potential of –0.86 V vs. SCE (**Fig. 4.20**). The onset potential is

defined as the intersect between the maximum initial slope of the reduction peak with the baseline, which are both extrapolated to the onset potential in **Figure 4.20**. Measurement of the reduction potential of the PPNO/TFAA adduct revealed that this complex is easier to reduce, with a peak reduction potential of –0.91 V vs. SCE in MeCN with an onset reduction at –0.65 V vs. SCE (**Fig. 4.21**).

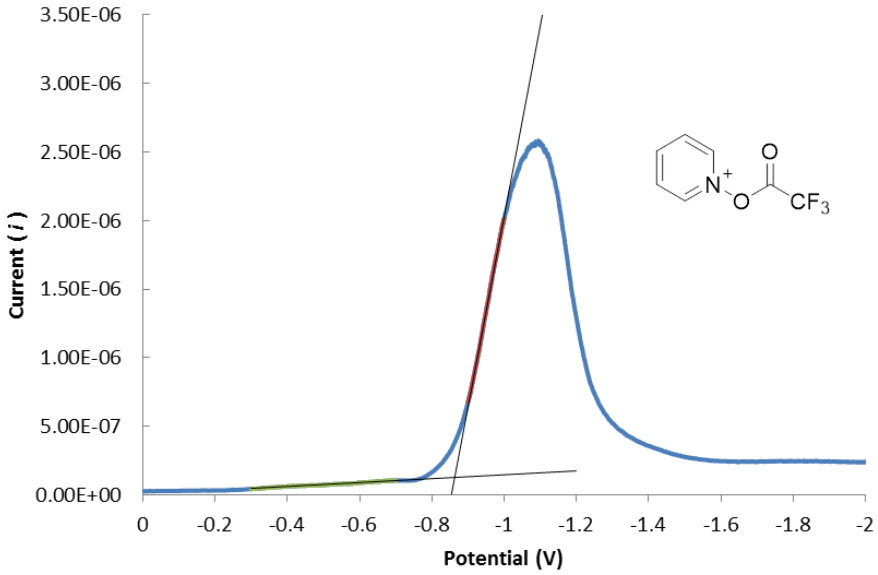

Figure 4.20 DPV analysis of the PNO/TFAA adduct in MeCN

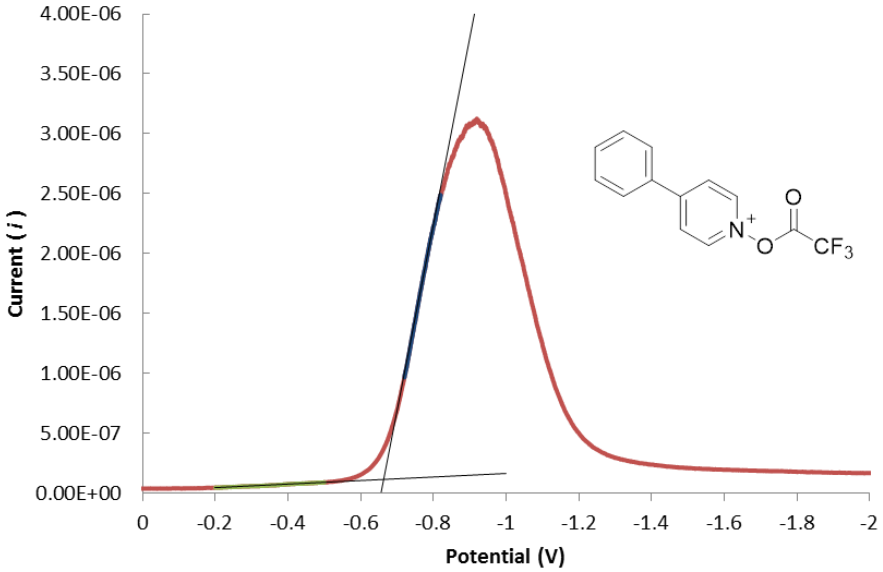

Figure 4.21 DPV analysis of the PPNO/TFAA adduct in MeCN

With this electrochemical comparison of the two optimal *N*-oxides in hand, we turned back to measuring quenching data for the two species. Concomitant with our discovery that PPNO was a good promoter of this reactivity we observed a slight effect of oxygen on the reaction conditions, and as a consequence we re-ran all of our quenching data in the absence of oxygen (**Fig. 4.22**). While the purpose of this experiment is the qualitative demonstration of fluorescence quenching, it is acknowledged that the quenching data for the PPNO/TFAA adduct is slightly curved and may be exhibiting second-order behavior.

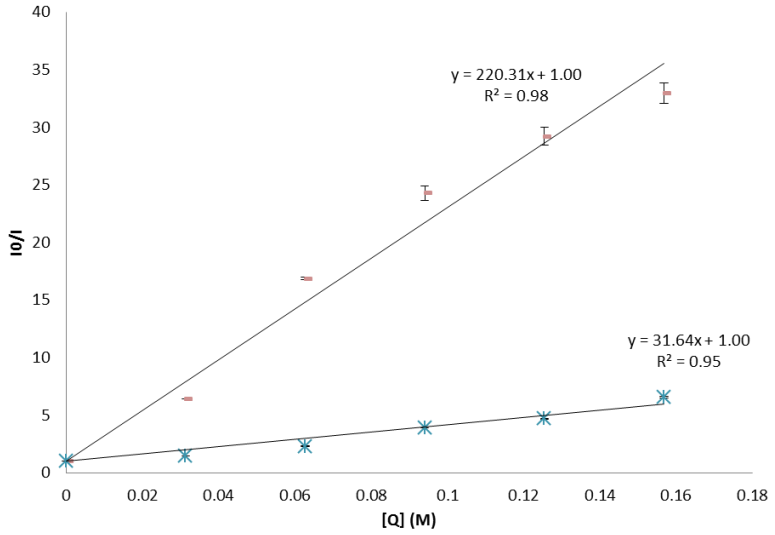

Figure 4.22 Quenching data for PPNO/TFAA (red) and PNO/TFAA (blue)

With our mechanistic expectations about the behavior of the catalyst confirmed through electrochemical and fluorescence experiments, we turned our attention to the evaluation of the background reaction observed in the absence of catalyst (**Table 4.2**, entries 21-22). As this reaction was not observed in the absence of light, we first looked at the absorbance spectra of each mixture of components in solution to determine the identity of the absorbing chemical species.

Unsurprisingly, neither mesitylene nor TFAA absorb near the visible region of the spectrum, with absorbance maxima well below 300 nm (**Fig. 4.23**). The absorbance of PPNO stretches slightly into the visible region, and the combination of mesitylene with PPNO did not result in significant absorbance changes—at these concentrations (0.4M), the slight differences may be due to a solvent effect which mesitylene exhibits on the absorbance of PPNO. Interestingly, when TFAA is added to the PPNO solution, a significant absorbance in the visible region is observed, with a peak absorbance around 389 nm. The addition of mesitylene to this mixture forms an even stronger absorbance with slightly red-shifted λ_{max} at 392 nm.

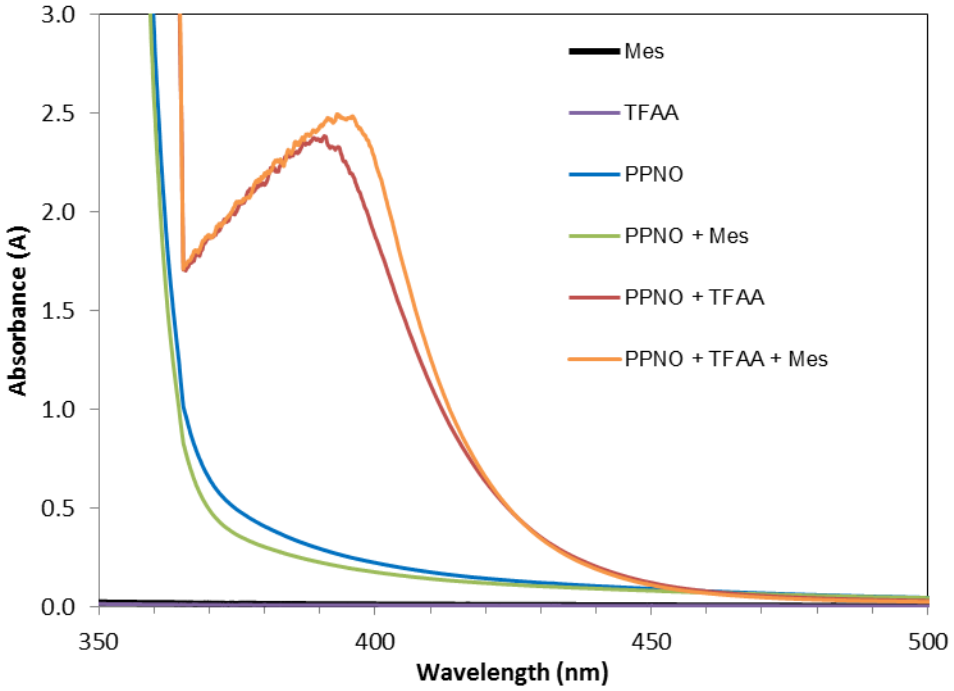

Figure 4.23 Absorbance of individual components and combinations in solution

With this data in hand, we next examined the absorbance behavior of the PPNO/TFAA mixture. We postulated early on that the electron-rich substrates were forming donor-acceptor complexes with the pyridinium reagent, but were quite surprised by a similar absorbance being displayed by the PPNO/TFAA mixture. To evaluate the cause of this phenomenon, the UV-Vis spectrum of a number of samples were obtained, with the concentration of PPNO maintained constant but with varied equivalents of TFAA (**Fig. 4.24**). With half an equivalent of TFAA, the largest absorbance was observed. As PPNO does not form this absorbance by itself, we postulate that this absorbance may be attributable to an intermolecular interaction between acylated and non-acylated PPNO, wherein these two species form an electron donor-acceptor complex (EDA). EDA complexes form between an electron-rich and electron poor species in solution, which forms a new electronic transition which is often observable in the visible spectrum.[185] Key to the proposition that these complexes are present is the fact that *this absorbance is not observed if all components are not present*.

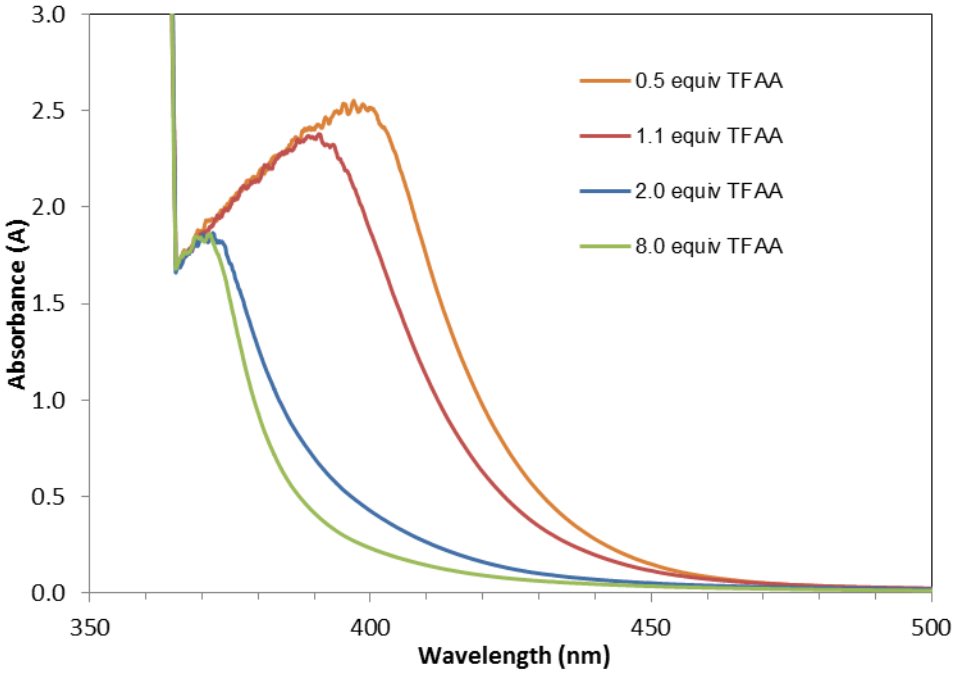

Figure 4.24 Varied absorbance profiles of PPNO with varied equivalents of TFAA

Interestingly, variations of the amounts of TFAA resulted in both changes in absorbance intensity and wavelength. These shifts in wavelength suggest significant changes in structure, because the energetics of the absorbance transition is changing. What is furthermore indicative from the data in **Figure 2** is the fact that upon the addition of sufficient amounts of TFAA (2 equivalents) the absorbance coalesces into a peak which does not shift any further in terms of either intensity or wavelength. This suggests that at sufficient levels of TFAA, all the PPNO present in the solution is acylated, and that this species has an absorbance maximum centered at 370 nm. When less TFAA is present, larger absorbance peaks are observable, which we postulate may be attributable to EDA complexes of various macromolecular structure in solution.

In a simple case, the EDA interaction between PPNO and acylated PPNO may be represented by complex **A** in **Figure 4.25**; however, many EDA complexes are not limited to a 1:1 stoichiometry, and consequently many options exist for the identity of this complex, including a 1:2 or 2:1 species. We speculate that this complex is due to an electronic interaction

between PPNO and acylated PPNO, but the exact structure of this interaction is currently not known to us. It is likely that the structure of this proposed EDA interaction changes based on equivalents of TFAA added, because there is a clear energetic change (λ_{max} shift) with varied equivalents of TFAA, and it is possible that oligomeric complexes with more complex stoichiometry are formed.

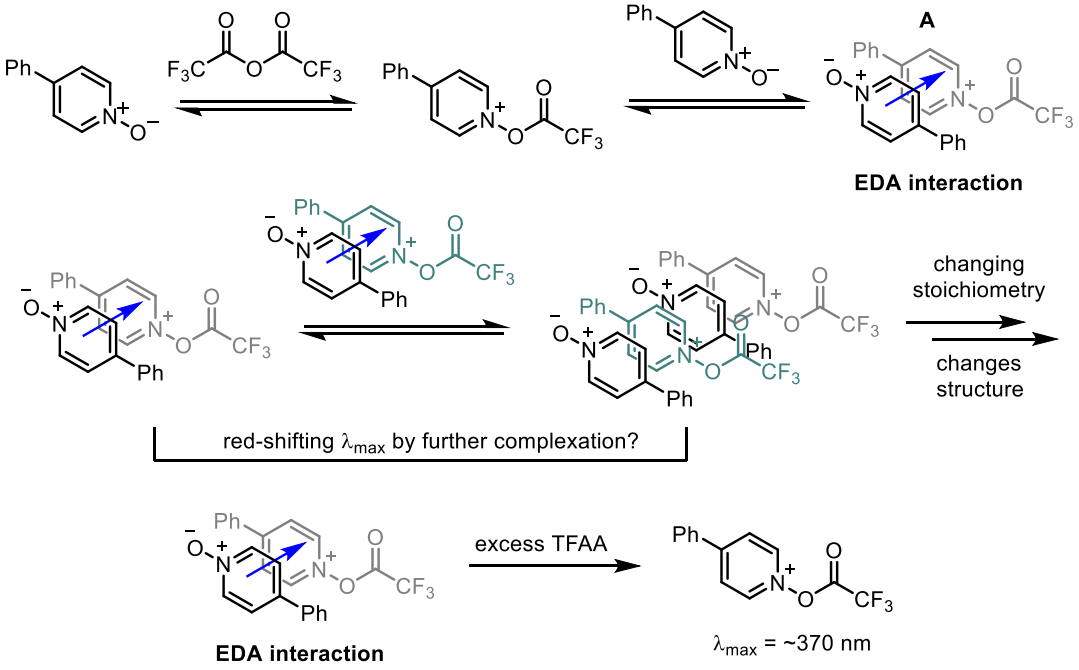

Figure 4.25 Possible interactions contributing to reagent absorbance

We then turned our attention to the evaluation of substrate interaction with the reagent itself. We chose to evaluate these interactions by using PPNO and TFAA in a 1:2 ratio, as the identity of the adduct is thought to be understood at these ratios, and the absorbance of this species is minimized in relation to other ratios with less TFAA. Combining this reagent adduct with a single equivalent of mesitylene, naphthalene, and trimethoxybenzene, we obtained increasingly absorbing bands in the visible spectrum (**Fig. 4.26**). Interactions of this type have been observed and studied previously by Kochi, who demonstrated for *N*-acyloxy pyridinium salts that the charge-transfer transition energy ($h\nu_{CT}$) trends linearly with the ionization potential

(I_p) of the donor in question.[186] We have demonstrated that this relationship holds true for this system, as the transition energy of each of these absorbances trends linearly with donor I_p (**Fig. 4.27**). Benzene does not form an EDA complex with the reagent, as is evidenced by its off-trend point in **Figure 4.27**.

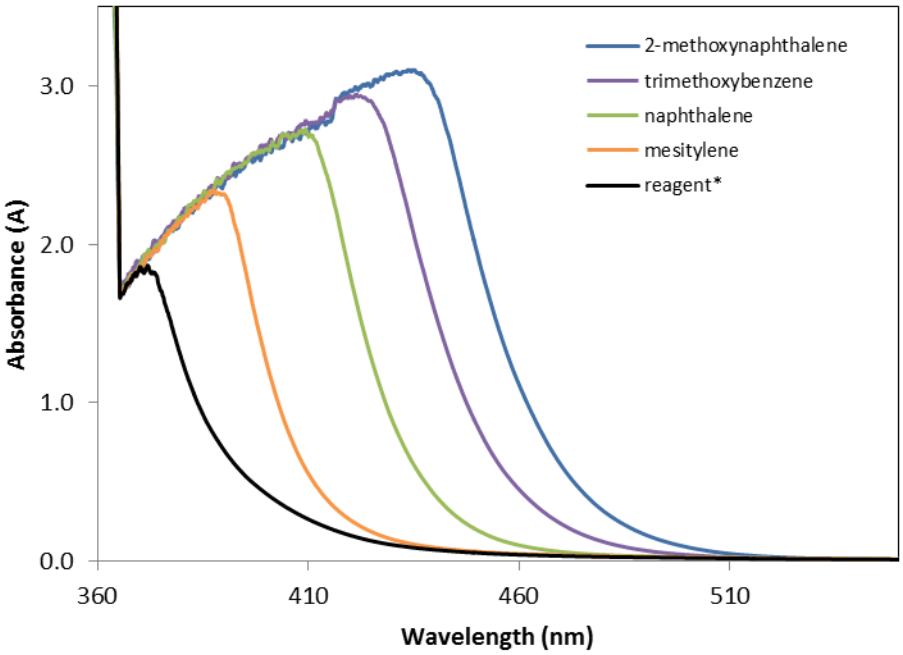

Figure 4.26 EDA absorbances with electron-rich substrates

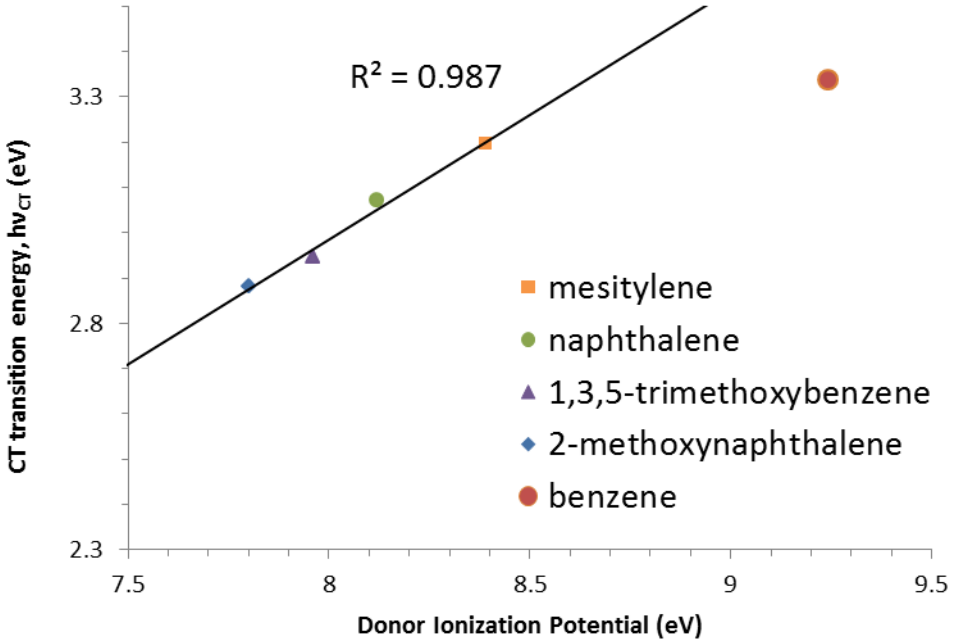

Figure 4.27 Transition energies trend linearly with donor ionization potential

The implications of these EDA complexes are fairly significant for the chemistry at hand, although the degree to which these complexes are operative is highly substrate dependent; however, from these accumulated data a mechanistic picture is beginning to take shape. Based upon the quenching and electrochemical data, it is clear that the photocatalyst drives the reaction forward through direct reduction of the acyloxy pyridinium salt from its photoexcited state (**Fig. 4.28**). This reduction forms the CF_3 radical through initial fragmentation of the reagent's N–O bond, followed by fast decarboxylation to extrude CO_2. Following the formation of this reactive intermediate, its electron-poor nature dictates its selective addition to an electron-rich substrate, which forms a dearomatized radical intermediate. Subsequent oxidation and deprotonation are the likely steps in this pathway, although examples of the opposite order of operations (i.e. deprotonation then oxidation) have been reported for much more basic systems.[187]

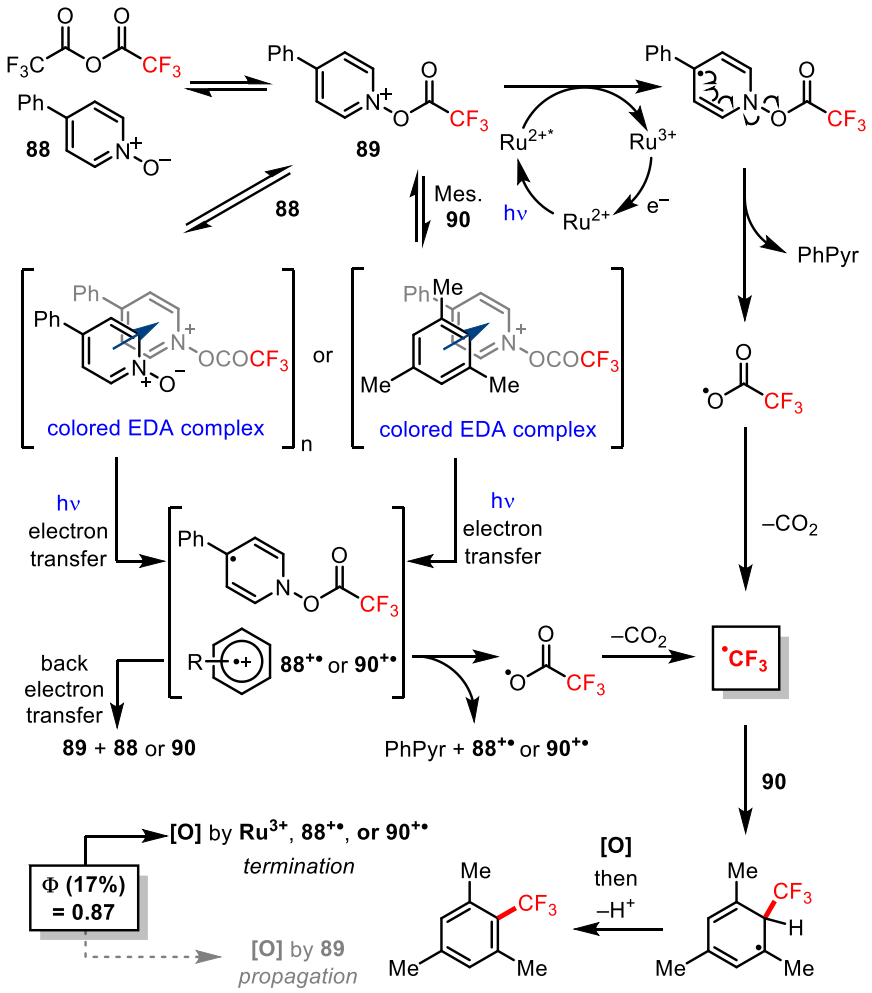

Figure 4.28 Mechanistic proposal

The UV-Vis studies of these reaction systems also suggest another pathway to product exists in the form of EDA complex formation. EDA complexes are proposed to be formed both between electron-rich substrates and the acylated *N*-oxide, as well as between acylated and non-acylated forms of the *N*-oxide by itself. These complexes absorb light, and then can fragment upon single-electron transfer to form the arene radical cation as well as the trifluoroacetyl carboxylate radical, providing another pathway to the formation of the CF_3 radical. These complexes do not have to fragment, and can undergo back-electron-transfer to regenerate starting

material; however, the fragmentation events of similar materials have been measured, and these structures are known to undergo extremely fast fragmentations.

One alternative for the re-aromatization process aside from direct oxidation by the catalyst is a propagative pathway, in which the re-oxidation of the ring could be promoted by another equivalent of reagent. Propagative pathways in photoredox catalysis have been proposed in a number of contexts, with strong experimental evidence for these pathways arising from quantum yield measurements.[188] Quantum yield is defined as the yield of product per absorbed photon, and describes the requirements of light for a given reaction.[189] If a reaction has a quantum yield of >>1, this suggests that there are propagative pathways at work, as only one photon is required to form multiple equivalents of product. Conversely, if a quantum yield is much lower than one, this suggests that a reaction is not very propagative, as many equivalents of light must be utilized to form product. In this way, light requirements for a given reaction can provide significant insight into a reaction mechanism. The quantum yield of the trifluoromethylation chemistry was measured for both the PNO and PPNO systems in order to compare the efficiency of reaction as a function of light absorbance (**Fig. 4.29**). While the quantum yield with PPNO is slightly higher, neither reaction provided a quantum yield greater than 1.0, suggesting that propagation is not a dominant pathway in the transformation, and that the photocatalyst is likely involved in the re-aromatization step.

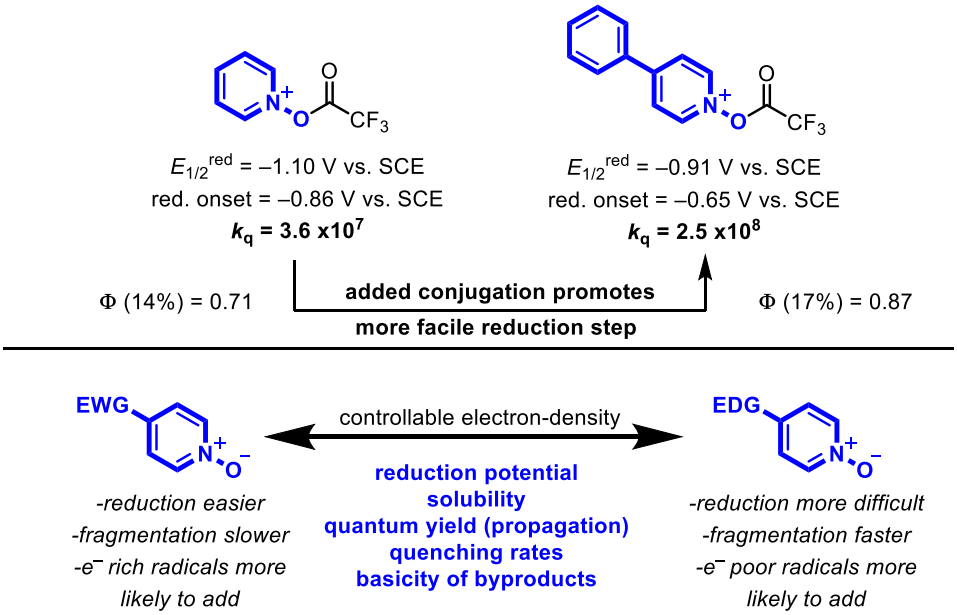

Figure 4.29 Mechanistic effects of pyridine substitution

Conclusions

In conclusion, this work has elucidated conditions in which TFAA can be used as an efficient CF_3 source for a scalable trifluoromethylation reaction. This chemistry is limited to electron-rich substrates, and currently the scope is not large; however, we have begun to tease apart mechanistic aspects of this chemistry which will ideally provide further insight for the design of better reagent systems.

One significant challenge standing in the way of this chemistry is the incompatibility of TFAA with free OH or NH groups. While TFAA is ideal for this work, perhaps eventually the use of TFA of HCF_3 will be compatible with photoredox catalysis, and this may overcome some of the limitations of the current system. Nevertheless, this work demonstrates that through the rational design of reaction conditions, chemicals which have been traditionally recalcitrant can be activated for reactivity under milder conditions.

While the yields of reactions using PNO as the activating reagent are somewhat low, it is nevertheless an extremely inexpensive reaction system compared to all other CF_3 sources. Current scalable state-of-the-art work consists of the use of stoichiometric copper, which is acceptable but not ideal for large scale application. The hope is that further developments in this arena will further improve the scope of relevance for photoredox catalysis, and ideally this work will be truly useful for the synthesis of industrially relevant compounds.

Experimental

General information & Reaction Apparatus:

All chemicals were used as received. Reactions were monitored by TLC and visualized with a dual short wave/long wave UV lamp. Column flash chromatography was performed using 230-400 mesh silica gel or via automated column chromatography. Preparative TLC purifications were run on silica plates of 1000 μm thickness. NMR spectra were recorded on Varian MR400, Varian Inova 500, Varian Vnmrs 500, or Varian Vnmrs 700 spectrometers. Chemical shifts for ^{1}HNMR were reported as δ, parts per million, relative to the signal of $CHCl_3$ at 7.26 ppm. Chemical shifts for ^{13}CNMR were reported as δ, parts per million, relative to the center line signal of the $CDCl_3$ triplet at 77.0 ppm. Chemical shifts for ^{19}FNMR were reported as δ, parts per million, relative to the signal of a trifluorotoluene internal standard at -63.72 ppm. The abbreviations s, br. s, d, dd, br. d, ddd, t, q, br. q, qi, m, and br. m stand for the resonance multiplicity singlet, broad singlet, doublet, doublet of doublets, broad doublet, doublet of doublet of doublets, triplet, quartet, broad quartet, quintet, multiplet and broad multiplet, respectively. IR spectra were recorded on a Perkin-Elmer Spectrum BX FT-IR spectrometer fitted with an ATR accessory. Mass Spectra were recorded at the Mass Spectrometry Facility at the Department of Chemistry of the University of Michigan in Ann Arbor, MI on an Agilent Q-TOF HPCL-MS with ESI high resolution mass spectrometer. LED lights and the requisite power box and cables were purchased from Creative Lighting Solutions (http://www.creativelightings.com) with the following item codes: CL-FRS5050-12WP-12V (4.4W blue LED light strip), CL-FRS5050WPDD-5M-12V-BL (72 W LED strip), CL-PS94670-25W (25 W power supply), CL-PS16020-150W (150 W power supply), CL-PC6FT-PCW (power cord), CL-TERMBL-5P

(terminal block). A reaction performed with a 24 W CFL placed 5 cm from the vial provided identical results.

Unless stated otherwise, all reactions were run on a 0.8mmol scale in a 2 dram vial equipped with stir bar and septum. The light apparatuses used to irradiate the reactions were constructed from test tube racks and wrapped with three 4W LED strips. Reactions were run only in slots marked by an X in the picture below so as to keep a moderate distance from the light source (~2.5 cm). At this distance the temperature of the reactions did not exceed 35 ˚C.

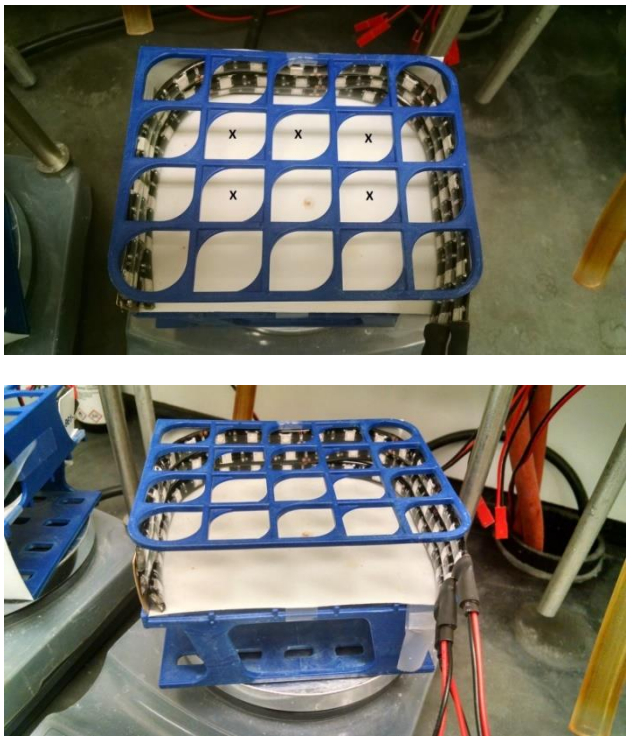

Optimized Trifluoromethylation Procedure:

For most reported substrates, both procedures 1 and 2 were performed. The reaction mixtures obtained by superior conditions (as judged by lack of byproduct formation in preference to

higher yields) were then purified as described. In select circumstances, the reactions were amenable to the use of more equivalents of pyridine-*N*-oxide and TFAA (procedure 3).

Procedure 1:

To a 2 dram vial equipped with a stir bar was added pyridine *N*-oxide (76 mg, 0.80 mmol, 1.0 equiv), $Ru(bpy)_3Cl_2 \cdot 6H_2O$ (6.0 mg, 1.0 mol%), and substrate (0.80 mmol). The combined materials were then dissolved in MeCN (2.0 ml) and stirred to form a homogeneous solution. Trifluoroacetic anhydride (120 µl, 190 mg, 0.88 mmol, 1.1 equiv) was then added to the resulting solution. The vial was equipped with a screw-on cap with septum, and a 25 gauge needle was placed through the septum for the duration of the reaction. Three 4.4 W LED light strips (positioned 2.5 cm away) were turned on and the reaction was allowed to run for 12-15 hours before the light source was removed. Trifluorotoluene (98 µl, 0.80 mmol) was added as a stoichiometric internal standard. A sample of the reaction was removed and diluted with $CDCl_3$ for NMR analysis. The trifluorotoluene signal was referenced to -63.72 ppm. Workup was performed by diluting the reaction with CH_2Cl_2 and washing with 1N HCl, followed by saturated $NaHCO_3$ and then brine. The organic layer was dried over sodium sulfate before filtering and concentrating at 40 ˚C under reduced pressure.

Procedure 2:

Procedure 2 is identical to Procedure 1 except 152 mg of pyridine-*N*-oxide (1.6 mmol, 2.0 equiv) and 237 µl of trifluoroacetic anhydride (353 mg, 1.68 mmol, 2.1 equiv) were used.

Procedure 3:

Procedure 2 is identical to Procedure 1 except 304 mg of pyridine-*N*-oxide (3.2 mmol, 4.0 equiv) and 902 µl of trifluoroacetic anhydride (1.34 g, 6.4 mmol, 8.0 equiv) were used, and the reaction was run for 24 hours.

1,4-dimethoxy-2-(trifluoromethyl)benzene[190] (48)

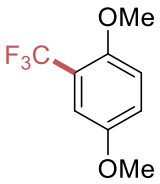

Procedure 1: 26% yield (FNMR)

Procedure 2: 45% yield (FNMR)

The reaction was run according to **Procedure 2** and was purified by column chromatography (0% to 15% CH_2Cl_2 in hexanes) to afford the title compound (51 mg, 21%, volatile) and remaining starting material (17 mg, 10%). The acquired ^{1}HNMR spectrum as identical to that reported in the literature;

^{1}HNMR ($CDCl_3$, 500 MHz): δ 7.12 (d, *J* = 2.8 Hz, 1H), 7.02 (dd, *J* = 9.1, 2.8 Hz, 1H), 6.94 (d, *J* = 9.1 Hz, 1H), 3.86 (s, 3H), 3.80 (s, 3H);

methyl 2-(trifluoromethyl)benzoate,[191] methyl 3-(trifluoromethyl)benzoate[192] and methyl 4-(trifluoromethyl)benzoate[193] (49)

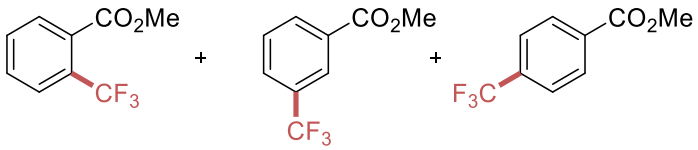

Procedure 1: 24% yield (FNMR, 13:4:7, o:m:p)

Procedure 2: 44% yield (FNMR, 23:8:13, o:m:p)

The reaction was run according to **Procedure 2** and was purified by preparative TLC (1:1 CH_2Cl_2:hexanes) to yield the inseparable isomers as a clear oil (37 mg, 23%) in a 4.2:1.0:1.7 ratio (o:m:p). The ^{1}HNMR of the obtained mixture matched each of the known products.

^{1}HNMR ($CDCl_3$, 500 MHz): δ 8.31 (s, 1H, *meta*), 8.24 (d, *J* = 7.5 Hz, 1H, *meta*), 8.16 (d, *J* = 8.4 Hz, 2H, *para*), 7.82 (d, *J* = 7.8 Hz, 1H, *meta*), 7.79-7.78 (complex m, 1H, *ortho*), 7.76-7.75 (complex m, 1H, *ortho*), 7.71 (d, *J* = 8.4 Hz, 2H, *para*), 7.63-7.58 (m, overlap, 2H *ortho*, 1H *meta*), 3.95 (s, 3H, *meta*), 3.95 (s, 3H, *para*), 3.93 (s, 3H, *ortho*).

methyl 4-methoxy-2-(trifluoromethyl)benzene and methyl 4-methoxy-3-(trifluoromethyl)benzene (50)

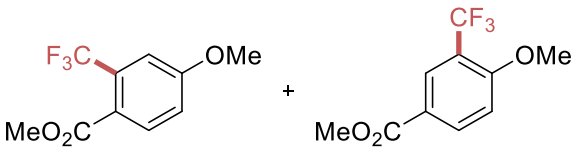

The reaction was run according to **Procedure 3**. Upon completion, the reaction was worked up and purified by preparative TLC (100% CH_2Cl_2) to provide the title compounds in a 2:3 regioisomeric mixture (90.3 mg, 48%) along with recovered starting material (35.1 mg, 26%) and methyl 4-methoxy-3,6-dioxocyclohexa-1,4-diene-1-carboxylate (10.3 mg, 7%). The product regioisomers were characterized as a mixture:

^{1}HNMR ($CDCl_3$, 500 MHz): δ 8.27 (d, *J* = 2.2 Hz, 1H, *major*), 8.20 (dd, *J* = 8.5, 2.2 Hz, 1H, *major*), 7.86 (d, *J* = 8.7 Hz, 1H, *minor*), 7.25 (d, *J* = 2.3 Hz, 1H, *minor*), 7.06 (dd, *J* = 8.7, 2.3 Hz, 1H, *minor*), 7.04 (d, *J* = 8.5 Hz, 1H, *major*);

^{13}CNMR ($CDCl_3$, 125 MHz): δ 166.5, 165.8, 161.7, 160.9, 135.1, 133.1, 131.0 (q, J_{CF} = 32.4 Hz), 129.0 (q, J_{CF} = 4.8 Hz), 123.1 (q, J_{CF} = 271.8 Hz), 123.0 (q, J_{CF} = 273.7), 122.5 (q, J_{CF} = 1.9 Hz), 122.1, 118.7 (q, J_{CF} = 31.5 Hz), 115.8, 113.3 (q, J_{CF} = 6.0 Hz), 111.5, 56.2, 55.7, 52.5, 52.2;

^{19}FNMR ($CDCl_3$, 465 MHz): δ -60.90 (*minor*), -63.89 (*major*);

IR (neat): 3106, 3018, 2963, 2849, 1728, 1707, 1618, 1582, 1509, 1424, 1264, 1236, 1138, 1115, 1016;

HRMS (ESI) *m/z* calculated for $C_{10}H_{10}F_3O_3$ ([M+H]+) 235.0577, found 235.0574.

(trifluoromethyl)benzene (51)

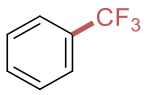

Procedure 1: 25% yield (FNMR)

Procedure 1 (10 equiv benzene): 45% yield (FNMR)

Each reaction for this substrate was quenched with methanol before adding trifluoroethanol as an internal standard (0.8 mmol, 58 µl). Due to the wide availability of the product, no purification was attempted on this reaction mixture. The proton and fluorine signals of the product were identical to those of a commercial sample.

4,6-dimethoxy-5-(trifluoromethyl)pyrimidine[130] (52)

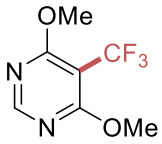

Procedure 1: 23% yield (FNMR)

Procedure 2: 37% yield (FNMR)

The reaction was run according to **Procedure 2** and purified by preparative TLC (10% EtOAc in hexanes) to provide the title compound as a white solid (50 mg, 30%) along with recovered starting material (14 mg, 13%). The acquired ^{1}HNMR spectrum matched that reported in the literature;

^{1}HNMR ($CDCl_3$, 500 MHz): δ 8.47 (s, 1H), 4.04 (s, 6H);

methyl 1-methyl-6-oxo-5-(trifluoromethyl)-1,6-dihydropyridine-3-carboxylate (53)

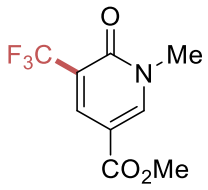

Procedure 1: 38% yield (FNMR)

Procedure 2: 48% yield (FNMR)

The reaction was run according to **Procedure 2** and was concentrated after 15 hours without workup. The crude residue was purified on SiO_2 (5% to 40% EtOAc) to provide the title compound (100 mg, 54%) as an off-white solid. Remaining starting material (8.0 mg, 6%) was eluted off the column in 65% EtOAc in hexanes.

^{1}HNMR ($CDCl_3$, 500 MHz): δ 8.37 (d, J = 2.3 Hz, 1H), 8.28 (d, J = 2.3 Hz, 1H), 3.90 (s, 3H), 3.66 (s, 3H);

^{13}CNMR ($CDCl_3$, 175 MHz): δ 163.6, 158.5, 146.6, 138.1 (q, J_{CF} = 5.2 Hz), 122.1 (q, J_{CF} = 271.1 Hz), 119.1 (q, J_{CF} = 31.4 Hz), 107.8, 52.3, 38.3;

^{19}FNMR ($CDCl_3$, 465 MHz): δ -67.23;

IR (neat): 3066, 2965, 1717, 1671, 1560, 1448, 1255, 1122;

HRMS (ESI) *m/z* calculated for $C_9H_9F_3NO_3$ ($[M+H]^+$) 236.0529, found 236.0529;

2,2,2-trifluoro-1-(1-phenyl-5-(trifluoromethyl)-1H-pyrrol-2-yl)ethan-1-one (54)

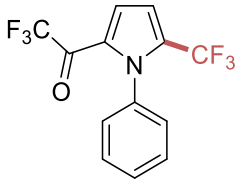

Procedure 1: 39% yield (FNMR)

Procedure 2: 53% yield (FNMR)

The reaction mixture from **Procedure 2** was purified by preparative TLC (10% EtOAc in hexanes) to afford the title compound (200 mg, 49%) as a clear oil along with recovered starting material (20 mg, 10%).

^{1}HNMR (MeCN-d_3, 500 MHz): δ 7.58-7.50 (m, overlap, 3H), 7.40-7.36 (m, overlap, 3H), 6.97 (d, J = 4.6 Hz, 1H);

^{13}CNMR ($CDCl_3$, 175 MHz): δ 170.2 (q, J_{CF} = 36.8 Hz), 136.5, 132.2 (q, J_{CF} = 38.1 Hz), 129.8, 129.0, 127.5, 125.5, 121.4 (q, J_{CF} = 4.1 Hz), 119.7 (q, J_{CF} = 269.8 Hz), 116.3 (q, J_{CF} = 290.9 Hz), 112.3 (q, J_{CF} = 3.2 Hz);

^{19}FNMR ($CDCl_3$, 470 MHz): δ -58.93, -73.30;

IR (neat): 3149, 1705, 1502, 1346, 1202, 1123;

HRMS (EI) *m/z* calculated for $C_{13}H_8F_6NO$ ($[M+H]^+$) 307.0432, found 307.0440.

tert-butyl 2-(trifluoromethyl)-1*H*-indole-1-carboxylate[194] (55)

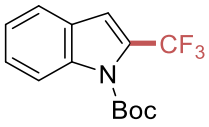

Procedure 1: 26% yield (FNMR)

Procedure 2: 19% yield (FNMR)

The reaction was run according to **Procedure 1** and purified on SiO_2 (100% hexanes) to afford the title compound (58 mg, 25%) as a clear oil, along with recovered starting material (26 mg, 15%). The acquired ^{1}HNMR spectrum was identical to that reported in the literature;

^{1}HNMR ($CDCl_3$, 500MHz): δ 8.29 (d, *J* = 8.1 Hz, 1H), 7.62 (d, *J* = 7.7 Hz, 1H), 7.45 (dd, *J* = 8.1, 7.7 Hz, 1H), 7.30 (dd, *J* = 7.7, 7.7 Hz, 1H), 7.14 (s, 1H), 1.68 (s, 9H);

3-methyl-2-(trifluoromethyl)benzofuran[158] (56)

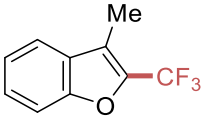

Procedure 1: 47% yield (FNMR)

The reaction was run according to Procedure 1. The crude reaction mixture was purified by preparative TLC (100% hexanes) and the title compound was isolated as a clear oil (39 mg, 37%). The acquired ^{1}HNMR spectrum matched that reported in the literature;

^{1}HNMR ($CDCl_3$, 500 MHz): δ 7.61 (d, *J* = 7.7 Hz, 1H), 7.52 (d, *J* = 8.2 Hz, 1H), 7.43 (dd, *J* = 7.7, 7.7 Hz, 1H), 7.33 (dd, *J* = 7.7, 7.7 Hz, 1H) 2.41 (q, J_{H-F} = 2.0 Hz, 3H);

5-(4-bromophenyl)-2-(trifluoromethyl)oxazole and 5-(4-bromophenyl)-4-(trifluoromethyl)oxazole (57)

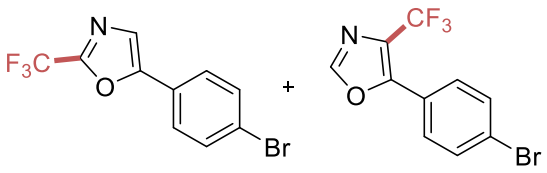

Procedure 1: 27% (FNMR) ~1:1 regioisomeric ratio

Procedure 2: 26% (FNMR) ~1:1 regioisomeric ratio

The reaction was run according to **Procedure 1** and purified on SiO_2 (1-5% EtOAc in hexanes) to provide 5-(4-bromophenyl)-2-(trifluoromethyl)oxazole (30 mg, 10%) and 5-(4-bromophenyl)-4-(trifluoromethyl)oxazole (22 mg, 7%) as white solids. In addition, starting material was recovered (100 mg, 45%) along with 1-(5-4-bromophenyl)oxazol-4-yl)-2,2,2-trifluoroethan-1-one (38 mg, 12%).

5-(4-bromophenyl)-2-(trifluoromethyl)oxazole

^{1}HNMR ($CDCl_3$, 700 MHz): δ 7.61 (d, J = 8.8 Hz, 2H), 7.57 (d, J = 8.8 Hz, 2H), 7.46 (s, 1H);

^{13}CNMR ($CDCl_3$, 175 MHz): δ 152.9, 150.0 (q, J_{CF} = 43.6 Hz), 132.4, 126.3, 125.1, 124.1, 122.8, 116.4 (q, J_{CF} = 270.4 Hz);

^{19}FNMR ($CDCl_3$ 470 MHz): δ -66.66;

IR (neat): 3146, 1677, 2587, 2478, 1406, 1202, 1137;

HRMS (EI) *m/z* calculated for $C_{10}H_6BrF_3NO$ ($[M+H]^+$) 291.9579, found 291.9574.

5-(4-bromophenyl)-4-(trifluoromethyl)oxazole

^{1}HNMR ($CDCl_3$, 700 MHz): 7.96 (s, 1H), 7.64 (d, J = 8.6 Hz, 2H), 7.55 (d, J = 8.6 Hz, 2H);

^{13}CNMR ($CDCl_3$, 175 MHz): δ 150.0 (q, J_{CF} = 3.2 Hz), 149.9, 132.2, 129.1 (q, J_{CF} = 2.0 Hz), 125.8 (q, J_{CF} = 39.5 Hz), 125.1, 124.6, 121.0 (q, J_{CF} = 268.4 Hz);

^{19}FNMR ($CDCl_3$ 470 MHz): δ -61.78;

IR (neat): 3121, 1678, 1617, 1586, 1514, 1489, 1384, 1125;

HRMS (EI) *m/z* calculated for $C_{10}H_5BrF_3NO$ ($[M]^+$) 290.9507, found 290.9516.

2-bromo-1,3,5-trimethyl-4-(trifluoromethyl)benzene (58)

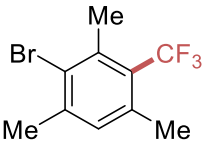

Procedure 1: 35% yield (FNMR)

Procedure 2: 48% yield (FNMR) with 4% yield of the double-addition product

Procedure 3: 65% yield (FNMR) with a 5:1 ratio of mono:di functionalized products

The reaction mixture from **Procedure 1** was purified by preparative TLC (100% hexanes) to afford 2-bromo-1,3,5-trimethyl-4-(trifluoromethyl)benzene as a clear oil (44 mg, 22%) along with 37 mg (23%) of recovered starting material;

^{1}HNMR ($CDCl_3$, 500 MHz): δ 6.96 (s, 1H), 2.57 (q, J_{HF} = 2.4 Hz, 3H), 2.43-2.40 (m, overlap, 6H);

^{13}CNMR ($CDCl_3$, 175 MHz): δ 141.6, 137.6, 135.6, 132.1, 127.6, 126.7 (q, J_{CF} = 28.6 Hz), 125.4 (q, J_{CF} = 276.6 Hz), 24.4, 21.7 (q, J_{CF} = 4.8 Hz), 21.5 (q, J_{CF} = 4.5 Hz);

^{19}FNMR ($CDCl_3$, 465 MHz): δ -54.10;

IR (neat): 2983, 1380, 1283, 1225, 1153, 1112;

HRMS (EI) *m/z* calculated for $C_{10}H_{11}BrF_3$ ($[M+H]^+$) 265.9918, found 265.9925.

2-bromo-1,3-dimethyl-4-(trifluoromethyl)benzene[158] (59)

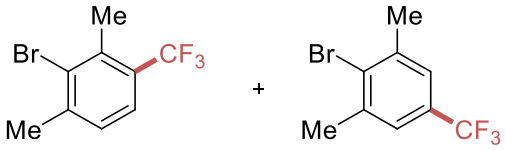

Procedure 1: 25% yield (FNMR, 5:1 regioisomeric mixture)

Procedure 2: 34% yield (FNMR, 5:1 regioisomeric mixture)

Procedure 3: 46% yield (FNMR, 5:1 regioisomeric mixture)

The reaction mixture from **Procedure 2** was purified by preparative TLC (100% hexanes) to afford the title compound in a 4:1 regioisomeric mixture (32 mg, 16%) along with 12 mg (8%) of recovered starting material. We were unable to separate the product regioisomers so they were characterized as a mixture;

^{1}HNMR ($CDCl_3$, 500 MHz): δ 7.48 (d, J = 8.1 Hz, 1H, *major*), 7.32 (s, 2H, *minor*) 7.16 (d, J = 8.1 Hz, 1H, *major*), 2.56 (s, 3H, *major*), 2.47 (s, overlap, 3H, *major*, 6H, *minor*);

^{13}CNMR ($CDCl_3$, 175 MHz): δ 142.7, 139.3, 130.0, 127.9 (q, J_{CF} = 28.6 Hz), 127.6, 124.3 (q, J_{CF} = 7.5 Hz), 124.0 (q, J_{CF} = 273.2 Hz), 23.9, 20.2 (q, J_{CF} = 2.0 Hz);

^{19}FNMR ($CDCl_3$, 465 MHz): δ -61.59 (*major*), -63.61 (*minor*);

IR (neat): 2972, 1385, 1307, 1180, 1121;

HRMS (EI) *m/z* calculated for $C_9H_9BrF_3$ ($[M+H]^+$) 251.9761, found 251.9765.

tert-butyl 5-bromo-2-(trifluoromethyl)-1H-pyrrolo[2,3-b]pyridine-1-carboxylate (60)

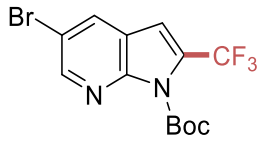

The reaction was run according to **Procedure 2** and purified via preparative TLC (5% EtOAc in hexanes) to yield the title compound (106 mg, 36%) as a white solid.

^{1}HNMR ($CDCl_3$, 500 MHz): δ 8.67 (d, J = 2.2 Hz, 1H), 8.11 (d, J = 2.2 Hz, 1H), 7.01 (s, 1H), 1.67 (s, 9H);

^{13}CNMR ($CDCl_3$, 175 MHz): δ 148.6, 147.7, 146.3, 132.6, 128.4 (q, J_{CF} = 39.9 Hz), 120.0 (q, J_{CF} = 268.6 Hz), 120.5, 115.2, 108.4(q, J_{CF} = 5.1 Hz), 86.6, 27.6;

^{19}FNMR ($CDCl_3$ 376 MHz): δ -59.77;

IR (neat): 2337, 2361, 1761, 1394, 1122, 844;

HRMS (ESI+) *m/z* calculated for $C_{13}H_{12}BrF_3N_2O_2Na$ ($[M+Na]^+$) 386.9927, found 386.9926.

3,3,3-trifluoro-1-phenylpropan-1-ol[195] (61)

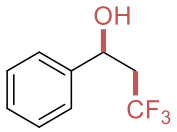

The reaction was run according to **Procedure 2** but with CH_2Cl_2 as the solvent. After 15 hours, the reaction was removed from the light source and diluted with 1.0 ml of MeOH. The reaction was stirred for an additional 60 minutes before adding 100 µl of 4N KOH solution and was then stirred for an additional 10 minutes. The reaction was then concentrated and purified on SiO_2 (100% hexanes to 5% EtOAc in hexanes) to provide the title compound (70 mg, 46%) as a colorless oil. The acquired ^{1}HNMR spectrum was consistent with that reported in the literature; ^{1}HNMR ($CDCl_3$, 400MHz): δ 7.41-7.31 (m, overlap, 5H), 5.10 (ddd, *J* = 9.6, 3.6, 3.2 Hz, 1H), 2.64 (tdd, *J* = 19.2, 15.2, 9.6 Hz), 2.46 (tdd, *J* = 19.2, 10.8, 3.6 Hz, 1H), 2.09 (d, *J* = 3.2 Hz, 1H).

(*E*)-4-(3,3,3-trifluoroprop-1-en-1-yl)benzonitrile[166] (62)

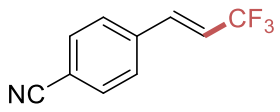

The reaction was run according to **Procedure 2** but with CH_2Cl_2 as the solvent. The following work up procedure to obtain **3** is un-optimized. After 15 hours, TFAA (110 µl, 1.0 equiv) was added to remove adventitious water, and the reaction was cooled to 0 ˚C. DBU (360 µl, 3.0 equiv) was added dropwise to the reaction to avoid reflux. Upon complete addition, the reaction was stirred for an additional 10 minutes before concentrating and purifying on SiO_2 (1% EtOAc in hexanes) to provide the title compound (90 mg, 56%) as a white solid. The acquired ^{1}HNMR spectrum was consistent with that reported in the literature;

^{1}HNMR ($CDCl_3$, 400MHz): δ 7.70 (d, *J* = 8.4 Hz, 2H), 7.56 (d, *J* = 8.4 Hz, 2H), 7.17 (dq, *J* = 16.3, 2.2 Hz, 1H), 6.31 (dq, *J* = 16.3, 6.4 Hz, 1H).

1,3-dimethyl-3-(2,2,2-trifluoroethyl)indolin-2-one[196] (64)

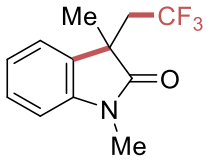

Procedure 1: 47% (FNMR)

Procedure 2: 53% (FNMR)

The reaction was run according to **Procedure 2** and was purified by preparative TLC (25% EtOAc in hexanes) to afford the title compound (78 mg, 40%) along with recovered starting material (20 mg, 14%). The acquired ^{1}HNMR spectrum was consistent with that reported in the literature;

^{1}HNMR ($CDCl_3$, 500MHz): δ 7.31 (dd, *J* = 7.8 Hz, 1H), 7.26 (d, 1H), 7.09 (dd, *J* = 7.8 Hz, 1H), 6.88 (d, *J* = 7.8 Hz, 1H), 3.24 (s, 3H), 2.82 (dq, *J* = 15.2, 10.7 Hz, 1H), 2.64 (dq, *J* = 15.2, 10.7 Hz, 1H), 1.41.

1,3,5-trimethyl-2-(trifluoromethyl)benzene[140] and 1,3,5-trimethyl-2,4-bis(trifluoromethyl)benzene[197] (69)

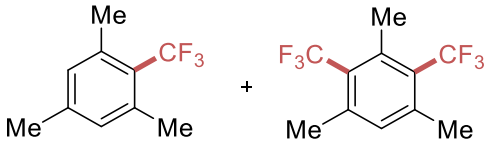

Procedure 1: 48% mono, 4% di (FNMR)

Procedure 2: 59% mono, 10% di (FNMR)

The reaction was run according to **Procedure 1** but using three equivalents of pyridine *N*-oxide (230 mg, 2.4 mmol) and 3.1 equivalents of TFAA (350 µl, 520 mg, 2.50 mmol). This was to ensure consumption of starting material, as its separation from the products is challenging. Upon completion of the reaction (49% mono, 20% di, ^{19}F NMR), the crude reaction was filtered through silica, and the resulting filtrate was concentrated to yield the title compounds (3:1, mono:di, 71 mg, 43%) as a clear oil. Further separation of the two products can be accomplished by preparative TLC (100% hexanes) to afford each product. The acquired ^{1}HNMR spectra were identical to those reported in the literature.

1,3,5-trimethyl-2-(trifluoromethyl)benzene

^{1}HNMR ($CDCl_3$, 500 MHz): δ 6.89 (s, 2H), 2.44 (q, J_{CF} = 3.3 Hz), 2.29 (s, 3H)

1,3,5-trimethyl-2,4-bis(trifluoromethyl)benzene

^{1}HNMR ($CDCl_3$, 500 MHz): δ 6.98 (s, 1H), 2.52 (spt, J_{HF} = 2.8 Hz, 3H), 2.47 (q, J_{HF} = 3.9 Hz, 6H)

1-methyl-3-(trifluoromethyl)pyridine-2(1*H*)-one[198] (70)

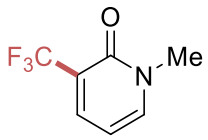

Procedure 1: 44% yield (FNMR)

Procedure 2: 41% yield (FNMR)

The reaction was run according to **Procedure 1** and was purified by column chromatography (0-40% EtOAc in hexanes) to afford a tan solid (57 mg, 40% yield). The acquired ^{1}HNMR spectrum was identical to that reported in the literature;

^{1}HNMR ($CDCl_3$, 500 MHz): δ 7.75 (d, *J* = 7.3 Hz, 1H), 7.50 (d, *J* = 7.3 Hz, 1H), 6.22 (dd, *J* = 7.3, 7.3 Hz);

1,3,7-trimethyl-8-(trifluoromethyl)-3,7-dihydro-1*H*-purine-2,6-dione[134] (71)

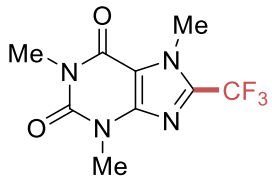

Procedure 1: 23% yield (FNMR)

Procedure 2: 41% yield (FNMR)

Procedure 3: 57% yield (FNMR)

The reaction was run according to **Procedure 3** except that due to low solubility the MeCN volume was raised to 4 ml. The substrate went into solution slowly over time. The reaction was purified on SiO_2 (10% EtOAc in hexanes) to afford the title compound (112.8 mg, 54%) as a white solid. The acquired ^{1}HNMR spectrum was identical to that reported in the literature;

^{1}HNMR ($CDCl_3$, 500 MHz): δ 4.16 (s, 3H), 3.59 (s, 3H), 3.42 (s, 3H);

tert-butyl 2-(trifluoromethyl)-1*H*-pyrrole-1-carboxylate and _tert_-butyl 2,5-bis(trifluoromethyl)-1*H*-pyrrole-1-carboxylate (72)

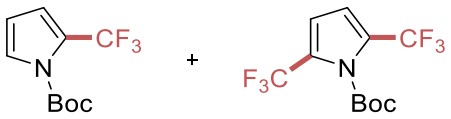

Procedure 1: 59% yield (FNMR) 55% mono, 4% bis, 15% starting material recovered

Procedure 2: 73% yield (FNMR) 37% mono, 36% bis

The reaction was run according to **Procedure 2** and was concentrated before running through a plug of silica gel with 100% DCM to decolorize the material. Concentration of the resulting filtrate provided the title compounds in a 1:1 mixture as a clear oil (160 mg, 74% yield). Further separation can be accomplished by preparative TLC (15% CH_2Cl_2 in hexanes) to afford the pure products. Products adopt a faint yellow hue upon further handling;

tert-butyl 2-(trifluoromethyl)-1*H*-pyrrole-1-carboxylate:

^{1}HNMR ($CDCl_3$, 700 MHz): δ 7.44 (dd, J = 3.3, 2.2 Hz, 1H), 6.74 (br apparent t, J = 2.2 Hz, 1H), 6.19 (dd, J = 3.4, 3.3 Hz, 1H);

^{13}CNMR ($CDCl_3$, 175 MHz): δ 147.4, 125.8, 121.7 (q, J_{CF} = 40.2 Hz), 120.5 (q, J_{CF} = 265.7), 117.8 (q, J_{CF} = 4.8 Hz), 109.6, 85.6, 27.7;

^{19}FNMR ($CDCl_3$ 470 MHz): δ -59.29;

IR (neat): 3151, 2986, 2938, 1752, 1305, 1320, 1284, 1124;

HRMS (EI) *m/z* calculated for $C_{10}H_{13}F_3NO_2$ ($[M+H]^+$) 235.0820, found 235.0813.

***tert*-butyl 2,5-bis(trifluoromethyl)-1*H*-pyrrole-1-carboxylate**:

^{1}HNMR ($CDCl_3$, 700 MHz): δ 6.71 (s, 2H), 1.62 (s, 9H);

^{13}CNMR ($CDCl_3$, 175 MHz): δ 146.0, 126.3 (q, J_{CF} = 41.6 Hz), 119.8 (q, J_{CF} = 119.8 Hz), 114.4 (q, J_{CF} = 4.1 Hz), 87.9, 27.3;

^{19}FNMR ($CDCl_3$, 470 MHz): δ -59.36;

IR (neat): 3151, 2988, 2933, 1778, 1296, 1257, 1133;

HRMS (EI) *m/z* calculated for $C_6H_4F_3N$ ($[M\text{-}Boc+H]^+$) 203.0170, found 203.0170.

(5-(trifluoromethyl)thiophen-2-yl)boronic acid MIDA ester: (73)

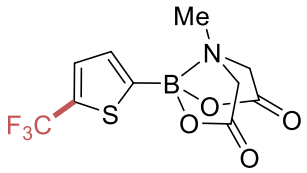

Procedure 1: 48% yield (FNMR)

Procedure 2: 64% yield (FNMR)

The reaction was run according to **Procedure 2** and was purified by column chromatography (20% MeCN in CH_2Cl_2) to afford a pink amorphous solid (~85% pure). This material was dissolved in a minimal volume of CH_2Cl_2 and diluted with diethyl ether. The product crashed out as a white suspension while the impurity (pink) oiled out on the bottom and sides of the vessel. The product slurry was decanted to provide the title compound in greater than 95% purity as a light pink amorphous solid (130 mg, 53%);

^{1}HNMR (CD_3CN, 400 MHz): δ 7.63-760 (m, 1H), 7.32-7.31 (m, 1H), 4.12 (d, J = 17.1, 2H), 3.96 (d, J = 17.1, 2H), 2.66 (s, 3H)

^{13}CNMR (CD_3CN, 175 MHz): δ 169.2, 135.3 (q, J_{CF} = 37.6 Hz), 134.8, 132.0 (q, J_{CF} = 3.3), 124.3 (q, J_{CF} = 267.7 Hz), 63.1, 49.0;

^{19}FNMR (CD_3CN 377 MHz): δ -55.53;

IR (neat): 3015, 1750, 1541, 1452, 1332, 1286, 1144, 1108, 1033, 1003, 817 ;

HRMS (EI) *m/z* calculated for $C_{10}H_{13}BF_3N_2O_4S$ ($[M+NH_4]^+$) 325.0637, found 325.0636.

(1-tosyl-5-(trifluoromethyl)-1*H*-pyrrol-2-yl)boronic acid MIDA ester

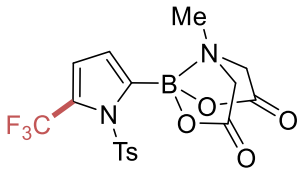

Procedure 1: 47% yield (FNMR)

Procedure 2: 57% yield (FNMR)

The reaction was run according to **Procedure 2** and was purified by filtration (20% MeCN in CH_2Cl_2) to afford a yellow amorphous solid (~85-90% pure). This material could be further purified by column chromatography (0-10% MeCN in DCM) to provide the title compound (164 mg, 46%) as a white solid:

^{1}HNMR (MeCN-d_3, 700 MHz): 7.72 (d, J = 8.3 Hz, 2H), 7.39 (d, J = 8.3 Hz, 2H), 7.02 (d, J = 3.7 Hz, 1H), 6.78 (d, J = 3.7 Hz, 1H), 4.08 (d, J = 17.6 Hz, 2H), 4.04 (d, J = 17.6 Hz, 2H), 2.88 (s, 3H), 2.41 (s, 3H);

^{13}CNMR (MeCN-d_3, 175 MHz): 169.6, 147.3, 137.4, 131.2, 129.2 (q, J_{CF} = 40.2 Hz), 127.9, 125.5, 121.7 (q, J_{CF} = 267.7 Hz), 120.9 (q, J_{CF} = 4.8 Hz), 66.0, 50.9, 22.0;

^{19}FNMR ($CDCl_3$, 470 MHz): -56.74; IR (neat): 2968, 1768, 1300, 1178, 1123, 1031;

HRMS (ESI) *m/z* calculated for $C_{17}H_{17}BF_3N_2O_6S$ ($[M+H]^+$) 445.0847, found 445.0850.

Batch Scale-Up Procedure:

General Procedure 4:

To a 500 mL recovery flask was added $Ru(bpy)_3Cl_2 \cdot 6H_2O$ (0.1 mol%), pyridine *N*-oxide (1.0, 2.0, 3.0, or 4.0 equiv.), MeCN, (2.5 mL/mmol substrate, standard reagent grade), the substrate (1.0 equiv), and the bright red homogenous solution was stirred for 2 minutes (Note the dissolution of pyridine *N*-oxide in MeCN is endothermic). Trifluoroacetic anhydride (1.1, 2.1, 3.1, or 4.1 equiv.) was added over 1 minute with no observable exotherm above 30 ˚C. The flask was placed within a 1L-jacketed beaker containing ^{i}PrOH, wrapped in a single 72W blue LED light strip and connected to a recirculating chiller set to 20 ˚C. The LED strip was turned on and after approximately 15 minutes the internal reaction temperature had reached a consistent 25-30 ˚C. After the requisite period of time the reaction mixture was worked up and purified as stated. Typically the reactions darken over time which did not represent a significant problem until the reaction was conducted on 100 g scale.

Note: The LED strip becomes hot during operation and thus the jacketed beaker was employed to regulate the temperature of the reaction. This set up is un-optimized and was used for its ease of operation.


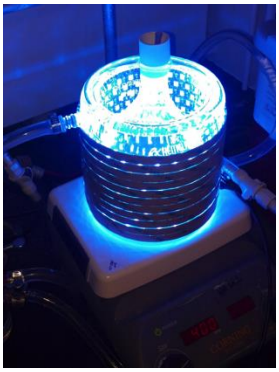


(**a**) (**b**) (**c**)

Representative reaction set up shown for Caffeine which was the only heterogeneous mixture at the outset of the reaction (**a**). The 72 W LED has significant brightness and we typically shielded the set up with aluminum foil to protect our eyes (**b**). Typically the solution darkens over the course of the reaction (**c**).

1,3,5-trimethyl-2-(trifluoromethyl)benzene and 1,3,5-trimethyl-2,4-bis(trifluoromethyl)benzene (69), 5 grams

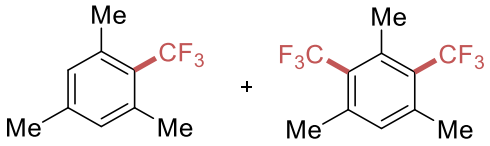

The reaction was run according to **Procedure 4.** $Ru(bpy)_3Cl_2•6H_2O$ (31.1 mg, 0.042 mmol, 0.1 mol%), pyridine *N*-oxide (11.9 g, 125 mmol, 3.0 equiv), MeCN (100 mL), mesitylene (5.00 g, 41.6 mmol, 1.0 equiv), and TFAA (27.1 g, 130 mmol, 3.1 equiv). After 46 h the crude dark red/black reaction mixture was concentrated to a black oil, diluted with hexane (20 mL) and filtered through a silica column (6 inch x 1.5 inch) eluting with hexanes. The colorless hexanes solution (~400 mL) was dried with Na_2SO_4 then filtered and concentrated (40 ˚C, 150 mbar) to yield the title compounds (4.80 g, 4:1 mono:di, 58%) as a clear colorless oil in accordance with the spectroscopic details previously reported (*vide supra*).

1-methyl-3-(trifluoromethyl)pyridine-2(1*H*)-one (70), 5 grams

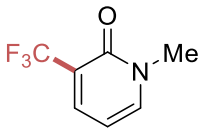

The reaction was run according to **Procedure 4.** $Ru(bpy)_3Cl_2 \bullet 6H_2O$ (34.3 mg, 0.046 mmol, 0.1 mol%), pyridine *N*-oxide (4.36 g, 45.8 mmol, 1.0 equiv), MeCN (115 mL), 1-methyl-2-pyridone (5.00 g, 45.8 mmol, 1.0 equiv), and TFAA (10.6 g, 50.4 mmol, 1.1 equiv). After 16.5 h the crude dark red reaction mixture (35% yield by ^{19}F NMR) was diluted with CH_2Cl_2 (150 mL) then washed with 1N HCl (200 mL), sat $NaHCO_3$ (200 mL), dried with Na_2SO_4 then filtered and concentrated to yield a crude dark brown/black solid. The crude material was purified via column chromatography (50% EtAOc:Hexanes) to yield the title compound (2.56 g, 32%) as a light pink solid in accordance with the spectroscopic details previously reported (*vide supra*).

1,3,7-trimethyl-8-(trifluoromethyl)-3,7-dihydro-1*H*-purine-2,6-dione (71), 5 grams

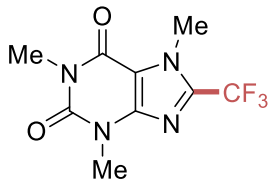

To a 500 mL recovery flask was added $Ru(bpy)_3Cl_2 \bullet 6H_2O$ (19.3 mg, 0.026 mmol, 0.1 mol%), pyridine *N*-oxide (9.79 g, 103.0 mmol, 4.0 equiv), MeCN (250 mL), caffeine (5.0 g, 25.75 mmol, 1.0 equiv), and the bright red heterogeneous solution was stirred for 2 minutes (Note the dissolution of pyridine *N*-oxide in MeCN is endothermic and the solubility of caffeine in MeCN is low). TFAA (43.26 g, 206 mmol, 8.0 equiv) was added and the flask was placed within a 1L-jacketed beaker containing ^{i}PrOH, wrapped in a single 72W blue LED light strip and connected to a recirculating heater/chiller set to 20 ˚C. The LED strip was turned on and after approximately 15 minutes the internal reaction temperature had reached a consistent 25-30 ˚C. After 20 h the crude dark red reaction mixture (61% yield by ^{19}F NMR) was concentrated to remove the MeCN, diluted with EtOAc (200 mL) then washed with water (200 mL), sat $NaHCO_3$ (200 mL), and water (200 mL). The brown solution was dried with Na_2SO_4 then filtered and concentrated to yield a crude brown solid that was chromatographed on SiO2 (5% EtOAc to 10% EtOAc in hexanes) to yield the title compound (3.88 g, 58%) as a light brown solid in accordance with the spectroscopic details previously reported (*vide supra*).

tert-butyl 2-(trifluoromethyl)-1_H_-pyrrole-1-carboxylate and _tert_-butyl 2,5-bis(trifluoromethyl)-1_H_-pyrrole-1-carboxylate (72), 5 grams

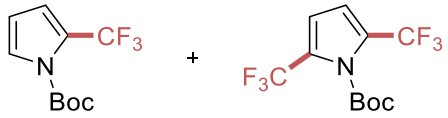

The reaction was run according to **Procedure 4.** $Ru(bpy)_3Cl_2•6H_2O$ (22.4 mg, 0.030 mmol, 0.1 mol%), pyridine *N*-oxide (5.69 g, 59.8 mmol, 2.0 equiv), MeCN (100 mL), *N*-Boc-pyrrole (5.00 g, 29.9 mmol, 1.0 equiv), and TFAA (13.2 g, 62.8 mmol, 2.1 equiv). After 15 h the crude dark red reaction mixture (50% yield mono 13% di by ^{19}F NMR) was diluted with CH_2Cl_2 (150 mL) then washed with 1N HCl (200 mL), sat $NaHCO_3$ (200 mL), dried with Na_2SO_4 then filtered and concentrated to yield a crude dark brown oil. This was diluted with hexane (20 mL) and filtered through a silica column (6 inch x 1.5 inch) eluting with hexanes. The colorless hexanes solution (~400 mL) was dried with Na_2SO_4 then filtered and concentrated to yield the title compound (4.50 g, 4:1 mono:di, 61%) as a yellow oil in accordance with the spectroscopic details previously reported (*vide supra*). The yellow oil could be further purified to remove the color via Kugelrohr distillation (75–80 ˚C, 1 mbar) to provide (4.02 g, 4:1 mono:di, 53%).

(5-(trifluoromethyl)thiophen-2-yl)boronic acid MIDA ester (73), 5 grams

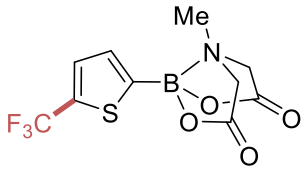

The reaction was run according to **Procedure 4** but using a 100 mL round-bottom-flask. $Ru(bpy)_3Cl_2•6H_2O$ (15.8 mg, 0.021 mmol, 0.1 mol%), pyridine *N*-oxide (4.01 g, 42.2 mmol, 2.0 equiv), MeCN (55 mL), thiophen-2-yl boronic acid MIDA ester (5.04 g, 21.1 mmol, 1.0 equiv), and TFAA (9.30 g, 44.3 mmol, 2.1 equiv). After 15 h the crude dark pink reaction mixture (57% yield by ^{19}F NMR) was concentrated to ~10 mL then diluted with CH_2Cl_2 (150 mL) then washed with 1N HCl (100 mL), twice with sat $NaHCO_3$ (100 mL), dried with Na_2SO_4 then filtered and concentrated to yield a crude pink foam. The crude material was purified via column chromatography (5% MeCN:CH_2Cl_2 to 10% MeCN:CH_2Cl_2) to yield the title compound (2.52 g, 39%) as a white solid in accordance with the spectroscopic details previously reported (*vide supra*). Significant material is lost during column chromatography as the SM and product have very similar RF.

tert-butyl 5-bromo-2-(trifluoromethyl)-1H-pyrrolo[2,3-b]pyridine-1-carboxylate (74), 5 grams

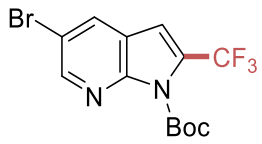

The reaction was run according to **Procedure 4** but using a 100 mL round-bottom-flask. $Ru(bpy)_3Cl_2•6H_2O$ (15.8 mg, 0.017 mmol, 0.1 mol%), pyridine *N*-oxide (3.20 g, 33.6 mmol, 2.0 equiv), MeCN (55 mL), *tert*-butyl 5-bromo-2-(trifluoromethyl)-1H-indole-1-carboxylate (5.00 g, 16.8 mmol, 1.0 equiv), and TFAA (7.42 g, 35.3 mmol, 2.1 equiv). After 15 h the crude dark red reaction mixture (34% yield by ^{19}F NMR) was diluted with CH_2Cl_2 (100 mL) then washed with 1N HCl (100 mL), sat $NaHCO_3$ (100 mL), dried with Na_2SO_4 then filtered and concentrated to yield a crude solid. The crude material was purified via column chromatography (0% to 5% Hexane:EtOAc) then recrystallized from hexanes to yield the title compound (1.68 g, 27%) as a white solid in accordance with the spectroscopic details previously reported (*vide supra*).

Cross-coupling of 74 and 74

tert-butyl 2-(trifluoromethyl)-5-(5-(trifluoromethyl)thiophen-2-yl)-1H-indole-1-carboxylate (75)

Following the procedure of Burke et al.15 To a 25 mL RBF with a stir bar was added tert-butyl 5-bromo-2- (trifluoromethyl)-1H-pyrrolo[2,3-b]pyridine-1-carboxylate (297 mg, 1.0 mmol, 1.0 equiv), (5- (trifluoromethyl)thiophen-2-yl)boronic acid MIDA ester (368 mg, 1.2 mmol, 1.2 equiv), SPhos (41.1 mg, 0.1 mmol, 0.1 equiv), Pd(OAc)2 (11.2 mg, 0.005 mmol, 0.05 equiv) and the flask was evacuated and backfilled with nitrogen 3 times. 1,4-Dioxane (55 mL) was added and the solution stirred for 10 minutes followed by the addition of K2PO4 (2.5 mL 3M (aq) and sparged for 30 mins with N2) and the mixture was heated to 60 ˚C for 4.5 h. The dark brown solution was cooled to rt, added to a separatory funnel, diluted with 1N NaOH (10 mL) and extracted with Et2O (3 × 25 mL). The combined organics were dried with Na2SO4 then filtered through celite and concentrated to yield a crude brown solid. The crude material was purified via column chromatography (5% Hexane:EtOAc) to yield the title compound (274 mg, 63%) as a white solid.

^{1}HNMR ($CDCl_3$, 700 MHz): δ 8.88 (d, J = 2.2 Hz, 1H), 8.13 (d, J = 2.2 Hz, 1H), 7.44 (d, J = 2.9 Hz 1H), 7.28 (d, J = 2.9 Hz 1H), 7.10 (s, 1H), 1.68 (s, 9H);

^{13}CNMR ($CDCl_3$, 175 MHz): δ 149.4, 146.7, 146.0, 144.6, 131.2 (q, J_{CF} = 38.7 Hz), 129.8 (q, J_{CF} = 3.8 Hz), 128.6 (q, J_{CF} = 39.8 Hz), 128.1, 125.5, 123.9, 122.3 (q, J_{CF} = 268.7 Hz), 120.4 (q, J_{CF} = 268.5 Hz), 119.3, 109.4 (q, J_{CF} = 4.9 Hz), 86.8, 27.8;

^{19}FNMR ($CDCl_3$, 376 MHz): δ -55.50, -58.71;

IR (neat): 1761, 1397, 1306, 1286, 1231, 1139, 1122, 1107, 842, 802;

HRMS (ESI^+) m/z calculated for $C_{19}H_9F_6NO_2S$ ($[M+H]^+$), 437.0753 found 437.0757.

Halogenation/Demethylation of 66

methyl 6-bromo-5-(trifluoromethyl)nicotinate (68)

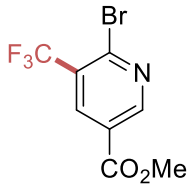

This reaction is un-optimized. To a 15 mL sealed pressure tube with a stir bar was added methyl 1-methyl-6-oxo-5-(trifluoromethyl)-1,6-dihydropyridine-3-carboxylate (100 mg, 0.43 mmol, 1.0 equiv), $POBr_3$ (610 mg, 2.13 mmol, 5.0 equiv) and PBr_3 (80.8 μL, 0.85 mmol, 2.0 equiv). The tube was flushed with N_2 then sealed and heated to 120 ˚C for 24 h. The black solution was cooled in an ice/water bath then cautiously quenched with ice cold water (5 mL over 5 min, patience is advised as there is typically a delay before addition of water causes a violent quenching of the excess reagents) followed by conc. NH_4OH (3 mL). The heterogeneous solution was diluted with water (50 mL) and CH_2Cl_2 (50 mL) in a beaker then transferred to a separatory funnel. The layers were separated, the aqueous layer extracted with CH_2Cl_2 (50 mL), and the combined organics were dried with Na_2SO_4 then filtered and concentrated to yield a light brown solid. The crude material was purified via column chromatography (0% to 5% Hexane:EtOAc) to yield the title compound (77 mg, 64%) as a white solid.

^{1}HNMR ($CDCl_3$, 400 MHz): δ 9.09 (d, J = 1.8 Hz, 1H), 8.53 (d, J = 1.8 Hz, 1H), 4.00 (s, 3H);

^{13}CNMR ($CDCl_3$, 175 MHz): δ 164.0, 153.3, 144.1, 137.3, (q, J_{CF} = 5.0 Hz), 128.1 (q, J_{CF} = 33.8 Hz), 125.3, 122.0 (q, J_{CF} = 273.2 Hz), 53.2

^{19}FNMR ($CDCl_3$ 376 MHz): δ -63.77;

IR (neat): 3064, 1727, 1595, 1568, 1432, 1407, 1250, 1129, 1047, 963, 770;

HRMS (APCI) *m/z* calculated for $C_8H_6BrF_3NO_2$ ($[M+H]^+$), 283.9526 found 283.9529.

methyl 6-chloro-5-(trifluoromethyl)nicotinate[144]: (67)

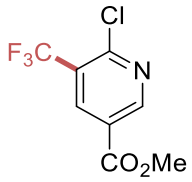

This reaction is un-optimized. To a 15 mL sealed pressure tube with a stir bar was added methyl 1-methyl-6-oxo-5-(trifluoromethyl)-1,6-dihydropyridine-3-carboxylate (100 mg, 0.43 mmol, 1.0 equiv), $POCl_3$ (396 μL, 4.25 mmol, 10.0 equiv) and PCl_5 (177 mg, 0.85 mmol, 2.0 equiv). The tube was flushed with N_2 then sealed and heated to 120 ˚C for 24 h. The black solution was cooled in an ice/water bath then cautiously quenched with ice cold water (5 mL over 5 min) followed by conc. NH_4OH (3 mL). The heterogeneous solution was diluted with water (50 mL) and CH_2Cl_2 (50 mL) in a beaker then transferred to a separatory funnel. The layers were separated and the aqueous layer was extracted with CH_2Cl_2 (50 mL) and the combined organics were dried with Na_2SO_4 then filtered and concentrated to yield a light yellow oil that solidified on standing. The crude material was purified via column chromatography (0% to 5% Hexane:EtOAc to yield (48 mg, 47%) as a white solid. The acquired ^{1}HNMR spectrum was consistent with that reported in the literature;

^{1}HNMR ($CDCl_3$, 500MHz): δ 9.14 (d, *J* = 2.0 Hz, 1H), 8.60 (d, *J* = 2.0 Hz, 1H), 4.00 (s, 3H).

Trifluoromethylation of *N*-Boc-pyrrole (18.4 gram scale)

***tert*-butyl 2-(trifluoromethyl)-1*H*-pyrrole-1-carboxylate and *tert*-butyl 2,5-bis(trifluoromethyl)-1*H*-pyrrole-1-carboxylate (72)**

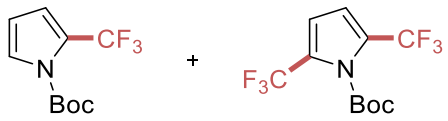

The reaction was run according to **Procedure 3.** $Ru(bpy)_3Cl_2 \bullet 6H_2O$ (82.5 mg, 0.11 mmol, 0.1 mol%), pyridine *N*-oxide (21.0 g, 220 mmol, 2.0 equiv), MeCN (375 mL), *N*-Boc-pyrrole (18.4 g, 110 mmol, 1.0 equiv), and TFAA (48.6 g, 231 mmol, 2.1 equiv). After 15 h the crude dark red reaction mixture (59% yield mono 12% di by ^{19}F NMR) was diluted with CH_2Cl_2 (350 mL) then washed with 1N HCl (400 mL), sat $NaHCO_3$ (200 mL), dried with Na_2SO_4 then filtered and concentrated to yield a crude dark brown oil. This was diluted with hexane (100 mL) and filtered through a silica column (6 inch x 1.5 inch) eluting with hexanes. The colorless hexanes solution (1000 mL) was dried with Na_2SO_4 then filtered and concentrated to yield the title compounds (15.8 g, 5:1 mono:di, 57%) as a colorless oil in accordance with the spectroscopic details previously reported (*vide supra*).

Trifluoromethylation of *N*-Boc-pyrrole (101 gram scale)

***tert*-butyl 2-(trifluoromethyl)-1*H*-pyrrole-1-carboxylate and *tert*-butyl 2,5-bis(trifluoromethyl)-1*H*-pyrrole-1-carboxylate (72)**

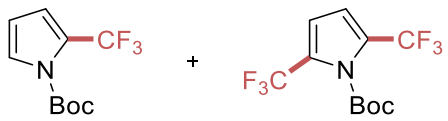

To a 3 neck 3L RBF fitted with an overhead stirrer and thermometer placed within a desiccator (See **picture below**), was added *N*-Boc-pyrrole (101 g, 605 mmol, 1.0 equiv), MeCN (1000 mL),

$Ru(bpy)_3Cl_2•6H_2O$ (453 mg, 0.61 mmol, 0.1 mol%) and pyridine *N*-oxide (115 g, 1210 mmol, 2.0 equiv) washed in with MeCN (250 mL). This heterogeneous solution was stirred until the pyridine *N*-oxide had fully dissolved (~ 2 minutes) at which time the internal reaction temperature was 15 ˚C. TFAA (267 g, 1271 mmol, 2.1 equiv) was added portion-wise over 2 minutes with a concurrent exotherm to 35 ˚C. The bright red solution was irradiated with a single strip of 72 W (total power) LEDs that were air cooled from a flow or air within the desiccator, with the internal reaction temperature consistent at 35 ˚C over the course of the reaction. The homogenous solution was stirred for 62 h after which it was deemed by ^{19}F NMR to have stalled at 33% yield mono, 2% yield di (13:1 mono:di). As the reaction becomes increasingly dark over time we attribute the reduced reactivity to a factor of light penetration, the same total light intensity being used for 20 g and 100 g scale. Attempts to separate the residual *N*-Boc-pyrrole from the product via repeated distillation were unsuccessful and thus no further purification was undertaken. Research is underway to establish the cause of the solution darkening over time as well as further studies on scale employing a stronger (higher W) light source with a more optimized reaction set up.

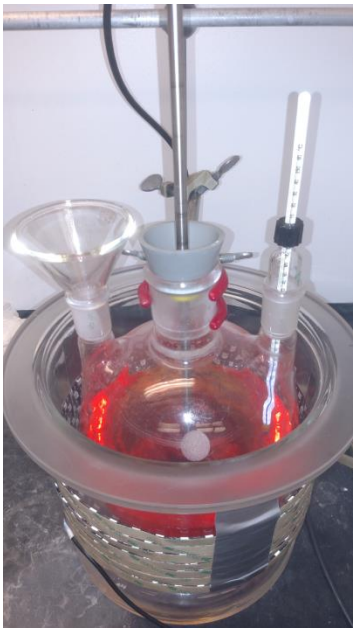

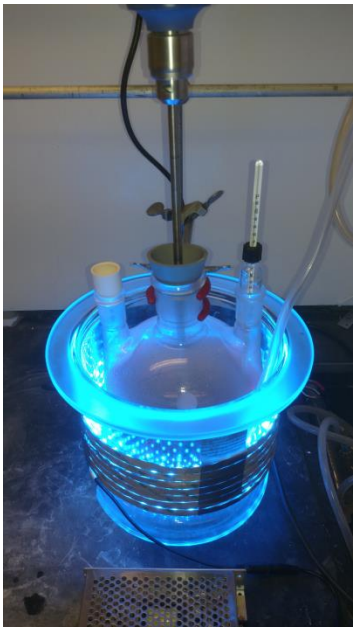

100 g batch reaction set up.

Reaction in continuous flow

tert-butyl 2-(trifluoromethyl)-1_H_-pyrrole-1-carboxylate and _tert_-butyl 2,5-bis(trifluoromethyl)-1_H_-pyrrole-1-carboxylate (72)

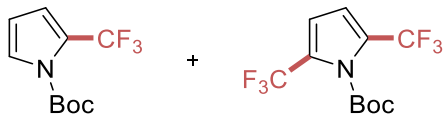

The following set up and conditions are un-optimized and serve as a proof of concept as to the ability to perform this reaction at steady state conditions in flow. No direct comparisons between batch and flow have been made at this time, as neither process is fully optimized or demonstrated on a wide selection of substrates.

A flow trifluoromethylation of 20 grams of *N*-Boc-pyrrole was performed using the Vapourtec® E-series integrated flow chemistry system equipped with a UV-150 photochemical reactor (http://www.vapourtec.co.uk). This UV-150 reactor was equipped with a 450 nm light source (24W Radiant Output) and a dichroic mirror. The PFA reactor cartridge (part no. 50-1287) possessed a 10 ml internal volume, with 1.3 mm internal diameter and 0.15 mm wall thickness. For reliable steady-state elution times, a known length of tubing (28 cm, supplied by Vapourtec®) connected each pump to a static T mixer (purchased from Upchurch Scientific via the Idex website, https://www.idex-hs.com, part P-632) with another 28 cm section leading from the T mixer to the reactor (1/2 of this volume was attributed to each reagent stream for a total length of 42cm of tubing each before the reactor). A further 115 cm of tubing led from the outlet of the reactor to a collection valve (Vapourtec® collection valve kit). The back-pressure regulator was adjusted to supply 4 bar of back pressure at 1 ml min^{-1} flow rate. Solution A contained TFAA (37.25 ml, 263.7 mmol, 2.1 equiv) and was made up to a volume of 189 ml.

Solution B contained $Ru(bpy)_3Cl_2 \cdot 6H_2O$ (94.0 mg, 0.126 mmol, 0.1 mol%), pyridine *N*-oxide (23.89 g, 251.2 mmol, 2.0 equiv), *N*-Boc-pyrrole (21.00 g, 125.6 mmol, 1.0 equiv) and was made up to a total volume of 189 mL with MeCN. Each solution was pumped at a flow rate of 0.5 ml/min to result in a 1 ml/min flow rate after the T mixer. A total volume of 372 ml of solution (186 ml of each solution) was pumped over a span of 6 hours and 12 minutes, with a steady state collection of 360 minutes (360 ml of 0.33M solution collected). An analysis of the final reaction solution yielded 77% yield (FNMR vs. trifluorotoluene) of the final product in 46% yield mono, 31% yield di (3:2 mono:di). The collected solution was concentrated (minimum pressure 150 mbar at 40 ˚C), diluted with CH_2Cl_2 (400 ml), washed with 1N HCl (400 ml) and sat. $NaHCO_3$ (400 ml). The aqueous layer from the bicarbonate wash was extracted with an additional 200 ml of CH_2Cl_2, and the organics were combined, washed with brine, over Na_2SO_4 and filtered. The resulting solution was concentrated (minimum pressure 150 mbar at 40 ˚C) to a dark brown oil. This was diluted with hexane (200 ml) and filtered through a plug of silica (10 in. x 1.5 in.), followed by a wash with 300 ml of hexanes. The resulting solution was concentrated (minimum pressure 150 mbar at 40 ˚C) to yield the title product as a clear oil (23.1 g, 3:2 mono:di, 71% yield) in accordance with the spectroscopic details previously reported (*vide supra*).

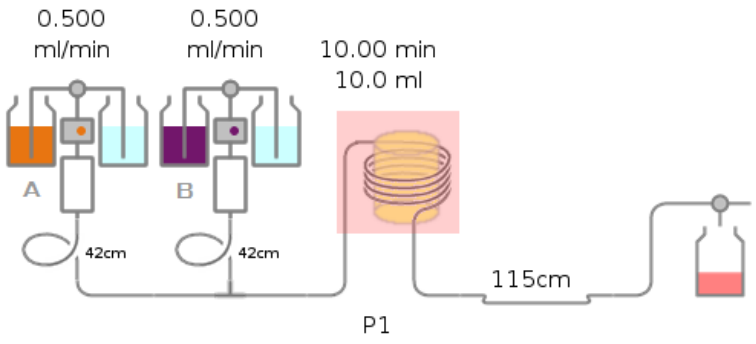

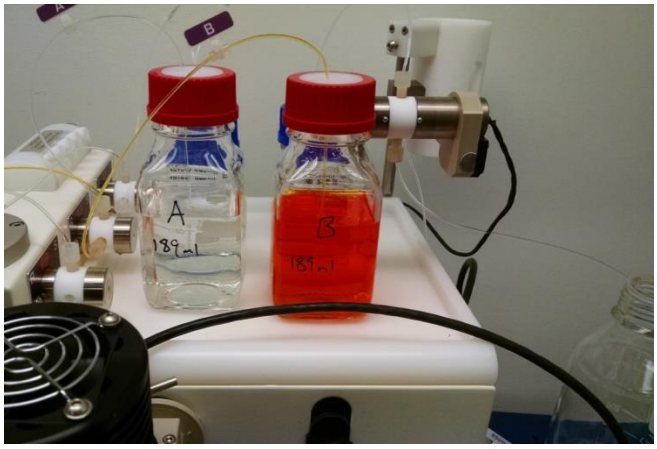

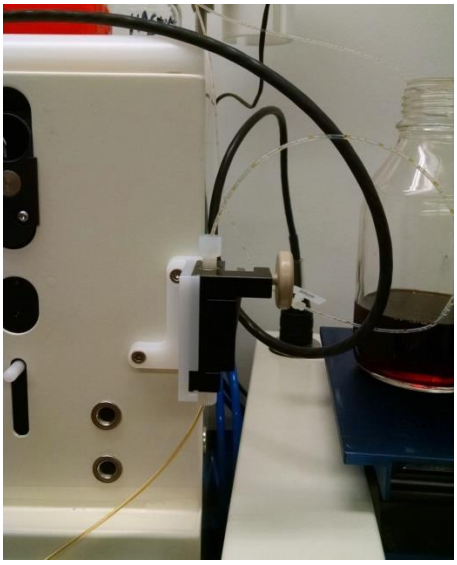

Schematic of Vapourtec® E-series photo reactor setup used for reaction scale-up (top), with images of the prepared solutions (middle) and observable outgassing of the reaction solution as it exits the back-pressure regulator (bottom). Solutions A and B are referred to in the flow procedure, which can be found in the Supplementary Methods section.

Improvements to original pyridine *N*-oxide conditions:

All chemicals were used as received. Reactions were monitored by TLC and visualized with a dual short wave/long wave UV lamp. Column flash chromatography was performed using 230-400 mesh silica gel or via automated column chromatography. Preparative TLC purifications were run on silica plates of 1000 μm thickness. NMR spectra were recorded on Varian MR400, Varian Inova 500, Varian Vnmrs 500, or Varian Vnmrs 700 spectrometers. Chemical shifts for ^{1}H NMR were reported as δ, parts per million, relative to the signal of $CHCl_3$ at 7.26 ppm. Chemical shifts for ^{13}C NMR were reported as δ, parts per million, relative to the center line signal of the $CDCl_3$ triplet at 77.0 ppm. Chemical shifts for ^{19}F NMR were reported as δ, parts per million, relative to the signal of a trifluorotoluene internal standard at -63.72 ppm. *N*-oxide screening experiments were quantitatively analyzed by ^{19}F NMR with a relaxation delay of 1s, while later optimization experiments (entries 13 through 23) and all other internal standard yields were quantified by ^{19}F NMR with a 5s relaxation delay. The abbreviations s, br. s, d, dd, br. d, ddd, t, q, br. q, qi, m, and br. m stand for the resonance multiplicity singlet, broad singlet, doublet, doublet of doublets, broad doublet, doublet of doublet of doublets, triplet, quartet, broad quartet, quintet, multiplet and broad multiplet, respectively. IR spectra were recorded on a Perkin-Elmer Spectrum BX FT-IR spectrometer fitted with an ATR accessory. Mass Spectra were recorded at the Mass Spectrometry Facility at the Department of Chemistry of the University of Michigan in Ann Arbor, MI on an Agilent Q-TOF HPCL-MS with ESI high resolution mass spectrometer. Fluorescence, actinometry, and quantum yield measurements were performed with a Fluoromax-2 fluorimeter equipped with a 150W Xe arc lamp. UV-VIS measurements were obtained on a Shimadzu UV-1601 UV-VIS Spectrometer. LED lights and the requisite power box and cables were purchased from Creative Lighting Solutions

(http://www.creativelightings.com) with the following item codes: CL-FRS5050-12WP-12V (4.4W blue LED light strip), CL-PS94670-25W (25 W power supply), CL-PC6FT-PCW (power cord), CL-TERMBL-5P (terminal block).

Optimization and Control Experiments for Table 4.2:

All optimization experiments were performed on a 0.8 mmol scale at 0.4 M concentration unless stated otherwise, with the equivalents or reagents used, atmosphere, catalyst loadings found in Table 4.2.

Entries 1-16: To a 2 dram vial equipped with a stir bar was added the *N*-oxide derivative (0.4–1.6 mmol, 0.5–2.0 equiv.), $Ru(bpy)_3Cl_2•6H_2O$ (6.0 mg, 1.0 mol%), and substrate (0.80 mmol). The combined materials were then dissolved in dry MeCN (2.0 ml) and stirred briefly (~1 minute). Trifluoroacetic anhydride (120 µl, 190 mg, 0.88 mmol, 1.1 equiv.) was then added to the resulting solution. The vial was equipped with a screw-on cap with septum, and a short length of PFE tubing was placed through a hole in the septum to allow for air exchange (pictured) for the duration of the reaction. Three 4.4 W LED light strips were turned on and the reactions allowed to proceed for 12 hours before removal of the light source. Trifluorotoluene (98 µl, 0.80 mmol) was added as a stoichiometric internal standard. A sample of the reaction was removed and diluted with $CDCl_3$ for NMR analysis. The trifluorotoluene signal was referenced to δ -63.72. Product peaks in the crude ^{19}F NMR were integrated with 1,3,5-trimethyl-2-(trifluoromethyl)benzene observed at δ -54.70 (s, 3F) and 1,3,5-trimethyl-2,4-bis(trifluoromethyl)benzene observed at δ -53.89 (s, 6F).

Entries 17-23: Procedurally identical to entries 1-16, with key differences. For reactions with 0.1 mol% catalyst (**entries 19, 20, 23, 24**), 500 µl of a solution 1.2 mg/ml $Ru(bpy)_3Cl_2•6H_2O$ in dry MeCN (0.6 mg, 0.1 mol%) was added in lieu of 500 µl of solvent. Reactions were degassed (**entries 17-24**) upon dissolution of catalyst, *N*-oxide, and mesitylene in dry MeCN by sparging of the solution with nitrogen for 30 seconds, followed by the addition of TFAA (not degassed) under a stream of nitrogen. The reactions were quickly sealed with a rubber-lined screw on cap, and wrapped with parafilm. Light exclusion (**entry 23**) was achieved by wrapping the reaction in foil (before addition of TFAA) while placing the vessel in front of the light source so as to match the temperature profile of the other reactions. Before analysis of the light-exclusion experiment, methanol (500 µl) was added via syringe and the reaction was allowed to stir for 5 minutes before exposure to light during analysis.

Preparation of CF_3 compounds with 4-Ph-PNO:

General Procedure:

To a 2 dram vial equipped with a stir bar was added 4-phenylpyridine *N*-oxide (0.8–3.2 mmol, 1.0–4.0 equiv.) and substrate (0.80 mmol) followed by 500 ul of a 1.2 mg/ml solution of $Ru(bpy)_3Cl_2•6H_2O$ (0.6 mg, 0.1 mol%). The combined materials were then diluted with dry MeCN (1.5 ml) and stirred briefly to form a heterogeneous solution, with the *N*-oxide only partially dissolved when used in higher equivalents. The reaction was sparged with nitrogen gas for 30 seconds with a glass pipette, followed by the addition of trifluoroacetic anhydride (120 µl, 190 mg, 0.88 mmol, 1.1-4.1 equiv.) under a stream of nitrogen, which is then removed as the vial is simultaneously sealed with a rubber-lined screw-on cap. The trifluoroacetic anhydride solubilizes any remaining solid *N*-oxide within seconds to minutes. Three 4.4 W LED light strips were turned on and the reactions allowed to proceed for 3–12 hours before removal of the light source. Trifluorotoluene (98 µl, 0.80 mmol) was added as a stoichiometric internal standard. A sample of the reaction was removed and diluted with $CDCl_3$ for NMR analysis, with the trifluorotoluene signal referenced to δ -63.72. Workup conditions were substrate-dependent.

1,3,5-trimethyl-2-(trifluoromethyl)benzene[140] and 1,3,5-trimethyl-2,4-bis(trifluoromethyl)benzene[197] (69)

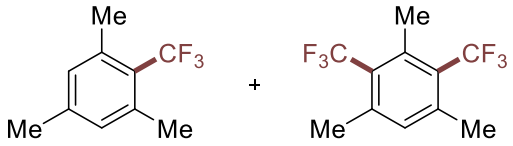

Following the general procedure, using 4-phenylpyridine *N*-oxide (273.9 mg, 1.6 mmol, 2.0 equiv.) and TFAA (237 µl, 1.68 mmol, 2.1 equiv.), the reaction was run for 12 hours. ^{19}F NMR analysis of the crude reaction mixture vs. the injected trifluorotoluene standard revealed the volatile title compounds 1,3,5-trimethyl-2-(trifluoromethyl)benzene [^{19}F NMR ($CDCl_3$, 500 MHz): δ -54.70 (s, 3F, **65% yield**)] and 1,3,5-trimethyl-2,4-bis(trifluoromethyl)benzene [^{19}F NMR ($CDCl_3$, 500 MHz): δ -53.89 (s, 3F, **14% yield**)] in a 4.6:1 ratio. The isolation and characterization of these compounds has previously been reported.[199]

(trifluoromethyl)benzene (51)

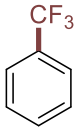

Following the general procedure, using 4-phenylpyridine *N*-oxide (137.0 mg, 0.8 mmol, 1.0 equiv.) as the limiting reagent, TFAA (124 µl, 0.88 mmol, 1.1 equiv.), and benzene (713 µl, 8.0 mmol, 10.0 equiv.), the reaction was run for 12 hours. Upon completion, the reaction was quenched with methanol (500 µl) and removed from the light source. Trifluoroethanol (58 µl, 0.8 mmol) was added as internal standard. Due to the wide availability and volatility of the product, no purification was attempted on this reaction mixture. The proton and fluorine signals of the product were identical to those of a commercial sample. **79% yield (^{19}F NMR)**.

4-(tert-butyl)-1-methoxy-2-(trifluoromethyl)benzene[200] (76)

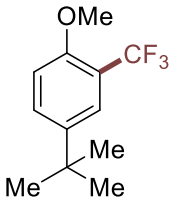

Following the general procedure, using 4-phenylpyridine *N*-oxide (273.9 mg, 1.6 mmol, 2.0 equiv.) and TFAA (237 µl, 1.68 mmol, 2.1 equiv.), the reaction was run for 5 hours. ^{19}F NMR analysis of the crude reaction mixture vs. the injected trifluorotoluene standard revealed the volatile title compound in **59% yield**. The reaction was partitioned with 1N HCl and diluted with dichloromethane. The organic phase was separated, washed with sat. $NaHCO_3$, brine, and dried over sodium sulfate before filtering and concentrating. The crude reaction mixture was purified by prep TLC (100% hexanes run up x2) to yield to title compound as a volatile, clear oil (R_f = 0.32, hexanes). ^{1}H NMR ($CDCl_3$, 400 MHz): δ 7.56 (d, J = 2.4 Hz, 1H), 7.50 (dd, J = 8.8, 2.4 Hz, 1H), 6.94 (d, J = 8.8 Hz, 1H), 3.88 (s, 3H), 1.31 (s, 9H); ^{13}C NMR ($CDCl_3$, 175 MHz): δ 155.2 (q, J_{CF} = 1.4 Hz), 142.9, 129.9, 123.9 (q, J_{CF} = 272.5 Hz), 123.89 (q, J_{CF} = 4.8 Hz), 118.0 (q, J_{CF} = 30.7 Hz), 111.7, 55.9, 34.2, 31.3; ^{19}F NMR ($CDCl_3$, 470 MHz): δ -63.13 (s); IR (neat): 2965, 1620, 1589, 1509, 1325, 1280, 1253, 1119, 1057; HRMS (EI) *m/z* calculated for $C_{12}H_{15}F_3O$ ($[M]^+$) 232.1075, found 232.1077.

1-methyl-3-(trifluoromethyl)pyridine-2(1H)-one[199,198] (70)

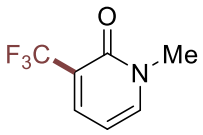

Following the general procedure using 4-phenylpyridine *N*-oxide (137.0 mg, 0.8 mmol, 1.0 equiv.) and TFAA (124 µl, 0.88 mmol, 1.1 equiv.), the reaction was run for 15 hours. ^{19}F NMR analysis of the crude reaction mixture vs. the injected trifluorotoluene standard revealed the title compound in **50% yield**. The reaction was partitioned with 1N HCl and diluted with ethyl acetate. The organic phase was separated and washed with sat. $NaHCO_3$, brine, and dried over sodium sulfate before filtering and concentrating. Re-extraction of the combined and basified aqueous phase (basified further with sat. $NaHCO_3$) led to full material recovery, while the initial acidic workup conditions result in a significant loss of material. The crude reaction mixture was purified on silica gel with 0-50% EtOAc in hexanes to yield the title compound (71.8 mg, **51% yield**) as a tan solid. The characterization of this compound has previously been reported.[199]

methyl 1-methyl-6-oxo-5-(trifluoromethyl)-1,6-dihydropyridine-3-carboxylate (66)

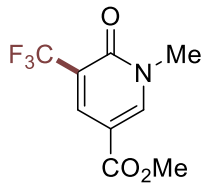

Following the general procedure using 4-phenylpyridine *N*-oxide (273.9 mg, 1.6 mmol, 2.0 equiv.) and TFAA (237 µl, 1.68 mmol, 2.1 equiv.), the reaction was run for 15 hours. ^{19}F NMR analysis of the crude reaction mixture vs. the injected trifluorotoluene standard revealed the title compound in **49% yield**. The reaction mixture was diluted with ethyl acetate and washed with sat. $NaHCO_3$. The aqueous layer was washed twice with ethyl acetate, and the combined organic layers were washed with brine, dried over sodium sulfate, and concentrated. The crude reaction mixture was purified by prep TLC (20% CH_2Cl_2 in EtOAc) to yield the title compound (93.0 mg, **49% yield**) as a tan solid. The characterization of this compound has been previously reported.[199]

4,6-dimethoxy-5-(trifluoromethyl)pyrimidine (52)

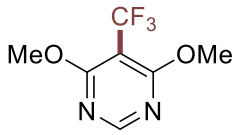

Following the general procedure using 4-phenylpyridine *N*-oxide (237.9 mg, 1.6 mmol, 2.0 equiv.) and TFAA (451 µl, 3.2 mmol, 4.0 equiv.), the reaction was run for 12 hours. ^{19}F NMR analysis of the crude reaction mixture vs. the injected trifluorotoluene standard revealed the title compound in **39% yield**. The reaction mixture was diluted with ethyl acetate and was partitioned with 1N HCl. The organic phase was separated, washed with sat. $NaHCO_3$, brine, and dried over sodium sulfate before filtering and concentrating. The crude reaction mixture was purified by prep TLC (30% EtOAc in hexanes) to yield the title compound (53.0 mg, **32% yield**) as a clear crystalline solid. The characterization of this compound has previously been reported.[199]

tert-butyl 2-acetyl-5-(trifluoromethyl)-1H-pyrrole-1-carboxylate (77)

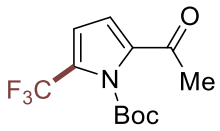

Following the general procedure, using 4-phenylpyridine *N*-oxide (273.9 mg, 1.6 mmol, 2.0 equiv.) and TFAA (237 µl, 1.68 mmol, 2.1 equiv.), the reaction was run for 5 hours. ^{19}F NMR analysis of the crude reaction mixture vs. the injected trifluorotoluene standard revealed the title compound in **70% yield**. The reaction was partitioned with 1N HCl and diluted with dichloromethane. The organic phase was separated, washed with sat. $NaHCO_3$, brine, and dried over sodium sulfate before filtering and concentrating. The crude reaction mixture was purified on silica gel with 50% dichloromethane in hexanes to yield the title compound (157.2 mg, **71% yield**) as a clear oil (R_f = 0.3, 70% dichloromethane in hexanes). ^{1}H NMR ($CDCl_3$, 500 MHz): δ 6.80 (d, J = 3.6 Hz, 1H), 6.61 (d, J = 3.6 Hz, 1H), 2.48 (s, 3H), 1.61 (s, 9H); ^{13}C NMR ($CDCl_3$, 100 MHz): δ 187.8, 147.8, 135.1 (q, J_{CF} = 1.8 Hz), 126.5 (q, J_{CF} = 40.1 Hz), 119.9 (q, J_{CF} = 268.6 Hz), 116.1, 112.2 (q, J_{CF} = 3.4 Hz), 86.8, 27.0, 26.7; ^{19}F NMR ($CDCl_3$, 470 MHz): δ -59.82; IR (neat): 2988, 1775, 1679, 1550, 1372, 1248, 1125; HRMS (ESI) *m/z* calculated for $C_7H_6F_3NO$ [(M–Boc+H)$^+$] 177.0401, found 177.0404.

1-(tert-butyl) 2-methyl 5-(trifluoromethyl)-1H-pyrrole-1,2-dicarboxylate (78)

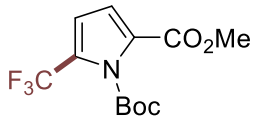

Following the general procedure, using 4-phenylpyridine *N*-oxide (273.9 mg, 1.6 mmol, 2.0 equiv.) and TFAA (237 µl, 1.68 mmol, 2.1 equiv.), the reaction was run for 3 hours. ^{19}F NMR analysis of the crude reaction mixture vs. the injected trifluorotoluene standard revealed the title compound in **63% yield**. The reaction was partitioned with 1N HCl and diluted with dichloromethane. The organic phase was separated, washed with sat. $NaHCO_3$, brine, and dried over sodium sulfate before filtering and concentrating. The crude reaction mixture was purified on silica gel with 10%–30% dichloromethane in hexanes to yield the title compound (140.1 mg, **60% yield**) as a clear oil (R_f = 0.14, 40% dichloromethane in hexanes). ^{1}H NMR ($CDCl_3$, 700 MHz): δ 6.80 (d, J = 3.8 Hz, 1H), 6.61 (d, J = 3.8 Hz, 1H), 3.87 (s, 3H), 1.61 (s, 9H); ^{13}C NMR ($CDCl_3$, 175 MHz): δ 160.2, 147.2, 127.8, 125.6 (q, J_{CF} = 125.6 Hz), 119.9 (q, J_{CF} = 267 Hz), 116.1, 112.8 (q, J_{CF} = 3.6 Hz), 86.9, 52.1, 27.1; ^{19}F NMR ($CDCl_3$, 470 MHz): δ -59.66; IR (neat): 2989, 1777, 1728, 1558, 1373, 1247, 1123; HRMS (EI) *m/z* calculated for $C_7H_6F_3NO_2$ ($[M\text{-}Boc+H]^+$) 193.0351, found 193.0351.

2,2,2-trifluoro-1-(1-phenyl-5-(trifluoromethyl)-1H-pyrrol-2-yl)ethan-1-one (79)

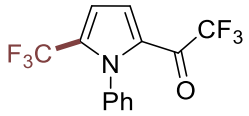

Following the general procedure, using 4-phenylpyridine *N*-oxide (273.9 mg, 1.6 mmol, 2.0 equiv.) and TFAA (237 µl, 1.68 mmol, 2.1 equiv.), the reaction was run for 7 hours. ^{19}F NMR analysis of the crude reaction mixture vs. the injected trifluorotoluene standard revealed the title compound in **59% yield** with 22% remaining starting material. The use of more equivalents of reagent did not result in higher yields of product, but further consumed the starting material. The reaction was partitioned with 1N HCl and diluted with dichloromethane. The organic phase was separated, washed with sat. $NaHCO_3$, brine, and dried over sodium sulfate before filtering and concentrating. The crude reaction mixture was purified by prep TLC (10% ethyl acetate in hexanes) to yield the title compound (143.0 mg, **58% yield**) as a clear oil (R_f = 0.53, 25% dichloromethane in hexanes). The isolation and characterization of this compound has previously been reported.[199]

(5-(trifluoromethyl)thiophen-2-yl)boronic acid MIDA ester (73)

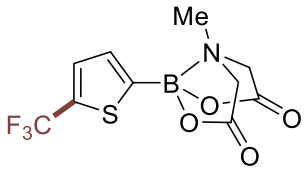

Following the general procedure, using 4-phenylpyridine *N*-oxide (547.8 mg, 3.2 mmol, 4.0 equiv.) and TFAA (463 µl, 3.28 mmol, 4.1 equiv.) with 4 ml total of dry MeCN (0.2M) the reaction was run for 12 hours. ^{19}F NMR analysis of the crude reaction mixture vs. the injected trifluorotoluene standard revealed the title compound in **73% yield**. The use of fewer equivalents of reagent at shorter reaction times provided comparable yields of product, but incompletely consumed the starting material, which was inseparable from the product. The reaction was partitioned with 1N HCl and diluted with dichloromethane. The organic phase was separated, washed with brine, and dried over sodium sulfate before filtering and concentrating. The crude reaction mixture was purified on silica gel. Pyridine derivatives were flushed off the column with ~750 ml of 2% methanol in diethyl ether[201] before the product was eluted with 10% MeCN in CH_2Cl_2 (179.7 mg, **73% yield**) as an amorphous, off-white solid (R_f = 0.44, THF). The isolation and characterization of this compound has previously been reported.[199]

(1-(tert-butoxycarbonyl)-5-(trifluoromethyl)-1H-pyrrol-2-yl)boronic acid MIDA ester (80)

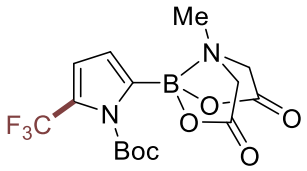

Following the general procedure, using 4-phenylpyridine *N*-oxide (410.9 mg, 2.4 mmol, 3.0 equiv.) and TFAA (350 µl, 2.48 mmol, 3.1 equiv.) with 4 ml total of dry MeCN (0.2M) the reaction was run for 12 hours. It should be noted that for this substrate the reaction mixture gets very dark upon exposure to light, which limits conversion at higher concentrations (0.4M). ^{19}F NMR analysis of the crude reaction mixture vs. the injected trifluorotoluene standard revealed the title compound in **75% yield**. The reaction was filtered through silica gel with 50% MeCN in CH_2Cl_2 and concentrated. The crude reaction mixture was purified on silica gel. Pyridine derivatives were flushed off the column with ~750 ml of 2% methanol in diethyl ether before the product was eluted with 10% MeCN in CH_2Cl_2 as an off-white solid (R_f = 0.43, 25% MeCN in CH_2Cl_2). This material was further purified by preparative TLC (25% MeCN in CH_2Cl_2) to yield the title compound as a white solid (190.6 mg, **62%**). ^{1}H NMR ($CDCl_3$, 500 MHz): δ 6.72 (d, *J* = 3.6 Hz, 1H), 6.68 (d, *J* = 3.6 Hz, 1H), 4.18 (d, *J* = 16.8 Hz, 2H), 3.95 (d, *J* = 16.8 Hz, 2H), 3.00 (s, 3H), 1.57 (s, 9H); ^{13}C NMR ($CDCl_3$, 175 MHz): δ 169.7, 150.8, 125.5 (q, J_{CF} = 38.8 Hz), 121.9 (q, J_{CF} = 265.7 Hz), 121.7, 117.4 (q, J_{CF} = 4.1 Hz), 87.8, 65.9, 50.5, 27.6; ^{19}F NMR ($CDCl_3$, 470 MHz): δ –58.01; IR (neat): 2999, 1741, 1564, 1454, 1334, 1220, 1126, 1032; HRMS (EI) *m/z* calculated for $C_{10}H_{10}BF_3N_2O_4$ [(M–Boc+H)$^+$] 290.0686, found 290.0687.

(5-(trifluoromethyl)furan-2-yl)boronic acid MIDA ester (81)

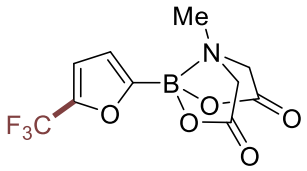

Following the general procedure, using 4-phenylpyridine *N*-oxide (273.9 mg, 1.6 mmol, 2.0 equiv.) and TFAA (237 µl, 1.68 mmol, 2.1 equiv.), the reaction was run for 6 hours. ^{19}F NMR analysis of the crude reaction mixture vs. the injected trifluorotoluene standard revealed the title compound in **60% yield**. The reaction was filtered through silica gel with 50% MeCN in CH_2Cl_2 and concentrated. The crude reaction mixture was purified on silica gel. Pyridine derivatives were flushed off the column with ~750 ml of 2% methanol in diethyl ether[201] before the product was eluted with 10% MeCN in CH_2Cl_2 (137.8 mg, **59% yield**) as an amorphous, off-white solid (R_f = 0.46, 20% MeCN/CH_2Cl_2). ^{1}HNMR (MeCN-*d3*, 700 MHz): δ 6.99 (d, *J* = 3.2 Hz, 1H), 6.85 (d, *J* = 3.2 Hz, 1H), 4.12 (d, *J* = 17.3 Hz, 2H), 3.96 (d, *J* = 17.3 Hz, 2H), 2.70 (s, 3H); ^{13}C NMR (MeCN-*d3*, 175 MHz): δ 169.3, 145.4 (q, J_{CF} = 41.8 Hz), 120.9 (q, J_{CF} = 267.7 Hz), 120.5, 113.8 (q, J_{CF} = 2.7 Hz), 63.1, 48.6; ^{19}F NMR ($CDCl_3$, 470 MHz): δ -64.95; IR (neat): 2953, 1757, 1605, 1462, 1309, 1279, 1218, 1173, 1125, 1102, 1050, 1009, 936; HRMS (ESI) *m/z* calculated for $C_{10}H_9BF_3NO_5$ ($[M]^+$) 309.0864, found 309.0866.

tert-butyl 2-(trifluoromethyl)-1H-pyrrole-1-carboxylate (72)

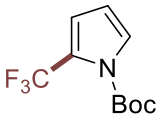

Following the general procedure using 4-phenylpyridine *N*-oxide (137.0 mg, 0.8 mmol, 1.0 equiv.) and TFAA (124 µl, 0.88 mmol, 1.1 equiv.), the reaction was run for 15 hours. ^{19}F NMR analysis of the crude reaction mixture vs. the injected trifluorotoluene standard revealed trifluoromethylated pyrrole in **65% yield** (6:1 ratio mono:bis). Tert-butyl 2-(trifluoromethyl)-1H-pyrrole-1-carboxylate: ^{19}F NMR ($CDCl_3$, 470 MHz): δ -59.29 (s, 3F, **56% yield**). Tert-butyl 2,5-bis(trifluoromethyl)-1H-pyrrole-1-carboxylate: ^{19}F NMR ($CDCl_3$, 470 MHz): δ -59.36 (s, 3F, **9% yield**). The isolation and characterization of this compound has been previously reported.[199]

Tert-butyl 2,5-bis(trifluoromethyl)-1H-pyrrole-1-carboxylate (82)

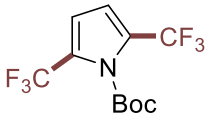

Following the general procedure using 4-phenylpyridine *N*-oxide (410.9 mg, 2.4 mmol, 3.0 equiv.) and TFAA (350 µl, 2.48 mmol, 3.1 equiv.), the reaction was run for 15 hours. ^{19}F NMR analysis of the crude reaction mixture vs. the injected trifluorotoluene standard revealed trifluoromethylated pyrrole in **63% yield** (1:8 ratio mono:bis). Tert-butyl 2-(trifluoromethyl)-1H-pyrrole-1-carboxylate: ^{19}F NMR ($CDCl_3$, 470 MHz): δ -59.29 (s, 3F, **7% yield**). Tert-butyl 2,5-bis(trifluoromethyl)-1H-pyrrole-1-carboxylate: ^{19}F NMR ($CDCl_3$, 470 MHz): δ -59.36 (s, 3F, **56% yield**). The isolation and characterization of this compound has been previously reported.[199]

1,3-dimethyl-3-(2,2,2-trifluoroethyl)indolin-2-one (64)

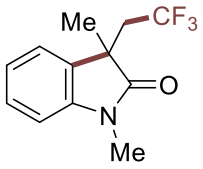

Following the general procedure using 4-phenylpyridine *N*-oxide (273.9 mg, 1.6 mmol, 2.0 equiv.) and TFAA (451 µl, 3.2 mmol, 4.0 equiv.), the reaction was run for 12 hours. ^{19}F NMR analysis of the reaction mixture cannot be accurately accomplished due to peak overlap of the product with a minor impurity. The reaction was partitioned with 1N HCl and diluted with ethyl acetate. The organic phase was separated, washed with sat. $NaHCO_3$, brine, and dried over sodium sulfate before filtering and concentrating. The crude reaction mixture was purified by column chromatography (0% to 50% ethyl acetate in hexanes) to yield the title compound (89.5 mg, **46% yield**). The isolation and characterization of this compound has been previously reported.[199]

1-(tert-butyl) 2-methyl 5-(perfluoroethyl)-1H-pyrrole-1,2-dicarboxylate (83)

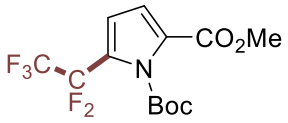

Following the general procedure, using 4-phenylpyridine *N*-oxide (137.0 mg, 0.8 mmol, 1.0 equiv.) and pentafluoropropionic anhydride (174 µl, 0.88 mmol, 1.1 equiv.), the reaction was run for 6 hours. ^{19}F NMR analysis of the crude reaction mixture vs. the injected trifluorotoluene standard revealed the title compound in **80% yield**. The reaction was partitioned with 1N HCl and diluted with dichloromethane. The organic phase was separated, washed with sat. $NaHCO_3$, brine, and dried over sodium sulfate before filtering and concentrating. The crude reaction mixture was purified by column chromatography (30% dichloromethane in hexanes) to yield the title compound (198.9 mg, **72% yield**) as a clear oil (R_f = 0.1, 25% dichloromethane in hexanes).

^{1}H NMR ($CDCl_3$, 700 MHz): δ 6.87 (d, J = 3.8 Hz, 1H), 6.58 (d, J = 3.8 Hz, 1H), 3.87 (s, 3H), 1.61 (s, 9H);

^{13}C NMR ($CDCl_3$, 175 MHz): δ 159.8, 147.7, 127.3, 123.1 (t, J_{CF} = 27.2 Hz), 118.5 (qt, J_{CF} = 287.1, 38.1 Hz), 116.1, 113.6 (app. tq, J_{CF} = 5.7, 1.9 Hz), 110.3 (tq, J_{CF} = 252.7, 40.1 Hz), 87.1, 52.1, 27.0;

^{19}F NMR ($CDCl_3$, 376 MHz): δ -84.23 (3F), -107.82 (2F);

IR (neat): 2991, 1782, 1726, 1546, 1373, 1250, 1207, 1133, 1096, 1034;

HRMS (EI) *m/z* calculated for $C_8H_6F_5NO_2$ [(M–Boc+H)$^+$] 243.0319, found 243.0314.

(5-(perfluoroethyl)thiophen-2-yl)boronic acid MIDA ester (84)

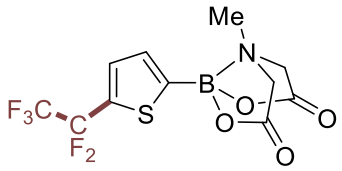

Following the general procedure, using 4-phenylpyridine *N*-oxide (410.9 mg, 2.4 mmol, 3.0 equiv.) and pentafluoropropionic anhydride (517 µl, 2.48 mmol, 3.1 equiv.) with 4 ml total of dry MeCN (0.2M) the reaction was run for 12 hours. ^{19}F NMR analysis of the crude reaction mixture vs. the injected trifluorotoluene standard revealed the title compound in **95% yield**. The reaction was partitioned with 1N HCl and diluted with dichloromethane. The organic phase was separated, washed with brine, and dried over sodium sulfate before filtering and concentrating. The crude reaction mixture was purified on silica gel. Pyridine derivatives were flushed off the column with ~750 ml of 2% methanol in diethyl ether[201] before the product was eluted with 10% MeCN in CH_2Cl_2 (260.0 mg, **91% yield**) as an amorphous, off-white solid (R_f = 0.33, 20% MeCN in CH_2Cl_2).

^{1}H NMR (MeCN-*d3*, 700 MHz): δ 7.62 (d, *J* = 3.5 Hz, 1H), 7.36 (dt, *J* = 3.5 Hz, J_{CF} = 1.9 Hz, 1H), 4.12 (d, *J* = 17.2 Hz, 2H), 3.96 (d, *J* = 17.2 Hz, 2H), 2.65 (s, 3H);

^{13}C NMR (MeCN-*d3*, 175 MHz): δ 168.9, 134.9, 133.0 (t, J_{CF} = 29.7 Hz), 132.9 (t, J_{CF} = 5.4 Hz), 119.9 (qt, J_{CF} = 285.4, 40.9 Hz), 113.7 (tq, J_{CF} = 251.4, 39.5 Hz), 62.8, 48.7;

^{19}F NMR (MeCN-*d3*, 376 MHz): δ -86.08 (br. s, 3F), -105.14 (s, 2F);

IR (neat): 3011, 1760, 1535, 1459, 1337, 1285, 1258, 1196, 1165, 1030, 980;

HRMS (ESI) *m/z* calculated for $C_{11}H_9BF_5NO_4S$ [$(M+H)^+$] 358.0338, found 358.0344; *m/z* calculated for $C_{11}H_9BF_5NO_4SNa$ [$(M+Na)^+$] 380.0159, found 380.0159.

4-(tert-butyl)-1-methoxy-2-(perfluoroethyl)benzene (85)

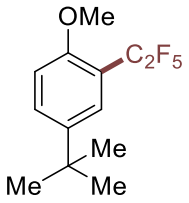

Following the general procedure, using 4-phenylpyridine *N*-oxide (410.9 mg, 2.4 mmol, 3.0 equiv.) and pentafluoropropionic anhydride (489 µl, 2.48 mmol, 3.1 equiv.), the reaction was run for 8 hours. ^{19}F NMR analysis of the crude reaction mixture vs. the injected trifluorotoluene standard revealed the title compound in **81% yield**. The reaction was partitioned with 1N HCl and diluted with dichloromethane. The organic phase was separated, washed with sat. $NaHCO_3$, brine, and dried over sodium sulfate before filtering and concentrating. The crude reaction mixture was purified by prep TLC (100% hexanes run up x2) to yield the title compound as a clear oil (R_f = 0.57, 10% dichloromethane in hexanes).

^{1}H NMR ($CDCl_3$, 400 MHz): δ 7.53-7.49 (m, overlap, 2H), 6.95 (d, J = 8.4 Hz, 1H), 3.85 (s, 3H), 1.31 (s, 9H);

^{13}C NMR ($CDCl_3$, 175 MHz): δ 156.0 (t, J_{CF} = 2.7 Hz), 143.2, 130.2, 125.6 (t, J_{CF} = 8.5 Hz), 119.5 (qt, J_{CF} = 287.5, 39.5 Hz), 115.9 (t, J_{CF} = 115.9 Hz), 113.9 (tq, J_{CF} = 254.8, 41.6 Hz), 112.2, 56.0, 34.2, 31.3;

^{19}F NMR ($CDCl_3$, 376 MHz): δ -84.89 (3F), -112.60 (2F);

IR (neat): 2961, 1617, 1510, 1464, 1268, 1194, 1074, 1030, 991;

HRMS (EI) *m/z* calculated for $C_{13}H_{15}F_5O$ [$(M)^+$] 282.1043, found 282.1042.

(perfluoroethyl)benzene (86)

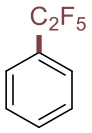

Following the general procedure, using 4-phenylpyridine *N*-oxide (137.0 mg, 0.8 mmol, 1.0 equiv.) as the limiting reagent, pentafluoropropionic anhydride (174 µl, 0.88 mmol, 1.1 equiv.), and benzene (713 µl, 8.0 mmol, 10.0 equiv.), the reaction was run for 12 hours. Upon completion, the reaction was quenched with methanol (500 µl) and removed from the light source. ^{19}F NMR analysis of the crude reaction mixture vs. the injected trifluorotoluene standard revealed the title compound in **76% yield**. Due to the volatility of the product, no purification was attempted on this reaction mixture. The fluorine signals of the product were consistent to those reported in the literature: in one report,[202] values are listed vs. trifluorotoluene (referenced to δ 0.0) with positive values to high field, and are reproduced here with trifluorotoluene referenced to δ -63.72: ^{19}F NMR (no solvent reported, 60 MHz): δ -119.3 (m, 2F), -88.9 (t, J_{FF} = 1.7 Hz, 3F); Another report[203] reports the shifts in toluene-*d8* (δ -84, -113), while yet another[204] reports the shifts in benzene-*d6* (δ -84.86, -114.75). Our data: ^{19}F NMR ($CDCl_3$, 470 MHz): δ -85.78 (s, 3F), -115.95 (s, 2F).

1-(tert-butyl) 2-methyl 5-(perfluoropropyl)-1H-pyrrole-1,2-dicarboxylate (87)

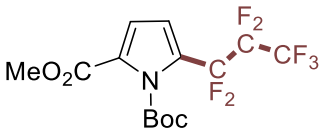

With heptafluorobutyric anhydride:

Following the general procedure, using 4-phenylpyridine *N*-oxide (273.9 mg, 1.6 mmol, 2.0 equiv.) and heptafluorobutyric anhydride (412 µl, 1.68 mmol, 2.1 equiv.), the reaction was run for 4 hours. ^{19}FNMR analysis of the crude reaction mixture vs. the injected trifluorotoluene standard revealed the title compound in **78% yield**. The reaction was partitioned with 1N HCl and diluted with dichloromethane. The organic phase was separated, washed with sat. $NaHCO_3$, brine, and dried over sodium sulfate before filtering and concentrating. The crude reaction mixture was purified by column chromatography (10-30% dichloromethane in hexanes) to yield the title compound (225.9 mg, **72% yield**) as a clear oil (R_f = 0.31, 50% CH_2Cl_2 in hexanes).

^{1}H NMR ($CDCl_3$, 400 MHz): δ 6.89 (dt, J = 4.0, 1.2 Hz, 1H), 6.59 (d, J = 4.0 Hz, 1H), 3.87 (s, 3H), 1.60 (s, 9H);

^{13}C NMR ($CDCl_3$, 175 MHz): δ 159.9, 147.7, 127.2, 123.1 (t, J_{CF} = 29.3 Hz), 117.9 (qt, J_{CF} = 287.5, 34.7), 116.1, 114.1 (t, J_{CF} = 5.4 Hz), 112.5 (tt, J_{CF} = 254.8, 32.7 Hz). 108.4 (ttq, J_{CF} = 265.0, 38.1, 38.1 Hz), 87.1, 52.1, 27.0 Hz;

^{19}F NMR ($CDCl_3$, 376 Hz): -81.01 (t, J_{FF} = 9.5 Hz, 3F), -105.91 (ap. sxt, tq, J_{FF} = 9.5, 8.9 Hz, 2F), -125.84 (t, J_{FF} = 8.9 Hz, 2F):

IR (neat): 2984, 1784, 1727, 1546, 1437, 1373, 1248, 1202, 1154, 111, 1088, 838, 741;

HRMS (EI) *m/z* calculated for $C_9H_6F_7NO_2$ [$(M)^+$] 293.0287, found 293.0291.

With heptafluorobutyryl chloride:

Following the general procedure, using 4-phenylpyridine *N*-oxide (273.9 mg, 1.6 mmol, 2.0 equiv.) and heptafluorobutyryl chloride (251 µl, 1.68 mmol, 2.1 equiv.), the reaction was run for 4 hours. ^{19}FNMR analysis of the crude reaction mixture vs. the injected trifluorotoluene standard revealed the title compound in **67% yield**. The reaction was partitioned with 1N HCl and diluted with dichloromethane. The organic phase was separated, washed with sat. $NaHCO_3$, brine, and dried over sodium sulfate before filtering and concentrating. The crude reaction mixture was purified by column chromatography (10-30% dichloromethane in hexanes) to yield the title compound as a clear oil (193.2 mg, **61% yield**).

Background EDA Reaction Controls

For each substrate type, control reactions without catalyst were performed to determine the degree of contribution of the EDA mechanism to the overall transformation. These were specifically designed to probe substrate-specific effects, and consequently a ratio of 2:1 TFAA:4-Ph-pyridine *N*-oxide was employed for these reactions, despite the fact that optimized conditions in the manuscript utilize a 1.1:1 ratio. This is to eliminate the contribution of the putative "self-complexation" between acylated and non-acylated *N*-oxide, which also results in productive chemistry. The reactions below were performed on 0.2 mmol scale (0.4 M in MeCN, 0.5 ml MeCN), with 2 equivalents of 4-Ph-PNO and 4 equivalents of TFAA

With $Ru(bpy)_3Cl_2$ vs.
No Photocatalyst

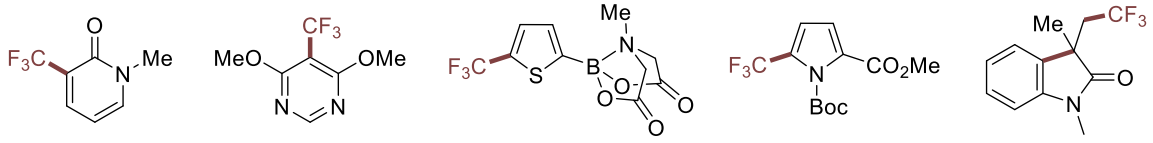

44% **24%**	**42%** **17%**	**65%** **18%**	**49%** **12%**	**44%** **45%**
70	**52**	**73**	**78**	**64**

UV-Vis Studies:

All UV-VIS measurements were performed on a Shimadzu UV-1601 UV-VIS Spectrometer. Samples were prepared using dry MeCN as the solvent. Measurements were taken in 1cm path length quartz cuvettes at room temperature and were not degassed.

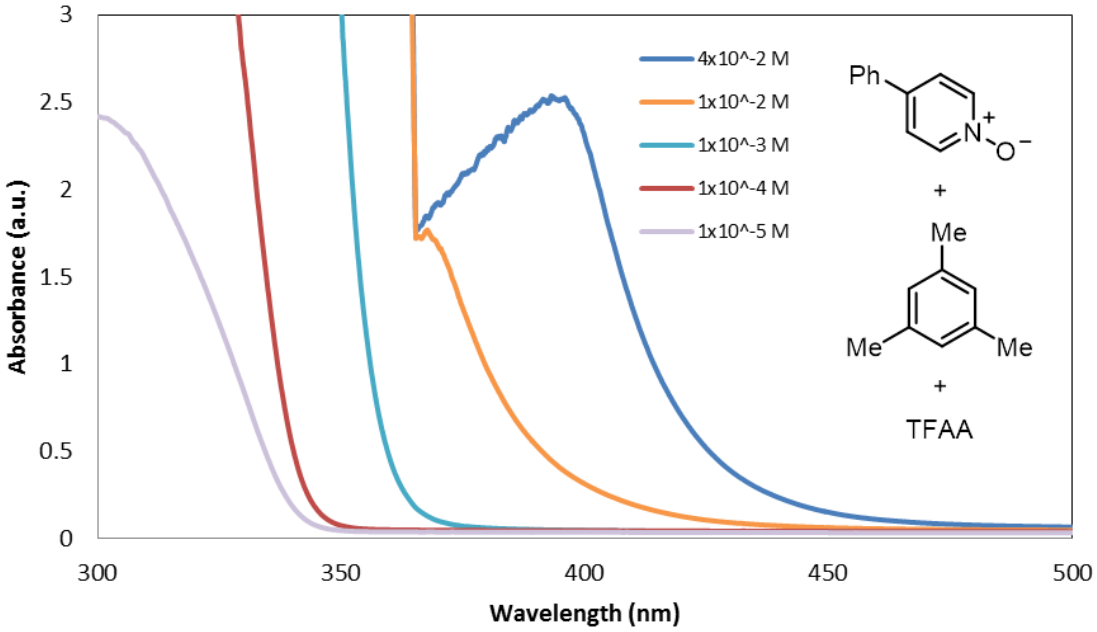

Evaluation of the various component contributions to the EDA absorbance at 0.4M is performed earlier in this chapter; however, these effects were seen at lower concentrations as well, with donor arene clearly being essential for the proposed EDA absorbance (orange curve, above). Visible light absorbance by the reagent can also be seen at these concentrations.

As expected, visible absorbance of the EDA complex are higher for more electron donating arenes (below). Below optical absorbance spectra of various reaction components are displayed at a standardized concentration of 0.1M in dry MeCN. Components were mixed in relevant stoichiometry, resulting in a 0.1 M concentration for each component except for TFAA, which was present in 0.11 M concentration. PPNO stands for 4-phenylpyridine *N*-oxide.

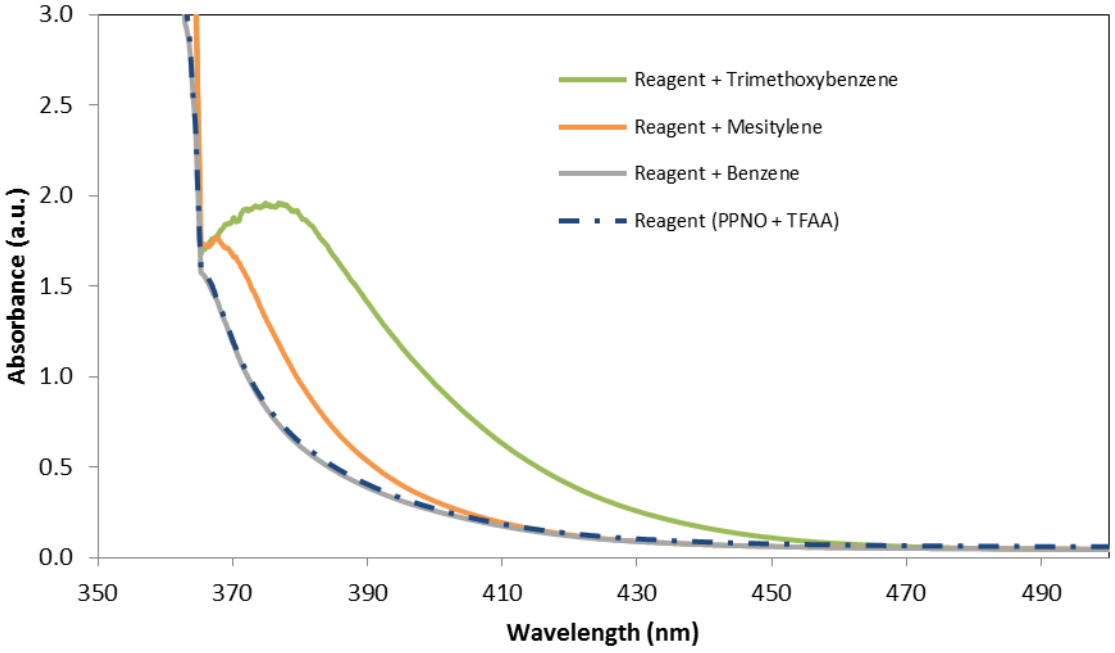

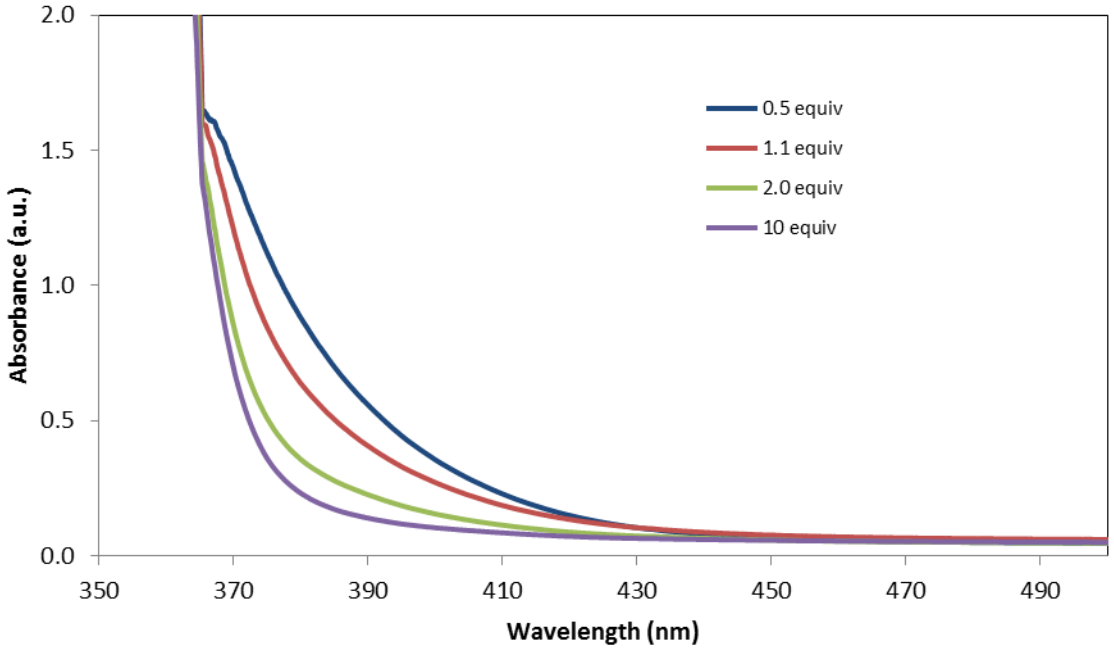

Optical absorbance spectra of 4-phenylpyridine *N*-oxide at 0.1 M concentration with varying concentrations of TFAA in dry MeCN.

At 0.1 M, the 4-phenylpyridine *N*-oxide/TFAA mixture has a shouldered peak at 365 nm, but the actual peak is obscured by strong aryl absorbance, presumably from the pyridinium moiety itself. Nevertheless, TFAA titration studies at these lower concentrations do not suggest a shifting in absorption wavelength and merely result in absorbance intensity differences between 365 nm and 450 nm (above).

Starting Material Consumption vs. Time

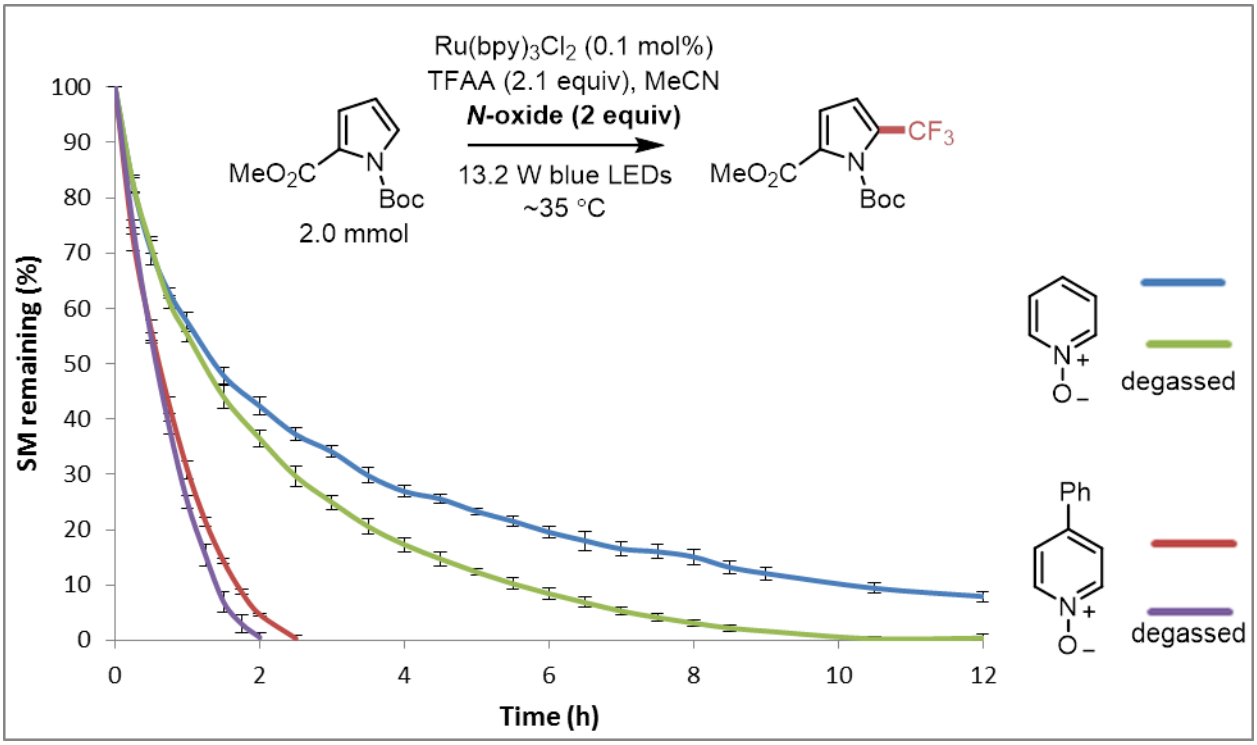

Effects of pyridine *N*-oxide choice on starting material consumption. In every case, degassed reaction mixtures (green, purple) consumed starting material faster than non-degassed mixtures (blue, red). Each reaction profile is the average of three runs, with error bars in each direction representing one standard deviation for each time point.

Electrochemical Measurements

The measurement of reduction potentials for the acylonium salts reported in this manuscript cannot be accurately performed through cyclic voltammetry analysis. The observed signal using cyclic voltammetry has variations in shape and peak potential from run to run, and the peak shape in particular is dependent upon sweep rate. Literature precedent in this area for alkylated pyridine *N*-oxides suggests that these molecules can undergo extremely fast ("barrierless") fragmentation upon single-electron reduction (k_{obs} on the order of 1.8×10^{12} s^{-1} for

1-methoxy-4-phenylpyridinium and $4.1x10^{12}$ s^{-1} for 1-methoxypyridinium).[205] Furthermore, another paper concerning similar structures reports that "[r]eduction potentials of *N*-methoxypyridinium salts are not readily accessible through conventional electrochemical techniques because of the relatively fast reductive cleavage of these compounds."[184]

Differential pulse voltammetry (DPV) was performed to obtain the reduction potentials of the various pyridine *N*-oxide/anhydride combinations, and reproducible potentials were obtained through these methods. Measurements were performed with a model CHI660C multi-potentiostat from CH Instruments. Measurements were performed with a glassy carbon working electrode, Pt auxiliary electrode, Ag/AgCl reference electrode, Bu_4NPF_6 electrolyte (0.1 M in MeCN), and analyte (pyridine-N-oxide:TFAA, 1:1, 0.01 M) with the following settings: Incr E (V) = 0.001, Amplitude (V) = 0.005, Pulse Width (sec) = 0.05, Sampling Width (sec) = 0.01, Pulse Period (sec) = 0.5.

All voltammograms are reported/displayed ***after*** conversion to voltage vs. SCE, where:

$$\mathbf{V_{SCE} = V_{AgCl} - 0.05\ V}$$

Onset potentials are estimated based on the intersection of the baseline and onset slope.

Quenching Studies:

Quenching data was obtained using a Fluoromax-2 Fluorimeter. All quenching data was recorded using a quartz cuvette with a stir bar at between 24.5 and 25.5 ˚C with $Ru(bpy)_3Cl_2$ (9.97×10^{-6} M) in dry, degassed MeCN (sparged for 5 minutes). Excitation was performed at 452 nm with emission measured at 615 nm. All values are the average of three measurements.

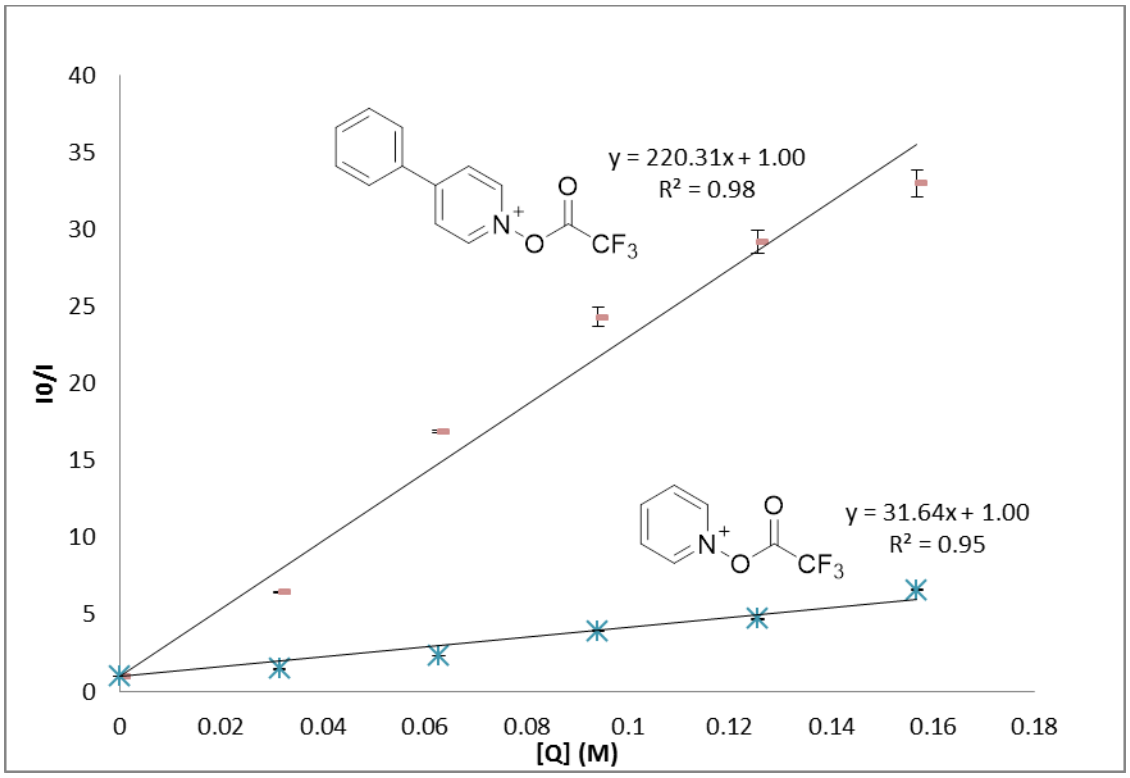

Stern-Volmer Quenching of $Ru(bpy)_3Cl_2$ with 4-phenylpyridine *N*-oxide (PPNO)/TFAA or with pyridine *N*-oxide (PNO)/TFAA. For each measurement the concentration of quencher refers to the concentration of the *N*-oxide, which is the limiting reagent in a ratio of 1.0:1.1 in relation to TFAA.

From the data above, quenching rates (k_q) may be extracted based on the following equation:

$$\frac{I_0}{I} = k_q \tau_0 [Q] + 1$$

Where τ_0 represents the catalyst excited state lifetime[3] at 25 ˚C in MeCN, for which we used a value of 0.87 μs.[206]

	k_q (M^{-1} s^{-1})
pyridine *N*-oxide/TFAA	**3.6×10^7**
4-Ph-pyridine *N*-oxide/TFAA	**2.5×10^8**

For the 4-Ph-pyridine *N*-oxide/TFAA mixture, the calculated quenching rate is likely a lower bound for the value, as higher concentrations of quencher begin to absorb very slightly at 452 nm:

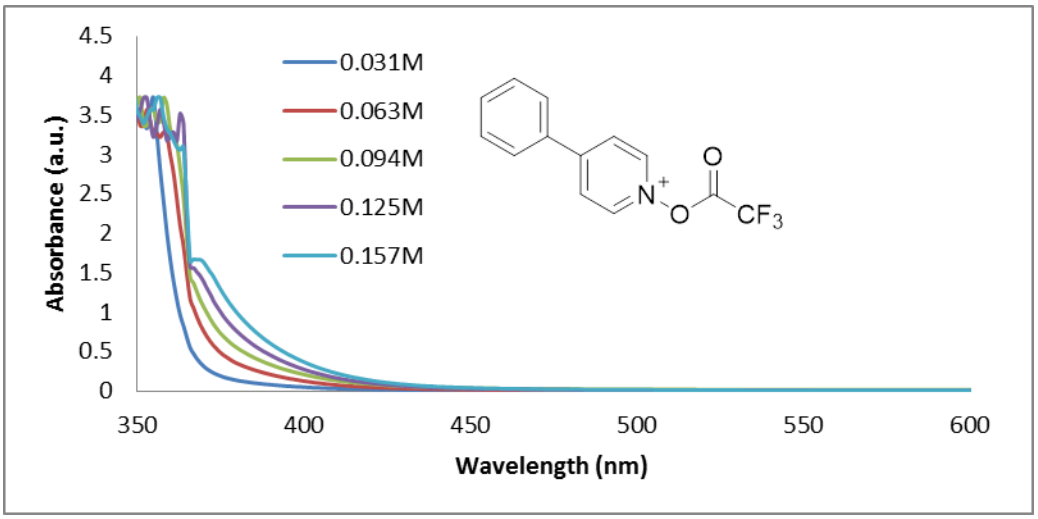

Optical absorbance spectra of the 4-Ph-pyridine *N*-oxide/TFAA mixture (1.0:1.1 ratio) at the various concentrations used in the quenching experiment.

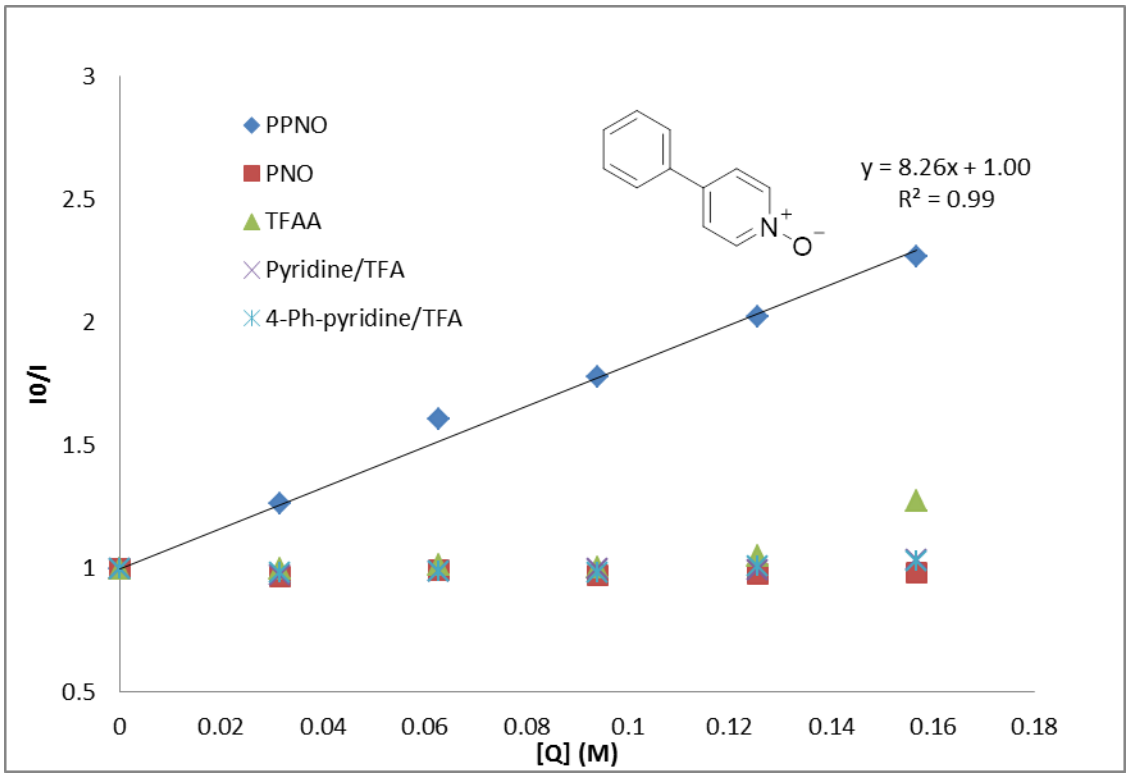

Stern-Volmer Quenching of $Ru(bpy)_3Cl_2$, component controls. Of the individual components of the reaction, only 4-phenylpyridine *N*-oxide (PPNO) quenched the photocatalyst, while PNO, TFAA, 4-phenylpyridinum trifluoroacetate, and pyridinium trifluoroacetate did not quench the catalyst.

Quantum Yield Measurements

Quantum yield experimental design was based on the procedure by Cismesia and Yoon.[188] Experiments were performed using a Fluoromax-2 Fluorimeter equipped with a 150 W Xenon Arc lamp. Actinometry was performed with potassium ferrioxalate trihydrate. The procedure for determining photon flux, as described by Cismesia and Yoon, is reproduced below:

> "The photon flux of the spectrophotometer was determined by standard ferrioxalate actinometry. A 0.15 M solution of ferrioxalate was prepared by dissolving 2.21 g of potassium ferrioxalate hydrate in 30 mL of 0.05 M H_2SO_4. A buffered solution of phenanthroline was prepared by dissolving 50 mg of phenanthroline and 11.25 g of sodium acetate in 50 mL of 0.5 M H_2SO_4. Both solutions were stored in the dark. To determine the photon flux of the spectrophotometer, 2.0 mL of the ferrioxalate solution was placed in a cuvette and irradiated for 90.0 seconds at λ = 436 nm with an emission slit width at 10.0 nm. After irradiation, 0.35 mL of the phenanthroline solution was added to the cuvette. The solution was then allowed to rest for 1 h to allow the ferrous ions to completely coordinate to the phenanthroline."

At this point, our protocol differed slightly from the published protocol. Our absorbance measurements in the 1 cm quartz cuvette at 510 nm for the Fe^{2+} phenanthroline complex were above 2.0 absorbance units, and were deemed too high for accurate quantification. Instead, we obtained the absorbance of the solutions at 510 nm after transferring some of the solution to a 1 mm (0.1 cm) path length cuvette, which provided absorbance units an order of magnitude lower. An additional sample was prepared exactly as above, was not irradiated, and upon development with the phenanthroline solution for 1 hour its absorbance was measured at 510 nm in the 1 mm path cuvette. The amount of Fe^{2+} was quantified according to the equation below.

> "Where V is the total volume (0.00235 L) of the solution after addition of phenanthroline, ΔA is the difference in absorbance at 510 nm between the irradiated and non-irradiated solutions, l is the path length… [0.100 cm], and ε is the molar absorptivity at 510 nm (11,100 L mol^{-1} cm^{-1})."

$$\text{mol } Fe^{2+} = \frac{V \cdot \Delta A}{l \cdot \varepsilon} = \frac{0.00235 \text{ L} \cdot 0.234009}{0.100 \text{ cm} \cdot 11{,}100 \text{ L mol}^{-1}\text{cm}^{-1}} = 4.95 \text{ x } 10^{-7} \text{ mol } Fe^{2+}$$

Photon flux was then determined as follows:

$$\text{photon flux} = \frac{\text{mol } Fe^{2+}}{\Phi \cdot t \cdot f} = \frac{4.95 \text{ x } 10^{-7} \text{ mol}}{1.01 \cdot 90 \text{ s} \cdot 0.99907} = 5.46 \text{ x } 10^{-9} \text{einstein s}^{-1}$$

Φ = the quantum yield of ferrioxalate at 0.15 M and λ=436 nm

f = fraction of light absorbed at λ=436 nm, which can be determined from the equation $f = 1 - 10^{-A}$. The absorbance spectrum of the non-irradiated 0.15 M ferrioxalate solution was taken and is shown below. The absorbance at 436 nm was found to be 3.03186, which results in a value of 0.99907 for f.

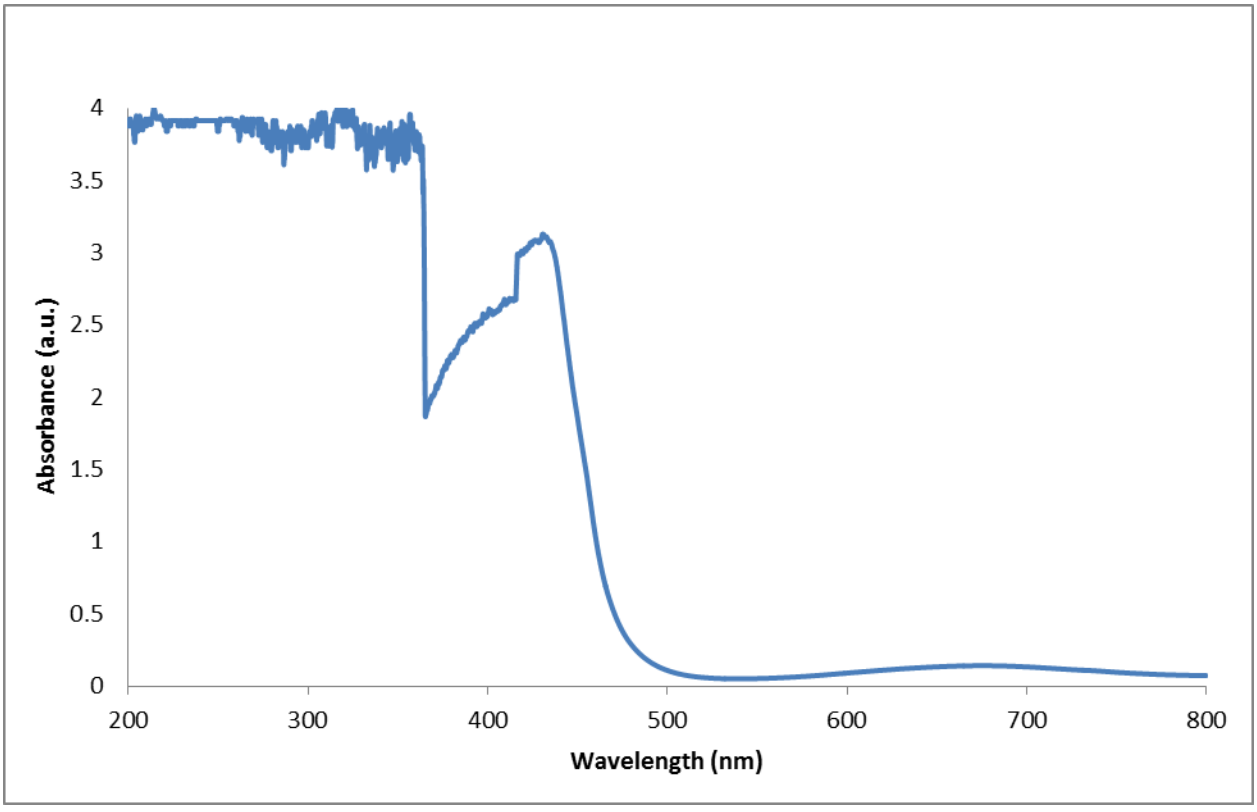

Optical absorbance spectrum for $K_3Fe(C_2O_4)_3$, 0.15 M in 0.05M H_2SO_4. The absorbance of the sample at 436 nm is 3.03186, which means that >99.9% of incident light is absorbed at this wavelength.

Quantum yield of the trifluoromethylation of mesitylene under standard conditions was determined as follows:

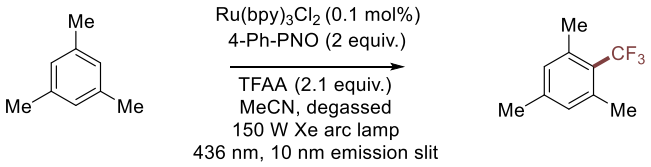

In a dark room, 4-phenylpyridine *N*-oxide (273.9 mg, 1.6 mmol, 2.0 equiv.), and mesitylene (111 µL, 96.2 mg, 0.80 mmol, 1.0 equiv.) were combined in a 1 cm path length cuvette equipped with stir bar. 500 µl of a solution 1.2 mg/ml $Ru(bpy)_3Cl_2 \bullet 6H_2O$ in dry MeCN (0.6 mg, 0.1 mol%) was added to the cuvette, followed by 1.5 ml of dry MeCN. The solution was sparged for 30 seconds, followed by the addition of TFAA (237 µl, 353 mg, 2.1 equiv., not degassed) under a stream of nitrogen. The reaction was quickly sealed with a screw on cap, and wrapped with parafilm. Light exclusion was achieved by wrapping the reaction in foil until the reaction was placed in the fluorimeter. The sample-holder was pre-equilibrated to 35 ˚C, and the reaction sample was allowed to equilibrate to this temperature over 10 minutes. The sample was stirred and irradiated at 436 nm with a 10 nm slit width for 28,800 s (8 h). After irradiation, 0.5 ml of methanol was added to the reaction solution. After stirring for an additional 2 minutes, trifluorotoluene (98 µl, 0.8 mmol, 1.0 equiv.) was added as an internal standard, and the reaction was analyzed by ^{19}F NMR. The reaction yielded 17% (0.136 mmol) of 1,3,5-trimethyl-2-(trifluoromethyl)benzene.

The quantum yield was calculated as follows:

$$\Phi = \frac{\text{mol product}}{\text{flux}\cdot t \cdot f} = \frac{1.36\ \text{x}10^{-4}\text{mol}}{5.46\ \text{x}10^{-9}\text{einstein}\ \text{s}^{-1} \cdot 28800\ \text{s} \cdot 1.00} = 0.87$$

Where f is the fraction of light absorbed at λ=436 nm, which can be determined from the equation $f = 1 - 10^{-A}$. The absorbance spectrum of the non-irradiated 0.15 M ferrioxalate

solution was taken and is shown below. The absorbance at 436 nm was found to be 3.389282, which results in a value > 0.999 for f.

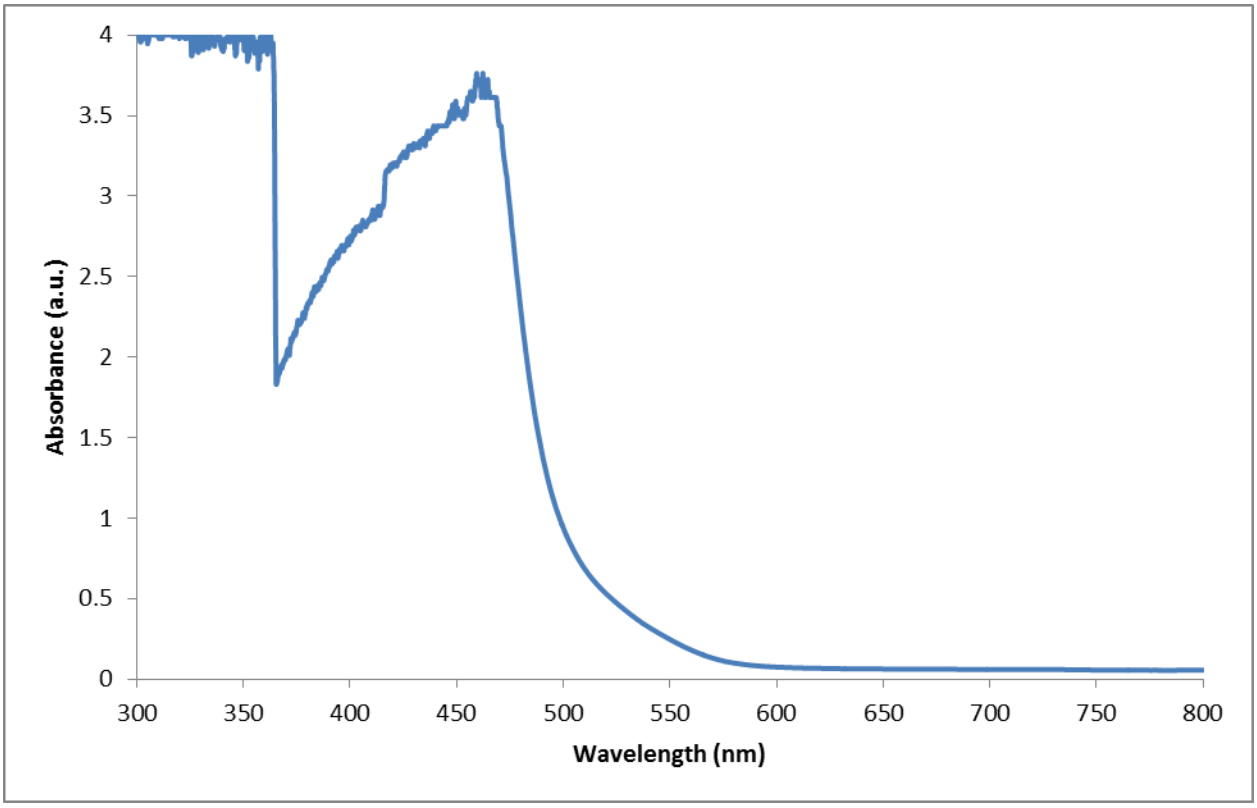

Optical absorbance spectrum for the full reaction mixture (0.4 M in MeCN). Reactant stoichiometry is 1.0 : 2.0 : 2.1 for mesitylene, 4-phenylpyridine *N*-oxide, and TFAA, respectively, with 0.1 mol% $Ru(bpy)_3Cl_2$. The absorbance of the sample at 436 nm is 3.389282, which means that >99.9% of incident light is absorbed at this wavelength.

Bibliography:

[1] Yoon, T. P.; Ischay, M. A.; Du, J. *Nature Chem.* **2010**, *2*, 527–532.

[2] Prier, C. K.; Rankic, D. A.; MacMillan, D. W. C. *Chem. Rev.* **2013**, *113*, 5322–5363.

[3] Juris, A.; Balzani, V.; Barigelletti, F.; Campagna, S.; Belser, P.; Von Zelewsky, A. *Chem. Coord. Rev.* **1988**, *84*, 85–277.

[4] Kalyanasundaram, K. Coord. Chem. Rev. 1982, 46, 159–244.

[5] Demas, J. N.; Crosby, G. A. *J. Am. Chem. Soc.* **1971**, *93*, 2841–2847.

[6] Kober, E. M.; Sullivan, B. P.; Meyer, T. J. *Inorg. Chem.* **1984**, *23*, 2098–2104.

[7] Kakutani, T.; Morihiro, Y.; Senda, M.; Takahashi, R.; Matsumoto, K. *Bull. Chem. Soc. Jpn.* **1978**, *51*, 2847–2854.

[8] Tucker, J. W.; Stephenson, C. R. J. *J. Org. Chem.* **2012**, *77*, 1617–1622.

[9] Antizar-Ladislao, B. *Environ. Int.* **2008**, *34*, 292–308.

[10] Nicewicz, D. A.; MacMillan, D. W. C. *Science* **2008**, *322*, 77–80.

[11] Ischay, M. A.; Anzovino, M. E.; Du, J.; Yoon, T. P. *J. Am. Chem. Soc.* **2008**, *130*, 12886–12887.

[12] Linsay Smith, J. R.; Masheder, D. *J. Chem. Soc., Perkin Trans. 2* **1976**, 47–51.

[13] Narayanam, J. M. R.; Tucker, J. W.; Stephenson, C. R. J. *J. Am. Chem. Soc.* **2009**, *131*, 8756–8757.

[14] Shi, L.; Xia, W. *Chem. Soc. Rev.* **2012**, *41*, 7687–7697.

[15] Hu, J.; Wang, J.; Nguyen, T. H.; Zheng, N. *Beilstein J. Org. Chem.* **2013**, *9*, 1977–2001.

[16] Beatty, J. W.; Stephenson, C. R. J. *Acc. Chem. Res.* **2015**, *48*, 1474–1484.

[17] Lindsay Smith, J. R.; Masheder, D. *J. Chem. Soc., Perkin Trans. 2* **1976**, 47–51.

[18] For the oxidation potential of Et_3N vs. $AgNO_3$ in MeCN, converted to SCE in **Figure 1.4**, see: Newman, J. D. S.; Blanchard, G. J. *Langmuir* **2006**, *22*, 5882–5887.

[19] Estimation of the pKa of the α-C−H bond of the triethylamine radical cation was performed according to eq. 19 found in: Nicholas, M. de P.; Arnold, D. R. *Can. J. Chem.* **1982**, *60*, 2165–2179.

[20] Dombrowski, G. W.; Dinnocenzo, J. P.; Farid, S.; Goodman, J. L.; Gould, I. R. *J. Org. Chem.* **1999**, *64*, 427–431.

[21] Estimation of the α-C−H BDE for the triethylamine radical cation was performed with BDE values from ref. 20 according to: Wayner, D. D. M.; Dannenberg, J. J.; Griller, D. *Chem. Phys. Lett.* **1986**, *131*, 189–191.

[22] Lewis, F. D.; Ho, T.-I. *J. Am. Chem. Soc.* **1980**, *102*, 1751–1752.

[23] Lewis, F. D.; Ho, T.-I. *J. Org. Chem.* **1994**, *116*, 4211–4220.

[24] Zhang, X.; Yeh, S.-R.; Hong, S.; Freccero, M.; Albini, A.; Falvey, D. E.; Mariano, P. S. *J. Am. Chem. Soc.* **1994**, *116*, 4211–4220.

[25] Anne, A.; Hapoit, P.; Moiroux, J.; Neta, P.; Saveant, J.-M. *J. Am. Chem. Soc.* **1992**, *114*, 4694–4701.

[26] Yoon, U. C.; Su, Z.; Mariano, P. S. In *CRC Handbook of Organic Photochemistry and Photobiology*, 2nd ed.; Horspool, W., Lenci, F., Eds.; CRC Press, Boca Raton, FL, 2004; Vol. 2, pp 101-1–101-20.

[27] Schmittel, M.; Burghart, A. *Angew. Chem., Int. Ed. Engl.* **1997**, *36*, 2550–2589.

[28] Tucker, J. W.; Narayanam, J. M. R.; Krabbe, S. W.; Stephenson, C. R. J. *Org. Lett.* **2010**, *12*, 368–371.

[29] Furst, L.; Matsuura, B. S.; Narayanam, J. M. R.; Tucker, J. W.; Stephenson, C. R. J. *Org. Lett.* **2010**, *12*, 3104–3107.

[30] Condie, A. G.; González-Gómez, J. C.; Stephenson, C. R. J. *J. Am. Chem. Soc.* **2010**, *132*, 1464–1465.

[31] Freeman, D. B.; Furst, L.; Condie, A. G.; Stephenson, C. R. J. *Org. Lett.* **2012**, *14*, 94–97.

[32] Xuan, J.; Feng, Z. J.; Duan, S. W.; Xiao, W.-J. *RSC Adv.* **2012**, *2*, 4065–4068.

[33] Mathis, C. L.; Gist, B. M.; Frederickson, C. K.; Midkiff, K. M.; Marvin, C. C. *Tetrahedron Lett.* **2013**, *54*, 2101–2104.

[34] Xiao, T.; Li, L.; Lin, G.; Mao, Z.; Zhou, L. *Org. Lett.* **2014**, *16*, 4232–4235.

[35] Feng, Z. J.; Xuan, J.; Xia, X. D.; Ding, W.; Guo, W.; Chen, J. R.; Zou, Y. Q.; Lu, L.; Q.; Xiao, W.-J. *Org. Biomol. Chem.* **2014**¸ *12*, 2037–2040.

[36] Rueping, M.; Zhu, S.; Koenigs, R. M. *Chem. Commun.* **2011**, *47*, 8679–8681.

[37] Rueping, M.; Vila, C.; Koenigs, R. M.; Pscharny, K.; Fabry, D. C. *Chem. Commun.* **2011**, *47*, 2360–2362.

[38] Zhao, G.; Yang, C.; Guo, L.; Sun, H.; Chen, C.; Xia, W. *Chem. Commun.* **2012**, *48*, 2337–2339.

[39] Fu, W.; Guo, W.; Zou, G.; Xu, C. *J. Fluorine Chem.* **2012**, *140*, 88–94.

[40] Xie, J.; Xue, Q.; Jin, H.; Li, H.; Cheng, Y.; Zhu, C. *Chem. Sci.* **2013**, *4*, 1281–1286.

[41] Zou, Y. Q.; Lu, L. Q.; Fu, L. *Angew. Chem., Int. Ed.* **2011**, *50*, 7171–7175.

[42] Xu, G.-Q.; Li, C.-G.; Liu, M.-Q.; Cao, J.; Luo, Y.-C.; Xu, P.-F. *Chem. Commun.* **2016**, *52*, 1190–1193.

[43] DiRocco, D. A.; Rovis, T. *J. Am. Chem. Soc.* **2012**, *134*, 8094–8097.

[44] Bergonzini, G.; Schindler, C. S.; Wallentin, C.-J.; Jacobsen, E. N.; Stephenson, C. R. J. *Chem. Sci.* **2014**, *5*, 112–116.

[45] Wayner, D. D. M.; Dannenberg, J. J.; Griller, D. *Chem. Phys. Lett.* **1986**, *131*, 189–191.

[46] Kohls, P.; Jadhav, D.; Pandey, G.; Reiser, O. *Org. Lett.* **2012**, *14*, 672–675.

[47] Pandey, G.; Jadhav, D.; Tiwari, S. K.; Singh, B. *Adv. Synth. Catal.* **2014**, *356*, 2813–2818.

[48] Dai, X.; Cheng, D.; Guan, B.; Mao, W.; Xu, X.; Li, X. *J. Org. Chem.* **2014**, *79*, 7212–7219.

[49] Ju, X.; Li, D.; Li, W.; Yu, W.; Bian, F. *Adv. Synth. Catal.* **2012**, *354*, 3561–3567.

[50] Miyake, Y.; Nakajima, K.; Nishibayashi, Y. *J. Am. Chem. Soc.* **2012**, *134*, 3338–3341.

[51] Zhu, S.; Das, A.; Bui, L.; Zhou, H.; Curran, D. P.; Rueping, M. *J. Am. Chem. Soc.* **2013**, *135*, 1823–1829.

[52] Zhang, P.; Xiao, T.; Xiong, S.; Dong, X.; Zhou, L. *Org. Lett.* **2014**, *16*, 3264–3267.

[53] Miyake, Y.; Nakajima, K.; Nishibayashi, Y. *Chem. Eur. J.* **2012**, *18*, 16473–16477.

[54] McNally, A.; Prier, C. K.; MacMillan, D. W. C. *Science*, **2011**, *334*, 1114–1117.

[55] Prier, C. K.; MacMillan, D. W. C. *Chem. Sci.* **2014**, *5*, 4173–4178.

[56] Noble, A.; MacMillan, D. W. C. *J. Am. Chem. Soc.* **2014**, *136*, 11602–11605.

[57] Maity, S.; Zhu, M.; Shinabery, R. S.; Zheng, N. *Angew. Chem., Int. Ed.* **2012**, *51*, 222–226.

[58] Nguyen, T. H.; Maity, S.; Zheng, N. *Beilstein J. Org. Chem.* **2014**, *10*, 975–980.

[59] Haga, M.-A.; Dodsworth, E. S.; Eryavec, G.; Seymour, P.; Lever, A. B. P. *Inorg. Chem.* **1985**, *24*, 1901–1906.

[60] Wang, J.; Zheng, N. *Angew. Chem., Int. Ed.* **2015**, *54*, 11424–11427.

[61] Wang, C.; Ren, X.; Xie, H.; Lu, Z. *Chem. Eur. J.* **2015**, *21*, 9676–9680.

[62] Lu, Z.; Parrish, J. D.; Yoon, T. P. *Tetrahedron*, **2014**, *70*, 4270–4278.

[63] Cai, S.; Zhao, X.; Wang, X.; Liu, Q.; Li, Z.; Wang, D. Z. *Angew. Chem., Int. Ed.* **2012**, *51*, 8050–8053.

[64] Zuo, Z.; MacMillan, D. W. C. *J. Am. Chem. Soc.* **2014**, *136*, 5257–5260.

[65] Vlček Jr., A. *Coord. Chem. Rev.* **2000**, *200-202*, 933–978.

[66] Ferrere, S.; Gregg, B. A. *J. Am. Chem. Soc.* **1998**, *120*, 843–844.

[67] Creutz, C.; Chou, M.; Netzel, T. L.; Okumura, M.; Sutin, N. *J. Am. Chem. Soc.* **1980**, *102*, 1309–1319.

[68] Li, F.; Gentemann, S.; Kalsbeck, W. A.; Seth, J.; Lindsey, J. S.; Holten, D.; Bocian, D. F. *J. Mater. Chem.* **1997**, *7*, 1245–1262.

[69] Scaltrito, D. V.; Thompson, D. W.; O'Callaghan, J. A.; Meyer, G. J. *Coord. Chem. Rev.* **2000**, *208*, 243–266.

[70] Pirtsch, M.; Paria, S.; Matsuno, T.; Isobe, H.; Reiser, O. *Chem. Eur. J.* **2012**, *18*, 7336–7340.

[71] Henry, M. S. *J. Am. Chem. Soc.* **1977**, *99*, 6138–6139.

[72] Brunschwig, B.; Sutin, N. *J. Am. Chem. Soc.* **1978**, *100*, 7568–7577.

[73] Creutz, C.; Sutin, N. *Inorg. Chem.* **1976**, *15*, 496–499.

[74] Blaskó, G.; Cordell, G. A. In The Alkaloids; Brossi, A., Suffness, M., Eds.; Academic Press: San Diego, CA, 1990; Vol. 37, p 1–76.

[75] http://www.who.int/medicines/publications/essentialmedicines/18th_EML.pdf

[76] Neuss, N., Neuss, M. N. In *The Alkaloids*; Brossi, A., Suffness, M., Eds.; Academic: San Diego, CA, 1990; Vol. 37, p 229–240.

[77] Ishikawa, H.; Colby, D. A.; Seto, S.; Va, P.; Tam, A.; Kakei, H.; Rayl, T. J.; Hwang, I.; Boger, D. L. *J. Am. Chem. Soc.* **2009**, *131*, 4904–4916.

[78] Sundberg, R. J.; Smith, S. Q. In *The Alkaloids*; Academic Press: Waltham, MA, 2002; Vol. 59, p 281–376.

[79] Keuhne, M. E.; Markó, I. In *The Alkaloids*; Academic Press: Waltham, MA, 2002; Vol. 59, p 77–131.

[80] Pereira, D. M.; Ferreres, F.; Oliviera, J. M. A.; Gaspar, L.; Faria, J.; Valentão, P.; Sottomayor, M.; Andrade, P. B. *Phytomedicine* **2010**¸ *17*, 646–652.

[81] Prakash, V.; Timasheff, S. N. *Biochemistry* **1991**, *30*, 873–880.

[82] Langlois, N.; Gueritte, F.; Potier, P. *J. Am. Chem. Soc.* **1976**, *98*, 7017–7024.

[83] Vucovic, J.; Goodbody, A. E.; Kutney, J. P.; Misawa, M. *Tetrahedron* **1988**, *44*, 325–331.

[84] Tabakovic, I.; Gunic, E.; Gasic, M. J. *J. Chem. Soc., Perkin Trans. 2* **1996**, 2741–2745.

[85] Sundber, R. J.; Hunt, P. J.; Desos, P.; Gadamasetti, K. G. *J. Org. Chem.* **1991**, *56*, 1689–1692.

[86] Kutney, J. P.; Cretney, W. J.; Hadfield, J. R.; Hall, E. S.; Nelson, V. R. *J. Am. Chem. Soc.* **1970**¸ *92*, 1704–1707.

[87] Sundberg, R. J.; Desos, P.; Gadamasetti, K. G.; Sabat, M. *Tetrahedron Lett.* **1991**, *32*, 3035–3038.

[88] Cocquet, G.; Rool, P.; Ferroud, C. *Tetrahedron Lett.* **2001**, *42*, 839–841.

[89] Gormann, M.; Neuss, N.; Cone, N. J. *J. Am. Chem. Soc.* **1965**, *87*, 93–99.

[90] Brown, R. T.; Hill, J. S.; Smith, G. F.; Stapleford, K. S. J. *Tetrahedron*, **1971**, *27*, 5217–5228.

[91] Carroll, W. A.; Greico, P. A. *J. Am. Chem. Soc.* **1993**, *115*, 1164–1165.

[92] Cheng, B.; Sunderhaus, J. D.; Martin, S. F. *Org. Lett.* **2010**, *12*, 3622–3625.

[93] Gotoh, H.; Sears, J. E.; Eschenmoser, A.; Boger, D. L. *J. Am. Chem. Soc.* **2012**, *134*, 13240–13243.

[94] Tucker, J. W.; Zhang, Y.; Jamison, T. J.; Stephenson, C. R. J. *Angew. Chem., Int. Ed.* **2012**, *51*, 4144–4147.

[95] Agami, C.; Couty, F.; Evano, G. *Org. Lett.* **2000**, *2*, 2085–2088.

[96] Bettiol, J.-L.; Sundberg, R. J. *J. Org. Chem.* **1993**, *58*, 814–816.

[97] Bau, R.; Jin, K. K. *J. Chem. Soc., Perkin Trans. 1* **2000**, 2079–2082.

[98] Sears, J. E.; Boger, D. L. *Acc.Chem. Res.* **2015**, *48*, 653–662.

[99] Cordell, G. A.; Saxton, J. E. In *The Alkaloids*; Academic Press: Waltham, MA, 1981; Vol. 20, p 1–295.

[100] Schreiber, S. L. *Tetrahedron* **1980**, *21*, 1027–1030.

[101] Kotani, S.; Osakama, K.; Sugiura, M.; Nakajima, M. *Org. Lett.* **2011**, *13*, 3968–3971.

[102] Neuss, N.; Gorman, M. *Tetrahedron*, **1961**, *2*, 206–210.

[103] Gorman, M.; Neuss, N.; Cone, N. J. *J. Am. Chem. Soc.* **1965**, *87*, 93–99.

[104] Wheeler, S. E.; Houk, K. N.; Schleyer, P. v. R.; Allen, W. D. *J. Am. Chem. Soc.* **2009**¸ *131*, 2547–2560.

[105] Schleyer, P. v R.; Williams, J. E. Jr. *J. Am. Chem. Soc.* **1970**, *92*, 2377–2386.

[106] Khoury, P. R.; Goddard, J. D.; Tam, W. *Tetrahedron* **2004**, *60*, 8103–8112.

[107] Gaussian 09, Revision D.01, M. J. Frisch, G. W. Trucks, H. B. Schlegel, G. E. Scuseria, M. A. Robb, J. R. Cheeseman, G. Scalmani, V. Barone, B. Mennucci, G. A. Petersson, H. Nakatsuji, M. Caricato, X. Li, H. P. Hratchian, A. F. Izmaylov, J. Bloino, G. Zheng, J. L. Sonnenberg, M. Hada, M. Ehara, K. Toyota, R. Fukuda, J. Hasegawa, M. Ishida, T. Nakajima, Y. Honda, O. Kitao, H. Nakai, T. Vreven, J. A. Montgomery, Jr., J. E. Peralta, F. Ogliaro, M. Bearpark, J. J. Heyd, E. Brothers, K. N. Kudin, V. N. Staroverov, R. Kobayashi, J. Normand, K. Raghavachari, A. Rendell, J. C. Burant, S. S. Iyengar, J. Tomasi, M. Cossi, N. Rega, J. M. Millam, M. Klene, J. E. Knox, J. B. Cross, V. Bakken, C. Adamo, J. Jaramillo, R. Gomperts, R. E. Stratmann, O. Yazyev, A. J. Austin, R. Cammi, C. Pomelli, J. W. Ochterski, R. L. Martin, K. Morokuma, V. G. Zakrzewski, G. A. Voth, P. Salvador, J. J. Dannenberg, S. Dapprich, A. D. Daniels, Ö. Farkas, J. B. Foresman, J. V. Ortiz, J. Cioslowski, and D. J. Fox, Gaussian, Inc., Wallingford CT, 2009.

[108]. Zeches, M.; Debray, M. M.; Ledouble, G.; Le Men-Olivier, L.; Le Men, J. *Phytochemistry* **1975**, *14*, 1122–1124.

[109]. Gorman, M.; Neuss, N.; Cone, N. J.; Deyrup, J. A. *J. Am. Chem. Soc.* **1960**, *82*, 1142–1145.

[110]. Kuehne, M. E.; Wilson, T. E.; Bandarage, U. K.; Dai, W.; Yu, Q. *Tetrahedron* **2001**, *57*, 2085–2094.

[111]. Kuehne, M. E.; Bornmann, W. G. *J. Org. Chem.* **1989**, *54*, 3407–3420.

[112]. Kuehne, M. E.; Bandarage, U. K.; Hammach, A.; Li, Y.-L.; Wang, T. *J. Org. Chem.* **1998**, *63*, 2172–2183.

[113] Ritter, S, K, *C&EN*, **2015**, *93*, 27.

[114] Müller, K.; Faeh, C.; Diedrich, F. *Science* 2007, 317, 1881–1886.

[115] Bégué, J.-P.; Bonnet-Delpon, D. *J. Fluorine Chem.* **2006**, *127*, 9992–1012.

[116] Isanbor, C.; O'Hagan, D. *J. Fluorine Chem.* **2006**, *127*, 303–319.

[117] Kirk, K. L. *J. Fluorine Chem.* **2006**, *127*, 1013–1029.

[118] Wang, J. W.; Sánchez-Roselló, M.; Aceña, J. L.; d. Pozo, C.; Sorochinsky, A. E.; Fustero, S.; Soloshonok, V. A.; Liu, H. *Chem. Rev.* **2014**, *114*, 2432–2506.

[119] Leroux, F.; Jeschke, P.; Schlosser, M. *Chem. Rev.* **2005**, *105*, 827–856.

[120] Black, W. C.; Bayly, C. I.; Davis, D. E.; Desmarias, S.; Falgueyret, J.-P.; Léger, S.; Li, C. S.; Massé, F.; McKay, D. J.; Palmer, J. T.; Mercival, M. D.; Robichaud, J.; Tsou, N.; Zamboni, R. *Bioorg. Med. Chem. Lett.* **2005**, *15*, 4741–4744.

[121] Siegemund, G.; Schwertfeger, W.; Feiring, A.; Smart, B.; Behr, F.; Vogel, H.; McKusick, B. Fluorine Compounds, Organic. In *Ullmann's Encyclopedia of Industrial Chemistry*; Wiley, 2002.

[122] Banks, R. E. *J. Fluorine Chem.* **1994**, *67*, 193–203.

[123] McCulloch, A.; Lindley, A. A. *Atmos. Environ.* **2007**, *41*, 1560–1566.

[124] Naumann, D.; Tyrra, W.; Kock, B. *J. Fluorine Chem.* **1994**, *67*, 91–93.

[125] Krishnamurti, R.; Bellew, D. R.; Prakash, G. K. S. *J. Org. Chem.* **1991**, *56*, 984–989.

[126] Umemoto, T.; Ishihara, S. *J. Fluorine Chem.* **1998**, *92*, 181–187.

[127] Umemoto, T.; Ishihara, S. *Tetrahedron Lett.* **1990**, *31*, 3579–3582.

[128] Matoušek, V.; Pietrasiak, E.; Schwenk, R.; Togni, *J. Org. Chem.* **2013**, *78*, 6763–6768.

[129] Ye, Y.; Sanford, M. S. *J. Am. Chem. Soc.* **2012**, *134*, 9034–9037.

[130] Sladojevich, F.; McNeill, E.; Börgel, J.; Zheng, S.-L.; Ritter, T. Condensed-phase, halogen-bonded CF_3I and C_2F_5I adducts for perfluoroalkylation reactions. *Angew. Chem., Int. Ed.* **2015**, *54*, 3712–3716.

[131] Tordeux, M.; Langlois, B.; Wakselman, C. *J. Org. Chem.* **1989**, *54*, 2452–2453.

[132] Wakselman, C.; Tordeux, M. *Bull. Soc. Chim. Fr.* **1986**, 868.

[133] Ji, Y.; Brueckl, T.; Baxter, R. D.; Fujiwara, Y.; Seiple, I. B.; Su, S.; Blackmond, D. G.; Baran, P. S. *Proc. Natl. Acad. Sci. U. S. A.* **2011**, *108*, 14411–14415.

[134] Fujiwara, Y.; Dixon, J. A.; O'Hara, F.; Funder, E. D.; Dixon, D.; Rodriguez, R. A.; Baxter, R. D.; Herlé, B.; Sach, N.; Collins, M. R.; Ishihara, Y.; Baran, P. S. *Nature*, **2012**, *492*, 95–99.

[135] Swartz, F. *Bull. Soc. Chim. Belg.* **1933**, *42*, 102–103.

[136] Dolbier, W. R. Jr. *Chem. Rev.* **1996**, *96*, 1557–1584.

[137] Matsui, K.; Tobita, E.; Ando, M.; Kondo, K. *Chem. Lett.* **1981**, 1719–1720.

[138] Kondratenko, N. V.; Vechirko, E. P.; Yagupolskii, L. M. *Synthesis*, **1980**, 932–933.

[139] Carr, G. E.; Chambers, R. D.; Holmes, T. F.; *J. Chem. Soc., Perkin Trans. 1* **1988**, 921–926.

[140] Li, Y.; Chen, T.; Wang, H.; Zhang, R.; Jin, K.; Wang, X.; Duan, C. *Synlett*, **2011**, *12*, 1713–1716.

[141] Chen, M.; Buchwald, S. L. *Angew. Chem., Int. Ed.* **2013**, *52*, 11628–11631.

[142] Langlois, B. R.; Roques, N. *J. Fluorine Chem.* **2007**, *128*, 1318–1325.

[143] Su, D.-B.; Duan, J.-X.; Chen, Q.-Y. *Tetrahedron Lett.* **1991**, *32*, 7689–7690.

[144] Mulder, J. A.; Frutos, R. P.; Patel, N. D.; Qu, B.; Sun. X.; Tampone, T. G.; Gao, J.; Sarvestani, M.; Eriksson, M. C.; Haddad, N.; Shen, S.; Song, J. J.; Senanayake, C. H. *Org. Process Res. Dev.* **2013**, *17*, 940–945.

[145] Depecker, C.; Marsouk, H.; Trevin, S.; Devynck, J. *New J. Chem.* **1999**, *23*, 739–742.

[146] Tanabe, Y.; Matsuo, N.; Ohno, N. *J. Org. Chem.* **1988**, *53*, 4582–4585.

[147] Lai, C.; Mallouk, T. E. *J. Chem. Soc., Chem. Commun.* **1993**, 1359–1361.

[148] Shi, G.; Shao, C.; Pan, S.; Yu, J.; Zhang, Y. *Org. Lett.* **2015**, *17*, 38–41.

[149] Sawada, H.; Nakayama, M. *J. Fluorine Chem.* **1990**, *46*, 423–431.

[150] Koike, T.; Akita, M.; *Top. Catal.* **2014**, *57*, 967–974.

[151] Nagib, D. A.; Scott, M. E.; MacMillan, D. W. C. *J. Am. Chem. Soc.* **2009**, *131*, 10875–10877.

[152] Slinker, J. D.; Gorodetsky, A. A.; Lowry, M. S.; Wang, J.; Parker, S. Rohl, R.; Bernhard, S.; Malliaras, G. C. *J. Am. Chem. Soc.* **2004**, *126*, 2763–2767.

[153] Andrieux, C. P.; Gelis, L.; Medebielle, M.; Pinson, J.; Saveant, J. M. *J. Am. Chem. Soc.* **1990**, *112*, 3509–3520.

[154] Pham, P. V.; Nagib, D. A.; MacMillan, *Angew. Chem., Int. Ed.* **2011**, *50*, 6119–6122.

[155] Nguyen, J. D.; Tucker, J. W.; Konieczynska, M. D.; Stephenson, C. R. J. *J. Am. Chem. Soc.* **2011**, *133*, 4160–4163.

[156] Wallentin, C.-J.; Nguyen, J. D.; Finkeiner, P.; Stephenson, C. R. J. *J. Am. Chem. Soc.* **2012**, *134*, 8875–8884.

[157] Iqbal, N.; Choi, S.; Kim, E.; Cho, E. J. *J. Org. Chem.* **2012**, *77*, 11383–11387.

[158] Nagib, D. A.; MacMillan, D. W. C. *Nature* **2011**, *480*, 224–228.

[159] Tang, X.-J.; Thomoson, C. S.; Dolbier, W. R. Jr. *Org. Lett.* **2014**, *16*, 4594–4597.

[160] Yasu, Y.; Koike, T.; Akita, M. *Angew. Chem., Int. Ed.* **2012**, *51*, 9567–9571.

[161] Yasu, Y.; Koike, T.; Akita, M. *Org. Lett.* **2013**, *15*, 2136–2139.

[162] Tomita, R.; Yasu, Y.; Koike, T.; Akita, M. *Angew. Chem., Int. Ed.* **2014**, *53*, 7144–7148.

[163] Noto, N.; Miyazawa, K.; Koike, T.; Akita, M. *Org. Lett.* **2015**, *17*, 3710–3713.

[164] Tomita, R.; Koike, T.; Akita, M. *Angew. Chem., Int. Ed.* **2015**, *54*, 12923–12927.

[165] Tomita, R.; Yasu, Y.; Koike, T.; Akita, M. *Beilstein J. Org. Chem.* **2014**, *10*, 1099–1106.

[166] Yasu, Y.; Koike, T.; Akita, M. *Chem. Commun.* **2013**, *49*, 2037–2039.

[167] Wei, Q.; Chen, J.-R.; Hu, X.-Q.; Yang, X.-C.; Lu, B.; Xiao, W.-J. *Org. Lett.* **2015**, *17*, 4464–4467.

[168] Mizuta, S.; Engle, K. M.; Verhoog, S.; Galicia-López, O.; O'Duill, M.; Médebielle, M.; Wheelhouse, K.; Rassias, G.; Thompson, A. L.; Gouverneur, V. *Org. Lett.* **2013**, *15*, 1250–1253.

[169] Pitre, S. P.; McTiernan, C. D.; Ismaili, H.; Scaiano, J. C. *ACS Catal.* **2014**, *4*, 2530–2535.

[170] Xie, J.; Yuan, X.; Abdukader, A.; Zhu, C.; Ma, J. *Org. Lett.* **2014**, *16*, 1768–1771.

[171] Wilger, D. J.; Gesmundo, N. J.; Nicewicz, D. A. *Chem. Sci.* **2013**, *4*, 3160–3165.

[172] Straathof, N. J. W.; Gemoets, H. P. L.; Wang, X.; Schouten, J. C.; Hessel, V.; Noël, T. *ChemSusChem* **2014**, *7*, 1612–1617.

[173] Straathof, N. J. W.; Tegelbeckers, B. J. P.; Hessel, V.; Wang, X.; Noël, T. *Chem. Sci.* **2014**, *5*, 4768–4773.

[174] Cantillo, D.; de Frutos, O.; Rincón, J. A.; Mateos, C.; Kappe, C. O. *Org. Lett.* **2014**, *16*, 896–899.

[175] Barton, D. H. R.; Crich, D.; Motherwell, W. B. *J. Chem. Soc., Chem. Commun.* **1983**, *17*, 939–941.

[176] Barton, D. H. R.; Lacher, B.; Zard, S. Z. *Tetrahedron* **1986**, *42*, 2325–2328.

[177] Fleming, I. Frontier Orbitals and Organic Chemical Reactions. Chichester: John Wiley & Sons, **1976.**

[178] Okada, K.; Okamoto, K.; Morita, N.; Okubo, K.; Oda, M. *J. Am. Chem. Soc.* **1991**, *113*, 9401–9402.

[179] Allen, L. J.; Cabrera, P. J.; Lee, M.; Sanford, M. S. *J. Am. Chem. Soc.* **2014**, *136*, 5607–5610.

[180] Fukuzumi, S.; Kotani, H.; Ohkubo, K.; Ogo, S.; Tkachenko, N. V.; Lemmetyinen, H. *J. Am. Chem. Soc.* **2004**, *126*, 1600–1601.

[181] Seybold, P. G.; Gouterman, M.; Callis, J. *Photochem. and Photobiol.* **1969**, *9*, 229–242.

[182] Benniston, A. C.; Harriman, A.; Li, P.; Rostron, J. P.; v. Ramsesdonk, H. J.; Groenveld, M. M.; Zhang, H.; Verhoeven, J. W. *J. Am. Chem. Soc.* **2005**. *127*, 16054–16064.

[183] Flamigni, L.; Barieri, A.; Sabatini, C.; Ventura, B.; Berigelletti, F. *Coord. Chem. Rev.* **2007**, *281*, 143–203.

[184] Shulka, D.; Ahearn, W. G.; Farid, S. *J. Org. Chem.* **2005**, *70*, 6809–6819.

[185] Lima, C. G. S.; Lima, T. d. M.; Duarte, M.; Jurberg, I. D.; Paixão, M. W. *ACS Catalysis* **2016**, *6*, 1389–1407.

[186] Lee, K. Y.; Kochi, J. K. *J. Chem. Soc., Perkin Trans. 2* **1992**, 1011–1017.

[187] Dewanji, A.; Muraka, S.; Curran, D. P.; Studer, A. *Org. Lett.* **2013**, *15*, 6102–6105.

[188] Cismesia, M. A.; Yoon, T. P. *Chem. Sci.* **2015**, *6*, 5426–5434.

[189] Kärkäs, M. D.; Matsuura, B. S.; Stephenson, C. R. J. *Science* **2015**, *349*, 1285–1286.

[190] Ye, Y., Lee, S. H., & Sanford, M. S. *Org. Lett.* **2011**, *13*, 5464–5467.

[191] Lishchynskyi, A.; Novikov, M. A.; Martin, E.; Escudero-Adán, E. C.; Novák, P.; Grushin, V. V. *J. Org. Chem.* **2013**, *78*, 11126–11146.

[192] Khan, B. A.; Buba, A. E.; Gooβen, L. J. *Chem. Eur. J.* **2012**, *18*, 1577–1581.

[193] Danoun, G.; Bayarmagnai, B.; Grünberg, M. F.; Gooβen, L. J. *Angew. Chem., Int. Ed.* **2013**, *52*, 7972–7975.

[194] Liu, T.; Shen, Q. *Org. Lett.* **2011**, *13*, 2342–2345.

[195] Li, Y.; Studer, A. *Angew. Chem., Int. Ed.* **2012**, *51*, 8221–8224.

[196] Li, L.; Deng, M.; Zheng, S. C.; Xiong, Y. P.; Tan, B.; Liu, X. Y. *Org. Lett.* **2014**, *16*, 504–507.

[197] Kino, T.; Nagase, Y.; Ohtsuka, Y.; Yamamoto, K.; Uragachi, D.; Tokuhisa, K.; Yamakawa, T. *J. Fluorine Chem.* **2010**, *131*, 98–105.

[198] Cui, L.; Matusaki, Y.; Tada, N.; Miura, T.; Uno, B.; Itoh, A. *Adv. Synth. Catal.* **2013**, *355*, 2203–2207.

[199] Beatty, J. W.; Douglas, J. J.; Cole, K. P.; Stephenson, C. R. J. *Nat. Commun.* **2015**, *6*, 7919.

[200] Wiehn, M. S.; Vinogradova, E. V.; Togni, A. *J. Fluorine Chem.* **2010**, *131*, 951.

[201] Li, J.; Ballmer, S. G.; Gillis, E. P.; Fujii, S.; Schmidt, M. J.; Palazzo, A. M. E.; Lehmann, J. W.; Morehouse, G. F. Burke, M. S. *Science*, **2015**, *347*, 1121.

[202] Kobayashi, Y.; Kumadaki, I. *J. Chem. Soc., Perkin Trans. 1*, **1980**, 661.

[203] Escudero-Adan, E. C.; Grushin, V. V.; Martinez Belmonte, M.; Tomashenko, O. A. Angew. Chem. Int. Ed. 2011, 50, 7655.

[204] Maleckis, A.; Sanford, M. S. *Organometallics*, **2014**, *33*, 2653.

[205] Lorance, E. D.; Kramer, W. H.; Gould, I. R. *J. Am. Chem. Soc.* **2003**, *126*, 14071–14078.

[206] Kaizu, Y.; Ohta,H.; Kobayashi, K.; Kobayashi, H. *J. Photochem.* **1985**, *30*, 93–103.